The Influence of Machine-Part Measuring Strategies for Coordinate Measuring Devices on the Precision of the Measured Values

Jana Moravčíková, Peter Pokorný

Slovak University of Technology in Bratislava, Faculty of Materials Science and Technology in Trnava, J. Bottu 25, 917 24 Trnava, Slovak Republic
jana.moravcikova@stuba.sk, peter.pokorny@stuba.sk

Abstract: This article describes various strategies of measurement and their influence on the accuracy of measured parameters. Maintaining and, in particular, increasing the accuracy of production plays a key role in production companies. Coordinates-based measuring technology enables measuring parameters with a high degree of accuracy, depending on the measuring method used and specific conditions. The scanning system available to the CMM has a significant impact on the result of the measuring. The measuring experiment is executed on a calibration ring of a known size using the PRISMO Ultra coordinate-measuring machine. The goal of the experiment is an analysis of the effect of measuring strategies while measuring a machine-part on the values of roundness and diameter of the calibration ring. This includes a change of measuring method, scanning rate, diameter of the scanning stylus, as well as the evaluation filter. The RONDCOM 60A high-precision measuring device is designed to establish reference values of roundness for the proposed experiment measurement. This paper focuses on the analysis of the impact of conditions of measuring roundness and diameter of the calibration ring on the results of the measurements.

Keywords: coordinate measuring; measurement strategy; accuracy; roundness; diameter

1 Introduction

Production technologies, as well as measuring methods, are currently showing a trend towards increased accuracy. The required geometric and dimensional accuracy of a produced machine-part depends to a large degree on the accuracy of the machine tools and their abilities. It was a subject of the study [1, 2, 3, 4]. The precision of the produced part also determines the conditions of its assemblage and, therefore, the outcome of the assembly process. Along with increased accuracy practical requirements also arose for controlling highly precise dimensions. Coordinate measuring machines (CMM) are often currently used to

cover this need [5]. These machines are highly precise with a low degree of measurement uncertainty. The method of scanning points has a significant effect on measurement accuracy, evaluation methods and measurement conditions [6, 7, 8].

2 Description of Experimental Portion

2.1 The Characteristics of the Measured Part and the Measuring Device

A calibration etalon, a ring of a known diameter of 25 mm (Fig. 1) was used for the execution of the measuring plan. This etalon was awarded a calibration certificate issued by Kontroltech, s.r.o., Dubnica nad Váhom, a calibration company. The calibration center is a calibration laboratory approved by the Slovak National Accreditation Service, according to the STN EN ISO/IEC 17025:200 standard. The calibration ring has a precisely defined internal diameter that was measured in the calibration center at the h/2 defined height. The key parameters of the ring are shown in Table 1.

Table 1
Key parameters of the ring declared by the calibration center

Ring	Nominal size D [mm]	Actual size D [mm]	Coordinates
1	Ø25.0000	Ø25.0046	x, y

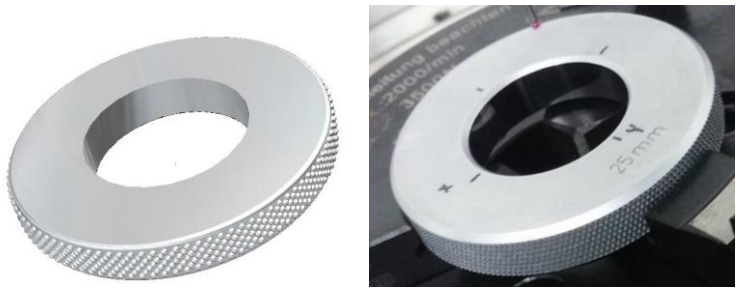

Figure 1
Inspection calibration ring

The measuring devices used for the execution of this experimental work were:
RONDCOM 60A
CMM ZEISS PRISMO Ultra

These devices are located in Heavy Laboratories of the Faculty of Materials Science and Technology in Trnava of the Slovak University of Technology in Bratislava, Slovakia.

RONDCOM 60A (Fig. 2) is a special device for measuring roundness with high precision. The machine enables high productivity of measurements due to its automated settings. Measuring takes place on a special table of the machine with air-bearings that have a rotational precision up to 20 nm, (MPEE = 0.015 + 6H/10000 μm), where H is height from table surface to measuring point. Its granite construction is a sign of the long-term stability of the machine [9].

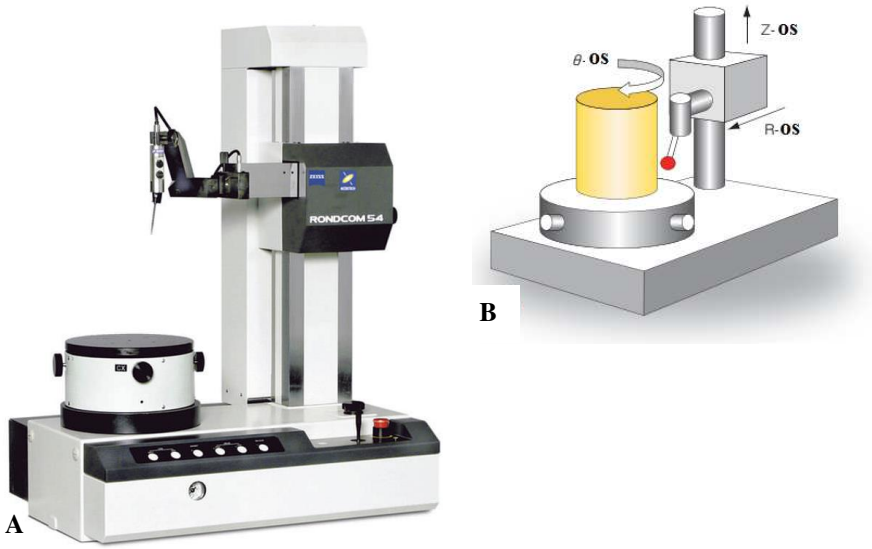

Figure 2
Measuring equipment: A – Roundcom 60A. B – Measurement principle

CMM ZEISS PRISMO Ultra - enables maximum precision at high-speed scanning. The device uses a computer-controlled correction of all dynamic influences on the measuring device.

Device construction [10]:

- A very stiff lightweight portal, thanks to the combination of ceramics and composite materials based on carbon fibres.
- All axes are on air-bearings. Axis X: 8 air-bearings, axis Y: 8 air-bearings, axis Z: 5 air-bearings.
- Elastomer buffering of vibrations and covered conductor paths, including measuring gauges for use in the vicinity of production.

CMM PRISMO Ultra by ZEISS (Fig. 3) is therefore ideal for tasks in the area of research, development and quality control, as well as for calibration of test units

and calibers. The relation (CARL ZEISS, 2015): MPEE = ± (0.5 + L/350) [mm] establishes the maximum permitted error (MPEE) [11].

A VAST Gold fixed measuring sensor is part of the coordinate measuring device. This measuring sensor is capable of scanning with high precision through a contact method. Coordinate measuring devices may additionally be equipped with rotary tables, particularly for measuring rotating parts such as shafts, bearing rings, gear rings and transmission boxes. The RT-AB rotary table is set on air-bearings, functions quietly, has excellent radial and axial runout values and direct dynamic drive [10, 12].

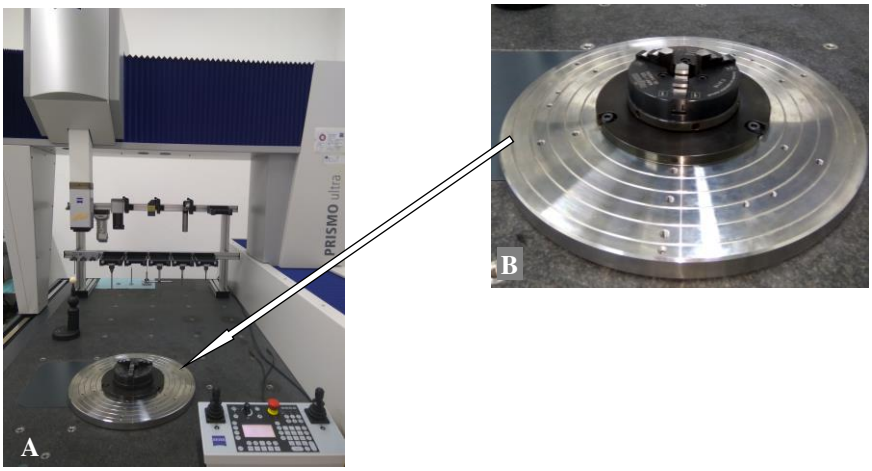

Figure 3
Measuring equipment: A – CMM PRISMO Ultra. B - Rotary table

2.2 Method and Structure of the Measurement

Measuring process using *RONDCOM 60A*:
1. Setup of the scanning system for the Ø1.5 mm sensor.
2. Leveling of the rotation table.
3. Calibration of the scanning system.
4. Setup and fastening of the measured part.
5. Leveling the part.
6. Creating a new measuring plan in the *ACCTee* program.
7. Defining measurement parameters in the *ACCTee* interface.
8. Execution of the measurement.

Measuring parameters for identifying roundness using the RONDCOM 60A device:
- Measuring method: semi-automatic.
- Number of scanned points: 3600.

- Measuring rate: 2 mm.s^{-1}, 4 mm.s^{-1}, 6 mm.s^{-1}, 8 mm.s^{-1}, 10 mm.s^{-1}.
- Measuring position: 5.10 mm in the Z axis.
- Evaluation method: Gauss.
- Filter used: Gauss, Spline.

Measuring process using PRISMO Ultra CMM:
1. Scanning strategy – creation of a measuring plan.
2. Setup of the scanning system for Ø1.5 mm, Ø3 mm and Ø5 mm sensors.
3. Reference sensor calibration.
4. Scanning system calibration.
5. Rotary table calibration.
6. Fastening the part into the rotary table clamps.
7. Creating a new measuring plan in the CALYPSO program.
8. Defining measuring parameters and evaluation in the CALYPSO interface.
9. Execution of the measurement.
10. Comparative analysis of scanned data against reference values.

A structure of experimental measuring was prepared for better orientation in the experiment (Figure 4). The structure clearly depicts the methods used for scanning: *VAST Gold* sensor / RT; monitored parameters – roundness/diameter; a change of the sensor radius Ø1.5/ Ø3/ Ø5; a change of measuring rate; a change of evaluation filter - Spline/Gauss.

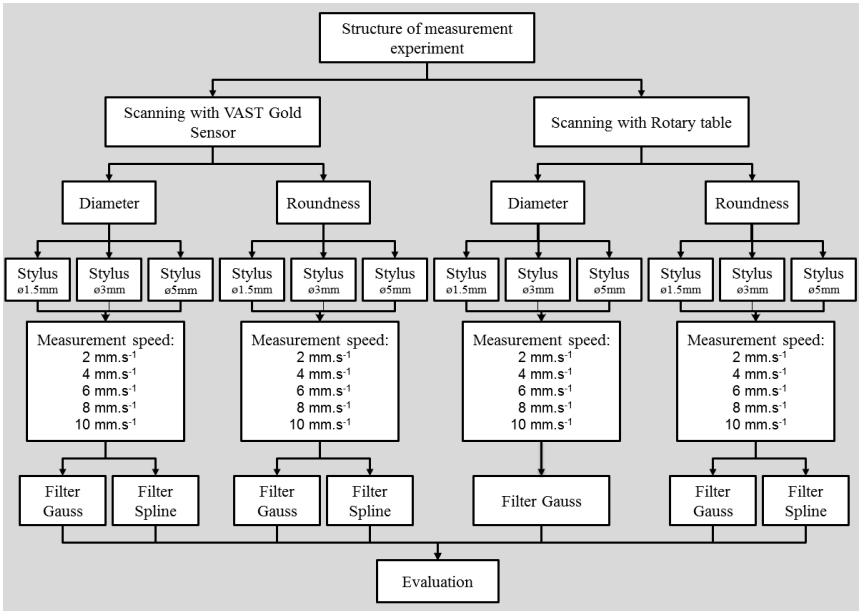

Figure 4
Structure of measuring

2.3 The Execution of the Experimental Portion of the Work experimentálnej časti práce

2.3.1 Preparation and Measuring Conditions

The experimental portion of the work was executed on the *RONDCOM 60A* device and is processed using *ACCTeePro* software. This software uses the *WINDOWS* operating system. It is a special software for identifying parameters of surfaces, contours and shape-characteristics of a part [9]. The device scanning system is set at h/2 height, meaning 4.2 mm in the direction of the Z coordinate of the calibration ring and the stylus diameter is 1.5 mm.

The experimental portion of the work was executed using the ZEISS PRISMO *Ultra* coordinate measuring device with a maximum permitted error in length measurement 0,5+L/350 μm, a fixed *VAST Gold* sensor and a rotary table. The part was measured using a contact technology of scanning. Results of the experimental measurement are shown in Table 2.

Table 2

Conditions of the surrounding environment

Room temperature in the laboratory	+20 °C
Relative air humidity	60% ÷ 70%
Reference measuring temperature	20 °C
Sea-level elevation	100 ÷ 125 V: max. 3000 m 230 ÷ 240 V: max. 2000 m

Three scanning stylus of varied diameters were used during the execution of the experiment, according to Table 3. Calibration of scanning systems must be performed in order to achieve precise measurements. The calibration is always performed prior to the measurement of new parts and is intended to correct systemic errors using a calibration ball. The OS_RT scanning system, using a stylus with an 8 mm diameter, is designed for measuring and calibration using a rotary table. Calibration conditions are listed in Table 3.

Identification of sensors in the measuring plan:
- DP_ZS_1.5 – stylus with a Ø1.5 mm diameter,
- DP_ZS_3 – stylus with a Ø3 mm diameter,
- DP_ZS_5 – stylus with a Ø5 diameter.

Basic coordinate systems for the given part must be defined in the software in preparation for the CMM measurement. This process was performed by enabling the positioning of the coordinate system into the center of the calibration ring.

Table 3
Stylus calibration conditions

Sensor Diameter	Ø8 [mm]	Ø5 [mm]	Ø3 [mm]	Ø1.5 [mm]
Mode	Tenzor			
Sensor Geometry	Sphere			
Opening Angle	180°			
Dynamic Scanning	100%	100%	100%	100%
Calibration Ball Position	180˚ turning: 0˚			
Scanning Power	200 mN	200 mN	200 mN	100 mN

The measurements of diameter and roundness of the part - calibration ring are performed three times according to the structure stipulated in Figure 4. The measuring plan consisted of the following elements:

- Plane 1, Circle 1 – form a basic coordinate system
- Circle 2, Circle 4, Circle 6, Circle 8 and Circle 10 – elements intended for measurement with the Ø1.5 mm stylus.
- Circle 2_3mm, Circle 4_3mm, Circle 6_3mm, Circle 8_3 mm, Circle 10_3mm - elements intended for measurement with the Ø3 mm stylus.
- Circle 2_5mm, Circle 4_5mm, Circle 6_5mm, Circle 8_5 mm, Circle 10_5mm – elements intended for measurement with the Ø5 mm stylus.

The 'circle' element must be scanned in order to evaluate roundness. An example of a settings strategy for the measurement of the 'circle' element is shown in Figure 5. The following parameters must be set in order to measure this element:

- Scanning rate: 2 $mm.s^{-1}$, 4 $mm.s^{-1}$, 6 $mm.s^{-1}$, 8 $mm.s^{-1}$, 10 $mm.s^{-1}$.
- Number of scanning points: 3000.
- Angle range: 380°.
- Filter type: Gauss, Spline.

Figure 5 shows an example of the result evaluation settings of the 'circle' element measurements and Figure 6 shows filter settings for evaluation. The measurement plan (Fig. 7) is created and applied to the scanning of a ring with the *VAST Gold* stylus sensor and scanning with the activation of a rotary table. Two measurement plans were created and applied with the exact same conditions for evaluation:

- measurement plan for measuring with the *VAST Gold* fixed stylus without the activation of the rotary table,
- measurement plan for measuring with the *VAST Gold* fixed stylus with the activation of the rotary table (Fig. 7).

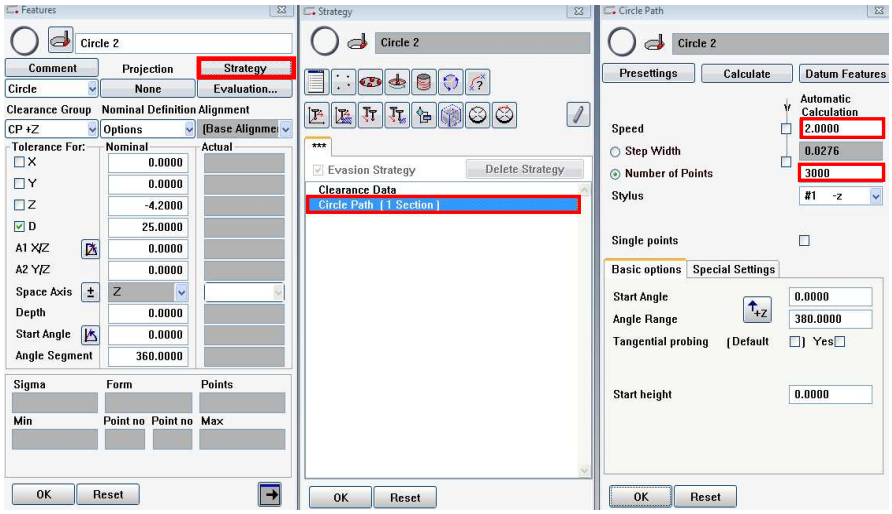

Figure 5

Settings strategy and number of scanning points in the CALYPSO interface

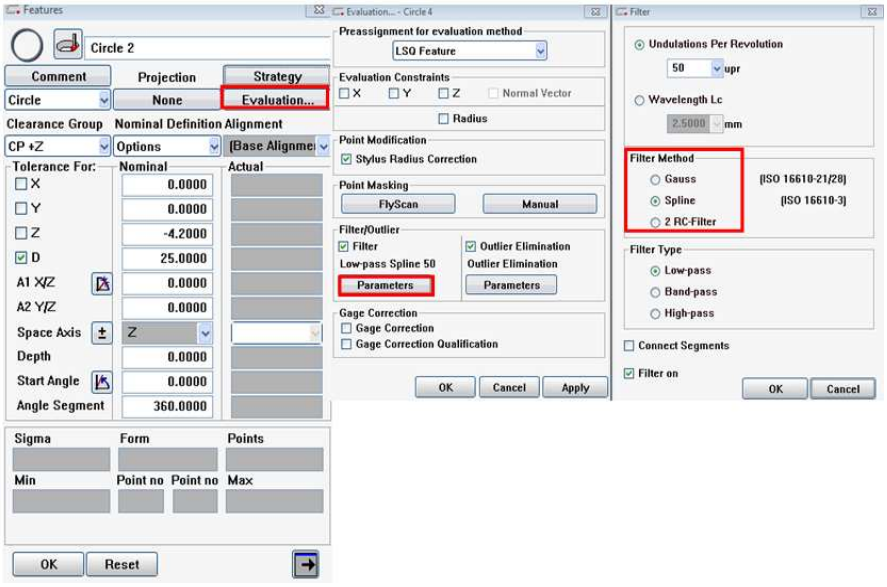

Figure 6

Filter settings for evaluation in the CALYPSO interface

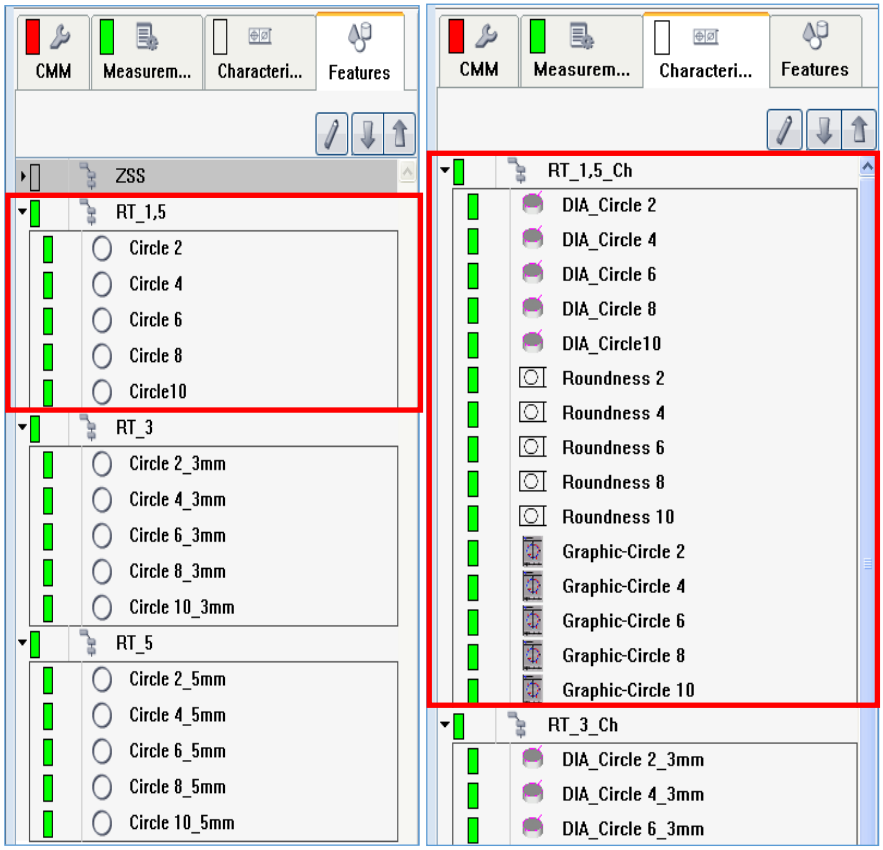

Figure 7

Overview of the measurement plan created in the CALYPSO interface: A – Element selection. B – Measurement characteristics

2.3.2 Execution of the Measurements

The measurement process began with the calibration of the RONDCOM 60A measuring device, calibration of the PRISMO Ultra CMM scanning systems and the calibration of the rotary table that is a part of the PRISMO Ultra CMM and is placed upon the working surface of the device. The calibration of the roundness was performed using gauge blocks (Fig. 8). Calibration process of the Ø1.5; Ø3; Ø5 and Ø8 mm styli was executed using a ceramic calibration ball of 30 mm diameter. The depiction of the rotary table calibration process using a calibration cylinder is shown in Figure 9. Using the calibration cylinder, the scanning system is able to automatically determine the placing of the rotary table and its parameters.

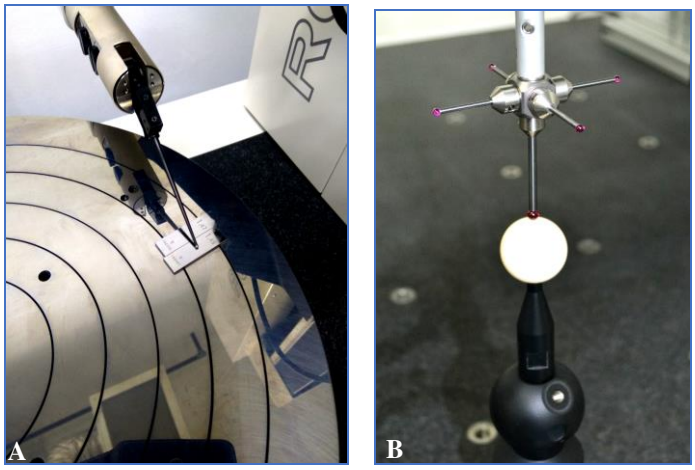

Figure 8
Calibration of the scanning systems: A – RONDCOM 60A. B - CMM PRISMO Ultra

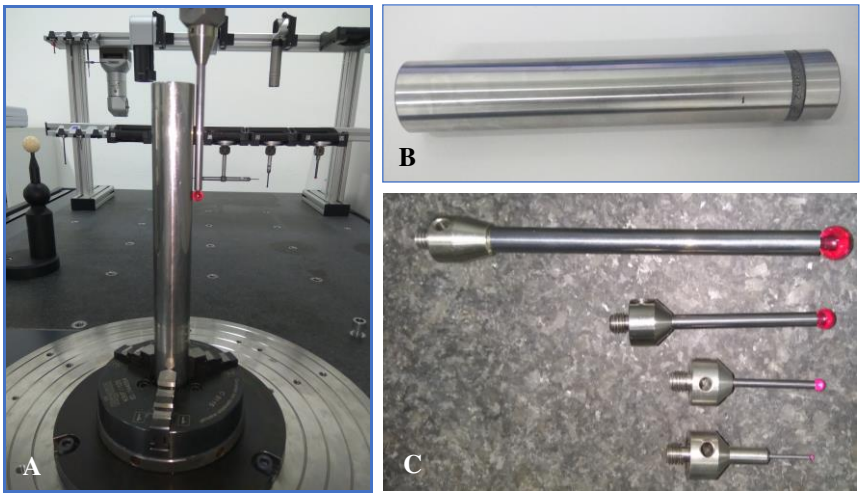

Figure 9
Calibration of the rotary table: A – calibration proces. B – calibration cylinder. C – Stylus

The calibration Ø25 mm ring was fastened to the rotary table of the RONDCOM 60A circle-measuring device and secured against shifting and turning. The roundness values obtained from the RONDCOM 60A measuring device are established as reference roundness values for the executed experiment. The placement of the calibration ring and the process of measuring roundness and diameter using the PRISMO Ultra CMM is depicted in Figure 10. When measuring with the use of the rotary table, the calibration ring was fastened into

the clamps of the rotary table, while in measuring using the fixed VAST Gold stylus, the ring was placed and fastened directly on the measuring table of the device. The final phase of the experiment was the setting off of the plan created in the CALYPSO interface. The scanning of the ring took place automatically through exchanging scanning stylus.

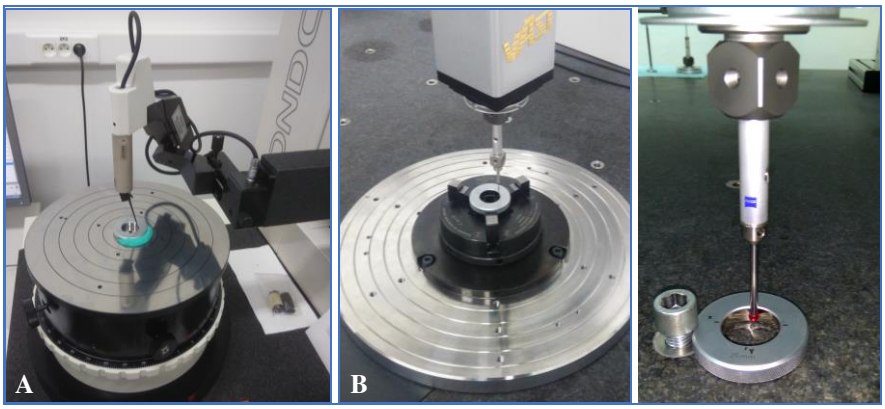

Figure 10
Execution of the measurement:
A - Measurement of the reference value using RONDCOM 60A
B - Measurement using the CMM PRISMO Ultra

2.4 Analysis and Evaluation of Results of the Experimental Work

Analysis against data scanned on the calibration ring was performed in order to analyze and evaluate the results of the experimental part of this work.

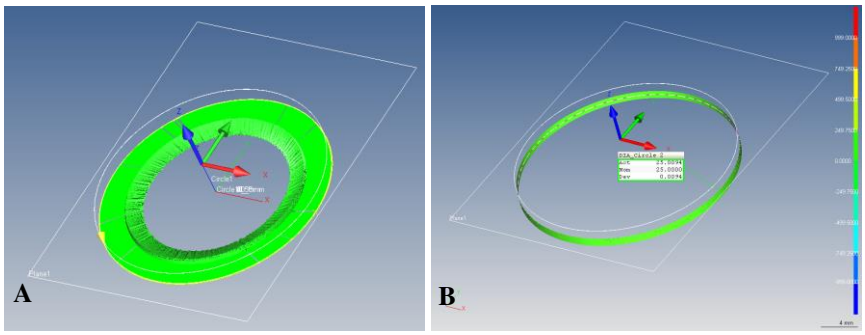

Figure 11
Measured points in the CALYPSO interface: A - Scanned element; B – Deviation of the ring diameter

A correlation between roundness tolerance and the diameter value declared by the calibration certificate was established for the values obtained from the RONDCOM 60A. After the scanning of the calibration ring, the software evaluated data in both a numeric and graphic form. The CAD window of the software provides a view of the scanned elements (Fig. 11).

2.4.1 Evaluation of Roundness Tolerance

The values measured by the RONDCOM 60A are listed in Table 4. These values were considered basic reference values for the evaluation of the roundness tolerance of the CMM PRISMO Ultra. The results of the experiment of measuring roundness obtained from the CMM PRISMO Ultra are shown in Tables 5 and 6.

Table 4
Measurement of roundness using the RONDCOM 60A – reference values

Measurement speed [mm.s^{-1}]	Roundness [μm]	
	Stylus **Ø1.5** mm	
	Filter GAUSS	Filter SPLINE
2	0.2650	0.2640
4	0.2710	0.2750
6	0.2730	0.2860
8	0.2800	0.3010
10	0.2880	0.2870

Table 5
Measurement of roundness using fixed VAST Gold stylus scanning

Measurement speed [mm.s^{-1}]	Roundness [μm]					
	Stylus **Ø1.5** mm		Stylus **Ø3** mm		Stylus **Ø5** mm	
	Filter GAUSS	Filter SPLINE	Filter GAUSS	Filter SPLINE	Filter GAUSS	Filter SPLINE
2	1.2760	1.2789	1.1798	1.1781	1.3686	1.3787
4	1.2592	1.2785	1.1545	1.1699	1.3455	1.3548
6	1.2312	1.2635	1.1741	1.1975	1.3643	1.3723
8	1.2322	1.2580	1.2115	1.2218	1.3872	1.3751
10	1.2368	1.2520	1.2571	1.2609	1.4114	1.4114

Table 6
Measurement of roundness with stylus scanning and a rotary table

Roundness [µm]							
Measurement speed [mm.s^{-1}]		Stylus Ø**1.5** mm		Stylus Ø**3** mm		Stylus Ø**5** mm	
		Filter GAUSS	Filter SPLINE	Filter GAUSS	Filter SPLINE	Filter GAUSS	Filter SPLINE
	2	1.1898	1.2037	1.1686	1.1433	1.1891	1.2056
	4	1.1569	1.1768	1.0197	1.0102	1.1681	1.1705
	6	1.1588	1.1818	1.1731	1.1191	1.1874	1.1873
	8	1.1969	1.2112	1.1494	1.1092	1.2199	1.2480
	10	1.2304	1.2467	1.1713	1.1971	1.2420	1.2540

The following influences were taken into consideration when evaluating roundness tolerance:

- The effect of the measuring method on roundness tolerance while changing the scanning rate.
- The effects of the scanning stylus diameter on roundness tolerance while changing the scanning rate.
- The effect of the filter on roundness tolerance while changing the scanning rate.

The relations are shown graphically in Figure 12 a, b, c, d.

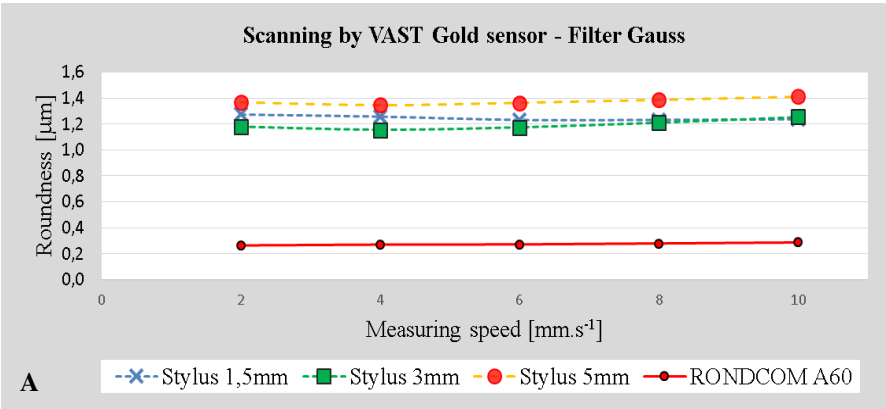

Figure 12
Evaluation of Roundness Tolerance: A – Scanning by VAST Gold sensor – filter Gauss. B – Scanning by VAST Gold sensor – filter Spline. C – Rotary table – filter Gauss. D – Rotary table – filter Spline

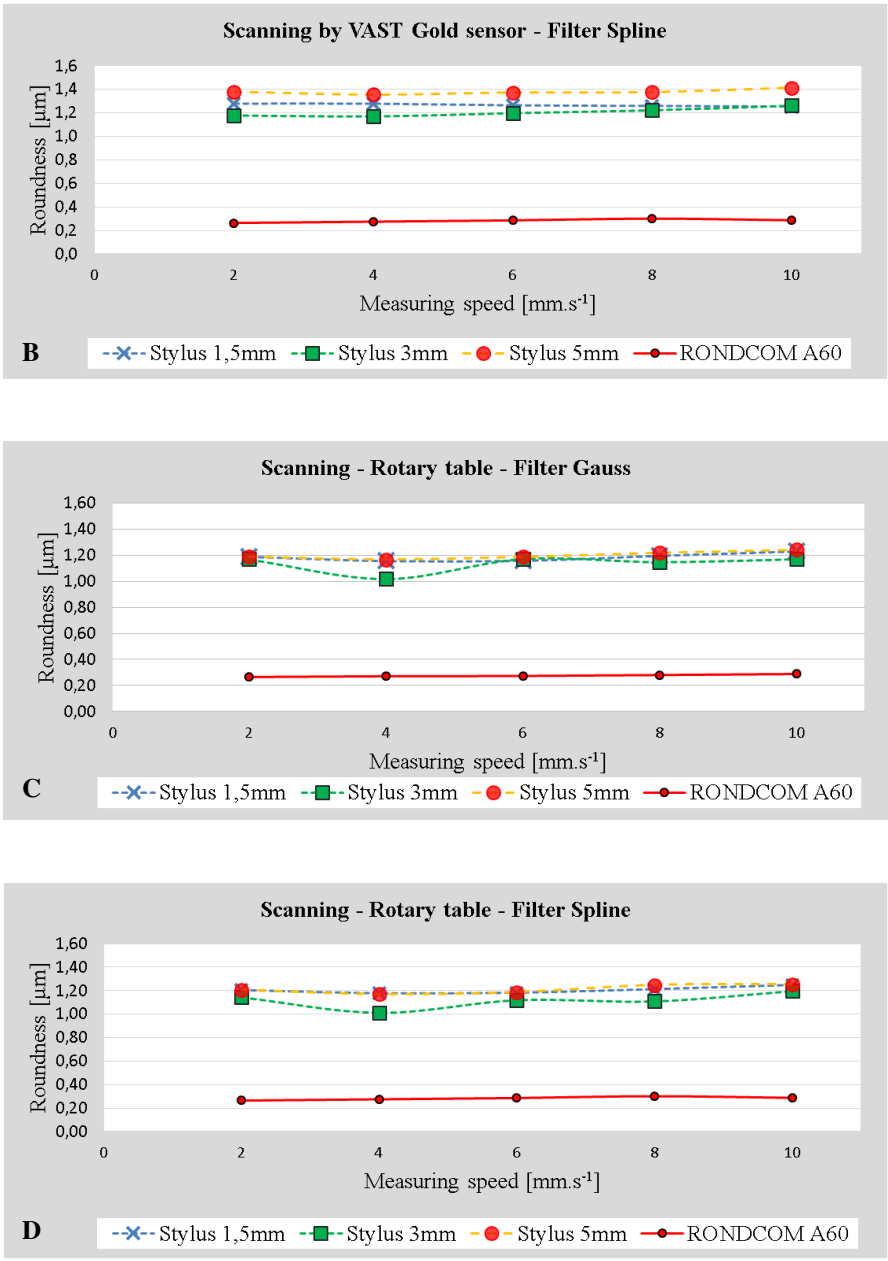

Figure 12

Evaluation of Roundness Tolerance: A – Scanning by VAST Gold sensor – filter Gauss. B – Scanning by VAST Gold sensor – filter Spline. C – Rotary table – filter Gauss. D – Rotary table – filter Spline

2.4.2 Diameter Measurement

The results of the experiment of diameter measurement measured using the CMM PRISMO Ultra are shown in Tables 7 and 8. The 25.0049 mm reference diameter of the ring was used based on the calibration certificate.

Table 7

Diameter measurement using the fixed VAST Gold stylus scanning

Diameter of ring [mm]							
Measurement speed [mm.s^{-1}]		Stylus Ø**1.5** mm		Stylus Ø**3** mm		Stylus Ø**5** mm	
		Filter GAUSS	Filter SPLINE	Filter GAUSS	Filter SPLINE	Filter GAUSS	Filter SPLINE
	2	25.00497	25.00496	25.00503	25.00503	25.00482	25.00482
	4	25.00493	25.00493	25.00502	25.00502	25.00482	25.00482
	6	25.00493	25.00493	25.00502	25.00502	25.00481	25.00481
	8	25.00492	25.00491	25.00488	25.00488	25.00480	25.00480
	10	25.00488	25.00488	25.00497	25.00497	25.00479	25.00479

Table 8

Diameter measurement using rotary table scanning

	Diameter of ring [mm]			
Measurement speed [mm.s^{-1}]		Stylus Ø**1.5** mm	Stylus Ø**3** mm	Stylus Ø**5** mm
		Filter GAUSS	Filter GAUSS	Filter GAUSS
	2	25.00713	25.00628	25.00284
	4	25.00715	25.00637	25.00297
	6	25.00716	25.00639	25.00307
	8	25.00716	25.00641	25.00311
	10	25.00717	25.00642	25.00311

The following influences were taken into consideration when evaluating the diameter measurement:

- The effect of the measuring method on diameter measurement while changing the scanning rate.
- The effect of the filter on diameter measurement while changing the scanning rate.
- The effects of the scanning *VAST Gold* stylus diameter on diameter measurement while changing the scanning rate.

The relations are shown graphically in Figure 13 a, b, c.

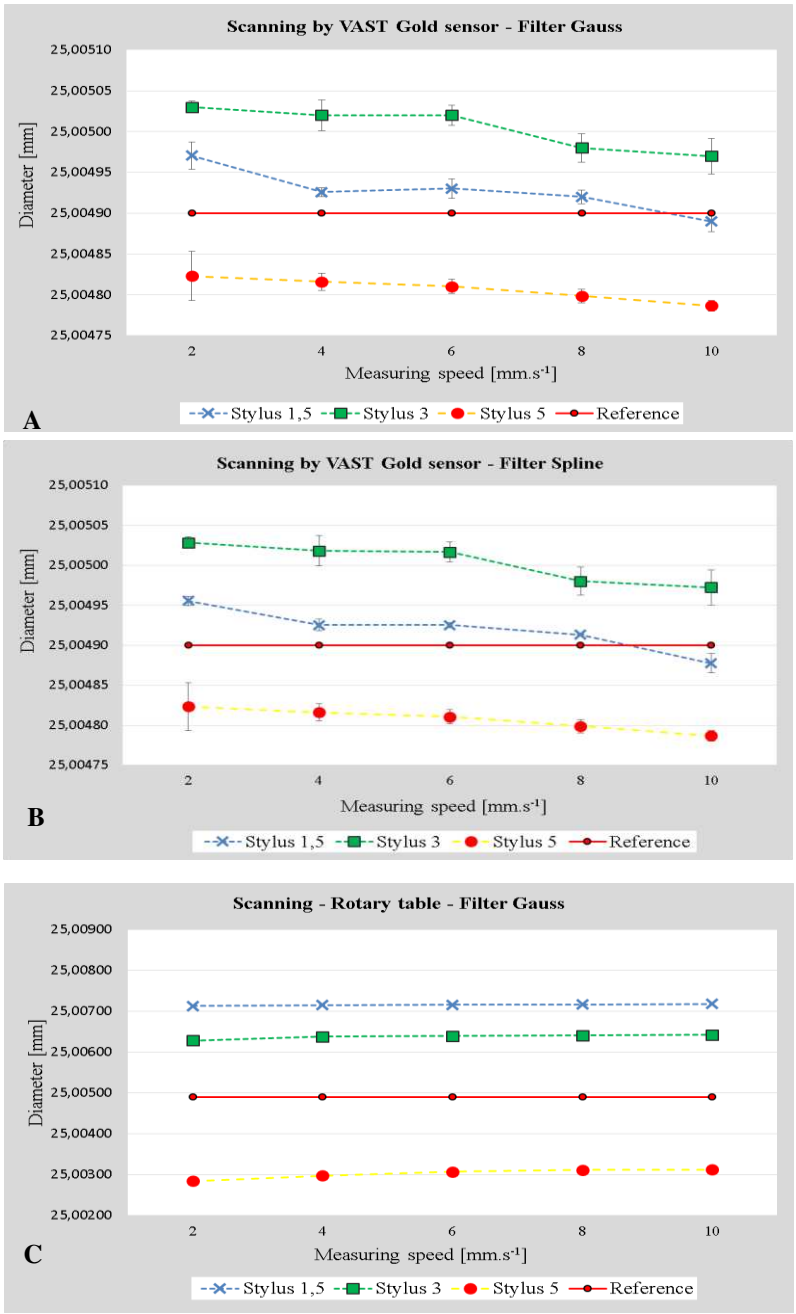

Figure 13
Evaluation of the Diameter: A – Scanning by VAST Gold sensor – filter Gauss. B – Scanning by VAST Gold sensor – filter Spline. C – Rotary table – filter Gauss

Evaluation and Conclusion

The evaluation of the extensive experiment is divided into three parts. The first part evaluates the effect of the method of measurement, the effect of the scanning stylus and the effect of the filter on the assessment of the roundness tolerance. In the second part of the evaluation, the effect of method, scanning stylus diameter and filter were established for the assessment of diameter. The last part focuses on a comparison of the graphic representation of roundness.

Roundness evaluation:

Effect of the method of measurement: measurement using a rotary table better corresponded to the reference value compared to the VAST Gold sensor method. However, the difference of roundness between both methods of measurement is within the range of (0 ÷ 0.2) μm.

Effect of the stylus diameter: The results from the Ø3 mm diameter best correspond with the declared etalon value. The difference in the result when measuring by Ø1.5 mm, Ø3 mm and Ø5 mm stylus is (0.1 ÷ 0.4) μm.

Effect of the filter: The Gauss and Spline filter does not have a significant effect on roundness measurement. The maximum difference was recorded when measuring with the VAST Gold stylus at the rate of 6 $mm.s^{-1}$ with Ø1.5 mm diameter. The difference of measured values in this case was 0.0323 μm. The best corresponding values for different filter evaluation were achieved in measuring roundness with a Ø3 mm stylus and the VAST Gold sensor.

Effect of scanning rate: The rate of 4 $mm.s^{-1}$ was established as the most suitable scanning rate in measuring with the rotary table and using a Ø3 mm stylus. The difference in roundness between the reference value and measured value for the Spline filter was 0.7402 μm and for the Gauss filter 0.7497 μm.

Graphic Comparison of Roundness

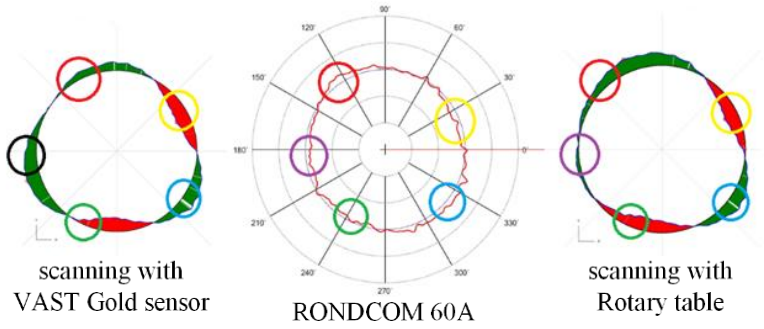

Figure 14

Graphic comparison of roundness. Scanning rate: 2 $mm.s^{-1}$_filter: GAUSS

Graphic results of the measurement show Figure 14 that the method of stylus scanning using a rotary table better corresponds with graphic results obtained using the RONDCOM 60A device. Circles identify similar areas in the same color. An area identified by a black circle indicates the least corresponding value.

Evaluation of the Diameter:

Effect of the method: The method of stylus scanning with the VAST Gold sensor best corresponds with the etalon value and is therefore more suitable than measurement using a rotary table.

Effect of the scanning stylus diameter: Values closest to the reference values were measured using the VAST Gold sensor at the scanning rate of 6 to 10 $mm.s^{-1}$ with the Ø1.5 mm stylus diameter. Diversion from the reference value at this scanning rate was a maximum of 0.03 μm.

Effect of the filter: The comparison of the Gauss and Spline filters shows negligible differences in the measurement results. When scanning using the VAST Gold sensor, the recorded divergences were in the range of (0 ÷ 0.02) μm. With the increase of scanning rate using the VAST Gold sensor, the measured values had a decreasing tendency. When measuring using the rotary table, the measured values had the opposite tendency, meaning that the measured diameter values increased with the increasing scanning rate.

As is apparent from this experiment, to precisely evaluate roundness, the best option is to use measurement with a rotary table, Ø3 mm stylus diameter, 4 $mm.s^{-1}$ scanning rate and the Spline filter. To measure diameter, the most suitable combination is VAST Gold sensor with an Ø1.5 mm stylus diameter, 6 to 8 $mm.s^{-1}$ scanning rate and the Spline filter. However, the use of the Gauss filter does not indicate significant differences for evaluating a diameter.

Acknowledgements

This contribution is a part of the VEGA project of Ministry of Education, Science, Research and Sport of the Slovak Republic, No. 1/0477/14 "Research of influence of selected characteristics of machining process on achieved quality of machined surface and problem free assembly using high Technologies" and the project Technical research and development infrastructure for contact and non-contact measurement methods", ITMS 26210120020, the Operational Program Research and Development financed by the European Regional Development Fund".

We support research activities in Slovakia / project is co-financed from EU funds.

References

[1] W. Xingsheng, X. Jieyu, Y. Yong, Z. Yongnian, F. Xiuqing, K. Min: *Use of Coordinate Measuring Machine to Measure Circular Aperture Complex Optical Surface*, Measurement, Vol. 100, 2017, pp. 1-6, ISSN 0263-2241, https://doi.org/10.1016/j.measurement.2016.12.038

[2] A. Keck, O. Sawodny, M. Gronle, T. Haist, W. Osten: *Active Compensation of Dynamic Errors in a Coordinate-Measuring Machine*, IFAC-PapersOnLine, Vol. 49, Issue 21, 2016, pp. 636-641, ISSN 2405-8963, https://doi.org/10.1016/j.ifacol.2016.10.672

[3] Syed Hammad Mian, Abdulrahman Al-Ahmari: *Enhance Performance of Inspection Process on Coordinate Measuring Machine*, Measurement, Vol. 47, 2014, pp. 78-91, ISSN 0263-2241, https://doi.org/10.1016/j.measurement.2013.08.045

[4] Z. He, J. Fu, X. Zhang, H. Shen: A Uniform Expression Model for Volumetric Errors of Machine Tools. International Journal of Machine Tools and Manufacture. Volume 100, January 2016, Pages 93-104

[5] D. H. Genest, Brown & Sharpe Manufacturing Company: Coordinate Measuring Machines. In *ASM Handbook,* Vol. 17, 1989. pp. 18-28

[6] A. Gąska, J. Sładek, K. Ostrowska, R. Kupiec, M. Krawczyk, W. Harmatys, P. Gąska, M. Gruza, D. Owczarek, R. Knapik, A. Kmita: *Analysis of Changes in Coordinate Measuring Machines Accuracy Made by Different Nodes Density in Geometrical Errors Correction Matrix*, Measurement, Vol. 68, 2015, pp. 155-163, ISSN 0263-2241, https://doi.org/10.1016/j.measurement.2015.02.056

[7] D. Zhao, Y. Bi, Y. Ke: *An Efficient Error Compensation Method for Coordinated CNC Five-Axis Machine Tools*, International Journal of Machine Tools and Manufacture, Vol. 123, 2017, pp. 105-115, ISSN 0890-6955, https://doi.org/10.1016/j.ijmachtools.2017.08.007

[8] J. Dupuis, C. Holst, H. Kuhlmann: *Improving the Kinematic Calibration of a Coordinate Measuring Arm Using Configuration Analysis*, Precision Engineering, Vol. 50, 2017, pp. 171-182, ISSN 0141-6359, https://doi.org/10.1016/j.precisioneng.2017.05.004

[9] ACCTee PRO. 2014 Available on: <http://www. zeiss .com /industrial-metrology/ende/products/systems/form-andsurface/>

[10] Š. Kender, Súradnicové meracie stroje, In *Electronic magazine Transfer of innovation*, TU Košice, Vol. 26, 2013 Available on:<https://www.sjf.tuke.sk/transferinovacii/pages/archiv/transfer/26-2013/pdf/233-235.pdf>

[11] ZEISS PRISMO, 2017 Available on: <https://www.zeiss.sk/metrologia/produkty/systemy/bridge-type-cmms/prismo.html>

[12] D. Flack: *Measurement Good Practice Guide No. 43,* Queen's Printer, Scotland, 2014.ISSN 1368-6550

Graph Irregularity and a Problem Raised by Hong

Tamás Réti

Bánki Donát Faculty of Mechanical and Safety Engineering, Óbuda University, Népszínház u. 8, H-1081 Budapest, Hungary, reti.tamas@bgk.uni-obuda.hu

Abstract: Starting with the study of the Collatz-Sinogowitz and the Albertson graph irregularity indices the relationships between the irregularity of graphs and their spectral radius are investigated. We also use the graph irregularity index defined as $Ir(G) = \Delta - \delta$, where Δ and δ denote the maximum and minimum degrees of G. Our observations lead to the answer for a question posed by Hong in 1993. The problem concerning graphs with the smallest spectral radius can be formulated as follows: If G is a connected irregular graph with n vertices and m edges, and G has the smallest spectral radius, is it true that $Ir(G) =1$? It will be shown that the answer is negative; counterexamples are represented by several cyclic graphs. Based on the previous considerations the problem proposed by Hong can be reinterpreted (refined) in the form of the following conjecture: If G is a connected irregular graph with n vertices and m edges, and G has the smallest spectral radius, then $Ir(G)=1$ if such a graph exists, and if not, then $Ir(G)=2$. Considering the family of unicyclic graphs for which $Ir(G) \geq 2$, we prove that among n-vertex irregular unicyclic graphs the minimal spectral radius belongs to the uniquely defined short lollipop graphs where a pendent vertex is attached to cycle C_{n-1}. Moreover, it is verified that among n-vertex graphs there exists exactly one irregular graph J_n having a maximal spectral radius and an irregularity index of $Ir(J_n)=1$. Finally, it is also shown that by using the irregularity index Ir(G) a classification of n-vertex trees into (n-2) disjoint subsets can be performed.

Keywords: irregularity indices; spectral radius; unicyclic graphs; lollipop

1 Introduction

For a graph G with n vertices and m edges, V(G) and E(G) denote the set of vertices and edges, respectively. Let d(u) be the degree of vertex u in G, and denote by uv an edge of G connecting vertices u and v. Denote by Δ and δ the maximum and minimum degree of G.

We use the standard terminology in graph theory, for notations not defined here we refer the reader to [1, 2, 3]. A graph is called regular, if all its vertices have the

same degree. A non-regular connected graph G is said to be irregular. Let $\rho(G)$ be the spectral radius of G and denote by $Cy = m - n + 1$ the cyclomatic number of a graph G. Because a tree graph is acyclic, its cyclomatic number is equal to zero. A connected graph G having $Cy(G) = k \geq 1$ cycles is said to be a k-cyclic graph.

A connected bidegreed bipartite graph $G(\Delta,\delta)$ is called semiregular if each vertex in the same part of bipartition has the same degree. An n-vertex unicyclic graph is a connected graph obtained by attaching a finite number of trees at vertices of a cycle. Because m = n for unicyclic graphs, their cyclomatic number equals one. The only regular unicyclic graphs are the cycles. By definition, let C(n,m) be the family of connected irregular graphs with n vertices and m edges, respectively. Consequently, C(n,n-1) denotes the set of trees, and C(n,n) denotes the set of irregular unicyclic graphs. It is immediate that for any connected irregular n-vertex graph, $1 \leq \Delta - \delta \leq n-2$. By definition, an n-vertex graph G is said to be *maximally irregular graph* if Ir(G) = n-2, and *weakly irregular graph* (WIR graph) if Ir(G) = 1. It is obvious that any connected WIR graph is a bidegreed graph.

The organization of this paper is as follows. In Section 2, we review some known irregularity indices, and their relations with the spectral radius of acyclic and various cyclic graphs. In Section 3, the Hong's problem is investigated with particular regard to unicyclic graphs. In Section 4, inequalities characterizing the irregularity of lollipop graphs are presented. In Section 5, it is proved that among n-vertex graphs there exists an irregular graph J_n having a maximal spectral radius and an irregularity index of $Ir(J_n)=1$. Moreover, a sharp upper bound is given for the spectral radius of n-vertex connected irregular graphs. In Section 6, it is shown that by using the irregularity index Ir(G) a classification of n-vertex trees into (n-2) disjoint subsets can be performed.

2 Relations between Graph Irregularity Indices and the Spectral Radius

By definition, a topological invariant IT(G) is called an irregularity index of a graph G if $IT(G) \geq 0$ and IT(G)=0 if and only if G is a regular graph. The majority of irregularity indices are degree-based, but there exist eigenvalue-based irregularity indices as well [6-19]. Widely used topological invariants are the Collatz–Sinogowitz irregularity index [6]

$$\varepsilon(G) = \rho(G) - \frac{2m}{n}$$

and the Albertson irregularity index [7],

$$AL(G) = \sum_{uv \in E} |d(u) - d(v)|$$

Among the degree-based irregularity indices, $Ir(G) = \Delta - \delta$ is one of the simplest topological graph invariants [8]. It is easy to see that for any m-edge connected graph

$$AL(G) = \sum_{uv \in E} |d(u) - d(v)| \leq mIr(G)$$

and equality holds if graph G is a regular or semiregular.

Weakly irregular graphs play a central role in the mathematical chemistry. Benzenoid graphs are bidegreed graphs composed of finite number hexagons (except C_6 cycle) [4]. They form a subset of WIR graphs because $\Delta=3$ and $\delta=2$ hold for them. The dual graphs of traditional trivalent fullerene graphs contain only vertices with degrees 5 and 6, consequently all dual fullerene graphs are WIR graphs with $\Delta - \delta = 6 - 5=1$ [5]. It is worth noting that semiregular WIR graphs with $\Delta=3$ and $\delta=2$ can be easily generated by performing a subdivision operation on edges of arbitrary 3-regular graphs. Complete bipartite graphs $K_{p,q}$ where $p\geq1$ and $q=p+1$ are also semiregular WIR graphs with $n=2p+1$ vertices and $m=p(p+1)$ edges. This observation implies that for any $n\geq3$ odd integer there is an n-vertex WIR graph isomorphic to an n-vertex complete bipatite graph.

As an example, in Fig.1, tricyclic WIR graphs with $\Delta=3$ and $\delta=2$ are depicted.

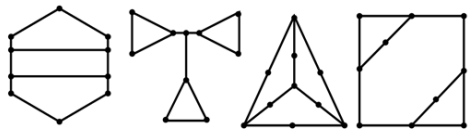

Figure 1
WIR graphs having identical vertex degree sequence

As can be seen, graphs J_C and J_D are semiregular, and J_C is generated by using a subdividing operation on the edges of K_4 complete graph.

The Collatz–Sinogowitz irregularity index has been extensively studied during the last two decades [10-19]. As can be seen, $\varepsilon(G)$ is a linear function of the spectral radius, consequently among graphs with n vertices and m edges the maximal irregularity index $\varepsilon(G)$ belongs to graphs with maximal spectral radius, and the minimal irregularity index $\varepsilon(G)$ belongs to graphs with minimal spectral radius. Similar phenomenon can be observed for some particular classes of graphs which are characterized by the irregularity index Ir(G.

2.1 Acyclic Graphs with Extremal Irregularity

Denote by P_n and $K_{1,n-1}$ the n-vertex paths and stars, respectively.

Lemma 1 Let T_n be an ($n \geq 3$)-vertex tree. Then $Ir(P_n)=1$ and $Ir(K_{1,n-1})=n-2$, consequently,

$1 = Ir(P_n) \leq Ir(T_n) \leq Ir(K_{1,n-1}) = n-2$.

In other words, the lower bounds are attained if T_n is the path P_n, and the upper bounds if T_n is the star $K_{1,n-1}$. Based on the Lemma 1 and using the known formulas published in Ref. [3] the following proposition is obtained:

Proposition 1 Let T_n be an n-vertex tree with $n \geq 3$ vertices. Then

$$\rho(T_n) \geq \rho(P_n) = 2\cos\left(\frac{\pi}{n+1}\right) \geq \sqrt{2} > Ir(P_n) = 1,$$

$$\rho(T_n) \leq \rho(K_{1,n-1}) = \sqrt{\Delta(K_{1,n-1})} = \sqrt{n-1} = \sqrt{Ir(K_{1,n-1})+1},$$

$$1 = Ir(P_n) < \rho(T_n) \leq \sqrt{Ir(K_{1,n-1})+1} = \sqrt{n-1}.$$

2.2 Maximally Irregular Cyclic Graphs

In what follows methods for constructing maximally irregular n-vertex cyclic graphs with Ir(G)=n-2 are presented.

Proposition 2 For any $n \geq 4$ positive integer there exists a maximally irregular n-vertex graph G_n with $m=(n-1)(n-2)/2+1$ edges having one vertex of degree 1, one vertex of degree n-1, and n-2 vertices of degree n-2.

Proof: Let K_{n-1} be a complete graph with n-1 vertices, where $n \geq 4$. By attaching one pendent edge to K_{n-1} we obtain the n-vertex graph G_n belonging to the family of kite graphs [30]. It is easy to see that the kite graph G_n has one vertex of degree 1, one vertex of degree n-1, and n-2 vertices of degree n-2.

Proposition 3 Denote by $G_n^{(k,p)}$ an n-vertex and k-cyclic graph composed of k triangles and $p=n-k-2 \geq 1$ pendent edges. Let us assume that k triangles have a sole common vertex u and all pendent edges are attached to vertex u. Then, $Ir(G_n^{(k,p)}) = k+p = n-2$

Proof: Consider the n-vertex cyclic graphs depicted in Fig. 2.

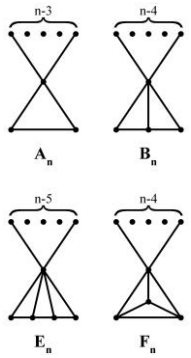

Figure 2
Four n-vertex and k-cyclic graphs with k= 1, 2 and 3

In Fig. 2 graphs A_n are unicyclic, B_n are bicyclic graphs, while E_n and F_n are non-isomorphic 3-cyclic graphs, respectively. It is easy to see that graphs denoted by A_n, B_n and E_n form subsets of $G_n^{(k,p)}$ graphs. Because k+p=n-2 is fulfilled, this implies that, $A_n = G_n^{(1,n-3)}$, $B_n = G_n^{(2,n-4)}$, and $E_n = G_n^{(3,n-5)}$.

Remark 1 According to results published in [25] a fundamental property of graphs A_n, B_n and F_n is that all of them have maximal spectral radius among n-vertex unicyclic, bicyclic and tricyclic connected graphs, respectively. From this observation it can be concluded that tricyclic graphs F_n have a larger spectral radius than graphs E_n.

Remark 2 It is interesting to note that among 6-vertex connected graphs there exist two non-isomorphic 3-cyclic graphs having identical minimal spectral radius of 2,732 and identical minimal irregularity index Ir=3-2=1.

2.3 Irregularity of Unicyclic Graphs

Structural properties of unicyclic graphs have been characterized in several papers [20-31]. As an example, consider the n-vertex sun graphs denoted by SG_n where $n \geq 6$ even integer. A sun graph SG_n is the graph on n=2k vertices obtained by attaching k pendent edges to a cycle C_k. [42]. (See Fig. 3)

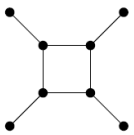

Figure 3
Sun graph SG_8

Sun graphs represent a particular subset of unicyclic graphs where $\Delta=3$ and $\delta=1$ hold [42]. For these graphs

$$\rho(SG_n) = 1+\sqrt{2} = 1+\sqrt{\Delta-\delta} = 1+\sqrt{Ir(SG_n)}\,.$$

As can be seen, the spectral radius and the irregularity index of sun graphs are constant numbers; they are independent of the vertex number and the graph diameter.

For the spectral radius of unicyclic graphs various upper bounds have been deduced [20-31].

Proposition 4 Let U be a unicyclic graph different from a cycle. Then

$$\rho(U) < 2\sqrt{\Delta-\delta} = 2\sqrt{Ir(U)}\,.$$

Proof: Hu in [20] verified that for a unicyclic graph with maximum degree Δ the inequality $\rho(G) \le 2\sqrt{\Delta-1}$ is valid, and equality holds if and only if G is a cycle. Because any unicyclic graph different from a cycle contains one or more pendent vertices, from this observation the result follows.

Hong in 1986 [40] and, independently Brualdi and Solheid [25] obtained a sharp upper bound for the spectral radius of unicyclic graphs.

Proposition 5 [40, 25]: Let U_n be an n-vertex unicyclic graph different from cycle C_n. Then

$$\rho(U_n) \le \rho(S_n^3)\,,$$

where S_n^3 denotes the graph obtained by joining any two vertices of degree one of the star $K_{1,n-1}$ by an edge. The upper bound is attained only when U_n is the graph S_n^3.

Remark 3 It should be noted that the set of S_n^3 graphs is identical to the family of unicyclic graphs A_n depicted in Fig. 2.

In 1993, Hong asked the following question (his Problem 3) [31]: *Let G be a simple irregular connected graph with n vertices and m edges. If G has the smallest spectral radius, is it true that $\Delta - \delta = Ir(G) = 1$?*

3 Investigating the Hong's Problem

Concerning the Hong's problem, it is easy to see that a necessary condition for the fulfillment of equality $Ir(G) = \Delta - \delta = 1$ is that the connected graph G must be a WIR graph. It is known that in the set C(n,n-1) of trees there is exactly one tree

(path P_n) which is a WIR graph. Moreover, paths P_n have minimal spectral radius among n-vertex trees. Unicyclic graphs other than cycles contain at least one pendent vertex of degree 1 and at least one vertex of degree not smaller than 3. As a consequence:

Proposition 6 For any irregular unicyclic graph $Ir(G) = \Delta - \delta \geq 2$ holds.

It is easy to show that there exist M and N, M > N positive integers such that all graphs in C(N,M) are not WIR graphs (that is $Ir(G) = \Delta - \delta \geq 2$ is fulfilled). This observation is demonstrated by simple examples.

Proposition 7 If N=6 and M=12, then the set C(6,12) of connected irregular graphs does not contain WIR graphs.

Proof: Set C(6,12) contains exactly 4 irregular graphs with cyclomatic number C_y=12-6+1=7. They are denoted by H_A, H_B, H_C, and H_D and are characterized by the following properties:

Degree sequence of H_A is [5,5,4,4,4,2] and $Ir(H_A) = 5 - 2 = 3$

Degree sequence of H_B is [5,5,5,3,3,3] and $Ir(H_B) = 5 - 3 = 2$

Degree sequence of H_C is [5,5,4,4,3,3] and $Ir(H_C) = 5 - 3 = 2$

Degree sequence of H_D is [5,4,4,4,4,3] and $Ir(H_D) = 5 - 3 = 2$

The minimal spectral radius belongs to graph H_D, namely $\rho(H_D) = 4{,}067$. In Fig. 4 these graphs taken from [32] are depicted.

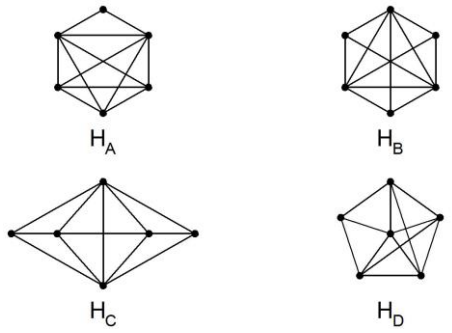

Figure 4
The four 6-vertex graphs from set C(6,12)

Proposition 8 If N=6 and M=9, then the set C(6,9) does not contain WIR graphs.

Proof: Set C(6,9) contains 18 irregular graphs with cyclomatic number C_y=9-6+1=4. None of them are WIR graphs. Among these 18 graphs the graph H_E depicted in Fig. 5 has the minimal spectral radius, $\rho(H_E) = 3{,}086$. The corresponding degree sequence is [4,3,3,3,3,2], so $Ir(H_E) = 2$.

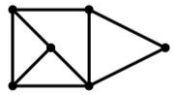

Figure 5
The 9-edge graph H_E from set C(6,9)

In what follows we deal with the construction of n-vertex irregular unicyclic graphs having minimal spectral radius. To do this, the introduction of some definitions and two lemmas are needed.

Lemma 2 [3, 33]: If H is a (not necessarily induced) subgraph of a graph G, that is $H \subset G$, then $\rho(H) < \rho(G)$.

Hoffman and Smith [34] defined *an internal path* of graph G as a walk $v_0,v_1,\ldots v_k$ ($k \geq 1$) such that the vertices $v_1,...,v_k$ are distinct (v_0, v_k do not need to be distinct), $d(v_k) > 2$, and $d(v_i) = 2$ whenever $0 < i < k$, holds.

Lemma 3 [30, 33]: Let uv be an edge of the n-vertex connected graph G and let G_{uv} be obtained from G by subdividing the edge uv of G. Let W_n, with $n \geq 6$ be the double-snake depicted in Fig. 6. If uv belongs to an internal path of G, and $G \neq W_n$, then $\rho(G_{uv}) < \rho(G)$.

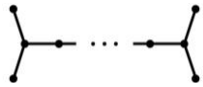

Figure 6
The double-snake graph W_n ($n \geq 6$)

The lollipop graphs are a subset of unicyclic graphs [30, 35-38]. A *lollipop Lo(n,k)* with $3 \leq k \leq n$ is a graph obtained from a cycle C_k and a path P_{n-k} by adding an edge between a vertex from the cycle and the endpoint from the path. Lollipop Lo(n,n-1) is called the short lollipop, while Lo(n,n) is the cycle C_n [36].

Proposition 9 The minimal spectral radius of an n-vertex unicyclic graph different from a cycle C_n belongs to uniquely defined short lollipop Lo(n,n-1) obtained by appending a cycle C_{n-1} ($n \geq 4$) to a pendent vertex u.

Proof: It is based on the application of two different graph transformation operations. A common feature of these transformations is that both of them decrease the spectral radii of unicyclic graphs.

i) Denote by Ω(n,k) the class of n-vertex irregular unicyclic graphs including a k-edge cycle C_k, where $3 \leq k \leq n-1$. Let $G_1 \in \Omega(n,k)$ be an arbitrary n-vertex unicyclic graph. Consider the finite sequence of unicyclic graphs $G_1 \supset G_2,...,\supset G_j,... \supset G_J$ obtained by deleting step-by-step pendent edges, in such a way, that $G_{j+1} = G_j - e$, where e is an

arbitrary pendent edge of G_j. According to Lemma 2, $G_{j+1} \subset G_j$ holds, consequently, as a result of consecutive edge-deleting operations $\rho(G_{j+1}) < \rho(G_j)$ is fulfilled. Because in the final step the corresponding vertex number is equal to k+1, we get the short lollipop graph Lo(k+1,k) composed of a k-edge cycle C_k and one pendent edge attached to C_k.

ii) In order to identify the n-vertex unicyclic graph with a minimal spectral radius, the lollipop graph Lo(k+1,k) must be further transformed. For this purpose, based on the concept outlined in Lemma 3, we have to create a sequence of subdividing transformations on the cycle C_k by increasing step-by-step the edge number of C_k until we obtain the lollipop graph Lo(n,n-1). (The final step of transformations is characterized by the case of k=n-1.) It is clear that in each step, our subdividing transformations are always performed on an edge belonging to an internal path of cycles considered. Moreover, from Lemma 3 it follows that as a result of subsequent subdividing operations we get a sequence of lollipop graphs with increasing vertex numbers and decreasing spectral radii, simultaneously. It is easy to see that the short lollipop graph Lo(n,n-1) obtained at the final step has the minimal spectral radius among all n-vertex irregular unicyclic graphs.

Remark 4 From the previous considerations it follows that for short lollipops Lo(n,n-1) having the minimal spectral radius the equality $\Delta - \delta = 3 - 1 = 2$ holds.

In Fig. 7, the concept for constructing n-vertex unicyclic graphs with the minimal spectral radius is demonstrated.

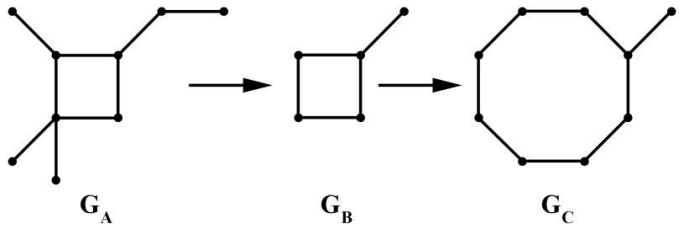

Figure 7
Transformations used for obtaining a unicyclic graph with the smallest spectral radius

Considering the three graphs shown in Fig. 7 it can be concluded that

i) graph G_A is a 9-vertex unicyclic graph with a spectral radius
$\rho(G_A) = 2{,}456$

ii) the 5-vertex lollipop graph G_B obtained from unicyclic G_A has the spectral radius $\rho(G_B) = \sqrt{(5+\sqrt{17})/2} = 2{,}1358$,

iii) the short lollipop graph G_C obtained from G_B represents the unique unicyclic graph having the minimal spectral radius $\rho(G_C) = 2{,}084$ among all 9-vertex unicyclic graphs.

Remark 5 In the family of n-vertex, non-isomorphic unicyclic graphs there are graphs having cycles C_k with different $k \geq 3$ edge numbers. The characteristic feature of the method used for identifying the n-vertex unicyclic graph with minimal spectral radius is that independently from the topological structure of graph G_1, in the final step we always obtain the same uniquely defined extremal lollipop graph Lo(n,n-1).

4 Some Considerations Related to Lollipop Graphs

Lemma 4 Boulet and Jouve in [37] verified that for the spectral radius of lollipop graphs Lo(n,k) the following universal upper bound holds

$$\rho(\mathrm{Lo}(n,k)) < \sqrt{5} = 2{,}236068$$

The value $\sqrt{5}$ seems to be the best upper bound for lollipop graphs. This claim is confirmed by computational results as well. For example, for lollipop Lo(8,3) one obtains that $\rho(\mathrm{Lo}(8,3)) = 2{,}2350$. (See computed spectral radii of 8-vertex unicyclic graphs summarized in [22]).

Remark 6 Let $k \geq 2$ a positive integer. It is easy to show that there exist infinitely many unicyclic graphs H_k with vertex number $n=3k$ for which

$$\rho(H_k) = \sqrt{5} = 2{,}236068 \text{ holds.}$$

Consider the infinite sequence of unicyclic graphs H_k depicted in Fig. 8. Graphs H_k having an identical degree set {1,2,3} and an arbitrary large diameter. They belong to the family of bipartite pseudo-semiregular graphs [48].

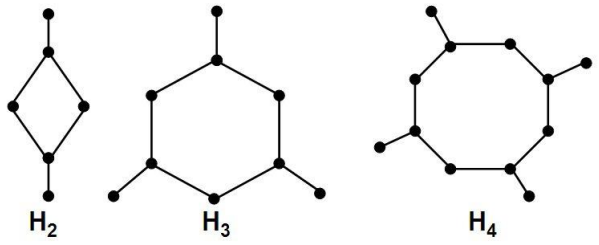

Figure 8
Unicyclic graphs H_k for k=2, 3, 4, with vertex number 6, 9, 12, ..

It is likely that there is no simple closed formula for computing the spectral radius of short lollipop graphs Lo(n,n-1). Supposing that a closed formula exists, this will be very complicated. As an example, consider the smallest lollipop graph Lo(4,3), having only 4 vertices.

In [39] the formula for calculating the spectral radius of the smallest lollipop graph Lo(4,3) is given. Namely, $\rho(\mathrm{Lo}(4,3)) = \theta_1 = 2{,}17009$ where θ_1 is one of the three roots of the polynomial defined by $\theta^3 - \theta^2 - 3\theta + 1 = 0$.

Woo and Neumayer [33] studied the structural properties of a particular class of unicyclic graphs called closed quipus. By definition, a *closed quipu* is a unicyclic graph G of maximum degree 3 such that all vertices of degree 3 lie on a cycle [30, 33]. This implies the following proposition:

Proposition 10 Because lollipop graphs form a subset of closed quipus it follows that in the family of n-vertex closed quipus the short lollipop Lo(n,n-1) has the smallest spectral radius.

Based on the previous considerations, the problem suggested by Hong can be modified (refined) in the form of the following conjecture: *If G is a connected irregular graph with n vertex and m edges, and G has the smallest spectral radius, then Ir(G)=1 if such a graph exists, and if not, then Ir(G)=2.*

Remark 7 From the relations between the spectral radius of unicyclic graphs and the corresponding Collatz-Sinogowitz irregularity index the following inequalities yield. For any n-vertex unicyclic graph U_n

$$\varepsilon(U_n) = \rho(U_n) - \frac{2m}{n} \geq \rho(\mathrm{Lo}(n, n-1)) - 2 > \rho(\mathrm{Lo}(n, n)) - 2 = 0 \cdot$$

Furthermore, from Lemma 4, one obtains that

$$\varepsilon(\mathrm{Lo}(n,k)) = \rho(\mathrm{Lo}(n,k)) - \frac{2m}{n} < \sqrt{5} - 2 = 0{,}236068 \cdot$$

5 WIR Graphs with Maximal Spectral Radius

The Hong'problem concerns WIR graphs. On the analogy of Hong's problem the following question can be asked: *Let G be a simple irregular connected graph with n vertices and m edges. If G has the maximal spectral radius, is it true that* $\Delta - \delta = Ir(G) = n-2$ *?*

The answer is negative. It is easy to show that for any $n \geq 4$ positive integer there always exists an n-vertex irregular graph J_n possessing the following properties: $Ir(J_n)=1$ and J_n has a maximal spectral radius among n-vertex irregular graphs.

Consider the unambiguously defined n-vertex irregular graph J_n obtained as $K_n - e$, where K_n is the n-vertex complete graph and e is an arbitrary edge of K_n. From the definition of graph J_n the following proposition is obtained:

Proposition 11 The n-vertex irregular graph J_n is characterized by the following properties:

i) J_n is the only n-vertex irregular graph having the maximal edge number equal to $m^* = n(n-1)/2 - 1$. This implies that J_n is the sole graph in the set $C(n, m^*)$.

ii) Because $\Delta(J_n) = n-1$ and $\delta(J_n) = n-2$, this implies that $Ir(J_n) = 1$.

iii) J_n has the maximal spectral radius among n-vertex irregular graphs [49].

iv) Using the formula published by Hong et al. [41], for the spectral radius of a connected irregular graph G one obtains that

$$\rho(G) \le \frac{n-3+\sqrt{n^2+2n-7}}{2},$$

and equality is fulfilled if and only if G is isomorphic to J_n.

Remark 8 Cioabă [43] proved that for a connected R-regular graph $G_{R,n}$ with n vertices

$$\frac{2}{n} > \Delta - \rho(G_{R,n} - e) > \frac{1}{nD}$$

holds. If $G_{R,n}$ is isomorphic to K_n then $\Delta(K_n) = \Delta(J_n) = n-1$. Because $D(J_n) = 2$, it follows that

$$\frac{2}{n} > n - 1 - \rho(J_n) > \frac{1}{2n}.$$

Remark 9 Let G be a connected graph with n vertices and m edges. If $n \ge 4$ and $m^* = n(n-1)/2 - 1$ then the known Hong's bound [44] represented by $\rho(G) \le \sqrt{2m - n + 1}$ slightly overestimates the spectral radii of graphs J_n:

$$\sqrt{2m^* - n + 1} = \sqrt{n^2 - 2n - 1} > \left(n - 3 + \sqrt{n^2 + 2n - 7}\right)/2 = \rho(J_n).$$

Remark 10 For example, if $J_4 = K_4 - e$, then for the spectral radius of the "diamond graph" J_4 one obtains that $\rho(J_4) = (1+\sqrt{17})/2)$.

6 Additional Considerations

The next inequalities represent some results relating to irregularity indices. Cioabă and Gregory have proved the following inequality [45]: Let G be a non-regular graph with n vertices and m edges having maximum degree Δ. Then

$$\varepsilon(G) = \rho - \frac{2m}{n} \geq \frac{(\Delta - \delta)^2}{4n\Delta} = \frac{Ir^2(G)}{4n\Delta}.$$

An interesting conjecture has been posed in [46]: For any connected non-regular graph G with n vertices

$$\Delta - \rho > \frac{\sqrt{\Delta - \delta}}{nD} = \frac{\sqrt{Ir(G)}}{nD}.$$

By a computer search the conjecture is verified for all connected graphs of order at most 8 [46].

Proposition 12 Let G be a connected graph. Then $2nVar(G) \geq Ir^2G) \geq 4Var(G)$ where

$$Var(G) = \frac{1}{n}\sum_{u \in V} d^2(u) - \left(\frac{2m}{n}\right)^2 \geq 0$$

is the degree-variance irregularity index proposed by Bell [9]. In the above formula equalities hold in both sides if and only if G is a regular graph.

Proof. In [47] Izumino et al. have proved that for a connected non-regular graph G with n vertices and m edges

$$Ir^2G) = (\Delta - \delta)^2 \geq 4Var(G)$$

Moreover, in [50] Gutman et al. verified that

$$Ir^2G) = (\Delta - \delta)^2 \leq 2nVar(G).$$

Proposition 13 Let G be a connected irregular graph with n vertices and m edges.

According to [19] consider the graph irregularity index IRF(G) defined by

$$IRFG) = \sum_{uv \in E} \big(d(u) - d(v)\big)^2$$

Then

$$Ir^2G) \geq \frac{1}{m} IRF(G) = \frac{1}{m}\big(F(G) - 2M_2(G)\big).$$

where

$$F(G) = \sum_{u \in V} d^3(u) \quad \text{and} \quad M_2(G) = \sum_{uv \in E} d(u)d(v),$$

and equality is valid if G is regular or semiregular.

Proof. In [19] it was shown that $IRF(G) = F(G) - 2M_2(G)$. This implies that

$IRFG) = F(G) - 2M_2(G) = \sum_{uv \in E} (d(u) - d(v))^2 \leq m(\Delta - \delta)^2$ where equality holds if G is regular or semiregular.

Using the irregularity index Ir(G) a classification of n-vertex trees into (n-2) disjoint subsets can be performed.

Proposition 14 Let $n \geq 4$ and $2 \leq q \leq n-1$ be positive integers. There exists at least one n-vertex tree T_q for which $Ir(T_q)=q-1$ holds.

Proof. The concept of generating the proper sequence of n-vertex trees T_q is based on the ordering of trees according to their maximum vertex degrees.

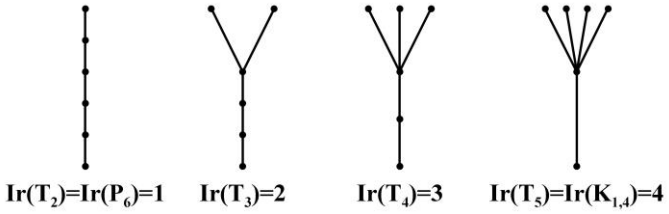

Figure 9
The sequence of T_q graphs with increasing irregularity (case of n=6)

As it is demonstrated in Fig. 9, for constructing the sequence of n-vertex trees T_q a simple graph transformation is used by which only the irregularity changes, but the vertex number n remains the same. Starting with path $T_2=P_n$, as a result of consecutive transformation steps, the maximum degree increases as $\Delta(T_{q+1}) = \Delta(T_q)+1$, and simultaneously the graph irregularity also increases according to $Ir(T_{q+1}) = Ir(T_q)+1$.

Based on previous considerations, the following conjecture is posed: *Let $n \geq 4$ and $2 \leq q \leq n-1$ be positive integers. There exists at least one n-vertex cyclic graph G_q for which $Ir(G_q)=q-1$ holds, except for unicyclic graphs with $q=2$.*

Acknowledgements

The author would like to thank Clive Elphick for valuable comments and suggestions on the drafts of this paper.

References

[1] C. Godsil, G. Royle, *Algebraic Graph Theory,* Springer-Verlag, Inc., New York, 2001

[2] N. Biggs, *Algebraic Graph Theory,* Cambridge Univ. Press, Cambridge, 1974

[3] D. Cvetković, M. Doob, H. Sachs, *Spectra of Graphs - Theory and Applications,* III. revised and enlarged edition, Johan Ambrosius Bart Verlag, Heidelberg – Leipzig, 1995

[4] I. Gutman, S. J. Cyvin, *Introduction to the Theory of Benzenoid Hydrocarbons,* Springer, Berlin, 1989

[5] P. W. Fowler, D. E. Manolopoulos: *An Atlas of Fullerenes*, Calendron Press, Oxford, 1995

[6] L. Collatz, U. Sinogowitz, Spektren endlicher Grafen, *Abh. Math. Sem. Univ. Hamburg,* **21** (1957) 63-77

[7] M. O. Albertson, The irregularity of a graph, *Ars Comb.* **46** (1997) 2019-225

[8] F. Goldberg, Spectral radius minus average degree: a better bound, math arxiv1407.4285 (2014)

[9] F. K. Bell, A note on the irregularity of a graph, *Linear Algebra Appl.***161** (1992) 45-54

[10] I. Gutman, P. Hansen, H. Mélot, Variable neighborhood search for extremal graphs. 10. Comparison of irregularity indices for chemical trees, *J. Chem. Inf. Model.* **45** (2005) 222-230

[11] R. Nasiri, G. H. Fath-Tabar, The second minimum of the irregularity of graphs, *El. Notes Discr. Math.* **45** (2014) 133-140

[12] H. Abdo, N. Cohen, D. Dimitrov, Graphs with maximal irregularity, *Filomat* **28** (2014) 1315-1322

[13] C. Elphick, P. Wocjan, New measures of graph irregularity, *El. J. Graph Theory Appl.* **2** (2014) 52-65

[14] I. Gutman, B. Furtula, C. Elphick, Three New/Old Vertex-Degree-Based Topological Indices, *MATCH Commun. Math. Comput. Chem.* **72** (2014) 617-632

[15] A. Hamzeh, T. Réti, An Analogue of Zagreb Index Inequality Obtained from Graph Irregularity Measures, *MATCH Commun. Math. Comput. Chem.* **72** (2014) 669-683

[16] D. Dimitrov, T. Réti, Graphs with equal irregularity indices, *Acta Polytech. Hung.* **11** (2014) 41-57

[17] B. Horoldagva, L. Buyantogtokh, S. Dorjsembe, I. Gutman, Maximum Size of Maximally Irregular Graphs, *MATCH Commun. Math. Comput. Chem.* **76** (2016) 81-98

[18] I. Gutman, Irregularity of Molecular Graphs, *Kragujevac J. Sci.* **38** (2016) 99-109

[19] T. Réti, E. Tóth-Laufer, On the Construction and Comparison of Graph Irregularity Indices, *Kragujevac J. Sci.* **39** (2017) 66-88

[20] S. Hu, The largest eigenvalue of unicyclic graphs, *Discrete Math.* **307** (2007) 280-284

[21] O. Rojo, New upper bounds on the spectral radius of unicyclic graphs, *Linear Algebra Appl.* **428** (2008) 754-764

[22] D. Cvetković, P. Rowlinson, Spectra of unicyclic graphs, *Graphs and Combinatorics,* **3** (1987) 7-23

[23] A. Yu, F. Tian, On the Spectral Radius of Unicyclic Graphs, *MATCH Commun. Math. Comput. Chem.* **51** (2004) 97-109

[24] Y. Hou, F. Tian, Unicyclic graphs with exactly two main eigenvalues, *Appl. Math. Lett.* **19** (2006) 1143-1147

[25] R. A. Brualdi, E. S. Solheid, On the spectral radius of connected graphs, *Publ. Inst. Math. (Beograd)* **39** (1986) 45-54

[26] S. K. Simić, On the largest eigenvalue of unicyclic graphs, *Publ. Inst. Math. (Beograd)* **42** (1987) 13-19

[27] F. Belardo, E. M. Li Marzi, S. K. Simić, Some results on the index of unicyclic graphs, *Linear Algebra Appl.* **416** (2006) 1048-1059

[28] F. Belardo, E. M. Li Marzi, S. K. Simić, On the spectral radius of unicyclic graphs with prescribed degree sequence, *Linear Algebra Appl.* **432** (2010) 2323-2334

[29] X. Chen, Y. Hou, The extreme eigenvalues and maximum degree of k-connected irregular graphs, *Linear Algebra Appl.* **463** (2014) 33-43

[30] D. Stevanović, *Spectral Radius of Graphs,* Academic Press, Amsterdam, 2015

[31] Y. Hong, Bounds of eigenvalues of graphs, *Discrete Math.* **123** (1993) 65 74

[32] D. Cvetković, M. Petrić, A table of connected graphs on six vertices, *Discrete Math.* **50** (1984) 37-49

[33] R. Woo, A. Neumayer, On Graphs Whose Spectral Radius is bounded by $3\sqrt{2}/2$, *Graphs and Combinatorics,* **23** (2007) 713-726

[34] A. J. Hoffman, J. H. Smith, On the spectral radii of topologically equivalent graphs, In M. Fiedler (Ed.) *Recent Advances in Graph Theory,* Academia Press Praha, 1975, pp. 273-281

[35] W. H. Haemers, X. Liu, Y. Zhang, Spectral characterization of lollipop graphs, *Linear Algebra Appl.* **428** (2008) 2415-2423

[36] M. Aouchiche, P. Hansen, A survey of automated conjectures in spectral graph theory, *Linear Algebra Appl.* **432** (2010) 2293-2322

[37] R. Boulet, B. Jouve, The lollipop graph is determined by its spectrum, *preprint submitted to Electron. J. Combin.* 2008, arXiv:0802.1035v1 [math.GM]

[38] Y. Zhang, X. Liu, B. Zhang, X. Yong, The lollipop graph is determined by its Q-spectrum, *Discrete Math.* **309** (2009) 3364-3369

[39] A. E. Brouwer and W. H. Haemers, *Spectra of graphs,* New York, Springer, 2011, p. 17

[40] Y. Hong, On the spectra of unicyclic graphs, *J. East China Norm. Univ. Nature. Sci. Ed.* **1** (1986) 31-34

[41] Y. Hong, J.-L. Shu, K. Fang, A Sharp Upper Bound of the Spectral Radius of Graphs, *J. Combin. Theory,* Series **B 81** (2001) 177-183

[42] M. Mirzakhah, D. Kiani, The sun graph is determined by its signless Laplacian spectrum, *Electron. J. Linear Algebra,* **20** (2010) 610-620

[43] S. M. Cioabă, The spectral radius and the maximum degree of irregular graphs. *Electron. J. Combin.* **14** (2007) #R38

[44] Y. Hong, A bound on the spectral radius of graphs, *Linear Algebra Appl.* **108** (1988) 135-139

[45] S. M. Cioabă, D. A. Gregory, Large matchings from eigenvalues, *Linear Algebra Appl.* **422** (2007) 308-317

[46] S. M. Cioabă, D. A. Gregory, V. Nikiforov, Extreme eigenvalues of nonregular graphs, *J. Combin. Theory,* Series **B 97** (2007) 483-486

[47] S. Izumino, H. Mori, Y. Seo, On Ozeki's Inequality, *J. of Inequal. and Appl.* **2** (1998) 235-253

[48] H. Abdo, D. Dimitrov, T. Reti, D. Stevanović, Estimation of the Spectral Radius of a Graph by the Second Zagreb Index, *MATCH Commun. Math. Comput. Chem.* **72** (2014) 741-751

[49] S. Friedland, Bounds on the Spectral Radius of Graphs with e Edges, *Linear Algebra Appl.* **101** (1988) 81-86

[50] I. Gutman, K. Ch Das, B. Furtula, E. Milovanović, Generalization of Szőkefalvi Nagy and Chebyshev inequalities with applications in spectral graph theory, *Appl. Math. Comput.* **313** (2017) 235-244

Cellular Automata Approach to Mathematical Morphology in the Triangular Grid

MohammadReza Saadat, Benedek Nagy

Department of Mathematics, Faculty of Arts and Sciences,
Eastern Mediterranean University, 99450 Famagusta,
North Cyprus, Mersin-10, Turkey
{mohammed.saadet | benedek.nagy}@emu.edu.tr

Abstract: Cellular automata are parallel computing devices working on a discrete time-scale. In the paper, each cell of the triangular grid has a state from the binary set (i.e., we have a binary pattern, an image, on the grid), and the state in the next time instant depends only on the actual state of the cell itself and the states of its side-neighbor cells. We illustrate their use in image synthesis, e.g., generating snowflakes, and in image analysis: some of our automata are connected to image processing operations, e.g., dilation and erosion. Computation of Hausdorff distance of two binary images on the triangular grid is also presented. In image processing, and especially in mathematical morphology, operations are local operations, and thus, cellular automata are apt to use. On the other side, the triangular grid is not a point lattice, thus the definition of translation based image operations is not always straightforward.

Keywords: parallel computing; cellular automaton; non-traditional grids; binary image processing; game of life; dilation; erosion; closing; opening; Hausdorff distance

1 Introduction

Cellular automata are widely used classical parallel computing models formulated by von Neumann, Ulam and Codd in the 1940's. These automata work on discrete grids, each cell has a state from a finite set and they are able, e.g., to do "self-reproduction". 2D models are widespread [7, 10, 24, 27]; "Game of Life" is one of the most popular cellular automata, it was introduced in 1970 by Conway [8, 9, 10, 23]. It is designed on a square grid where each cell has only 2 states: dead or alive. Many life-like automata have been studied since then (see, e.g, [5]). One of the most important properties of the cellular automata is the type of the grid. There are various two dimensional infinite grids: square, triangular, pentagonal and hexagonal grids. Digital image processing and mathematical morphology use discrete images represented on a grid. There are various algorithms which are based on the value of the cell and on the values of its neighbors. This fact gives us the possibility to

establish relations between specific cellular automata and morphological operations.

Image processing and image analysis are important parts of artificial and computational intelligence. The most used digital space is the square grid, it is used most frequently in applications as well. There are two other regular tessellations of the plane, the hexagonal and the triangular grids; they are also in a duality relation in terms of planar graphs. Because of some better properties some of the image processing algorithms are also developed for these grids [15, 18, 21, 13]. However, the triangular grid is not a point lattice, thus translation based local operations cannot be defined in a straightforward way. This is an important difference from the square and hexagonal lattices. In mathematical morphology, dilation and erosion are based on local translations, various approaches to extend their definitions to the triangular grid was shown recently in [1]. This paper is also motivated by the reason of lack of morphological operations described and analysed on the triangular grid. In various image processing applications parallel and distributed algorithms become important and popular, we will present parallel algorithms (cellular automata) for morphological operations.

In this paper, we are going to study cellular automata on the triangular grid giving some general characteristics. Some models can be connected to image processing techniques, especially parallel algorithms to dilation and erosion. Cellular automata were already introduced on the triangular grid [4], but with a larger neighborhood (for a Moore-type of neighbourhood having 12 neighbors). Here, in this paper, the smallest natural neighborhood (with 3 neighbors) is considered, that is analogous to the von Neumann neighbourhood used in the square grid.

2 Preliminaries

2.1 Cellular Automaton

A cellular automaton consists of a regular grid of cells with finite number of dimensions. Each cell has a finite number of states, such as “on” and “off” (In case of 2 states, it is called binary). For each cell, there is a set of cells called its neighbors. An initial state (time $t = 0$) is where each cell has one specified state (e.g., “on” or “off”). A new generation ($t + 1$) is created according to some fixed rules that specify the new state of each cell based on its current state and its neighbors’ states. The rules are the same for each cell and do not change. They are simultaneously applied to the whole grid. In the next subsection we recall a specific binary model.

2.2 Conway's Game of Life

The progress of the Game of Life, also known just as Life, is determined by its initial state, requiring no further input, thus it is a zero-player game. To "play" this game one creates an initial pattern and observes how it generates the next ones. It runs in a space of unlimited two-dimensional square grid. Each cell has two possible states, dead or alive, and interacts with its eight neighbors that are adjacent diagonally, vertically, or horizontally. This Moore neighborhood, also called chessboard neighborhood in image processing, is defined as

$$N(x,y) = \{(x',y') \big| x' \in \{x-1, x, x+1\}, y' \in \{y-1, y, y+1\}\} \backslash \{(x,y)\}$$

The game has simple rules which are as follow:

- **Birth:** a dead cell at time *t* with exactly 3 living neighbors will be alive at time *t* + 1.
- **Death:** a living cell at time *t* with less than 2 or more than 3 living neighbors will die at time *t* + 1.

The initial pattern is the system's seed. Each generation is a function of the previous one. The generation *t* + 1 is created by applying the game's rules simultaneously to each cell in the generation *t*. The rules are applied repetitively to create the next generations.

2.3 Triangular Grid

The Triangular Grid is also called isometric grid; it is a grid generated by tiling the plane regularly with equilateral triangles. Various coordinate systems can be used for this grid. Here we use the one which was described in [16, 17, 15]. Each cell has 3 coordinates, *i*, *j* and *k* where $i, j, k \in \mathbb{Z}$ and $i + j + k \in \{0,1\}$. See also Figure 1(a). There are 2 types of cell: type "*E*", even cells, where the sum of coordinates equals to 0 and type "*O*", odd cells, where the sum of coordinates equals to 1. Closest neighbors, also called side-neighbors are used throughout this paper. Two cells are neighbors if exactly one of their coordinates differs, and this difference is ±1. Consequently, each cell has 3 neighbors, the cells with which it shares a side. Even cells have odd neighbors and vice versa. Example of neighbors can also be seen in Figure 1(b) and (c), respectively.

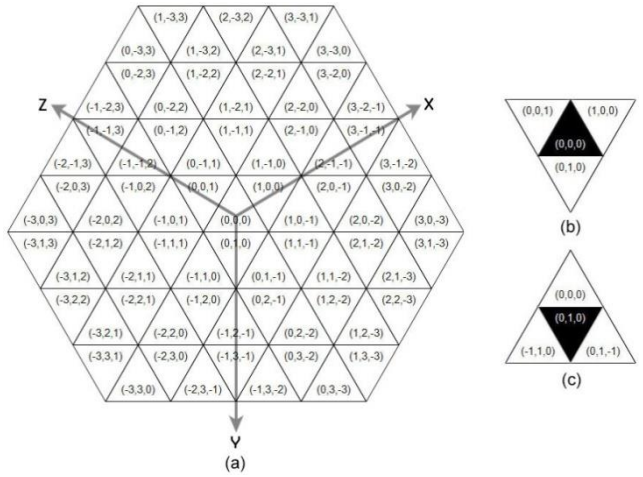

Figure 1
(a) Triangular grid. (b) A cell type "E" and (c) a cell type "O" with their neighbors

3 Definitions

Each cell has 2 possible *states*: dead or alive, they are represented by colors: black cells are alive, white cells are dead. A *pattern* is a set of living cells on the triangular grid. A *starting state* is just a finite pattern in the triangular grid.

The next definitions are somewhat analogous to the embedding hexagon of [20].

Definition 1. The *Bounding Hexagon* of a pattern is the smallest hexagon on the triangular grid which contains the pattern properly inside of itself. We use notation B for the Bounding Hexagon.

Let $H_1 = \left\{(x,y,z)\middle| \begin{matrix} x_{min}-1 \le x \le x_{max}+1, y_{min}-1 \le y \le y_{max}+1, \\ z_{min}-1 \le z \le z_{max}+1 \end{matrix}\right\}$, then

$B = \left\{(x,y,z) \in H_1 \middle| \begin{matrix} x = x_{min}-1 \text{ or } x = x_{max}+1 \text{ or } y = y_{min}-1 \text{ or} \\ y = y_{max}+1 \text{ or } z = z_{min}-1 \text{ or } z = z_{max}+1 \end{matrix}\right\}$.

Definition 2. *Outer Hexagon* is the smallest Hexagon on the triangular grid which contains the bounding hexagon properly inside of itself. We use notation O for the Outer Hexagon.

Let $H_2 = \left\{(x,y,z)\middle| \begin{matrix} x_{min}-2 \le x \le x_{max}+2, y_{min}-2 \le y \le y_{max}+2, \\ z_{min}-2 \le z \le z_{max}+2 \end{matrix}\right\}$, then

$O = \left\{(x,y,z) \in H_1 \middle| \begin{matrix} x = x_{min}-2 \text{ or } x = x_{max}+2 \text{ or } y = y_{min}-2 \text{ or} \\ y = y_{max}+2 \text{ or } z = z_{min}-2 \text{ or } z = z_{max}+2 \end{matrix}\right\}$.

See Figure 2, for examples.

Figure 2
A sample pattern (black), its bounding hexagon (blue) and its outer hexagon (green)

Definition 3. A *BS-Automaton* on the triangular grid consists of a starting state and its rule R that is a combination of 2 sets. The first set is called "Birth" (shortly "B") which shows the number of living cells needed in the neighborhood of a dead cell to make it alive. The second set is called "Survival" or "Stay alive" ("S") which shows the number of living cells needed in the neighborhood of a living cell to keep it alive.

$$R \in \{\mathrm{B}x\mathrm{S}y | x, y \in \{0,1,2,3\}^* \text{ are strings containing each of the numbers at most once}\}.$$

Since we have 3 neighbors, it is clear that B and S are subsets of $M = \{0,1,2,3\}$, and the above notation is used where string x contains the elements of B and y contains the elements of S. Both for B and S there are 2^4 possible sets, thus the total number of possible rules of BS-automata is 256. In the next section we show some of their properties.

4 Results

We start the section with some general observations.

Theorem 1. Any BS-automaton with rule R: $0 \in B$ and $3 \notin S$ leads to alternating states such that every second state consists of infinitely many living cells.

Proof: Based on the definition, the starting state is a set of finitely many living cells. If we consider the Outer Hexagon of the pattern, every cell outside of this hexagon is dead and has only dead neighbors. Since 0 is included in B, in the next step all these cells become alive, thus we have infinitely many living cells which have 3 living neighbors and only finitely many without 3 living neighbors. For the next generation, since 3 is not included in the set S, all these cells would die, and then, we have finitely many living cells and infinitely many dead cells. This property of the pattern is repeated by period 2. □

Further, we assume that our automaton is not of the previously described "flashing" type, and we deal with BS-automata with the condition $0 \notin B$.

Theorem 2. Any BS-automaton with rule R with $1 \in B$ leads to an unbounded growth (concerning the size of the pattern).

Proof. If we consider the Bounding Hexagon of the pattern, there would be 1 or more boundary cells which share an edge or a vertex with the Bounding Hexagon.

If at least 1 boundary cell shares an edge with the Bounding Hexagon, then at the next step, since $1 \in B$, its neighbor cell in the Bounding Hexagon becomes alive. This means that the new Bounding Hexagon is bigger than the previous one in this direction.

If none of the boundary cells share an edge with the Bounding Hexagon, then at the next step, at least one cell becomes alive such that it shares an edge with the Bounding Hexagon. Thus, even the new Bounding Hexagon would be the same size, at the next step, as we have shown in the previous part of the proof, the new Bounding Hexagon will be bigger.

The unlimited increase of the Bounding Hexagon shows the unbounded growth of the automaton. □

4.1 Case Studies with Growing Patterns

After some general results we are going to study some specific BS-automata.

Case B1S0123. In this automaton since *S* equals to *M*, any living cells live forever. By Theorem 2, there is no stable or periodic pattern. It usually makes the shape of snowflakes. It will never stop and it goes to infinity. Regardless of the type(s) of the starting cell(s) ("*E*" or "*O*"), it generates similar patterns. Figure 3 presents sample 1 where the starting state is a single cell of type "*O*". It also presents a real snowflake in the ending of the second line for the comparison. In Sample 2 the starting state is consisting of 2 separate cells with different types, as one can see on Figure 4, the growth of the pattern is very similar to the previous example. This automaton can be used for image synthesis.

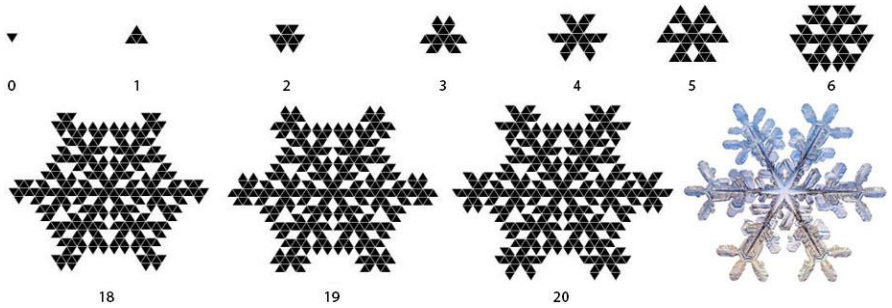

Figure 3
Automaton B1S0123, Sample 1, and a real snowflake[1] comparing to generation 20

[1] SnowCrystals.com. Web. 1 Jan. 2017. <http://www.snowcrystals.com/>

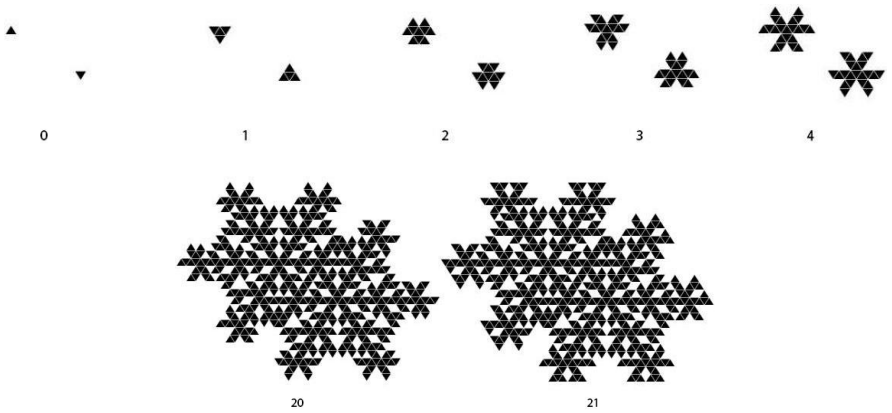

Figure 4
Automaton B1S0123, Sample 2

Case B1S123. Since the birth condition is 1, there is no stable pattern. Also there is no periodic pattern and it goes on to infinity. It generates inherently different patterns depending on the fact that the staring state includes only one type of cells or both types. If the starting state has only one type of cells, then after each step we have only one type of cells. In sample 3 the starting state consists of a single cell of type "*O*". It starts with type "*O*" and after that only type "*E*" cells are alive, and this property is repeated with period 2. See Figure 5. In the next sample the starting state is consisting of 2 adjacent cells with different types. Surprisingly, we got back very similar snowflake as we have seen in case of automaton B1S0123. Actually the two automata generate the same sequence of patterns from this start state. See Figure 6.

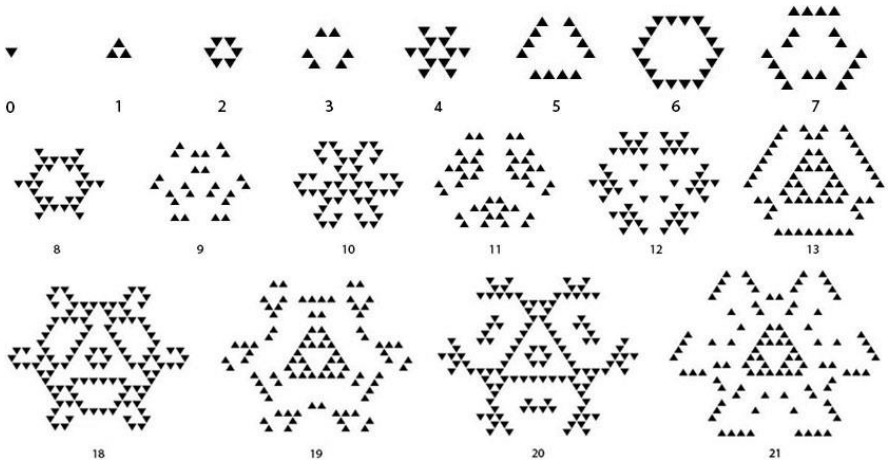

Figure 5
Automaton B1S123, Sample 3

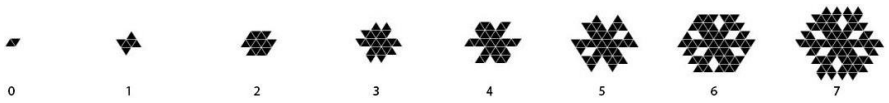

Figure 6
Automaton B1S123, Sample 4

Case B12S123. Since 1 is included in the set of birth conditions, there is no stable and no periodic pattern; it grows to infinity. If we start with one type of cells the method generates pattern similar to water's wave. In Sample 5, the starting state consists of a single cell of type "*O*". In each step we only have cells of one type. See Figure 7. This method has completely different behavior when we have both types of cells in the starting state. In such cases it fills the whole space easily and also, sometimes we may have finitely many holes. In sample 6 the starting state consists of 3 separate cells. There are 2 cells of type "*O*" and 1 cell of type "*E*". Figure 8 shows this example.

4.2 BS-Automata related to Image Processing

Case B2S0123. In this case any starting pattern will be transformed to a stable pattern soon and there is no infinite growth. Also since S equals to M, any living cells live forever. This automaton is a good tool for filling small spaces between cells. Sample 7 is transformed to a stable pattern in one generation, as it is shown in Figure 9 (2 left images).

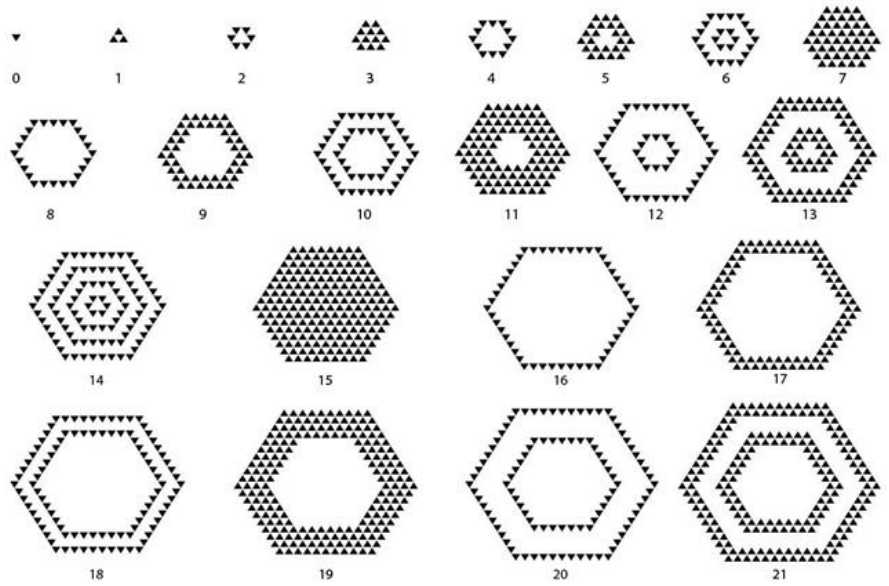

Figure 7
Automaton B12S123, Sample 5

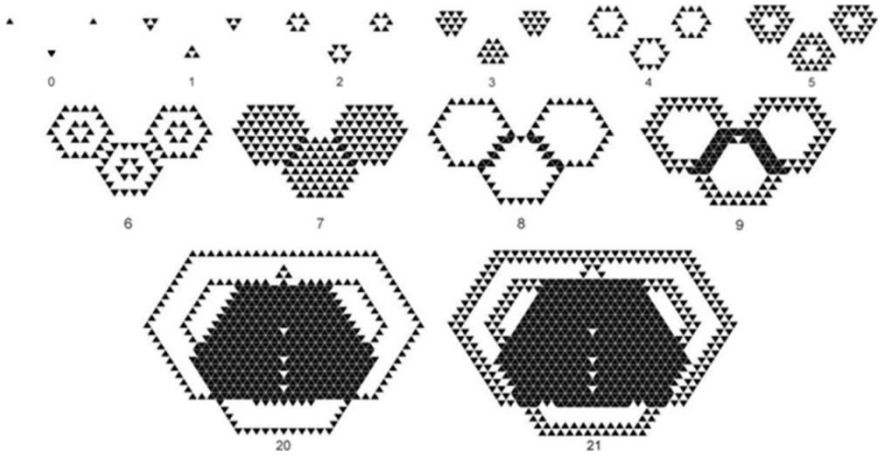

Figure 8
Automaton B12S123, Sample 6

Figure 9
B2S0123, Sample 7 (2 left images); Sample 8 (middle) and Sample 10 (right) are stable

In Sample 8, we have 2 lines with distance 1. This is a stable pattern and the automaton does not change the generation 0 (see Figure 9 (middle)). Next we add one single living cell to the left end. The automaton starts to fill the empty spaces between the 2 lines step by step and then arrives to a stable pattern on generation 11, as Figure 10 shows. However, it cannot be used to fill more than 1 cell width holes (Sample 10, in Figure 9).

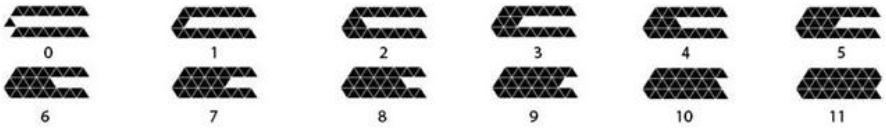

Figure 10
Automaton B2S0123, Sample 9

This automaton can be used for image recovery. In Sample 11 we have a set of living cells which should represent letter "Z". However, some of the living cells were deleted. The shape of Z is established after some generations. However, this automaton cannot filter out usual salt and pepper noises; see Sample 12 (Figure 12).

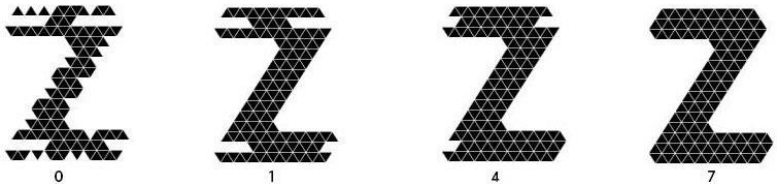

Figure 11
Automaton B2S0123, Sample 11, reconstruction of the character "Z"

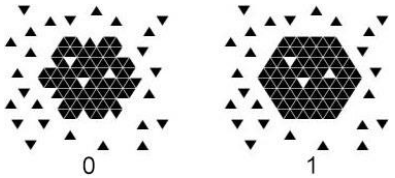

Figure 12
Automaton B2S0123, Sample 12

It could repair some patterns but couldn't remove the usual noises.

Case B2S123. This case is similar to the case B2S0123 but since 0 is not included in *S*, every living cell needs at least one living cell in its neighborhood to stay alive. With this automaton we have stable shapes and also periodic shapes (see Figure 13, Sample 13, left) but no infinite growth. This automaton gives us an important ability of Noise Filtering. Sample 14 is supposed to represent the word "Hi". Run of the automaton results to a stable pattern in 3 generations. (See Figure 13, Sample 14, middle.) This method still cannot filter inner noises (salt noise), see Figure 13, Sample 12, right.

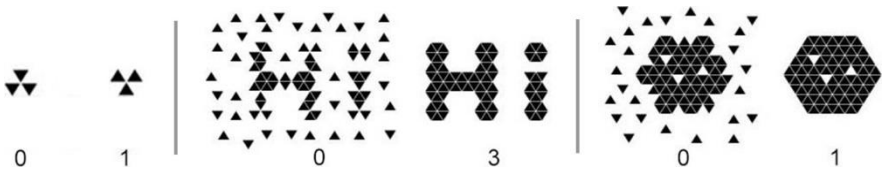

Figure 13
Automaton B2S123, Sample 13, an oscillator with period 2 (left), noise filtering on word "Hi", Sample 14 (middle) and Sample 12, (right)

Case B23S123. With this automaton we may have stable shapes and periodic shapes but not infinite growth. The automaton can be used to repair the shapes, to remove the outer noises (pepper) and to fill the inner noises (salt) at the same time, see Figure 14, left. Usage of this automaton also has some disadvantages. It will completely delete Sample 15 in 5 generations as it is shown in Figure 14 (right).

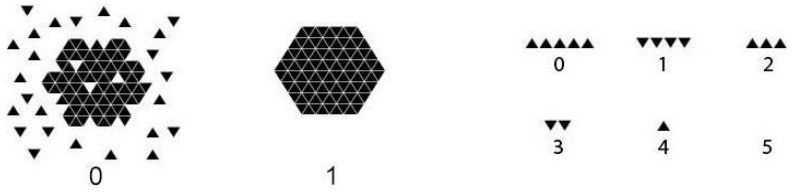

Figure 14
Automaton B23S123, Sample 12 (left), Sample 15 (right)

By the next examples we take the next step to the direction of image processing applications.

4.3 Pattern Recovery by Combining BS-Automata

Using a combination of two or more automata can help to recover the patterns and to filter the noises. One solution is to apply automaton B2S0123 first, then automaton B23S123 to the stable state obtained by automaton B2S0123 (we may call it middle state of the process). We used this method for Sample 16, see Figure 15. We have also tested the method on the Logo of our university (Eastern Mediterranean University, see Figure 16, left). Some noises are applied (2nd picture of Figure 16) on the original pattern and we used this image as the starting state. Figure 16 shows not only the original pattern and the starting state, but the middle state and final (stable) state as well. The finally obtained stable state is almost the same as the original pattern: the difference contains only 2 cells.

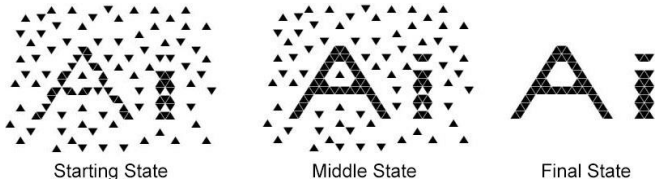

Figure 15
Pattern Recovery, Sample 16

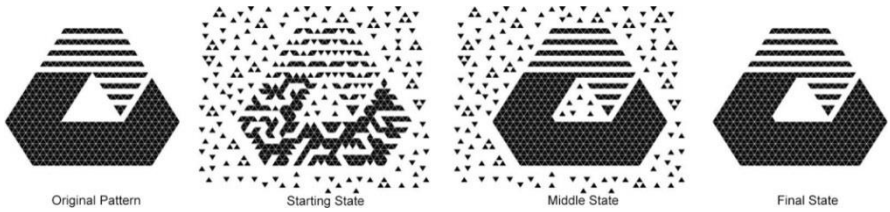

Figure 16
Pattern Recovery, Sample 17, Logo of the "Eastern Mediterranean University"

5 Morphologic Operations

Definition 4. The *dilation* of a pattern A on the triangular grid is a pattern $D(A)$ such that:

$$D(A) = \{q | q \in A \text{ or at least one of the neighbors of } q \text{ is an element of } A\}.$$

Definition 5. The *erosion* of a pattern A on the triangular grid is a pattern $E(A)$ such that:

$$E(A) = \{q | q \in A \text{ and all the neighbors of } q \text{ are elements of } A\}.$$

Note that the dilation and erosion above are done by the neighborhood used in this paper. In paper [1] similar operations are defined in a more general manner, instead of a fixed neighbourhood, various structural elements were used with various constraints. Allowing only vectors that translate the grid to itself, the strict approach is defined. In the weak approach each grid point can be used for translation. However, to describe our neighbourhood relation one may also need vectors with value (-1) as the sum of its coordinates, e.g., (-1,0,0). In the strong variants any three dimensional vectors are allowed to use, but only those triplets can be displayed which have 0 or +1 sum. Our special definition here is compatible only with this most general variant of operations of the mentioned paper having the following7-element set as structural element including the following 6+1 vectors {(0,0,1),(0,1,0),(1,0,0),(0,0,-1),(0,-1,0),(-1,0,0),(0,0,0)}.

By checking the definition of our automata one can establish the following:

Theorem 3. The automaton B123S0123 is equivalent to dilation.

Proof. Assume that $q \in D(A)$, then either $q \in A$ or there is a $q' \in A$ such that q and q' are neighbors. Let us run B123S0123 on A. Clearly if $q \in A$ then it is element of the resulted image because S0123, i.e., each pixel of A survives. If $q \notin A$ but there is a $q' \in A$ such that q and q' are neighbors, then q is also element of the resulted image because of B123.

Now, let us assume that q is an element of the resulted image of running B123S0123 on A, then either because of S0123, $q \in A$ or because of B123, there is a $q' \in A$ such that q and q' are neighbors which in both cases imply that $q \in D(A)$.

□

Theorem 4. The automaton BS3 is equivalent to erosion.

Proof. Assume that $q \in E(A)$, then $q \in A$ and also all of its neighbors are element of A. Let us run BS3 on A. Clearly if q is element of the resulted image, then because of S3, q and all of its neighbors are elements of A which means $q \in E(A)$.

□

Definition 6. The *opening* of a pattern A on the triangular grid is the pattern $D(E(A))$.

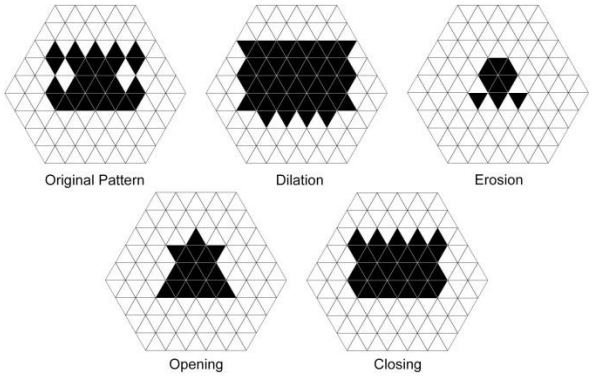

Figure 17
A pattern and its various morphologic transformations

Definition 7. The *closing* of a pattern A on the triangular grid is the pattern $E(D(A))$.

Similarly to the already shown combinations of BS-automata, one can apply 1 step with B123S0123 and then 1 step with BS3 to obtain the closing of the original pattern. Using these automata in the opposite order, the opening of the original image is obtained. See also Figure 17. Based on the distance of pixels measured by the length of the shortest path(s) connecting them through neighbor pixels (for more details we refer to, e.g., [16, 17, 15, 13]) we can also introduce the distance of patterns (see, e.g., [14]). This, so-called Hausdorff-distance, is used to measure, e.g., image similarities.

Definition 8. The *Hausdorff-distance* of two patterns A and B is defined as

$$d(A,B) = \max\left\{\max_{p\in A}\min_{q\in B} d(p,q), \max_{p\in B}\min_{q\in A} d(p,q)\right\}.$$

It is known that the Hausdorff-distance can be computed by dilations: By counting the minimum number of dilations that one needs to make on A to get a pattern $D^n(A)$ such that $D^n(A) \supseteq B$, and vice-versa, the minimal m such that $D^m(B) \supseteq A$, and finally taking the maximum of n and m gives exactly the value of $d(A,B)$ (see, e.g, [14]). Figure 18 shows an example. Obviously, the iterated dilations can be done by applying B123S0123 on both images.

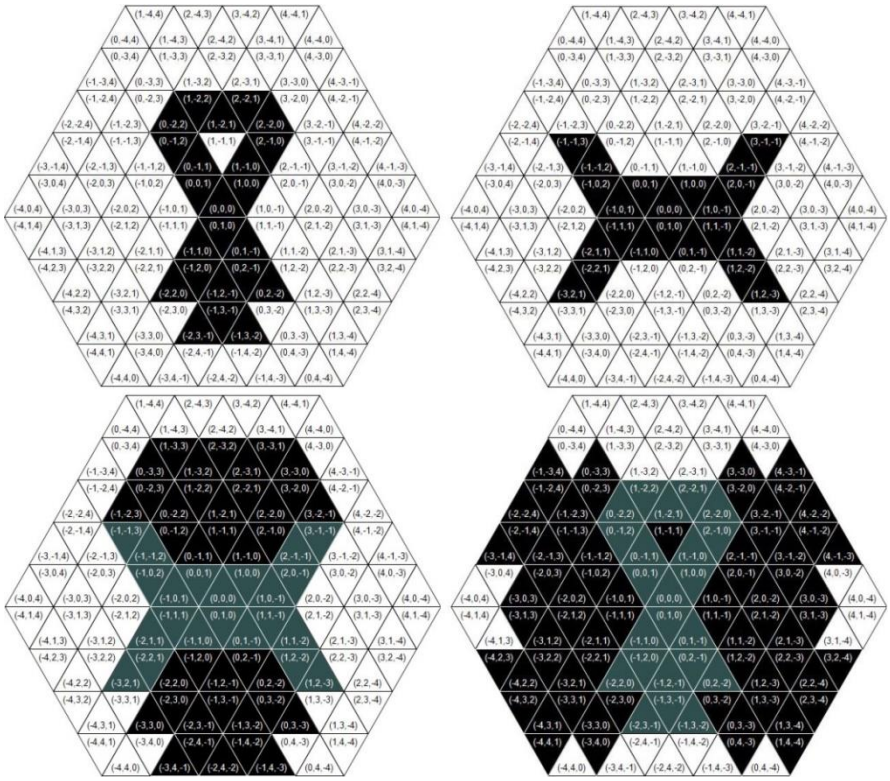

Figure 18

Patterns A and B (up), and their iterated dilation with 2 and 3 steps, respectively, resulting an image containing the other one, this yields to $d(A,B) = 3$

6 Literature Review

In this section the relation of our results and some results from the literature is shown. First we consider cellular automata related literature, then, we discuss also image processing algorithms, concentrating on those models that are defined on the triangular grid.

Cellular automata have already been defined and used in various grids. As we have already mentioned, in [4], Bays described cellular automata on the regular triangular grid, but based on 12 neighbors of the cells. In [4] stable patterns and gun like shapes were analysed in connection to Conway's Game of Life. Bays has also extended some notions on the pentagonal and hexagonal grids in [6]. In [11] it is analysed how messages can be transported in various grids based on a cellular automata approach. A new family of hexavalent networks stabilizing the symmetry axes,

providing the highest symmetry level for a 6–valent finite lattice is also presented there. In [19], the regular triangular grid is used (in its dual representation) to see how signals can spread on the grid based on various speed defined by neighborhood sequences. In [25] cellular automata on the regular triangular and hexagonal grids are used for path planning of robots based on artificial intelligence algorithms. In [3] cellular automata with memory are used to provide a reversible model on the triangular grid which may be helpful in bio- and physics related modelling and applications. In [26], triangles on specific topologically surfaces defined the grid of the cellular automata. In [29] the developments of the patterns are studied on any triangulated surface. Only grids with finitely many triangles are considered. Although the used grid is usually irregular triangular mesh, each triangle (except those that are on the boundary of the surface) has three neighbors, thus the rules of the automata are somewhat similar to those that we will define. However, the behaviour of the automata is different. In irregular meshes, no general coordinate system, no lanes, even and odd pixels are defined. Although cellular automata only on the square grid were used in [22], we should recall that, the authors used cellular automata for image processing applications such as noise removal and edge detecting. In this way, our paper can also be seen as a kind of extension of some of the results of [22] to the triangular grid. However we have used only deterministic cellular automata, while in [22] non deterministic model is considered for noise removal.

Morphological operations dilation and erosion are considered for the triangular grid in a more general and mathematical approach in [1, 2]. Our aim here was to show how cellular automata can be applied in mathematical morphology and other related image processing tasks on the triangular grid. We have shown also opening and closing and other image processing operations. About filtering operations, we briefly mention the median filtering. For binary images, in fact, this filtering assigns for each pixel the color of the majority of the pixels in its neighborhood. Notice that it works nicely on the square grid with both the usual used city block (von Neumann) and chessboard (Moore) neighborhood, since a pixel with their neighbors consist of 5 and 9 pixels, respectively [12]. However, this method does not work on the triangular grid using the closest neighbourhood, since a pixel with its 3 neighbors may have no majority color. On the triangular grid, median filter based on the 12 neighbors of the pixels can be defined, see, e.g., [28]. Considering the triangular grid with the closest neighbors, we may modify a little bit the original concept of the median filter. If we keep a pixel 0 only if the average of the value of the 4 pixel (the pixel and its 3 neighbors) is less than 0.5, and set it to 1 if this value is at least 0.5, we got a somewhat similar filter. In fact, a pixel is set to value 1, if at least 2 of the 4 pixels had value 1. Figure 19 shows how this filtering method can recover a noisy pattern (left). Applying it 35 times, the pattern is recovered (right) with a relatively small pixel error (18 pixels). By comparing this result to Fig. 16, we may see that our method with cellular automata shows a better performance (2 pixel error). Actually, our filtering method is based on morphological type of operations, as we have discussed.

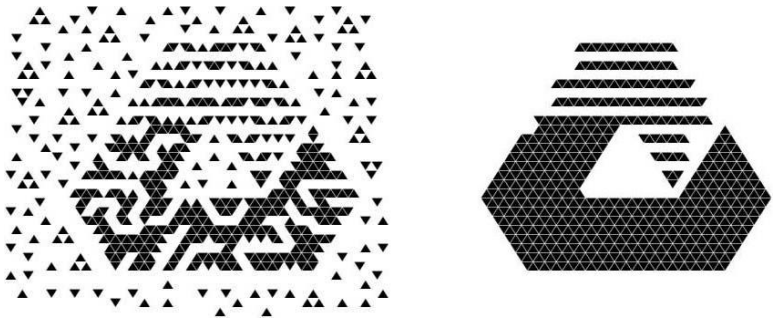

Figure 19
Pattern Recovery by a median like filter (the right figure, a stable pattern, is obtained after 35 steps)

Conclusions

In this paper various cellular automata are shown, some of them imply infinite growth of patterns; some of them reach a stable pattern or lead to a periodic behavior. Some of them are used to do some pattern recovery (step by step) filling concavities and holes; others can be used to remove noise. We have also shown how specific models can do dilation and erosion. These models are entirely parallel methods of computing. Based on them, further morphologic operations, the opening and closing were also computed. Further, by an iterative application of the automata for dilation, the Hausdorff distance of patterns on the triangular grid is computed. Parallel computing becomes very popular in practice, since more and more hardware devices support it, thus these approaches are valid alternatives to the traditional sequential computations (which are still frequently used on images).

In order to create the figures and find the properties of each case considered we have designed a Windows application using Microsoft Visual Studio 2015 platform. This software was used for the simulations presented.

References

[1] Abdalla M., Nagy B. (2017) Concepts of Binary Morphological Operations Dilation and Erosion on the Triangular Grid. In: Barneva R., Brimkov V., Tavares J. (eds) Computational Modeling of Objects Presented in Images. Fundamentals, Methods, and Applications. CompIMAGE 2016, Lecture Notes in Computer Science, Vol. 10149, Springer, Cham, 89-104

[2] Abdalla, M., Nagy, B. (2018) Dilation and Erosion on the Triangular Tessellation: an Independent Approach. IEEE Access, 6, 23108-23119

[3] Alonso-Sanz, R. (2007) A Structurally Dynamic Cellular Automaton with Memory in the Triangular Tessellation. Complex Systems, 17, 1-15

[4] Bays, C. (1994) Cellular Automata in the Triangular Tessellation. Complex Systems, 8(2), 127-150

[5] Bays, C. (2005) A Note on the Game of Life in Hexagonal and Pentagonal Tessellations. Complex Systems, 15(3), 245-252

[6] Bays, C. (2012) Cellular Automata in Triangular, Pentagonal and Hexagonal Tessellations. In: Meyers R. (eds) Computational Complexity. Springer, New York, pp. 434-442

[7] Delorme, M., Mazoyer, J., Cellular Automata: A Parallel Model, Springer, 1998

[8] Ewert, W., Dembski, W., Marks, R. J. (2015) Algorithmic specified complexity in the Game of Life. Systems, Man, and Cybernetics: Systems, IEEE Tr., 45(4), 584-594

[9] Gardner, M. (1970) Mathematical Games: The Fantastic Combinations of John Conway's New Solitaire Game "Life". Scientific American, 223(4), 120-123

[10] Herendi, T., Nagy, B.: Parallel Approach of Algorithms, Typotex, Budapest, 2014

[11] Hoffmann, R., Désérable, D. (2015) Routing by Cellular Automata Agents in the Triangular Lattice. In Robots and Lattice Automata (pp. 117-147) Springer, Cham

[12] Huang, T., Yang, G. J. T. G. Y., Tang, G. (1979) A Fast Two-Dimensional Median Filtering Algorithm. IEEE Transactions on Acoustics, Speech, and Signal Processing, 27(1) 13-18

[13] Kardos, P., Palágyi, K. (2017) On Topology Preservation of Mixed Operators in Triangular, Square, and Hexagonal Grids. Discrete Applied Mathematics, 216 (2017) 441-448

[14] Klette, R., Rosenfeld, A.: Digital Geometry: Geometric Methods for Digital Picture Analysis. Morgan Kaufmann, 2004

[15] Nagy, B (2004) Characterization of Digital Circles in Triangular Grid. Pattern Recognition Letters, 25 (2004) 1231-1242

[16] Nagy, B. (2001) Finding Shortest Path with Neighborhood Sequences in Triangular Grids, ISPA 2001, 2nd IEEE Int. Symp. Image and Signal Processing and Analysis, 55-60

[17] Nagy, B. (2002) Metrics based on Neighbourhood Sequences in Triangular Grids, Pure Mathematics and Applications - PU.M.A. 13, 259-274

[18] Nagy, B. (2007) Distances with Neighbourhood Sequences in Cubic and Triangular Grids. Pattern Recognition Letters, 28, 99-109

[19] Nagy, B. (2017) Application of Neighborhood Sequences in Communication of Hexagonal Networks, Discrete Applied Mathematics 216, 424-440

[20] Nagy, B., Barczi, K. (2013) Isoperimetrically Optimal Polygons in the Triangular Grid with Jordan-Type Neighbourhood on the Boundary. International Journal of Computer Mathematics, 90(8) 1629-1652

[21] Nagy, B., Lukic, T. (2016) Dense Projection Tomography on the Triangular Tiling. Fundam. Inform. 145, 125-141

[22] Popovici, A., Popovici, D. (2002) Cellular Automata in Image Processing. In Proceedings of the Fifteenth International Symposium on Mathematical Theory of Networks and Systems, D. S. Gilliam and J. Rosenthal, Eds., electronic proceedings, 6 pages

[23] Rendell, P. (2002) Turing Universality of the Game of Life. In collision-based computing (pp. 513-539) Springer, London

[24] Rozenberg, G., Bäck, T., Kok, J.N. (eds.) Handbook of Natural Computing. Springer 2012

[25] Tariq, J., Kumaravel, A. (2016) Construction of Cellular Automata over Hexagonal and Triangular Tessellations for Path Planning of Multi-Robots. 2016 IEEE International Conference on Computational Intelligence and Computing Research (ICCIC) 6 pages, IEEE (doi: 10.1109/ICCIC.2016. 7919686)

[26] Warne, D. J., Hayward, R. F. (2015) The Dynamics of Cellular Automata on 2-Manifolds is Affected by Topology. J. Cellular Automata, 10(5-6) 319-339

[27] Wolfram, S.: A New Kind of Science. Champaign, IL: Wolfram Media, 2002

[28] Yagou, H., Belyaev, A., Wei, D. (2002) Mesh Median Filter for Smoothing 3-D Polygonal Surfaces. In Cyber Worlds, 2002. Proceedings. First International Symposium on. IEEE. pp. 488-495

[29] Zawidzki, M. (2011) Application of Semitotalistic 2D Cellular Automata on a Triangulated 3D Surface. International Journal of Design & Nature and Ecodynamics, 6(1) 34-51

Possibility of Nuclear Cogeneration Development in the Region of Paks

Endre Börcsök[1,2], Ágnes Gerse[2], János Fülöp[1,3]

[1]Óbuda University, Bécsi út 96/b, 1034 Budapest, Hungary
borcsok.endre@energia.mta.hu

[2]Centre for Energy Research, Hungarian Academy of Sciences, Konkoly-Thege Miklós út 29-33, 1121 Budapest, Hungary, gerse.agnes@energia.mta.hu

[3]Institute forComputer Science and Control, Hungarian Academy ofSciences, Kende u. 13-17, 1111 Budapest, Hungary, fulop.janos@sztaki.mta.hu

Abstract: Almost half of the greenhouse gas emission from the energy sector in the world is related to heat demand. The development of nuclear cogeneration offers a convenient option for emission reduction; however, the examination of economic constrains is essential. This study focuses on the heat demand of households in the vicinity of Paks NPP and compares the economic and environmental aspects of several domestic heating alternatives. In the first part of our work, we analyze the competitiveness of nuclear cogeneration in the district heating sector. While in the second part we consider, the optimal heaters for different building typological groups by taking into account some economic and environmental aspects, the distance from Paks NPP and the heat demand density. We have found that the development of nuclear cogeneration is economically viable for the existing district heating network,above a carbon price of 5 Euro/ton of CO_2. In a region of high heat demand density, the nuclear cogeneration-based district heating can be competitive with stand-alone heaters, in particular when the environmental external costs are considered, as well.

Keywords: heat sector; district heating; cost-benefit analysis; optimization

1 Introduction

The present paper evaluates the potential reduction of greenhouse gas (GHG) emission from the domestic heat sector by harnessing nuclear cogeneration. The EU has adopted challenging carbon emission reduction targets that will require a substantive change in the energy sector. A district heating alternative, where the heat is produced by nuclear energy and transported by hot water pipe systems to the buildings, has a high potential to contribute to the achievement of these targets. International reports demonstrate numerous excellent examples for nuclear cogeneration; and based on world energy statistics, the direct heat consumption ratio

is around 1% globally [20]. In Hungary, nuclear energy-based district heating is an old-established method for low carbon residential heating. However, national statistics show that the heat consumption ratio at Paks NPP is far below the international level (Table 1). Paks NPP has four pressurized water reactors with freshwater cooling (VVER-440 Model V213) which supplyheat for 2600 households located at a distance of 4.5 km on average.

Table 1
Heat consumption ratio at Paks NPP [18]

Waste heat	Electricity	Heat consumption
65.7%	34%	0.3%

Although nuclear cogeneration has a negligible share in the Hungarian district heating sector nevertheless it is very cost effective as the heat price is extremely low in Paks (Table 2).

Table 2
District heating costs (for a 50 m^2 flat) in Hungary [8]. In Paks, the annual cost is far below the Hungarian average cost, however, the size of demand side is limited

Paks	Szarvas	Average
Nuclear	Geothermal	Natural gas
150.80 €/a	288.38 €/a	596.55 €/a

The first subject of this study was to identify the conditions where a nuclear energy-based district heating system (with transmission pipelines) could substitute a natural gas-based district heating system on a pure economic basis. In this part of the calculations, main input variables included fuel, nuclear heat and capital costs. The impact of different carbon prices was examined in a sensitivity analysis. The second part of this study was aimed at a cost comparison of nuclear-energy based district heating and conventional heating systems. This comparison was carried out using a standardized heat demand profile. The final results of the analysis enabled the assessment of the optimal heat supply portfolios in the subsequent part of this study where a general approach is presented for the selection of optimal residential heat supply portfolios, based on economic and environmental aspects. The resulting complex heat supply portfolios should be suitable to cover the seasonal heat demand profiles of different building typological groups. The guiding principle for the heat supply portfolio optimization was a distinction between the alternatives based on their fixed and variable costs. Fixed costs do not change with the energy production while variable costsare highly correlated to it. The alternatives that have moderate variable costs should cover the base load, while heaters having lower fixed costs should supply the peak demand. Although the main focus of this paper is the reduction of GHG emission, fixed and variable costs played a central role in the comparison of the heating alternatives.

2 Methodology

In the economic assessment of nuclear cogeneration, the fuel costs and the operation and maintenance (O&M) costs of existing natural gas-based district heating systems were considered as "base case"; they were compared to the costs of the nuclear heat supply, including the investment costs of a transmission pipe system and its corresponding O&M costs [1]. In a simple cost-benefit analysis, we focused on the payback time of the investment costs considering the decrease in heat production costs. The technical lifetime of the existing heaters was extended to the end of the examined time interval; therefore, the costs of a retrofit were beyond the scope of this study. It should, however, be noted that the technical lifetime of heat transmission pipelines is extremely long (50-60 years) compared to natural gas boilers (25-35 years) or to the remaining lifetime of Paks NPP (20-25 years). The time horizon for this study was defined around 20-40 years to reduce the uncertainty in the calculations; at the same time, an uninterrupted availability was assumed for the nuclear energy generation (future Paks II NPP). In the net present value (NPV) calculation, the investment costs are realized in the starting year (C_n, n=0) and were "discounted" to the present value of costs. As an extension of the district heating system, a pair of insulated pipelines of near-surface installation in rural land, several pump stations and a heat exchanger unit at the power plant were considered when calculating the net present value of costs [5]. Sizing has a strong influence on costs. In general, the transmission pipeline should have a capacity that is equivalent to 50% of the thermal peak demand and can cover 85% of the thermal energy consumption. The annual difference between the fuel and O&M costs of the natural gas-based heat supply and the nuclear energy-based heat supply (B_n; n=1,...,40) was discounted and summed up to the present value of benefits. The discount rate and the examined time horizon were chosen as r=4% and 40 years, respectively (1)-(3). The specific cost of the nuclear heat was estimated from the base load electricity prices, the efficiency of the nuclear power plant and the O&M costs of the transmission pipeline. In case of the existing natural gas-based district heating, the fuel and O&M costs of a thermal power plant were considered.

The present values of the stream of benefits and costs are as follows:

$$PV(B) = \sum_{n=0}^{N} \frac{B_n}{(1+r)^n}, \tag{1}$$

$$PV(C) = \sum_{n=0}^{N} \frac{C_n}{(1+r)^n}. \tag{2}$$

The assessment of the overall economic impact over the whole lifetime of the project was done by calculating the net present value:

$$NPV = PV(B) - PV(C). \tag{3}$$

Unfortunately, the long time horizon along with the assumption of constant fuel prices and O&M costs involves a degree of uncertainty in the calculations. Since

the forecasted costs (fuel and carbon price, neglected retrofit of gas boilers…) raise the revenues of the investment significantly, our calculations can be considered like a "worst-case study". A further question was whether the enlargement of the existing district heating network that is presently coupled with large-scale multi-flat buildings is appropriate. For a comparison, three building typological groups were defined: large-scale multi-flat buildings, medium-scale multi-flat buildings and single family houses with state-of-the-art heating alternatives [4]. In these three groups, the heat demand densities are different; and their influence on the capital costs of the extension of the district heating network is significant [14]. The comparison is based on a uniform assumption on the heat demand of households (a thermal peak load of 10.6 kW), disregarding the fact that the average area and the energy needs are different for the three building typological groups. The annual costs of residential heating for this standardized heat demand were compared to each other, respecting the technical lifetime of the alternatives (at a discount rate of 4%). Of course, we assumed ideal operating conditions when applying this approach; we took into account the maximum possible full load hours for the comparison of the alternatives, by calculating specific heat prices [3]. In addition to the techno-economic evaluation, also the impacts of the carbon emission prices and the external costs of the environmental impacts were taken into account as two separate assessments. The environmental impact assessment was based on the forecasted external costs of state-of-the-art technology options for year 2020 [15].

Subsequently, the optimal portfolios of heating alternatives for local communities were evaluated in the scope of this study: starting from a pure economic analysis (i.e. variable and fixed costs while neglecting carbon prices), involving the carbon costs additionally, and finally, the environmental impacts of the 25 technologies. The methodology of the transportation problem [6] was chosen to determine the optimal portfolio where the 25 alternatives ($a_1, \ldots a_{25}$) represent the supply points with set $I = \{1,\ldots,25\}$, and the three building typological groups are the demand points. The seasonality of the heat demand requires a detailed monthly data set for each building typological group ($w_1 \ldots w_{12}, w_{13} \ldots w_{24}, w_{25} \ldots w_{36}$) where $J = \{1,\ldots,36\}$. The alternatives represented by the supply points were assigned to the installed capacities ($p_1, \ldots p_{25}$). The monthly maximum (j) of heat generation e_{ij}can be calculated by using the installed capacity p_i. The value of e_{ij} is equal to the product of the installed capacity and the empirical utilization time $e_{ij} = h_{ij} \cdot p_i$ [10], [11]. Generally, the maximal value of empirical utilization time, which is approximately equivalent to a capacity factor of 50%, can be used constantly all over the year. However, in the cases of the air source heat pumps and the solar thermal alternatives [17], also a seasonal effect appears in the coefficienth_{ij}. The variable x_{ij} represents the actual amount of heat produced at supply point i in month j. For each unit of heat produced at the supply point i and shipped to the demand point j incurs a constant per unit variable cost (c_{ij}); nevertheless, instead of the general case,a more realistic constant per unit variable cost $c_i = c_{ij}$ was used in the present paper.

Although the described problem is essentially similar to the transportation problem [4], nevertheless, the facts that the p_i's are variables and they appear in the objective function with constant fixed cost coefficients (d_i), indicate that a slightly modified method is needed (Table 3).

Table 3
Variables of the transportation problem

heating alternatives	single family houses			medium-scale multi flat buildings			large-scale multi flat buildings			
Natural gas stand-alone heater	$x_{1,1}$	…	$x_{1,12}$	$x_{1,13}$	…	$x_{1,24}$	$x_{1,25}$	…	$x_{1,36}$	p_1
:	:		:	:		:	:		:	:
:	:		:	:		:	:		:	:
Solar thermal district heating	$x_{25,1}$		$x_{25,12}$	$x_{25,13}$		$x_{25,24}$	$x_{25,25}$		$x_{25,36}$	p_{25}
	w_1	…	w_{12}	w_{13}	…	w_{24}	w_{25}	…	w_{36}	

The demand constraints of the problem could be interpreted as

$$\sum_i x_{ij} = w_j \tag{4}$$

and the supply constraints in the form of $x_{ij} \le e_{ij} = h_{ij} p_i$. Based on the installed capacities p_i, as variables, the supply constraints can be converted into the form:

$$x_{ij} - h_{ij} \cdot p_i \le 0 \tag{5}$$

for each month and building typological group *j*. The variable x_{ij} could be interpreted as the "partialuse" of capacity p_{ij} in month *j*, with the formula: $x_{ij} = h_{ij} \cdot p_{ij}$, where $p_{ij} \le p_i$ for each alternative *i* and month *j*. Also, the constrains and sign restrictions $x_{ij} \ge 0$ need to be transformed:

$$p_{ij} \ge 0, \tag{6}$$

and after completing by the objective function

$$\sum_{i \in I} \left(d_i \cdot p_i + c_i \sum_{j \in J} h_{ij} \cdot p_{ij} \right) = z(\min) \tag{7}$$

the mathematical optimization results in a linear programming (LP) problem. The problem defined by (4)-(7) could be summarized in a standard form:

$$\sum_{i\in I}\sum_{j\in J} c_i \cdot h_{ij} \cdot p_{ij} + \sum_{i\in I} d_i \cdot p_i = z(\min) \tag{8}$$

$$\sum_i h_{ij} \cdot p_{ij} = w_j \tag{9}$$

$$p_i - p_{ij} \geq 0 \text{ for all } i \in I \text{ and } j \in J \tag{10}$$

$$p_{ij} \geq 0 \text{ and } p_i \geq 0 \text{ for all } i \in I \text{ and } j \in J \tag{11}$$

where the formulas (8) and (10) can be replaced by:

$$\sum_{i\in I}\sum_{j\in J} c_i \cdot h_{ij} \cdot p_{ij} + \sum_{i\in I} d_i \cdot p_i^* = z(\min) \;\; ; \quad p_i^* = \max_j \{p_{ij}\} \tag{12}$$

The optimal solution of this linear programming problem provides the preferential portfolio of the heating alternatives.

However, an alternative interpretation of the problem described above could be a continuous relaxation of the simple facility location problem [7]. The basic idea of this alternative interpretation is the new expression of z objective function with discrete Δp_{is} values, where $\sum_s \Delta p_{is} = p_i$. The solution of the simple facility location problem can be realized by a dynamic algorithm based on the knapsack problem. This approach, with a simple algorithm, is commonly used in the different fields of energy [9], [16]; however, this interpretation emphasizes the special characteristics of the results. The very first step of the algorithm is the definition of the knapsacks by increasing series of the constants of the demand constraints $w_j = \sum_i x_{ij}$ for all building typological groups j=$g(s)$, s=1,...,12. The knapsacks are defined by 12 demand increments $\Delta w_s = w_{g(s)} - w_{g(s-1)}$, $w_{g(0)} = 0$. Each knapsack s is represented by the increasing installed capacity of i alternatives $\sum_i h_{ig(s)} \cdot \Delta p_{is} = \Delta w_s$ to supply the Δw_s demand increments. Likewise, any s knapsacks and each alternative i are interlinked with $\left(d_i + c_i \sum_{k=s}^{12} h_{ig(k)} \right) \cdot \Delta p_{is}$ costs.

The most favourable $m(s)$ alternative supplies the Δw_s demand increments of the knapsacks s. At the same time, the dynamic algorithm of the knapsack problem generates the special structure of the monthly heat supply and the installed capacity in the most beneficial way,

$$\sum_{s=1}^{12} \left(d_{m(s)} + c_{m(s)} \sum_{k=s}^{12} h_{m(s)g(k)} \right) \cdot \Delta p_{m(s)s} = z'(\min) \tag{13}$$

that can be considered as an optimal solution to the simple facility location problem.

Proposition 1. The substitution of the monthly heat supply $h_{ij} \cdot p_i = w_{ij}$ from a given alternative *i* of installed capacity p_i in a mixed heat supply of $\sum_{l=1}^{n} h_{lj} \cdot p_{lj} = w_{ij}$ by newly installed capacities of p_l^*, $l \in \{1,...,n\}$ is disadvantageous in the optimization process, if p_i satisfies the following inequalities:

$$d_i \cdot p_i + c_i \sum_{j=1}^{12} h_{ij} \cdot p_i \le d_l \cdot p_l^* + c_l \sum_{j=1}^{12} h_{lj} \cdot p_l^* \quad \text{for each } l \in \{1,...,n\}. \tag{14}$$

*Proof.*Let Q be a selection of heating alternatives in an optimal solution. Then $\sum_{l \in Q} h_{lj} \cdot \overline{p}_{lj} = w_{ij}$ for all $j \in \{1,...,12\}$ where $\overline{p}_{lj} \le p_{lj}$. Consequently, the monthly heat supply w_{ij} for the whole year can be guaranteed by installed capacity $\overline{p}_l^*$. If we transform the arrangement of the monthly heat supply

$$\sum_{l \in Q} \left(d_l \cdot p_l^{**} + c_l \sum_{j=1}^{12} h_{lj} \cdot p_l^{**} \right) \le \sum_{l \in Q} \left(d_l \cdot \overline{p}_l^* + c_l \sum_{j=1}^{12} h_{lj} \cdot \overline{p}_{lj} \right) \text{ where } \quad p_l^{**} = \frac{\sum_{j=1}^{12} h_{lj} \cdot \overline{p}_{lj}}{\sum_{j=1}^{12} h_{lj}},$$

furthermore, for all p_l^{**} there exists a p_{il} where

$d_i \cdot p_{il} + c_i \sum_{j=1}^{12} h_{ij} \cdot p_{il} \le d_l \cdot p_l^{**} + c_l \sum_{j=1}^{12} h_{lj} \cdot p_l^{**}$, then along with the constrains (14)

and $p_i = \sum_{l \in Q} p_{il}$, these together result in

$$d_i \cdot p_i + c_i \sum_{j=1}^{12} h_{ij} \cdot p_i \le \sum_{l \in Q} \left(d_l \cdot \overline{p}_l^* + c_l \sum_{j=1}^{12} h_{lj} \cdot \overline{p}_{lj} \right) \qquad \blacksquare$$

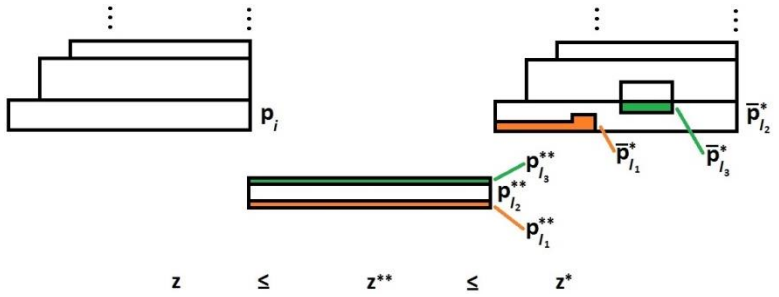

Figure 1
Knapsack replenishment with newly installed capacities

Based on these results, we conclude that a homogeneous supply of the monthly heat demand increments is more advantageous than the intermittent heat supply from newly installed capacity (Fig. 1).

Proposition 2. The substitution of the monthly heat supply from a given alternative i of an existing p_i installed capacity by the heat supply from an existing p_l installed capacity is disadvantageous if

$$d_i \cdot p_i^* + c_i \sum_{j=1}^{12} h_{ij} \cdot p_i^* \le d_l \cdot p_l^* + c_l \sum_{j=1}^{12} h_{lj} \cdot p_l^* \tag{15}$$

for all installed capacities $l \in \{1,...,n\}$ where $\sum_{j=1}^{12} h_{ij} \cdot p_i^* = \sum_{j=1}^{12} h_{lj} \cdot p_l^* = w_i$ (Fig. 2).

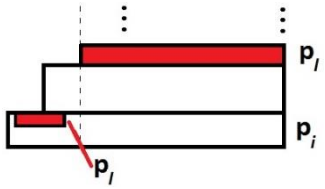

Figure 2
Knapsack replenishment with existing capacities

Proof. For each installed capacity $l \in H$ there exists an annual amount of heat supply $w_l = \sum_{j=1}^{12} h_{lj} \cdot p_{lj}$, $w_l < w_i$ such that

$$d_l \cdot p_l^* + c_l w_l \le d_i \cdot p_i^{**} + c_l w_l \quad \text{and} \quad p_i^{**} \le p_i^* \tag{16}$$

By the reason of constrains (15)-(16), we can identify the inequality $c_i < d_i \cdot \frac{p_i^{**} - p_i^*}{w_i - w_l} + c_l$ where the quotient $\frac{p_i^{**} - p_i^*}{w_i - w_l}$ cannot be positive, therefore $c_i < c_l$. Accordingly, the substitution of the heat supply from a given alternative i of an existing p_i^* installed capacity by another, existing alternative of heat supply, results in a higher objective function value. ■

The conclusion of the two propositions is that the supply of heat demand increments Δw_r should be provided in a homogeneous way for an optimal solution.

In the present study, the proposed problem was solved in the same way as a LP problem in GAMS environment [19], furthermore, by the dynamic algorithm of the knapsack problem. The negligible differences in the final results of the objective function values were related to round-off errors.

3 Results

The detailed analysis suggests that the substitution of the natural gas-based district heating by nuclear cogeneration can be beneficial, considering the lower fuel costs, O&M costs and carbon costs. The effects of two variables (heat demand e and distance of transport t) are crucial to the cost-benefit analysis. Analogously, the NPV of the optional extension of the nuclear cogeneration depends on variables e and t, therefore a multivariable NPV(e,t) function can be defined. The NPV(e,t) decreases as a function of the distance and increases as a function of the heat demand volume, i.e. $NPV_t'(e,t) < 0$ and $NPV_e'(e,t) > 0$. The limitcurve defined by NPV(e,t)=0 determines the minimal heat demand values where the investment can be economically viable. Based on the analysis, it is worth to compare the annual heat demand of some existing district heating networks in the region of Paks with the position of the limit curve.

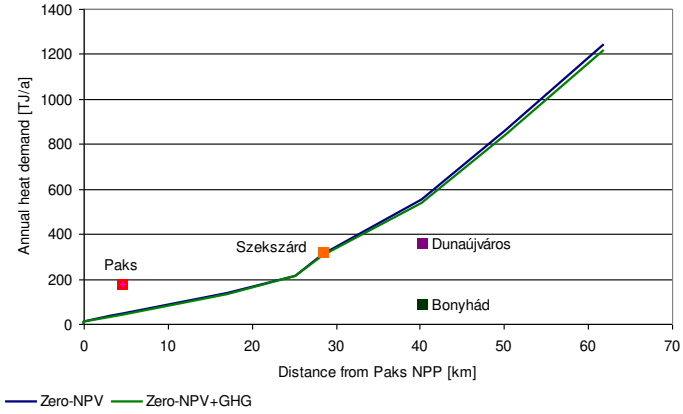

Figure 3

Towns in the region of Paks where the nuclear energy-based district heating can be competitive (40 years long payback period; 4% discount rate; carbon price of 5 Euro/ton of CO_2)

As it can be seen (Fig. 3), there are two towns, Paks (having an existing system) and Szekszárd that have sufficient heat demand to be supplied by nuclear heat in an economically viable way; both of them are above the limit-curve. On the basis of a partial sensitivity analysis, a supply to Dunaújváros would require a carbon price of at least 25 Euro/ton of CO_2,being considerably higher than the actual price (carbon emission price in 2015: 4.5-4.9 Euro/ton of CO_2). At present conditions, a nuclear-based heat supply is only feasible to Szekszárd where the payback period was evaluated at different carbon prices (Fig. 4).

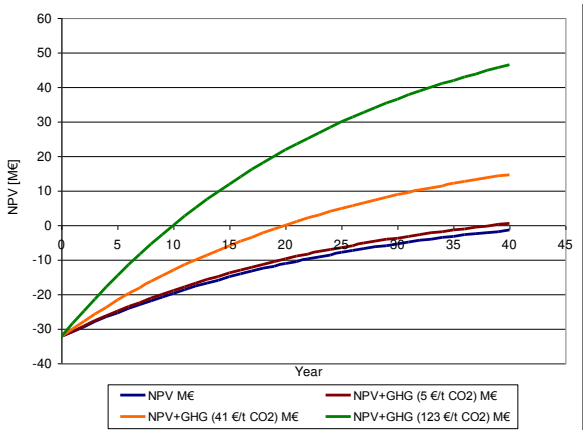

Figure 4

Time evolution of NPV for nuclear energy-based district heating at Szekszárd with different carbon prices

An increase in the carbon prices impacts the basic level of revenue and shortens the payback period of the project. In case of Szekszárd, the NPV of the investment reaches zero in 38 years when considering the present carbon price. In order to shorten the payback period to 20 years, a carbon price of 41 Euro/ton of CO_2 would be necessary; however, it should be noted that some low carbon scenarios predict even higher values than that in the energy sector. Shorter payback time seems to be not realistic as a payback time of 10 years would require a carbon price of 123 Euro/ton of CO_2.

As mentioned above, it was an important additional point of our study if the extension of the district heating network could be an economically viable solution to cover the expected increase in the heat demand [13]. This question was addressed from the point of view of the residential sector. The comparison of the heating alternatives was done by using a standardized heat demand profile for the three building typological groups and, additionally, the carbon price (17 Euro/ton of CO_2) and the external costs of environmental impacts were taken into account as two separate assessments. In comparison, the nuclear heat was the most favorable alternative for the large-scale multi flat buildings (LMB), by supposing a high penetration of the district heating network (Fig. 5). In case of the group consisting of medium-scale multi flat buildings (MMB), the nuclear district heating is competitive only when also the environmental external costs are considered in the assessment. Finally, the stand-alone heating could be the favorable option in cases of single family houses (SFH) as a result of the higher capital cost of the district heating installation.

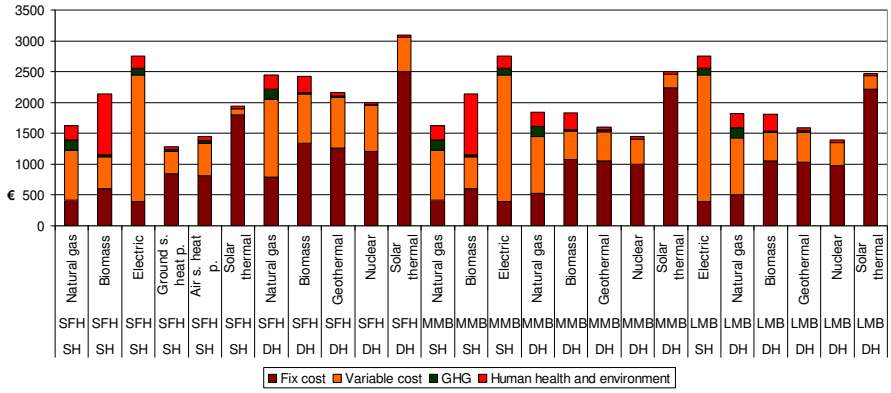

Figure 5

Annual cost of residential heating for a standardized case (140 m^2 ; 10.6 kW). The fixed cost of the nuclear district heating includes the costs of a 30 km transit pipeline. SH: Stand-alone heater; DH: District heating

The detailed comparison of the heating alternatives enables the selection of the optimal heat supply portfolios of the households, which are suitable to cover the seasonal heat demand profiles of the different building typological groups. Three portfolios were selected for each building typological group (Figure 6 and 7).

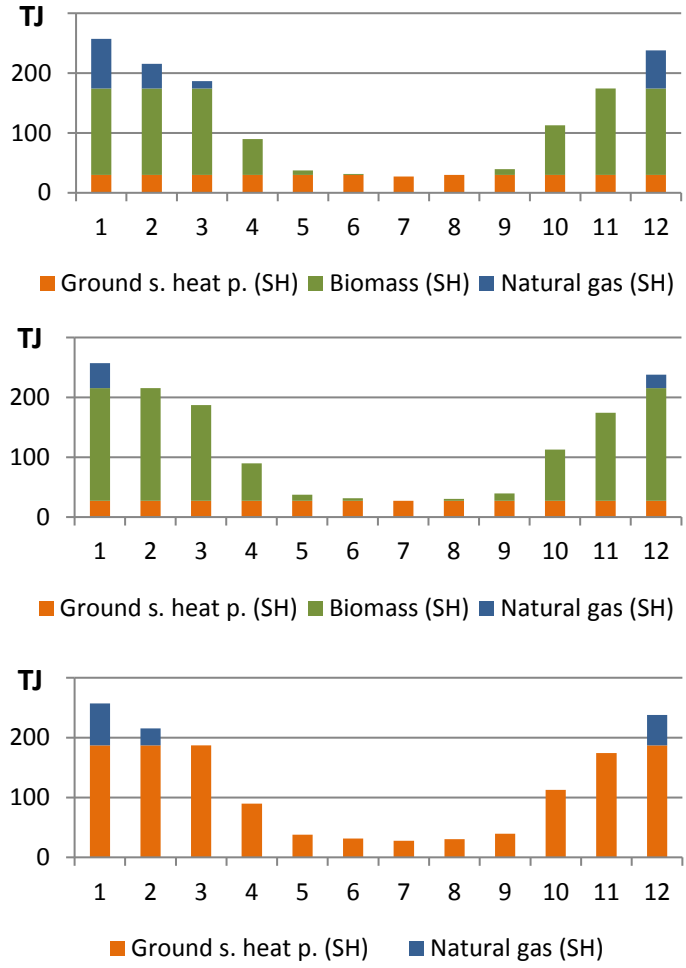

Figure 6

Optimal heat supply portfolios of single family houses for three cases: considering the fixed and variable costs only (top); including the carbon price additionally (middle) and finally, the external costs of environmental impacts (bottom)

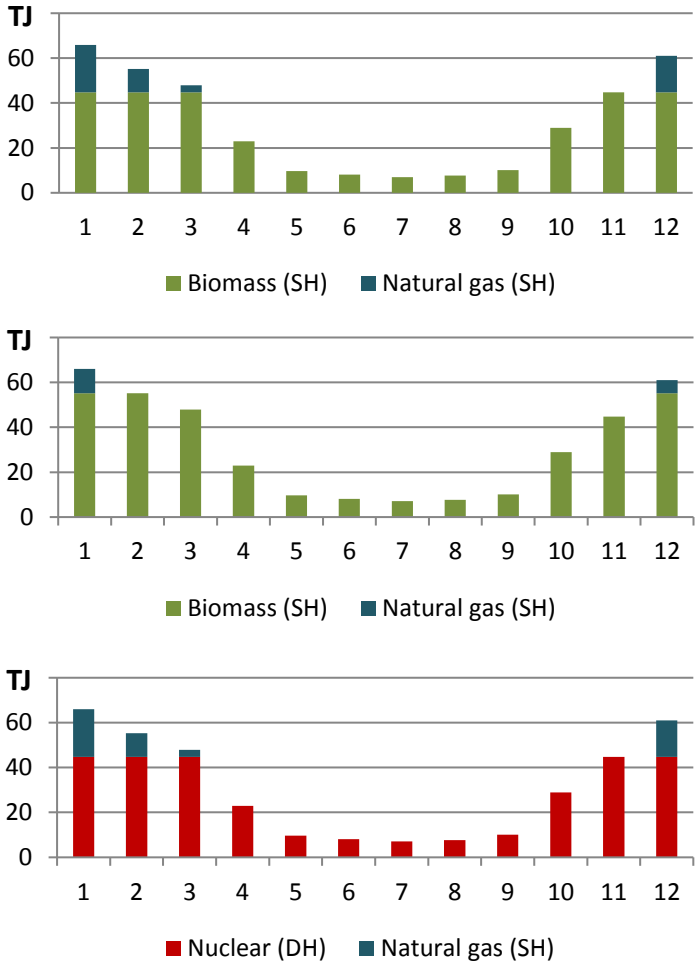

Figure 7

Optimal heat supply portfolios of medium-scale multi flat buildings for three cases: considering the fixed and variable costs only (top); includingthe carbon price additionally(middle) and finally, the external costs of environmental impacts (bottom)

In the first case, fixed and variable costs were considered only (neglecting carbon prices). In the second case, carbon prices were added, as well, and in the third case, also the external costs of the environmental impacts were taken into account. In cases of single family houses, the portfolios consist of three stand-alone heating technologies (biomass, ground source and natural gas-based heating). The base heat demand is supplied by ground source heat pumps while the peak load is covered by the natural gas based-heating; their ratio is different in the three scenarios. When

considering a carbon price of 17 Euro/ton of CO_2 in the assessment, the installed peak load capacity of 64 MW of natural gas-based heating decreases to a half of its initial value; at the same time, the installed capacity of ground source heat pumps is constantly 23 MW in both cases (i.e. carbon prices neglected vs. included). In the third case, where the external costs of environmental impacts were considered, as well, the biomass capacity that was significant in the first two cases (112 MW without carbon prices and 146 MW with carbon prices) is not part of the energy mix; the role of the biomass combustion was replaced by 145 MW installed capacity of ground source heat pumps.

In case of the medium-scale multi flat buildings, the share of the stand-alone heater technologies is reduced because of the building structure; at the same time, the higher heat load density makes the district heating more attractive economically. The peak load is covered by natural gas-based heating of 17 MW installed capacity. Similarly to the single family houses, the installed capacity of natural gas based heating halves after considering the carbon price. Furthermore, 35 MW installed capacity of stand-alone biomass heating was replaced by the nuclear district heating after taking into account the external costs of environmental impacts in addition to the carbon price.

In the building typological group of the large-scale multi flat buildings, the feasible, competitive heating technologies are, with no exception, the district heating-based alternatives. In the first assessment, the 29 MW of nuclear base demand capacity was complemented by 14 MW installed capacity of natural gas-based heat in peak load. The installed capacity of the nuclear-based district heating increases to 31 MW after considering the carbon price, and it reaches 36 MW after taking into account the external costs of the environmental impacts, as well.

Conclusions

The aim of this study was to identify the potential costs and benefits of the development of the nuclear energy-based district heating. The main benefit of moving towards the district heating is expected from the carbon emission savings it can provide. Since a conservative approach was applied in our calculations with no exception, results can be considered as "a worst-case study". At present conditions, Szekszárd is the only potential new location for nuclear-based heat consumption; however, the long payback period resulting from high capital costs and low carbon prices increases the risk of investment. Overall, we conclude that a governmental guarantee (assurance of nuclear heat in the long term) and the enlargement of the group of customers (by medium-scale multi flat buildings) could promote the investment. For single family houses, the low heat demand density is an obstacle to the development of the district heating, but the installation of heat pumps could contribute to reaching the carbon emission reduction targets. In the optimal heat supply portfolio calculation for households, the variable costs increase significantly when considering the external costs. Therefore, the alternatives of higher fixed costs could be competitive in the energy mix of the heat sector. The method presented in

our study was finalized by conducting a partial sensitivity analysis to assess the influence of carbon prices. However, the sensitivity analysis could be extended to any other variable by a statistical approach [12] or by multiobjective optimization [2].

Acknowledgement

The research of the second author was supported in part by OTKA grant K 111797. Finally, we thank János Osán and Tibor Orbán for their comments that greatly improved the manuscript.

References

[1] Andrews D., Riekkola K. A., Tzimas E., Serpa J., Carlsson J., Garcia P. N., Papaioannou I. Background Report on EU-27 District Heating and Cooling Potentials, Barriers, Best Practice and Measures of Promotion JRC Report 2012

[2] Börcsök E., Gerse A., Fülöp J. Applying Multiobjective Optimization for the Heat Supply in the Residential Sector in Budapest, 12th IEEE International Symposium on Applied Computational Intelligence and Informatics, SACI 2018 May 17-19, Timisoara, Romania

[3] Börcsök E., Talamon A., Török Sz. Possibility of Nuclear Cogeneration Development in the Region of Paks, NENE, 2016 Sept. 5-8, Portoroz, Slovenia

[4] Börcsök E., Talamon A., Török Sz. Socio-Economic Aspects of Nuclear Cogeneration Development in the Region of Paks, IAEA Technical Meeting, 2016 Nov. 21-23, Wien, Austria

[5] Büki G., Metzing J., Orbán T. Local Energy Supply 2014 [in Hungarian]

[6] Cornuejols G., Thizy J. M. A Primal Approach to the Simple Plant Location Problem, Alg. Disc. Meth. Vol. 3, No. 4, December 1982

[7] Dantzig G. B. Linear Programming and Extension, Princeton University Press August 1963

[8] District Heat Price Regulation for Different Consumer Groups 50/2011. (IX.30) directive of Ministry of National Development [in Hungarian]

[9] Göblyös B. Energy Mix Optimization in District Heating Sector, PhD Dissertation, Óbuda University 2016 [in Hungarian]

[10] Kádár P. Application of Optimization Techniques in the Power System Control, Acta Polytechnica Hungarica, Vol. 10, No. 5, 2013

[11] Kádár P. Pros and Cons of the Renewable Energy Application, Acta Polytechnica Hungarica, Vol. 11, No. 4, 2014

[12] Kharitonov V. V., Criteria of Return on Investment in Nuclear Energy, Nuclear Energy and Technology, Vol. 3, pp. 176-182, 2017

[13] Hartmann B., Börcsök E., Oláhné Groma V., Osán J., Talamon A., Török Sz., Alföldy-Boruss M. Multi-Criteria Revision of the Hungarian Renewable Energy UtilizationAction Plan – Review of the aspect of economy, Renewable and Sustainable Energy Reviews, Vol. 80, pp. 1187-1200, 2017

[14] Macadam J., Davies G., Cox J., Woods P., Turton A. The Potential and Costs of District Heating Networks, A report to the Department of Energy and Climate Change Pöyry 2009

[15] Mayer-Spohn O, Besl M. Documentation of the Life Cycle Inventory Data in CASES, CASES – Cost Assessment for Sustainable Energy Markets, Deliverable No. D6.1, October 2007

[16] Methodology for the WEM Wholesale Electricity Price Module, OECD IEA Report 2012

[17] Nyers J. COP and Economic Analysis of the Heat Recovery from Waste Water using Heat Pumps, Acta Polytechnica Hungarica, Vol. 13, No. 5, 2016

[18] Report of sustainability 2012, MVM Group 2013

[19] Roshenthal E. R., Brooke A., Kendrick D., Meeraus A., Raman R., GAMS A User's Guide.GAMS Development Corporation, Washington 1998

[20] World Energy Balances 2014 edition, OECD IEA Report, Paris 2014

Performance Analysis of Smart Grid Solutions in Distribution Power Systems

Nenad Katic

University of Novi Sad, Faculty of Technical Sciences, Trg Dositeja Obradovica 6, 21000 Novi Sad, Serbia, nenadkatic@uns.ac.rs

Abstract: Smart grid solutions are considered as a set of automation and telecommunication equipment connected to an intelligent master system, with aim to provide higher energy efficiency, optimized grid control and data processing. If applied in a power distribution network, it would include a wide set of smart applications for efficient operation, analysis, fault management, planning and optimization of grid operation. Together with field automation, as substation automation, feeder automation, remote terminal units and communication links, they constitute distribution automation management systems to provide higher efficiency and reduce cost of grid operation. In this paper, benefits and costs of a distribution automation management system is investigated and evaluated. The performance analysis is conducted considering the lifetime of the system, to manifest the profitability of the solution.

Keywords: Power Distribution; Smart Grid; Energy efficiency; Power system economics

1 Introduction

Opening of the electricity market and new regulations caused unbundling of vertically organized utilities into different companies, in the competitive market (e.g. generation, energy trade) or in further regulated (e.g. power transmission and distribution activity). Regulated power transmission and distribution companies (RPC) faced significant reduction of revenue (without energy trade) and increase of responsibility and penalties by regulation. In the new economic and technical environment, RPC are forced to significantly increase efficiency and reduce cost of operation, to be able to survive and operate positively. Smart Grid Solutions (SGS) provides this affect and are widely applied by RPCs. The challenge is quantification of benefits provided by SGS and comparison with related costs, to estimate the real profitability of such investments.

Power companies nowadays, implement different components of SGS with a common goal to increase efficiency of grid operation and reduce power losses, outage time and maintenance cost [1]–[4].

SGS are considered as set of advanced technologies aimed at improving the efficiency of grid operation, significantly improving reliability, quality and efficiency of power delivery, as well as reducing costs of power network operation. SGS include various technologies, as presented in Figure 1:

- *Smart Grid Control*: IT technologies applied in control centres of transmission or distribution companies, such as Advanced Distribution Management Systems (ADMS) for smart grid control, AMI/MDM for smart meter data management, Demand Response for management of consumption, GIS and Asset Management for asset data processing, etc.
- *Smart Power Grid:* operation technologies (OT) applied in power grid for automation of local operations (field automation systems): Substation automation systems, Remote Terminal Units (RTU), controllable Ring Main Units (RMU), Re-closers, Distributed Generators control, Electrical Vehicles management, Energy Storages control, etc,
- *Smart Consumption*: local control systems for smart management of energy consumption, as Building Management Systems, Industrial Control, Home Automation with smart meters, etc.

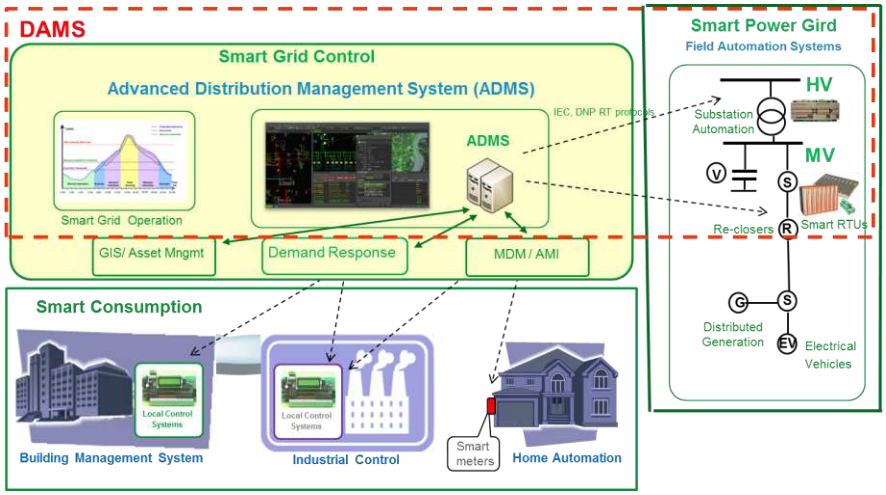

Figure 1
Smart Grid Solutions

Implementation of ADMS and Field automation solutions together can be referred as Distribution Automation Management System (DAMS). DAMS should reach various objectives, as advanced monitoring and control of distribution network; optimization and efficiency of network operation; reduction of power losses; reduction of power outage time, reduction of maintenance costs; efficient utilization of existing distribution facilities; postponement of investments; improvement of power quality, improvement of customer services; reduction of

operation costs and increase of revenue. DAMS should provide advanced tools for dynamic visualization, monitoring and control of electricity distribution network, as well as smart applications for operation analysis, planning and optimization. The system should be built on open standards and integrated with other IT systems in a Utility, to enable optimal network operation, decision making and design.

Smart grid efficiency is analysed in many research papers [1-7]. The key performance indicators related to smart grid efficiency are presented in [5], using the fuzzy analytic hierarchy process for the determination of overall smart grid efficiency. The analysis shows that the dominant performances of the optimal smart grid project are efficiency, security and quality of supply. Evolutionary computation is applied in optimization algorithms [6], used for smart power grid control and based on genetic algorithms, neural networks, heuristic algorithms and fuzzy methodologies [5, 6, and 7].

In this paper, the performance analysis of DAMS solution is presented, based on the main benefits in increasing efficiency, security and quality of supply. The operation benefits are evaluated in the second section of the paper, based on the sample of a real power distribution grid. The typical cost of DAMS implementation and operation cost during the lifetime of the system are evaluated in the third section. In the fourth section, the performance analysis is conducted considering the lifetime of the system, to manifest the profitability of the solution. Consequently, conclusion and references are provided.

2 Benefits of DAMS Implementation

Distribution Automation Management System (DAMS) is considered as implementation of ADMS and Field automation solutions together (Figure 1). In this section, DAMS benefits are analyzed and evaluated [4]. A sample of one real distribution network system (DNS) is used for the evaluation of benefits and costs. DNS is supplied by one Primary Substation (PSS 110/35 kV) and four Distribution Primary Substations (DPS 35/10 kV). DNS supplies 25,000 consumers (meters), over 350 km of 10 kV medium voltage (MV) network, by 40 MV feeders and 360 Secondary Substations (DSS 10/0,4 kV), as presented in Figure 2. DNS annual peak load is 50 MW. The annual injected electrical energy (AIEE) into DNS is approx. 200 GWh/year, with a commercial value of approx. 7,500,000 $/year (assuming wholesale price in range 35–40 $/MWh). The DNS total power losses are 10% (technical and non-technical losses).

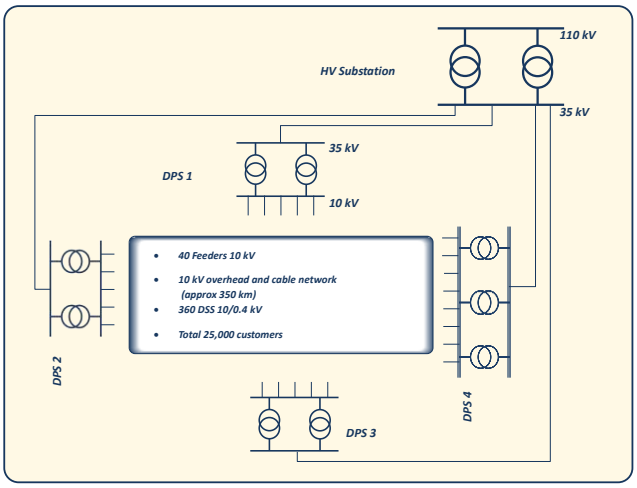

Figure 1
The example of a real Distribution Network

Implementation of DAMS should bring benefits in reduction of power losses; reduction of operation costs (reduced maintenance, outage time and non-supplied energy); reduction of network construction costs (improved utilization of facilities and postponement of investment) and in improving power quality. Such benefits are analyzed and evaluated in the following sections.

2.1. Reduction of Power Losses

Power losses are reported as the difference of the energy measured on entry points of the network and energy measured on consumption (customers) points, in one considered time period (typically one year). Technical power losses are related to energization of the network and power flow, while non-technical losses to problems with measurement and energy theft. Power losses are direct commercial loss to any RPC, since they have to be compensated by additional purchase of energy, as well as they contribute to pollution of environment. Therefore, there is always a high interest for reduction of losses and contribution of DAMS is presented in this section.

2.1.1. Optimal Feeder Reconfiguration

Power flow calculation [8] is based on the real-time state estimation and load profiles, providing real-time calculation of network operation state, for all transformers, feeders and laterals. Normally, distribution network is operated radially without loops, and if a feeder has connection to other feeders, the

connecting switch would be normally open. The normally open switches (NOS) are providing possibility for restoration of supply in case of incidents. In large distribution networks with hundreds of feeders, there are hundreds of NOS, which may be subject of optimization to reach certain objective (minimum power losses, improved voltages, reduced overloads, etc.). The optimization approach in DAMS function "Optimal Feeder Reconfiguration" (OFR) provides such a solution [9 - 12], based on optimization algorithm where all switches are closed and then opened with minimal current deviation, but using network model with only resistances for power lines [9]. If results are applied in a real network operation, experience is showing up to 20% reduction of technical (peak) power losses in the MV network, with insignificant costs of changing NOS locations. Since MV losses are approximately 30% of total (peak) power losses (including HV, MV, LV network and transformers), and since energy losses are lower due to variation of load in time, the reduction of total energy losses would be in the range of 4-5%, which is confirmed in field results [13]. The reduction of energy injection in distribution network would be in the range of 0,4–0,5 % AIEE, considering typical energy losses, and reduction of energy that RPC has to purchase 4–5%.

2.1.2. Volt/Var Control

DAMS function "Voltage/Var control" (VVC) provides optimization of voltages and reactive power flow in distribution network in a real time state [14-16], keeping voltages inside technical constraints, but reaching optimization objective. It calculates the "optimal" setting of the voltage regulation devices (on-load tap changers) and capacitor banks, according to selected objectives (minimal power losses, voltage deviation, power demand, and others). On the basis of areas whose voltages are influenced by these control devices and their action speeds, the voltage control problem is decomposed in space and time [15]. The space decomposition enables a solution of the distribution voltage control problem for the medium voltage network of each supply transformer (substation) separately. As well, the time decomposition enables a solution in the operation planning mode and the real time mode separately. The voltage control is each time stated as a constrained optimization problem. The network voltage profile quality is quantified by the damage (inconvenience) that electric consumers sustain due to steady state voltage deviations. Therefore, this damage is used as the optimization objective.

In case of minimal power losses objective, test results are showing 10% additional reduction of MV network power losses in coordination with OFR. The cumulative effect of VVC and OFR is providing reduction of AIEE up to 0,5%.

2.1.3. Reduction of Non-Technical Losses

DAMS Energy Audit application enables archiving energy injection (recorded by meters) and technical losses (calculated) in MV feeders and MV/LV transformers,

so that energy injection on the Low Voltage (LV) side is established, if not measured by specific meters. Technical losses in LV network can be calculated by DAMS applications, and then using billing data of LV customers "non-technical" losses can be allocated (theft, bad meters). Now, distribution transformers areas can be ranked according to the level of non-technical losses, and field crews sent to critical locations for control [17]. After reducing theft or metering failures, the injection of energy will be also reduced. The field results are showing reduction of non-technical energy losses minimum 0.5% of AIEE.

2.1.4. Total Reduction of Losses

In total, DAMS can contribute to 5–10% reduction of energy losses in distribution network, or 0.5 to 1% of AIEE.

In case of DNS (200 GWh energy injection), saving would be 1 to 2 GWh/year, or 35,000–75,000 $/year (using average wholesale price of 35–40 $/MWh), and divided by 25,000 customers (el.meters), is averaging **1.5-3** $/meter/year.

2.2. Reduction of Network Operation Costs

Network automation and DAMS is recently under implementation in many RPCs. Fault (outage) management is executed mostly manually with field crews, when a procedure may take several hours and customers along the feeder would suffer a long outage. The dispatcher has limited information about the network operational state. He faces the risk of making wrong decisions and extended outages, relying only on his experience, without any smart tools for decision support.

2.2.1. Direct Cost of Fault Management

DNS is having up to 150 MV feeder faults/year. In DNS without automation, the average duration of fault is approx. 2 hours, affecting 1000 customers or 1 MW of load, giving in average of 2 MWh of non-supplied energy per fault, or a total of 300 MWh energy of non-supplied energy per year (ENS). If the price of "distribution service" is approximately 4 c$/kWh (price that RPC is charging for services), then the lost revenue would be 12,000 $/year.

Additionally, due to frequent use of switching equipment in DNS with manual fault management, at least one circuit breaker would have to be replaced per year, because of the 300 switches on fault current (2–3 switches per fault), which has a cost of a minimum of 6,000 $/year. Similarly, at least 4 load switches should be replaced, because of 800 switches on load (5–6 switches per fault), which has a cost of a minimum of 16,000 $/year. The cost of field crew engagement for 800 switches in field (25 $/switch) is approx. 20,000 $/year.

The total direct cost of fault management in DNS, without DAMS, would be approx. 54,000 $/year.

2.2.2. Outage Compensation Cost

The liberalization of the electrical sector introduces compensations paid by RPC to customers because of outages, or exposure of RPC to penalties defined by the regulator. Regulation models are different in countries, but in many cases RPCs are exposed to additional cost for compensation of damages to customers, for example, RPCs in Holland pay compensation of 35$ to every customer for outages longer than 4 h (Netherlands Authority for Consumers and Markets). In some countries revenue and tariffs of RPC are exposed to penalties related to operation performance, for example, each hour lost cost RPC in UK approx. 20$/customer (Ofgem – UK Office of Gas and Electricity Market).

Exposure to penalties or outage compensation cost can be estimated, as ENS multiplied with the average service price and a multiplication factor, which can be in the range from 0 (no exposure) to 20 times (full exposure). If ENS in DNS is 300 MWh/year, then outage compensation costs in case of DNS would be in the range from 0 to 240,000 $/year. In most cases, exposure is not high, or outage compensation costs are paid rarely, so on average the ENS price should be multiplied approx. 5 times, and the average price of ENS can be assumed as 20 c$/kW. Thus, the average outage compensation cost in case of DNS would be 60,000 $/year.

2.2.3. Implementation of DAMS

Deployment of DAMS (ADMS and field automation) would significantly improve the fault management, reduce outage time, and reduce direct and compensation costs paid by RPC [4]. DAMS would require remote control of all HV Substation, remote control of certain number of MV load-switches (approx. 20%), implementation of fault detectors and central smart management system (ADMS). The fault would be located analytically, using algorithm for fault location, isolation and restoration [18], without need for many switching of equipment. The minimal necessary switching will be done remotely, and average outage time would be significantly reduced, almost 5 times, down to 15 – 20 minutes. In DNS, ENS would reduce to 60 MWh/year.

The lost revenue would decrease to 2,400 $/year because of ENS reduction. The maintenance cost would be significantly reduced: one breaker failure in two years (3,000 $/year) instead each year, one switch failure per year (4,000 $/year) instead of four failures, less crew engagement (200 switching, or 5,000 $/year). Thus, the total direct cost would decrease to 14,400 $/year. Compensation cost would decrease to 12,000 $/year (60 MWh x 20 c$/kWh). Therefore, the total saving after deployment of DAMS, would be 88,000 $/year, which equals 1.25% AIEE

or 3,5 $/meter. However, if exposure to penalties is considered in the higher range, then savings would be even higher.

DAMS can contribute to reduction of maintenance and network operation costs and provide savings of 1.25% AIEE, or **3,5 $/meter/year**.

2.3. Reduction of Network Construction and Development Costs

The network study and planning tools enable efficient utilization of existing distribution facilities with up to 20% postponement of investments in network constructions.

The normal construction of distribution facilities, due to new customer connections or resolving of power overloads, increases the number of distribution transformers on average 1% annually, as well as the length of MV power lines by 0.5%. In DNS, on average 4 new DSS and 2 kilometers of MV power lines should be built every year (4 x 30,000 + 2 x 90,000 = 300,000 $/year investments); however, with DAMS, investment would be postponed and reduced to 3 DSS and 1.6 km of MV power lines (234,000 $), giving a savings of approximately $66,000 annually.

The more efficient resolution of large outages using DAMS, by more efficient utilization of reserves in adjacent MV network, would postpone construction of new primary substations. *ADMS Large Area Restoration* functionality enables the efficient resolution of large HV supply transformer outages. In DNS, one DPS should be normally built every 10 years (1,000,000 $ investment); however investment can be postponed and save 50,000–80,000 $ per year in less depreciation or interest.

In total, reduction of network construction costs in DNS case would be in range 116,000-146,000 $/year, or 1.5-2.0% of AIEE. Therefore, DAMS can contribute to reduction of construction costs and provide savings of 1.5-2% AIEE, or **4,5-6 $/meter/year**.

2.4. Improved Power Quality

DAMS Voltage/Var Optimization application provides real-time regulation of on-load tap-changers on HV/MV transformers (PSS and PDS) and seasonal setting of off-load tap-changers on MV/LV transformers in DSS. Voltages are maintained within technical limits to provide power quality and minimize damages to customers due to voltage deviations. Additionally, voltages are maintained in optimal profile in dependence of the network operation state: in regular state reducing active and reactive losses; in emergency state reducing peak load; in extra energy state increasing demand. Guaranteed power quality can be provided

for special sensitive customers, as well as electricity sales can be impacted by changes of voltage level according to electricity market prices.

Testing results are showing savings of 0.5-1 % of AIEE, or **1,5–3 $/meter/year**.

2.5. Total Benefits

The total benefits of DAMS implementation, as well as DAMS benefits per type, are presented in the Table 1.

Table 1
DAMS total annual benefits

Benefit type	DAMS tool	Saving/year (% of AIEE*)	Saving/year ($/meter/year)
Reduction of energy losses	Optimal Feeder Reconfiguration, Volt/Var Control	0.5 - 1%	1.5 - 3
Reduction of network operation costs	Fault Management automation	1.25%	3.5
Reduction of network construction costs	Network construction planning and load forecast	1.5 - 2%	4.5 - 6
Improved power quality	Volt/Var Optimization	0.5 - 1%	1.5 - 3
Total Benefit		3.75 – 5.25%	11 – 15.5
Average Benefit		**4.6 %**	**14**
* Saving in % of the Annual Injected Electrical Energy (AIEE) into the distribution network			

The total benefits of DAMS implementation, as discussed in this section, should provide aggregated annual savings of 4.6% of AIEE, or **14 $/meter/year**.

3 Cost of DAMS Implementation

The costs of DAMS implementation encompass three areas [4]:

- *DAMS Software and IT hardware,* deployed in Main and Back-up data centres and Control Rooms (Dispatching Centres) of RPC, including costs of software licenses, engineering (design, configuration, data migration), delivery, testing, training, commissioning, support and maintenance.

- *Substation and Feeder automation,* including intelligent local master systems or remote terminal units (RTU) for local signal acquisition, processing and conversion, implemented in substations and overhead lines (pole mounted switches), with costs of equipment, delivery, commissioning, testing and maintenance.
- *Communication system* (radio links, fibre optic, public providers), including costs of system design, licenses for radio frequencies, delivery of equipment, testing commissioning, maintenance, or cost of subscription on communication providers.

Distribution automation principles recommend remote control of all NOS, as well as a certain number of MV load switches (e.g. on a third or half of the feeder) and fault detectors, to be able to execute a fast supply restoration and reduce outage time. Additionally, all supplying primary HV Substations and larger MV switching points should be under remote control. More RTUs in network would bring better results, but would rapidly increase investment cost. Some of the DAMS functions may be used for deeper analysis and design of the optimal level of automation, keeping investment inside a limited budget. The minimum level of investment in case of DNS is presented in Table 2.

Some old power equipment should be replaced to be controlled by automation systems (e.g. replacement of old air-insulated load-breakers with gas insulated Ring Main Units or Pole Mounted Switches), but power equipment is typically another line of investments. Since automation cost is considered from scratch However, many RPCs has already invested in certain automation equipment, it is assumed that the value of the existing automation equipment equals investment cost in replacement of old power equipment.

According to results of DNS investment analysis (Table 2), it can be generalized that DAMS investment costs typically consist of:

- DAMS SW/IT investment costs, which are in the range 5-8 $/customer (meter), depending on the network size and functionalities included. Typically, average price per meter is higher for smaller projects and lower for large projects, making 20% of the total DAMS investment,
- Communication systems are in the range of 4-8 $/meter, making 20% of the total DAMS investment.
- Cost of automation equipment with installation costs, this is the largest part, making 60% of the total DAMS investment, and it is in the range of 20-25 $/customer (meter),

The total investment costs in DAMS, as discussed in this section, are in the range of 29–41 $/meter, and for further analysis the average value of **35 $/meter** will be used. It equals 12% of AIEE value.

Table 2
DNS automation investment cost

DNS automation cost (25,000 customers/meters)	Unit price ($)	No of units	Price for DNS ($)	Price per customer ($/meter)
DAMS Software and IT hardware	125,000 - 200,000	1	125,000 – 200,000	5 - 8
PDS automation, RTU, cabling and interfaces	40,000 - 50,000	4	160,000 – 200,000	20 - 25
DSS, RTU, cabling and interfaces	4,000 - 5,000	25	100,000 – 125,000	
PMS, pole mounted switches, RTU and interfaces	3,000 - 4,000	70	210,000 – 280,000	
Distribution switching yard, RTU and interfaces	10,000	3	30,000	
Communication system: Fibre Optic interfaces, or radio equipment, interfaces, antennas, etc.	1,000 – 2,000	100	100,000 – 200,000	4 - 8
Total DAMS automation cost of DNS			725,000 – 1,035,000	29 - 41
Average DAMS cost ($/meter)				**35**

4 Cost Benefit Analysis

The cost–benefit economic analysis will be made comparing average annual costs and benefits of DAMS project, as well as comparing the total cost of ownership and total benefits over the lifetime of DAMS system [19] – [20].

4.1 The Method of Annual Costs

Profitability and attractiveness of an investment can be evaluated with the method of annual cost. In this method, cost and benefits in one year of operation are compared, assuming that they are not changing over the lifetime of the system. This is not fully correct because the value of money is changing over time, but for quick and simplified analysis this method can be used, mostly to show approximate profitability.

The annual cost of DAMS system operation can be evaluated taking into account annual investment cost (depreciation), operating cost and financial cost:

- Depreciation (d %) is calculated in economics as inverse value of the system lifetime, where the system lifetime is presented in years and depreciation in percentages. Depreciation is percentage of initial investment cost (I_0), which RPC should spend each year on "renewal" of the assets, so that assets never

lose value. If we assume the lifetime of DAMS as 10 years, then depreciation cost would be 10% of I_0.

- The operating and maintenance cost for using of the system (m %) are approximately 5% of I_0. Such cost typically include engagement of RPC's personnel, hardware and equipment maintenance, license subscriptions, etc.
- Financial cost (int %) includes average cost of capital, or interest in case of loan, taxes, etc., and they are in the range of 3-5% of I_0.

Thus, the annual cost of operating DAMS system ($C_{a,i}$) in year "i" can be expressed as in equations (1) and (2):

$$C_{a,i} = (d\% + m\% + \text{int}\,\%)\, I_0 \tag{1}$$

$$C_{a,i} = (10\% + 5\% + 5\%) I_0 = 20\ \%\ I_0 \tag{2}$$

If initial investment cost for DAMS implementation (I_0) is 35 \$/meter, according to section 3, then the annual cost of using DAMS is approx. 7 \$/meter/year.

The total annual benefit of DAMS operation ($B_{a,i}$) is calculated in chapter 2.5, resulting in 14 \$/meter/year.

Now, the annual profitability ($P_{a,i}$) of DAMS project is calculated as ratio of annual benefits ($B_{a,i}$) and costs ($C_{a,i}$), as expressed in equation (3):

$$P_{a,i} = \frac{B_{a,i}}{C_{a,i}} = \frac{14\ \$/meter}{7\ \$/meter} = 2 \tag{3}$$

Therefore, the method of annual cost is showing that DAMS projects have a very good profitability, because benefits will be twice higher then cost during each year of operation.

4.2 Discounting Method

The most accurate is the discounting method, which is considering the total cost over the lifetime of the system, or the total cost of ownership (TCO), comparing with the total benefits that system will provide over the lifetime or the total benefits of ownership (TBO).

Since the capital has to bring return over time, as discounting parameter is used "weighted average cost of capital" ($wacc$%). TCO can be expressed, as in equation (4):

$$C_{T,0} = TCO = \sum_{i=1}^{T} \frac{(d\% + m\% + \text{int}\,\%)_i\, I_0}{(1 + wacc\%)^i} \tag{4}$$

If we consider that annual costs are constant over time, then TCO can be expressed as in equation (5):

$$C_{T,0} = TCO = (d\% + m\% + \text{int}\,\%) I_0 \cdot \sum_{i=1}^{T} \frac{1}{(1+wacc\%)^i} \tag{5}$$

If discounting factor (*DF*) is introduced, and *wacc%* assumed 5%, then *DF* can be expressed as in equation (6):

$$DF = \sum_{i=1}^{T} \frac{1}{(1+wacc\%)^i} = \sum_{i=1}^{T} \frac{1}{(1+5\%)^i} = 7{,}72 \tag{6}$$

TCO can be expressed as in equation (7):

$$C_{T,0} = TCO = C_{a,i} \cdot DF = 20\% I_0 \cdot 7{,}72 = 1{,}54 \cdot I_0 \tag{7}$$

TCO of DAMS project, with the lifetime of 10 years, will be 1.54 times of initial investment, or 7,72 times of annual cost.

If I_0 is estimated on 35 \$/meter (Table 2), then TCO of DAMS project during 10 years will be **54 \$/meter**.

On the other side, TBO can be easily calculated in a similar way, equation (8):

$$B_{T,0} = TBO = B_{a,i} \cdot DF = B_{a,i} \cdot 7{,}72 \tag{8}$$

If annual benefit ($B_{a,i}$) is 14 \$/meter/year (Table 1), then TBO of DAMS project, during lifetime of 10 years, will be **108 \$/meter**.

The economic evaluation with discounting method is made using four typical economic parameters:

a) *Profitability* (*P*) – this economic factor describes the profitability of the project, using ratio of total benefits and costs during the project lifetime, as in equation (9):

$$P_{T,0} = \frac{TBO}{TCO} = \frac{108\,\$ / meter / 10\,years}{54\,\$ / meter / 10\,years} = 2 \tag{9}$$

DAMS projects are showing a high profitability, because benefits provided will be twice higher then all costs during the lifetime of the project.

b) *Payback* – this economic factor describes the time necessary for the return of investment, and the year when project starts to provide profit, as expressed in equation (10):

$$Payback = \frac{T}{P_{T,0}} = \frac{10\ years}{2} = 5\ years \tag{10}$$

DAMS projects are showing a good payback time of 5 years, and providing the profit in the following 5 years.

c) *Return on Investment* (*ROI*) – this economic factor describes the added value over invested amount, that project will bring during the lifetime, as expressed in equation (11):

$$ROI = \frac{TBO - TCO}{TCO} 100 = \frac{108 - 54}{54} 100 = 100\ \% \tag{11}$$

DAMS will create added value of 100%, which means that on each dollar spent, over two dollars will return.

d) *Internal Rate of Return* (*IRR*) – this economic factor describes how much the investment is attractive compared with the average cost of the capital. It is calculated as the discounting factor by which the *Net Present Value* (*NPV*) would equal to zero, or investment wouldn't bring any profit over lifetime, as expressed in equation (12):

$$NPV = -I_0 + \sum_{i=1}^{10} \frac{B_{a,i} - C_{a,i}}{(1 + IRR)^i} = 0 \tag{12}$$

NPV is the total profit over the lifetime discounted on the present date and then reduced by initial investment. If IRR is higher than average cost of capital, then the investment is attractive. In DAMS case, IRR is 15%, which is three times higher than average cost of capital (5%), showing high attractiveness of DAMS investment.

Economic analysis of DAMS projects is showing a high business attractiveness in any of four economic parameters: they are more than two times profitable, payback is half of the lifetime, return on investment is two times, and internal rate of return is very high.

4.3 Sensitivity Analysis

Sensitivity analysis was made to explore the impact of existing distribution automation levels on profitability of DAMS projects. Three scenarios were created:

a) Scenario A – *Typical state (TS)*: This is a typical situation in RPCs nowadays with small level of distribution automation (10-20% of the full automation level). This situation was considered in analysis of benefits in section 2 and costs in section 3. DAMS investment cost ($I_{0,TS}$) to reach full automation would be 35 $/meter, while annual benefits 14 $/meter/year (4,6% AIEE).

b) Scenario B – *Advanced state (AS)*: There are some advanced RPCs which recently invested more in automation, and already reached 30-40% of the full

automation level (e.g. North America, North Europe). In this case, investment cost I_0 would be lower than in Scenario A. If assumed that 2/3 of the full I_0 would be necessary, then ($I_{0,AS}$) in this case would be 22 $/meter. Also, benefits would be slightly lower, since certain benefits of outage reduction would already have been reached. If half of outage reduction benefits is already reached, then annual benefits would be in a range of 13 $/meter/year (4.3% AIEE).

c) Scenario C – *Full automation (FA):* There are a few very advanced RPCs which already reached the full automation (e.g. Japan, Singapore, Hong Kong, New York, etc.). In this case, further investment in automation is not necessary anymore, but it is necessary in DAMS system deployment (software and computer equipment). According to Table 2, only DAMS investment ($I_{0,FA}$) would be 8 $/meter. Benefits would also be lower, since fault management automation was already reached, but other benefit (e.g. power losses reduction, etc.) would produce at least 12 $/meter/year (4% AIEE).

The economic evaluation (discounting method) was made with scenarios A, B and C, using equations for TCO (7) and TBO (8), and DNS with 25,000 meters. The four typical economic parameters are calculated using equations 9–12, and results are presented in the Table 3.

Table 3
DAMS profitability with different automation levels

Scenario (autom.level)	TCO ($)	TBO ($)	P	ROI	IRR	PbT (years)
A – Typical state	1,347,500	2,702,000	2.00	100%	15%	5
B – Advanced state	847,000	2,509,000	2.96	196%	37%	3.38
C – Full automation	308,000	2,316,000	7.52	652%	130%	1.33

The sensitivity of four economic parameters on automation levels is presented graphically in Figures 3-6.

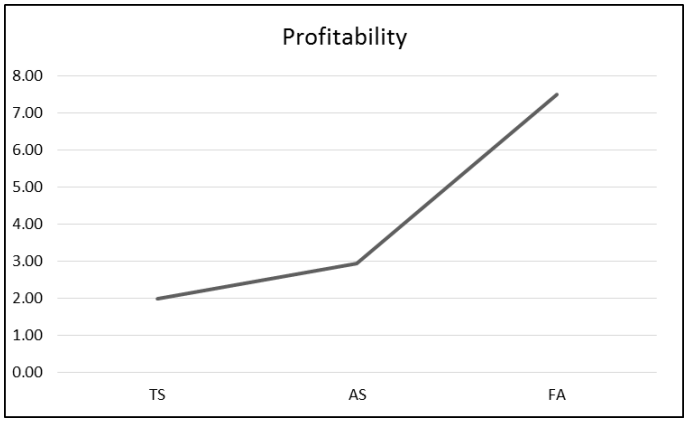

Figure 3
DAMS Profitability in different automation levels

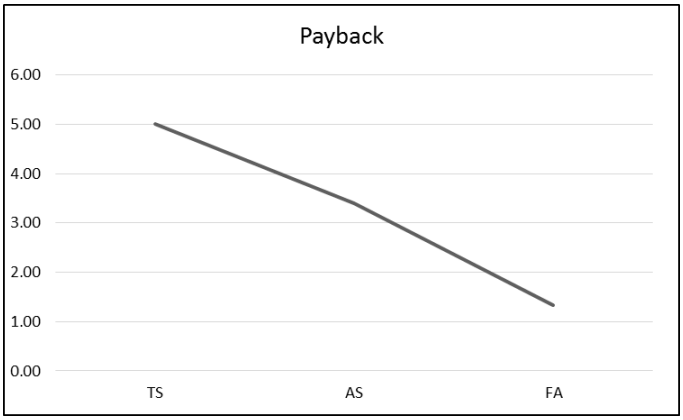

Figure 4
DAMS Payback time in different automation levels

The sensitivity analysis is clearly showing significant impact of automation level on profitability of DAMS projects. If existing automation level of the distribution network is higher, DAMS costs and TCO will be significantly lower because automation cost are highest. However, since most benefits are coming from software optimization features (reduction of power losses, postponement of constructions, power quality) TBO will keep high values. Consequently, all economic parameters will be much better. Profitability would increase by 3 times in case of advanced RPCs and up to 7 times in case of the full automation. Payback time would reduce over 3 years in case of advanced RPCs and down to 1 year in the full automation case. IRR and ROI would show much higher values creating high attractiveness of investments into DAMS.

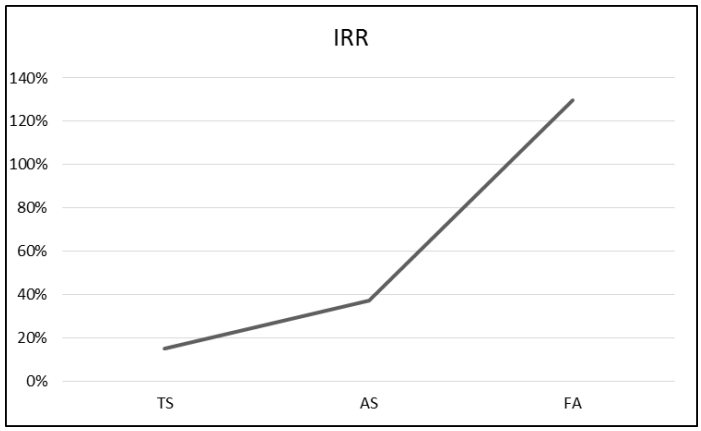

Figure 5
DAMS IRR in different automation levels

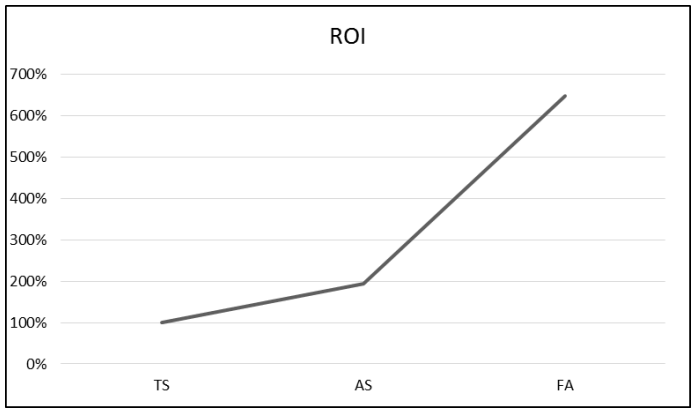

Figure 6
DAMS ROI in different automation levels

Conclusions

Investments in DAMS projects should be very profitable. The results of economic evaluation and sensitivity analysis are showing very good economic performance:

- *Good Profitability:* in most of regulated power distribution companies (RPCs) with small automation level nowadays, benefits would be *two times* higher than costs over the lifetime of a project. In RPCs with advanced automation level, profitability would be over *three times*. In case of the full automation, when investment is only in DAMS software and computer equipment, profitability would be even as much as *seven times*.

- *Short Payback time:* investment would return in 5 years in the low automation case, but in 3 years in the advanced case, or even in 1 year in the full automation case, showing a longer time for providing the profit.
- *High Return on Investment:* even in RPCs with small automation return on investment would be 100%, which means that on each dollar invested, two dollars will return. In advanced and fully automated RPCs, return would be even much higher, showing a high attractiveness of investment.
- *Attractive Internal Rate of Return:* in RPCs with small automation IRR (15%) is three times higher than average cost of capital, showing a very good attractiveness of investment. In advanced and full automated RPCs IRR is much higher, showing even higher attractiveness of investments in DAMS.

Finally, since not all DAMS benefits could be financially evaluated (e.g. improving safety on work, reducing damages, improving customer satisfaction, etc.), attractiveness of DAMS investment may be even higher.

References

[1] D. Molzahn, F. Dorfler, H. Sandberg: A Survey of Distributed Optimization and Control Algorithms for Electric Power Systems, IEEE Transactions on Smart Grid, Volume 8, issue 6, November 2017, pp. 2941-2962

[2] N. Katic: Profitability of Smart Grid Solutions Applied in Power Grid, Thermal Science, Vol. 20, Suppl. 2, 2016, pp. S371-S382

[3] S. Mohtashami, D. Pudjianto, G. Strbac: Strategic Distribution Network Planning with Smart Grid technologies, IEEE Transactions on Smart Grid, Volume 8, Issue 6, November 2017, pp. 2656-2664

[4] N. Katic: Benefits of Smart Grid Solutions in Open Electricity Market, Acta Polytechnica Hungarica, Vol. 10, No. 2, 2013, pp. 49-68

[5] A. Janjic, S. Savic, G. Janackovic, M. Stankovic, L. Velimirovic: Multi-Criteria Assessment of the Smart Grid Efficiency Using the Fuzzy Analytic Hierarchy Process, Facta Universitatis, Series: Electronics and Energetics, Vol. 29, No. 4, 2016, pp. 631-646

[6] V. Oduguwa, A. Tiwari, R. Roy: Evolutionary Computing in Manufacturing Industry: an Overview of Recent Applications, Applied Soft Computing, Vol. 5, No. 3, 2005, pp. 281-299

[7] A. Urmos, Z. Farkas, M. Farkas, T. Sandor, L. T. Kocsy, A. Nemcsics: Application of Self-Organizing Maps for Technological Support of Droplet Epitaxy, Acta Polytechnica Hungarica, Vol. 14, No. 4, 2017, pp. 207-224

[8] S. Cheng, D. Shirmohammadi: A Three-Phase Power Flow Method for Real-Time Distribution System Analysis; IEEE Trans. on Power System, Vol. 10, No. 2, May 1995, pp. 671-679

[9] D. Shirmohammadi, H. W. Wong: Reconfiguration of Electric Distribution Networks for Resistive Line Losses. IEEE Trans. on Power System 1989; Vol. 4, No. 2

[10] M. E. Baran, F. F. Wu: Network Reconfiguration in Distribution Systems for Loss Reduction and Load Balancing, IEEE Trans. On Power Delivery, Vol. 4, No. 2, April 1989

[11] I. Roytelman, V. Melnik, S. S. H. Lee, R. L. Lugtu: Multi-Objective Feeder Reconfiguration by Distribution Management System, IEEE Trans. on Power System, Vol. 11, No. 2, May 1996, pp. 661-667

[12] J. Cebrian, S. Rahman, N. Kagan: Restoration in Distribution Systems to Reduce Financial Losses Related to Process Trips, IEEE Transactions on Smart Grid, Volume 8, Issue 1, January 2017, pp. 219-227

[13] G. di Lembo, P. Petroni, Ch. Noce: Reduction of Power Losses and CO2 Emission: Accurate Network Data to Obtain Good Performances of DMS Systems, CIRED 20th Conference Prague, June 8-11, 2009, Prague, Czech Republic

[14] I. Roytelman, B. K. Wee, R. L. Lugtu: Volt/Var Control for Modern Distribution Management System, IEEE Trans. on Power System, Vol. 10, No. 3, August 1995, pp. 1454-1460

[15] V. Strezoski, N. Katic, D. Janjic: Voltage Control Integrated in Distribution Management Systems, Electric Power Systems Research, No. 60, 2001, pp. 85-97

[16] A. Hamouda, K. Zehar: Improvement of the Power Transmission of Distribution Feeders by Fixed Capacitor Banks, Acta Polytechnica Hungarica, Vol. 4, No. 2, 2007, pp. 47-62

[17] N. Katic, J. Katic: Reduction of Non-technical Power Losses as a Significant Improvement of Utilities' Operation Efficiency, SEEEI 2016, Electricity International Convention, Session TAM X, published in electronic form, Eilat, Israel, December 6-9, 2016

[18] A. Zidan and all: Fault Detection, Isolation and Service Restoration in Distribution Systems: State-of-The-Art and Future Trends, IEEE Transactions on Smart Grid, Volume 8, Issue 5, September 2017, pp. 2170-2185

[19] A. A. Sallam, O. P. Malik: Electric Distribution Systems, John Wiley & Sons, New Jersey, 2011

[20] D. Kirschen, G. Strbac: Power System Economics, John Wiley & Sons, England, 2004

Contact Problems in GaAs-based Solar Cells

Antal Ürmös[1], Zoltán Farkas[1], László Dobos[2], Szilvia Nagy[3], Ákos Nemcsics[1,2]

[1] Institute of Microelectronics and Technology, Óbuda University, Tavaszmező utca 17, H-1084 Budapest, Hungary

[2] Centre for Energy Research, Institute of Technical Physics and Materials Science, Konkoly Thege M. út 29-33, H-1121 Budapest, Hungary

[3] Department of Infocommunications, Széchenyi István University, Egyetem tér 1, H-9026 Győr, Hungary

e-mail: urmos.antal@kvk.uni-obuda.hu, farkas.zoltan@kvk.uni-obuda.hu, nagysz@sze.hu, nemcsics.akos@kvk.uni-obuda.hu

Abstract: The present work deals with contact problems of GaAs-based solar cells. In the introduction the most basic GaAs-based solar cell structures are introduced. Then, the energy and electronic properties are investigated. In the third part of this publication, the technological aspects of the metallization are discussed. Here the surface patterns are investigated, that are formed at the surface of the Au/GaAs and Au/TiN/GaAs material systems, as the effect of the annealing process. The further aim of these investigations to investigate, how the properties of ohmic contact depends on the properties of the material system. If these relations are known, the relationships between different morphologies and their electric qualities will be also known.

Keywords: solar cell; ohmic contacts; surface pattern; fractal dimension; structural entropy

1 Introduction

It is a well known fact that almost all of our energy sources originate with solar radiation, which is a renewable energy. One possible tool to directly utilize solar radiation, is the solar cell. The efficiency of solar cells is strongly influenced by the material band structure of the semiconductor. According to calculations, the optimal band gap is 1.4 eV. Such a material is, for example, GaAs. The efficiency of different solar cell structures may diverge from the theoretical calculations [1] in reality due to losses (thermal, reflection, recombination, etc) or due to cell construction issues (tandem, multiband solar cell, etc) [2].

This efficiency barrier can be surpassed with multiband devices. A limit of such methods of efficiency improvement is the finite number of the different semiconductors that can be integrated in a single solar cell. This newer barrier, in turn, can be surpassed by using multiple heterojunction or nanostructure type GaAs based solar cells. These devices utilize a wider wavelength interval of the solar spectrum.

Solar cells with single heterojunction GaAs-based structures are grown with metal-organic vapor phase deposition, and these solar cells are produced with lithography, heat treating and dry etching technology. The structures of these cells are shown in Fig. 1. The heterojunction is formed on a n-GaAs substrate. First, a buffer layer is grown on the substrate, and then a back surface field is formed. The base and emitter are formed on this layer then a window layer is deposited. The forward contact is a Ti/Pt/Au layer; the hind contact is an AuGe/Ni/Au layer.

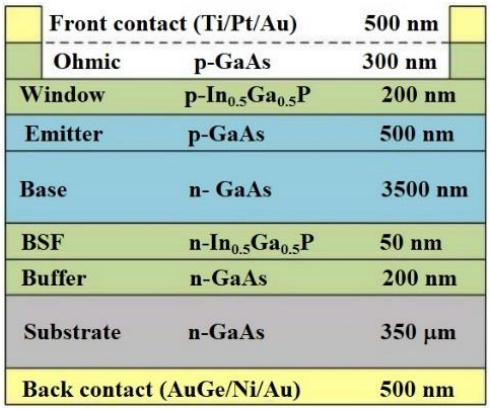

Figure 1
Structure of a single heterojunction GaAs solar cell (source: [3])

There are other possible structures as well. Such a possibility is GaAs thin layer on a flexible subtrate [4] or a sandwich structure of GaAs-Ge layers [5]. The goal regarding the latter structure was to increase the output current with Ge which has almost identical lattice constant than that of GaAs (Fig. 2). The 3 μm thick GaAs layer absorbs the greater proportion of the spectrum of Sun. The other parts of the spectrum is absorbed by Ge layer between 0.9 μm and 108 μm. The greater part of the spectrum is absored by the first 500 nm of the 5 μm thick Ge layer. The charge carriers that were generated in Ge drift to the GaAs layer and they are added to the charge carriers generated there. The quality of Ge and GaAs layers causes longer majority charge carrier lifetime thus the output current increases.

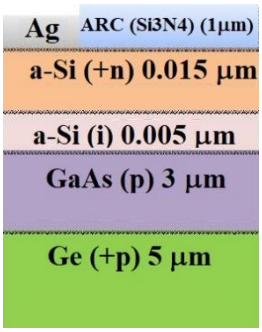

Figure 2
Structure of a single heterojunction ”sandwich” GaAs-Ge solar cell (source: [3])

Multiple heterojunction GaP/GaAs/Ge multiple bands solar cells are grown by metal-organic chemical vapor phase deposition or by molecular beam epitaxy. Multiple junction solar cells constist of single junction solar cells stacked onto each other. The structure of the multiple junction solar cells is such that the band gap of each layer is layer is thinner than that of the previous ones. The efficiency of these solar cells can be as high as 32%.

The group called nanostructure solar cells, is a special subgroup of the multiple junction solar cells [4] [5] [6]. In the case of this special subgroup, multiple qunatum dot layers can be found in the band gap. These devices are referred to as IBQD IBQD - Intermediate Band Quantum Dot Sc. Numerous authors have already published papers on these structures [7] [8] [9] [10] [11]. These quantum dot layers are ”inserted” between the usual p and n layers.

2 Electrical Aspects of the Contact

2.1 Energy Structure at the Contact Function

The contacts are vital parts of the GaAs based solar cells, since the device communictes with the environment through contacts. The III-V based compound semiconductors have several contact systems. The quality of these semiconductor systems play a key importance regarding the operation of solar cells and other electronic devices. The contact systems can be divided into two subcategories: Schottky and Ohmic ones. The latter will be discussed, in detail.

When discussing Schottky-effect the work function of metals is first taken into consideration. The work function is the difference between vacuum level and Fermi level of energy. This energy (exit work) is necessery for an electron to exit the surface of a metal and leave to the free space. The I-V characteristics of a Schottky contact is asymmetric, the Ohmic contact has a linear I-V characteristics, thus the

latter is independent of voltage polarity. In practice, a contact is considered Ohmic, if the voltage drop of metal-semiconductor transition is less than that of the bulk semiconductor. The Ohmic contact can be replaced by Rc contact resistance.

$$R_c = \left(\frac{dJ}{dV}\right)^{-1}\Big|_{V=0} \tag{1}$$

where J is current density and V is the voltage drop. The value of contact resistance in case of medium doped n semiconductor-metal transition is largely determined by thermal emission, thus:

$$R_c = \frac{k_B}{q*A*T} * e^{\frac{q*\Phi_{Bn}}{k_B*T}} \tag{2}$$

Equation (2) demonstrates that if the goal was to attain a low resistance then the lowest potential barrier must be attained at the metal-semiconductor transition. If the Ohmic contact is strongly doped then field emission (tunnel effect) is the dominant component. In the latter case contact resistance can be expressed as

$$R_c \approx e^{\left(\frac{2*\Phi_{Bn}}{h}\right)*\left(\sqrt{\frac{\varepsilon_0*\varepsilon_S*m_0}{N_D}}\right)} \tag{3}$$

Ohmic contact can be constructed several ways [12]. One possible solution is to choose a metal that has less work function than that of the n type semiconductor, thus the potential barrier between the metal and the compound semiconductor is thin enough that the electrons can tunnel through it in both directions. Another possible solution is to prepare a thin strongly doped layer of the same material as that of the substrate. This way a n^{++}/n or a p^{++}/p strongly doped weakly doped transition zone is prepared that decrease the thickness of metal/compound semiconductor potential barrier. Thus, the current flows thru the potential barrier via tunnel effect, because of the thin potential barrier and the low contact resistance. The third possible solution is to ”simulate” gradual heterojunction with small band gap material. This means that n^{++}-InAs/n-GaAs or n^{+}Ge/n-GaAs heterojunctions are formed by MBE technology. The fourth possible solution is to apply a not alloyed superlattice with short lattice constant. This structure contains GaN and small band gap InN layers. The latter is inserted between GaN layers in a sandwich like structure with InN cover layer that forms Ohmic contact with the GaN. The fifth solution is to increase the number of recombination centers on the surface of semiconductors with surface roughening. This way the surface acts as an infinite drain of majority charge carriers of the contact.

In addition to the high energy radiation damage, the incorporation of chemical contaminants into the semiconductor these recomibnation centers may cause the Fermi-level pinning [13] [14] [15]. This phenomenon may occur in bulk material, in the interface layer and on the surface as well.

In bulk material the Fermi-level may move between the valence band and conductance band. Generally electrically active crystal defects influence the Fermi level as well. Crystal defects that act as donors prevent other defects from acting as

acceptors. These defects free electrons and push Fermi level upwards in the band gap, meanwhile other defects trap electrons and push Fermi level downwards.

Forming a clean surface causes discontinuity in the external potential that leads to occurence of surface states. One must differentiate from mathematical point of view between the Shockley and Tamm states. The former stems from the pseudo free electron approximation, whence the latter stems from tight binding approximation. These states occure in high concentration that leads to Fermi-level pinning. The work function is almost independent of the location of bulk Fermi-level (doping level) which may be considered as pinned [16].

The study of Fermi level pinning near the interface is quite complicated, because of the multiple material on one hand and the several growing methods on the other hand. The barrier between the metal and semiconductor can be determined with the Schottky-Mott rule. This rule states that the thickness of the barrier is proportional with the difference of vacuum work function of the metal and the vacuum electron affinity of the semiconductor. This condition, called Schottky limit, is valid if there was no charge transfer between the metal and the semiconductor and there was no Fermi level pinning. Most of the materials do not show the phenomenon, because electric states are formed in the band gap of the semiconductor. These states contribute to charge transfer between the two materials and an electrostatic dipole is formed at the interface. The height of Schottky barrier is independent of work function and the Fermi level may be considered bended in this case. This condition is the Bardeen limit.

2.1.1 I-V Characteristics

The I-V characteristics of Schottky contacts can be measured in several ways. The possible methods are (1) measuring the photo reaction, (2) measuring I-V itself, and (3) and measuring C-V characteristics.

Similarly, the r_c specific contact resistance can be measured with multiple methods. Four ways of the possibilities [17] are (1) Cox-Strack method,(2) four point method, (3) Schockley extrapolation method, (4) transmission line method. In case of constant current density and homogenous surface of contact the R_c contact resistance may be obtained as:

$$R_c = \frac{r_c}{A} \tag{4}$$

The measured R resistance is approximately equal to R_c resistance in case of the most geometry of contact if $r_c \geq 0.01\ \Omega*cm^2$. For smaller values of r_c one must take into consideration the R_b spread resistance of the semiconductor and R_0 resistance of contact wires and the bulk resistance of the substrate of the semiconductor. For this reason the measured R resistance is:

$$R = R_c + R_b + R_0 \tag{5}$$

where R_b and R_0 depends on the geometry of metal/compound semiconductor.

It was supposed in the case of Cox-Strack method, that the contact is a circle with radius a, n-type film layer with specific resistance ρ and thickness of t [17] [18]. The spread reistance of the layer can be calculated as:

$$R_b = \frac{\rho}{a} * F \tag{6}$$

Where F is the function of a/t ratio. Experimentally, it was found that this function is approximately

$$F\left(\frac{a}{t}\right) = \frac{1}{\pi} * arctan\left(\frac{2*t}{a}\right) \tag{7}$$

It may be necessary to determine F more exactly in several cases [19]. If this value is known then the specific contact resistance will be:

$$r_c = \pi * a^2 * \left(R - \frac{\rho}{a} * F\left(\frac{a}{t}\right) - R_0\right) \tag{8}$$

It is necessary to metallize only one side of the slice, when using the four point method for obtaining r_c [20]. The thickness of the layer is t. The layer can be epitaxial layer on semiconductor substrate or uniformly doped bulk material. The specific resistance in this case will be:

$$r_c = \pi * a^2 * \left(\frac{V_1}{l} - \frac{V_1}{l} - \frac{\rho}{a} * F\left(\frac{a}{t}\right)\right) \tag{9}$$

The potential distribution on the surface is rather logarithmic than exponential according to other authors [21]. The specific contact resistance will be in this case:

$$r_c = \pi * a^2 * \left(\frac{V_1}{l} - \frac{V_1}{l} * \frac{\ln\left(\frac{3*s}{2*a} - \frac{1}{2}\right)}{2*\ln 2} - \frac{\rho}{a} * F\left(\frac{a}{t}\right)\right) \tag{10}$$

where v_1 and v_2 are the distance between the measurement point.

The crucial point of the Shokley method [22] [23], that $V(x)$ voltage drop is measured along the surface of the semiconductor layer with coplanar ohmic contacts. The extrapolated V_0 voltage is used through contacts and this way the r_c is found. Due to the R_s sheet resistance the contact resistance is not zero. The current is not distributed uniformly but concentrates under the contacts. The r_c kcontact resistance can be calculated by the extrapolation of linear voltage drop between two contacts, thus

$$r_c = R_b * L_T^2 \tag{11}$$

where L_T is the so called transferlength that in turn can be calculated with the following expression $L_T = -x / ln(V(x)/V_0)$.

The planar contact is considered a resistive power line according to the power line method [24] [25] [26]. The resistance in this model is the can be calculated from a uniform R_s sheet resistance and specific r_c contact resistance. The R_e total resitance can be calculated as:

$$R_e = \frac{(r_c * R_S)^{\frac{1}{2}}}{W} * \coth\left(d * \left(\frac{R_S}{r_c}\right)^{\frac{1}{2}}\right) \tag{12}$$

where W is the width and is the d length of the power line. Since generally $d^* (R_s/R_c)^{-2}$ the r_c contact resistance can be calculated as:

$$r_c = \frac{{R_e}^2 * W^2}{R_S} \tag{13}$$

The I-V characteristics can be visualized on the so-called Gummel plot as well (Fig. 3) [27]. The base and collector current are shown at the same time as a function of base-emitter voltage. The vertical scale (current scale) is logarithmic. A lot of diode paramteres can be calculated using this chart, eg. the DC amplification [28] or the factor of ideality [29]. The value of the latter can imply the presence of recombination centers of volume of those of surface. The recombination centres can cause various problems (eg. Fermi-level pinnings).

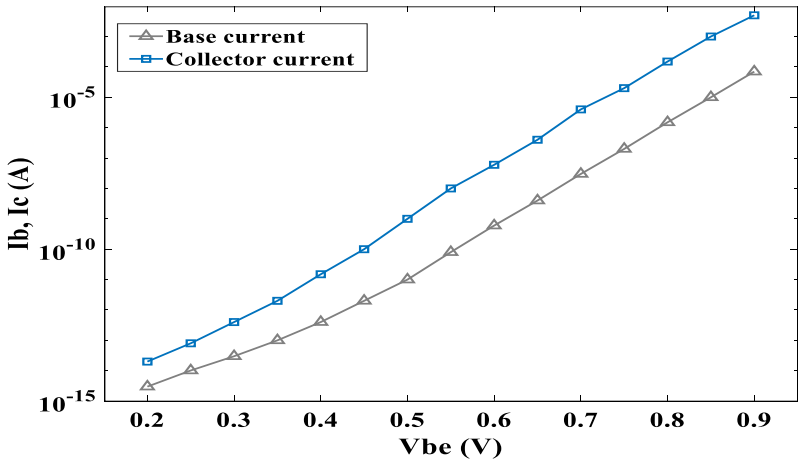

Figure 3
Gummel plot (source: [28])

Another possibility for examining the metal/compound semiconductor transition zone is the capacitance transient spectroscopy [30]. The crucial point of this method is the monitoring temporal change of charge density in the depleted zone of the diode. The thickness of this region is independent of the charge density. The thermal emission of the fixed position charge carriers causes capacitance change in the space-charge. This way information is received on trap states, and trap activation energy, the cross section of trap states and the concetration of traps. The capacitance of depleted layer changes due to thermal emission as follows:

$$C(t) = C_r * \left(1 - \frac{n_{T0}}{2 * N_D} * e^{\left(-\frac{t}{\tau_e}\right)}\right) \tag{14}$$

where the n_{T0} is the density of filled traps at $t = 0$ *sec,* C_r is the capacity of the diode if all the traps are empty at V_r voltage, τ_e is the time constant of emission ($\tau_e = 1 / e_n$, where e_n is the emission ratio). One variety of the process is the SCTS method [31].

Deep-level transient spectroscopy, DLTS is a robust and widely used measuresment method for determining the electrically acitve traps in the semiconductor [32] [33]. The DLTS is a correlation method where the transient of the capacity is multiplied with a correlation function (the signal of reference) and the product will be integrated.

Several parameters can be measure several parameters as the activation energy of defects, the trap cross sections and the density of traps.

There are no measurable surface and induced states and the metal/compound semiconductor transition zone is charge neutral in an ideal case [34]. Unfortunately this is not so in the case of eg. GaAs and several other semiconductor.

3 Technological Aspects of the Contacts

3.1 Metallization

As it was mentioned in section 2.1. the contacts have important role regarding the connection of the device and is environment. This is essential at Ohmic contacts, because in the case of several devices and several circuit applications the examination of physiscal and electric properties of bulk material requres good quality Ohmic contacts [35].

The Ohmic contacts can be fabricated in two ways [36]: (1) any metals deposited onto semiconductor the contact will be Ohmic (in situ ohmic contacts), (2) if the deposited metal is annealed properly then it will be Ohmic. In the latter case it is crucial to take in consideration: (1) the decomposition the surface of GaAs with the possible vaporing of As (2) the deviation in reactivity of GaAs that depends on the initial composition of the compound semiconductor (stochimetric ratio, presence of remaining oxides, contaminations, passivating chemical elements).

The change of I—V characteristics of some Ohmic contacts grown on n-GaAs and p-GaAs will be examined as result of annealing process.

Firstly, contacts made of gold on the surface of GaAs was examined [37]. On such solution is the application of Au-Ge/In Ohmic contacts on n-GaAs substrate [36]. One system of this kind is shown in Fig. 4 before annealing (A) and after annealing at 495 ^{o}C for 5 mintue (B).

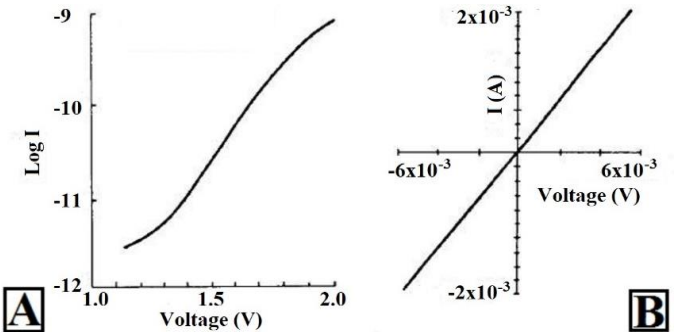

Figure 4
I-V characteristics of Au-Ge/In ohmic contact on n-GaAs substrate before annealing (A) and after annealing at 495 ºC for 5 minutes (B)

A problem is that this metal reacts with GaAs at a relatively low temperature (above 350 °C). Further problems are the occurence of all the three, the parasitic subtrate currents and the deep and shallow trap states [38]. For this reason several other solutions were found to substitute Au metalling.

Cu was used instead of Au in one experiment [39]. A Pd/Ge/Cu metalling was applied to n-type GaAs and Pt/Ti/Pt/Cu metalling was applied to p-type GaAs. A comparision of Au and Cu based metallizationon on n-GaAs (Fig. 5/A) and on p-GaAs (Fig. 5/B) substrate.

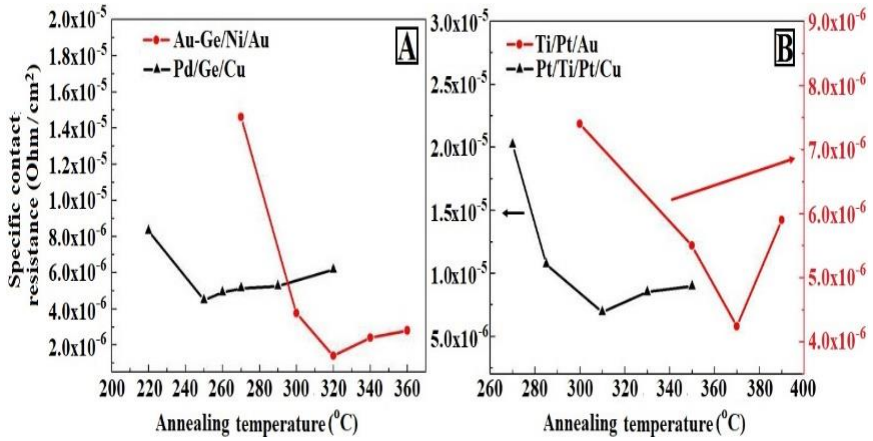

Figure 5
Comparision of Au and Cu metallization on n-GaAs (A) and on p-GaAs (B) substrate (source: [40])

The other possible solution also with Cu is Pd/Ge/Cu metallization on n-GaAs substrate [40]. This paper descibes an experiment annealing in N gas environment for 20 minutes between 150 ºC and 400 ºC. The authors examined the resistance of the contact as a function of annealing temperature with different Pd (Fig. 6/A) and different Ge layer thicknesses (Fig. 6/B).

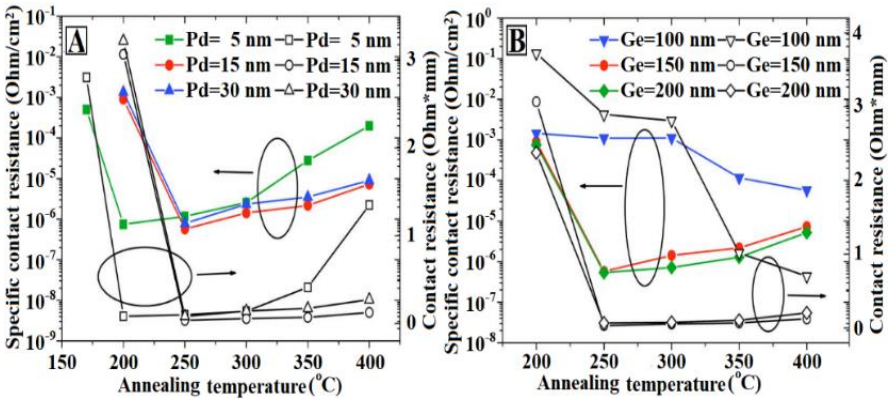

Figure 6

Comparision of Cu based metallizations as a function of thickness of Pd layer (A) and thickness of the Ge layer (B) (source: [41])

A third possible solution, a non-copper based one, is the NiGe metallization on n-GaAs [41]. The authors of this paper examined several samples with different metal layer thickness. Sample 3 shown in Fig. 7 the Ni layer is 75 nm and the Ge layer is 90 nm thick after 5 minutes annealing. The sample shown on Fig. 8 the authors applied 400 °C isoterm annealing and the specifice resistance was measured at identical time intervals. Sample 3 had a Ni layer thickness of 75 nm and that of Ge 90 nm, whence sample 5 had 15 nm thick first Ni layer and 72 nm Ge layer and the second Ni layer was 75 nm.

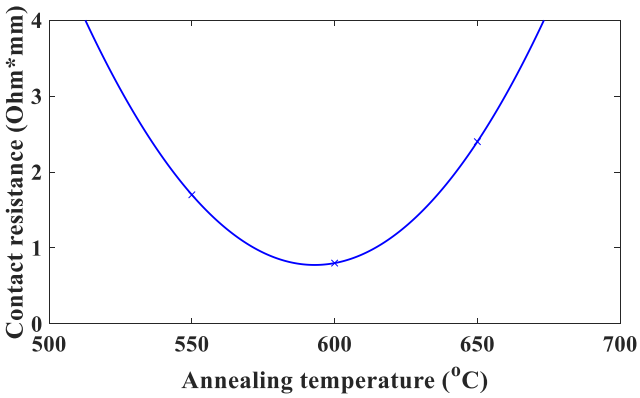

Figure 7

The Ni layer is 75 nm thick and the Ge layer 90 nm thick, after 5 minutes annealing between 550 °C and 650 °C (source: [42])

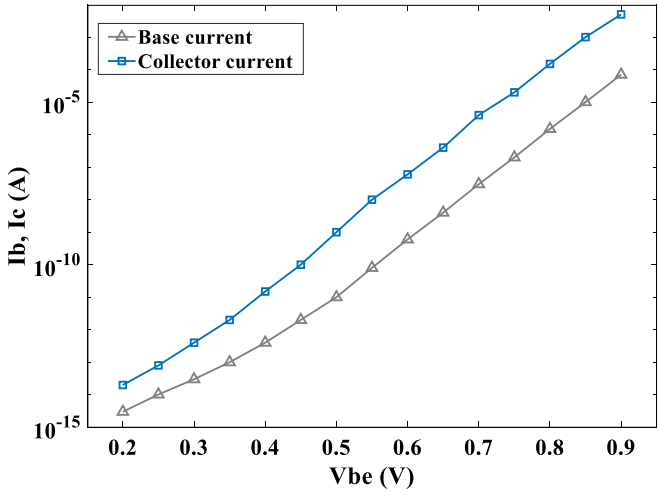

Figure 8

The contact resistance as a function of annealing time period (NiGe metallization), in case of sample 3 and sample 5, in 400 °C isotherm annealing (source: [42])

The fourth possible solution is application of NiSiW metallization [42]. The first Ni layer is 30 nm thick, the Si layer is 40 nm thick, the second Ni layer is 15 nm thick, thus the W layer is 40 nm in sample shown in Fig. 9. The specific contact resistance is shown as a function of temparature of annealing (Fig. 9/A) and as a function of time interval of annealing (Fig. 9/B).

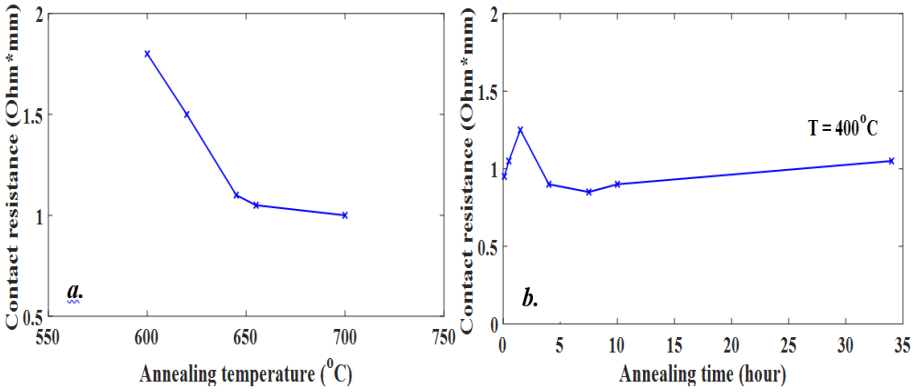

Figure 9

Values of contact resistance as a function of annealing time (NiSiW metallization), 400 °C isotherm annealing. The contact resistance is shown as a function of anneling temperature (A) and as a function of annealing time (B). (source: [42])

The fifth possible solution is application of Pd/Sn metallization on n-GaAs substrate [43]. The authors of the above mentioned paper applied a 32.4 nm thick Pd layer

and a 150 nm thick SN layer as metallization and the time interval of annealing was 30 minutes. The contact resistance- annealing temperature diagram can be seen in Fig. 10.

The sixth possible solution is to apply Pd/Ge metallization on n-GaAs substrate [44]. The sample was annealed for 30 minutes in N gas environment between 200 °C and 250 °C as mentioned in this paper. The contact showed increasingly ohmic characteristics with increasing annealing temperature as shown in Fig. 11/A. The contact resistance-annealing temperature diagram of the same material system is shown in Fig. 11/B.

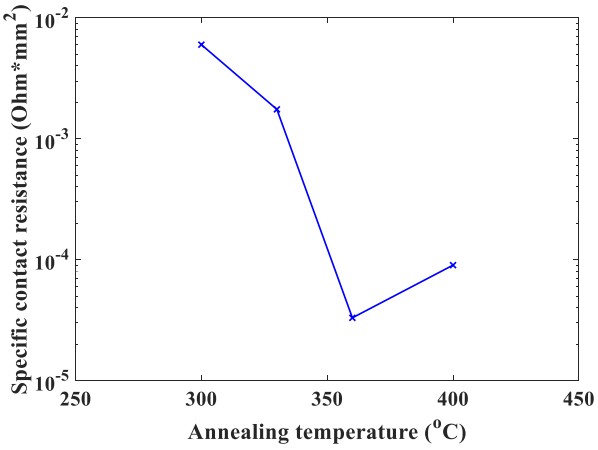

Figure 10

Contact resistance – annealing temperature diagram of Pd/Sn metallization (source: [43])

The selection of the contact material for compound semiconductors and the determining the appropriate thermal profile for different contact metallizations is a problematic area, and several researches are in progress. The main problem is that when a simple metal is used for GaAs metallization the system is instable in terms chemistry and thermal phenomena [45].

During the formation process of contact the extent to which the metal wets the surface under consideration has an important role. The wetting is the attachment ability of liquid phase material to a solid surface. This attachment ability is the macroscopic approach of intermolecular effects [46] [47] [48]. The degree of wetting depends on the balance of adhesive and cohesive forces. Wetting is related to solid, liquid and gasous phases as well. Wetting has an important role when the binding of two different materials is studied. Wetting has two types, reactive and non-reactive [49].

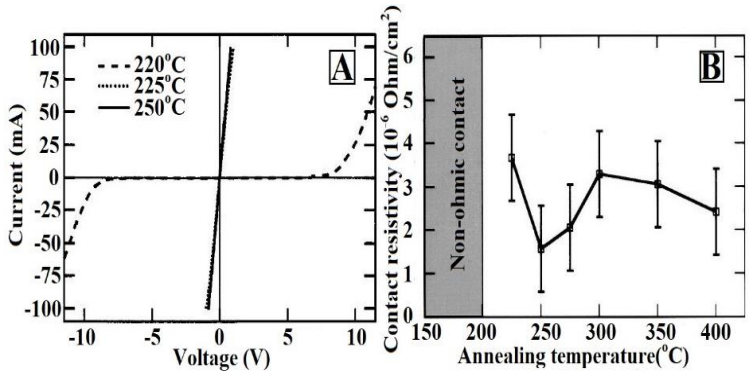

Figure 11
I-V diagram of Pd/Ge metallization with annealing temperature as parameter (A) and the contact resistance as a function of annealing temperature of the material system (B) (source: [44])

The properties of Ohmic contacts depend on the applied material system and the temperature of the applied annealing [50]. For this reason it is necessary to take into consideration two factors when examining the metal/compound semiconductor system during the annealing process [51] [35]. The first factor is the surface decomposition at relatively low temperature. It is the vaporization of volatile component. In case of GaAs the As is the volatile component [52] [53] [54]. The second factor is the varying reactivity of GaAs surface that depends on the initial structure of the substrate (stoichiometry, contaminants, residual oxides and presence of passivating materials). This temperature dependence was examined for material systems of Au/Pd [55], Pd [54], Au/Ge [56] [57] and Au/Ge/Ni [57] [58] [59] [60]. During the annealing process the volatile component evaporates. The volatile component if As in case of GaAs, and P in case of InP [55]. The result of thermal mutual effect in case of a thin layer system and compound semiconductor (eg. InP) was observed by scanning electron microscope [54] [61] [62] [63] [64] [65] [66]. The samples were examined in heated sample holder. Different surface features were produced by different material science processes (eg. Surface migration). The goal of the researchers was to determine the connection between the conditions of interaction, the materials involved and the attributes of the substrate. The temperature dependence of vaporized volatile component was examined in the given experimental arrangement. The amount of the vaporized component was measured by a quadropole mass spectrometer (EGA – evolved gas analysis). The electrical parameters of the fabricated contact were deduced then.

3.2 Geometrical Investigation

The metallization patterns that formed on the surface of GaAs contact can be described by multiple models. These models can be divided into two groups., the continuum and atomic ones. Such a nonlinear continuum model is the Kardar-Parisi-Zhang equation [67] [68] [69]:

$$\frac{\partial h(x,t)}{\partial t} = \upsilon * \Delta h(x,t) + \frac{\lambda}{2} * \left(\nabla h(x,t)\right)^2 + F + \eta(x,t) \tag{15}$$

where ν is the surface tension, t is the time, $h(x,t)$ is the height of interface at point x, λ is the wavelength, F is the incoming atomic flux, the $\eta(x,t)$ is the noise component (flux of the random inbound atoms. Atomic model eg. the so-called Kinetic Monte-Carlo algorithm [70] [71] [72], or the kinetic mean field model [73].

The surface can be charcterized, in addition to surface roughness, in other ways, eg. examining the surface patterns. Many surface pattern investigations are in the literature in case of GaAs substrate [54] [55] [57] and in case of InP substrate [74] [58] [61] as well. The biggest obstacle of the examination is the segmentation of clusters a difficult task to do. The contast may be weak thus it is hard to separate the cluster from the backgroud according to tone tresholds. This problem can be solved in multiple ways, eg. by the GOFM (grade of membership method) [75] [76], or by fractalmathematical methods [77] [78] [79], or by structural entropy [80] [81].

The crucial step of grade of membership method (GOFM) is to separate the surface and the structure with the subsequent function when examining the given surface pattern:

$$G(x) = \frac{1}{\Sigma_{j=1}^{n}\left(\frac{(x-v_i)^2}{(x-v_j)^2}\right)^{\frac{1}{m-1}}} \tag{16}$$

where x is the brightness of the pixel, v_i is the brightness of the pixel in the center of i^{th} cluster, n is the number of the clusters, m is the membership weight.

The surface patterns can be analysed by fractal theory as well. The fractals are infinitely complex, in terms of statistics „self similar", mathematical objects. In the countless different formation of fractals, there is at least one repetition that can be described by mathematical toolset [77] [78] [79].

The analyses utilizing the fractal theory can be found in [62] [74]. These analyses are based on in situ SEM images of the surface of contacts during the annealing process. These pictures were taken by L. Dobos et al, in a converted SEM. They provided the technical possibility of fast annealing processes at maximum of 700 °C. Bitmap (BMP) files were obtained by digitalizing SEM images. Further, the BMP images were processed by software [63].

The surface of a given, non-continuous thin layer is considered to be of fractal pattern if the black and white image of the surface has dimension between 1 and 2. The more regular and the more complete the coverage of the plane, the closer the dimension gets to 2.

The most widespread method of measurement of fractal dimensions of fractals in terms of mathematics (eg. bicolor images) is the so-called box-counting methodology elaborated by B. Mandelbrot [82] and Hausdorff [83].

In the course of our research Au, Pd and Au/Pd thin layers were deposited onto InP surface [74]. The data of the material system can be found in Table 1.

Table 1
The data of the examined material system

Orientation of substrate	Au/InP(111)	Pd/InP(100)	Au/Pd InP(100)
Layer thickness [nm]	60	50	85/50

Our goal was to thoroughly examine the surface morphology of Au, Pd and Au/Pd layers in terms of fractal patterns.

During the research the original records were cut. During the next step the records were converted to binary format according to Hausdorff measure. The boxes of diameter n necessary to cover the white pixels, were counted. This step was repeated with boxes of diameters of *n/2*, and so on until boxes of one pixel were reached.

If the logarithm of box count is plotted on a diagram as a function of number of the steps and a line is matched onto these points, then the fractal dimension is obtained.

In addition to fractal geometry, the same surfaces were examined by both filling factor and structural entropy methods. The structural entropy [80] [81] [84] [85] determines the localization type of probability distribution defined on lattices. In other words, this method defines the function according which the agglomerations of the probability distribution fade.

Let us have *n* lattice points of which only *m* points are filled. The filling factors are identical $p_i = 1/m$ and these values are $p_i = 0$ for the rest of lattice points. The structural entropy is that part of the entropy of the system which tells us accordingly, which functions, in the filled lattice, points decay. The shape of the fading is characterized by structural entropy which has the algebraic expression:

$$S_{str} = s - \ln d = \sum_{i=1}^{n} p_i * \ln p_i - ln \frac{1}{\sum_{i=1}^{n} p_i^2} \tag{17}$$

In case of two valued step like distribution the value will be zero because the Shannon entropy will be exactly *ln d*. For this reason, these calculations were carried out on grayscale images.

A variable that indicates the mean filling of a lattice point was introduced:

$$q = \frac{d}{n} = \frac{1}{n \sum_{i=1}^{n} p_i^2} \tag{18}$$

This variable is the filling ratio. If structural entropy was plotted as a function of filling ratio then it is observed that the graph of each fading functions (eg. the Gaussian function, the power functions etc.) is a well-defined curve on the $Q - S_{str}$ plane. If it was examined that which function fits the point of the distribution, then the type of fading can be determined [80] [86]. The underlying theory is detailed is [81]. The shaded area can be characterized by inequalities $0 < q < 1$ and $0 < S_{str} <$

-log q (Fig. 12). The structural entropy and localization factor can be used for analysis of AFM and in addition to, SEM records [87] [90].

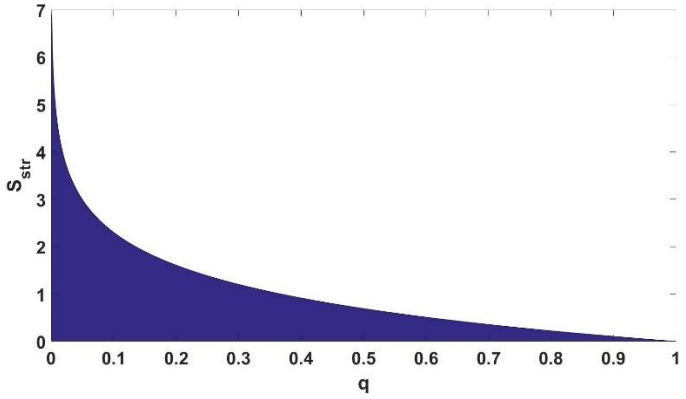

Figure 12

Allowed region of structural entropy plot

In the Fig. 13 the surface of the Au (60 nm) layer on GaAs (100) substrate (Fig. 13/a) at 400 ºC temperature, (Fig. 13/b) at 500 ºC temperature (Fig. 13/c) at 630 ºC temperature (magnitude is 500x).

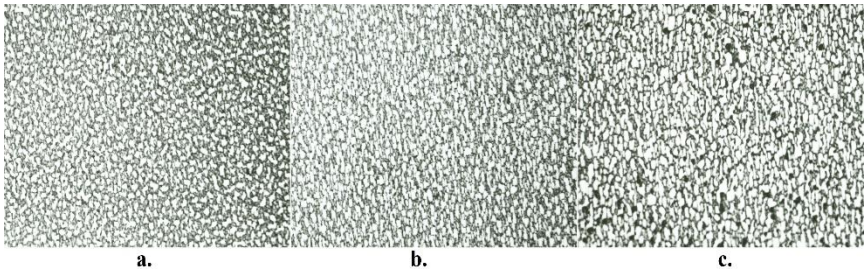

Figure 13

The surface of the Au (60 nm) layer on GaAs (100) substrate (a) at 400 ºC temperature, (b) at 500 ºC temperature, (c) at 630 ºC temperature (magnitude: 500x)

In the next two subchapters the Au/GaAs and Au/TiN/GaAs material systems are characterized by fractal dimension and by structural entropy as well.

3.2.1 Au/GaAs Material System

In the Au/GaAs system, the change of the fractal dimensions is shown in the Fig. 14, between 440 ºC and 600 ºC. In case of Fig. 14/b, the width of the Au layer is 40 nm and the fractal dimension decreases significantly in the function of the temperature. In case of Fig. 14/b the width of the Au layer is 60 nm and the fractal dimension is nearly constant. Probably the reason of this phenomena is the decreasing of the fractal dimension, which is caused by the evaporation of the illicit

component of the substrate (this is the As component, in case of GaAs). As it is shown in the Fig. 14, in case of the 40 nm Au layer thickness (Fig. 14/a), the evaporation of the illicit component is larger than in the case of the 60 nm Au layer (Fig. 14/b). According to this result, this phenomenon depends on the thickness of the Au layer.

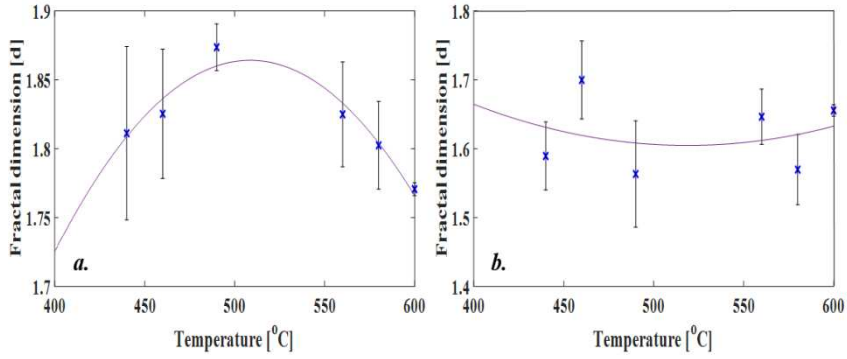

Figure 14
The change of the fractal dimension between 440 ºC and 600 ºC.
The width of the Au layer is (a) 40 nm and (b) 60 nm.

In Fig. 15, the structural entropy is shown, in case of 40 nm (Fig. 15/a) and in case of 60 nm (Fig. 15/b) Au layer width. The investigated temperature is 500 ºC. Based on Fig. 15, it is apparent, that the decay of the structural entropy is slower than the Gaussian function.

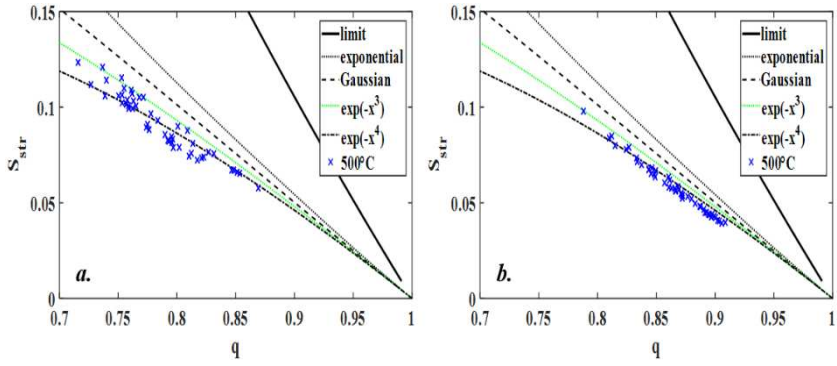

Figure 15
The structural entropy of the Au/GaAs system in 500 ºC temperature.
The width of the Au layer is (a) 40 nm and (b) 60 nm.

As it is visible in the Fig. 16, the localization factor between 440 ºC and 600 ºC also depends on the width of the Au layer. In case of the Fig. 16/b (60 nm Au layer width) the steepness is twice lager as the Fig. 16/a (40 nm Au layer width), between 440 ºC and 472 ºC, 472 ºC and 504 ºC, 504 ºC and 536 ºC.

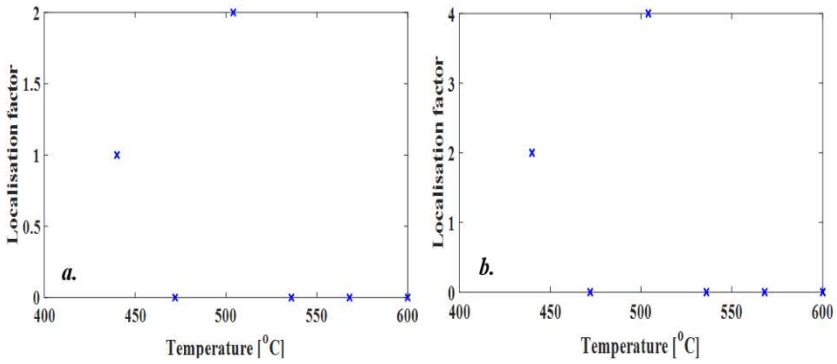

Figure 16
The change of the localization factor between 440 ºC and 600 ºC.
The width of the Au layer is (a) 40 nm and (b) 60 nm.

3.2.2 The Au-TiN/GaAs Material System

As it is shown in the Fig. 17/a, the fractal dimension in the 15 nm thick Au-TiN/GaAs layer is increasing in the function of the temperature. Unfortunately, the reason of this phenomenon is not known. In the Fig. 17/b, the fractal dimension decreases in the function of the temperature. The width of the Au-TiN layer is 25 nm, unfortunately more samples were not available.

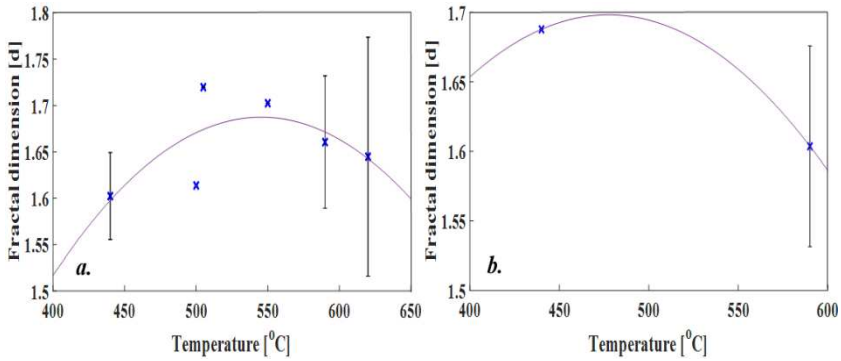

Figure 17
The change of the fractal dimension between 440 ºC and 600 ºC.
The width of the Au-TiN layer is (a) 15 nm and (b) 25 nm.

Similar to the previous material system, in the Fig. 18 it is also visible, that the structural entropy depends on the width of the TiN layer. The investigated temperature is 500 ºC. It is apparent, that the decay of the exponential curves structural entropy decays as a Gaussian (Fig. 18/b) or third-order exponential function (Fig. 18/a).

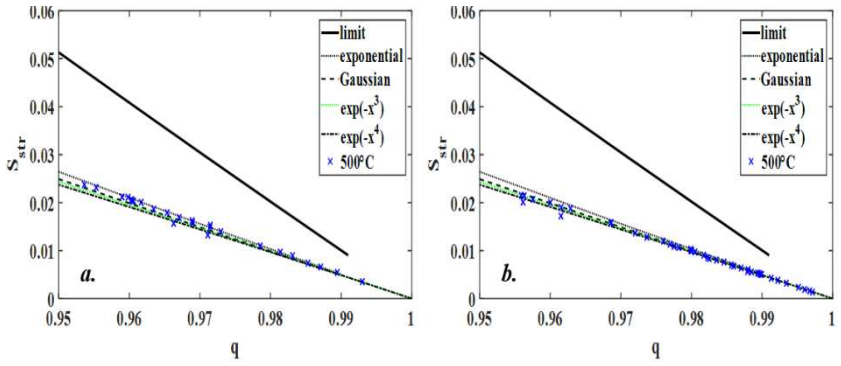

Figure 18

The structural entropy of the Au-TiN/GaAs in 500 °C.

The width of the Au-TiN layer is (a) 15 nm and (b) 25 nm.

As it is visible in the Fig. 19, the localization factor of the 15 nm thick Au-TiN/GaAs material system is third-order (Fig. 19/a). The localization factor of the 25 nm thick Au-TiN/GaAs material system is Gaussian (Fig. 19/b). The values of the localization factors are constant, so – in the investigated temperature range – of the localization factors are independent from the temperature.

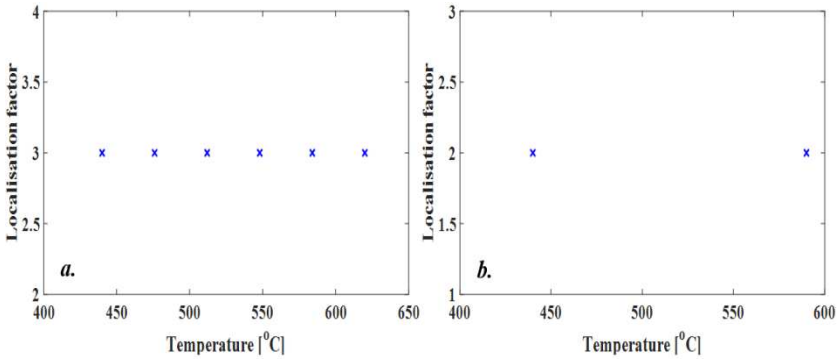

Figure 19

The change of the localization factor between 440 °C and 600 °C.

The width of the Au-TiN layer is (A) 15 nm and (B) 25 nm.

Conclusion

This paper focused on the electric and morphologic attributes of metal/compound semiconductor contacts. Detailed results were presented on electric qualities of Ohmic and Schottky contacts, on measurement technology and on different types of metallization, after the introduction. An examination of patterns on the surface of metallization was also explored. With the fabrication of solar cells in mind, the crucial point is the formation of internally homogeneous Ohmic contacts. The electric features and factors of lateral inhomogenity were summarized and the

obtained morpphologies were examined. The next phase of our work will be the relationships of different morphologies and their electric qualities.

References

[1] K. Kim, H-D. Nguyen, S. Mho, J. Lee, "Enhanced Efficiency of GaAs Single-Junction Solar Cells with Inverted-Cone-Shaped Nanoholes Fabricated Using Anodic Aluminum Oxide Masks," *International Journal of Photoenergy*, Vol. 2013, pp. 1-5, April 2013

[2] S. Moon, K. Kim, Y. Kim, J. Heo; J. Lee, "Highly efficient single-junction GaAs thin-film solar cell on flexible substrate," *Scientific Reports*, Vol. 6, p. 30107, February 2016

[3] N. Al Wahshi, A. Nayfeh, "Single junction GaAs - Ge stacked tandem cell," in *IEEE*, Denver, CO, USA, 2014, pp. 0295-0298

[4] M. Yamaguchi, T. Takamoto, K. Araki, N. Ekins-Daukes, "Multi-junction III-V solar cells: Current status and future potential," *Solar Energy*, Vol. 79, No. 1, pp. 78-85, July 2005

[5] S. Hegedus A. Luque, Ed., *Handbook of Photovoltaic Science and Engineering*, 2nd ed. England: Wiley, 2010

[6] J. Poortmans, V. Arkhipov, *Thin film solar cells: fabrication, characterization and applications*.: NJ:Wiley, 2006

[7] A. Luque, A. Martí, C. Stanley, "Understanding intermediate-band solar cells," *Nature Photonics*, Vol. 6, pp. 146-152, February 2012

[8] T. Noda, T. Mano, M. Elborg, K. Mitsuishi, K. Sakoda, "Fabrication of a GaAs/AlGaAs Lattice-Matched Quantum Dot Solar Cell," *J. Nonlinear Optic. Phys. Mat.*, Vol. 19, No. 4, pp. 681-686, 2010

[9] A. Benahmed, A. Aissat, A. Benkouider, J. P. Vilcot, "Modeling and simulation of InAs/GaAs quantum dots for solar cell applications," *Optik - International Journal for Light and Electron Optics*, Vol. 127, No. 7, pp. 3531-3534, April 2016

[10] C. Kerestes, S. Polly, D. Forbes, C. Bailey, A. Podell, J. Spann, P. Patel, B. Richards, P. Sharps, S. Hubbard, "Fabrication and analysis of multijunction solar cells with a quantum dot (In)GaAs junction," *Progress in Photovoltaics Research and Applications*, Vol. 22, No. 11, pp. 1172-1179, 2013

[11] Ákos Nemcsics, "Novel Alternative for the GaAs-based Self-organized Quantum-structure," *Óbuda University e-Bulletin*, pp. 193-199, 2011

[12] Li, Sheng S., "Metal–Semiconductor Contacts," in *Semiconductor Physical Electronics*.: Springer, 2006, pp. 2084-333

[13] D. Colleoni, G. Miceli, A. Pasquarello, "Origin of Fermi-level pinning at GaAs surfaces and interfaces," *J. Phys. Condens. Matter*, Vol. 26, No. 49, p. 492202, 2014

[14] M. D. Pashley, K. W. Haberern, R. M. Feenstra, P. D. Kirchner, "Different Fermi-level pinning behavior on n- and p-type GaAs(001)," *Phys. Rev. B*, Vol. 48, p. 4612, August 1993

[15] W. E. Spicer, N. Newman, C. J. Spindt, "‘‘Pinning’’ and Fermi level movement at GaAs surfaces and interfaces," *Journal of Vacuum Science & Technology A: Vacuum, Surfaces, and Films*, Vol. 8, pp. 2084-2089, 1989

[16] A. Zangwill, *Physics at Surfaces*. Cambridge, United Kingdom: Cambridge University Press, 1988

[17] G. Y. Robinson, "Schottky Diodes and Ohmic Contacts for the III-V Semiconductors," in *Physics and Chemistry of III-V Compound Semiconductor Interfaces*. New York and London, USA: Springer, 1985, pp. 73-163

[18] R. H. Cox, H. Strack, "Ohmic contacts for GaAs devices," *Solid-State Electronics*, Vol. 10, No. 12, pp. 1213-1218, December 1967

[19] R. D. Brooks, H. G. Mathes, "Spreading resistance between constant potential surfaces," *Bell Syst. Tech. J.*, Vol. 50, pp. 775-784, 1971

[20] L. E. Terry; R. W. Wilson, "Metalization systems for Si integrated circuits," *Proc. IEEE*, Vol. 57, pp. 1580-1586, 1969

[21] E. Kuphal, "Low resistance ohmic contacts to n- and p-InP," *Solid-State Electron.*, Vol. 24, pp. 69-78, 1981

[22] A. Goetzberger; R. M. Scarlett;, "Research and Investigation of Inverse Epitaxial UHF Power Transistor," Palo Alto, CA : NTIS Distributor, Palo Alto, CA, 1964

[23] P. L. Hower, W. W. Hooper, B. R. Cairns, R. D. Fairmen, D. A. Tremere, "The GaAs field-effect transistor," in *Semiconductors and Semimetals*, A. C. Beer R. K. Willardson, Ed. New York: Academic Press, 1973, Vol. 7, Ch. 3, pp. 147-200

[24] H. H. Berger, "Models for contacts to planar devices," *Solid-State Electron.*, Vol. 15, pp. 145-158, 1972

[25] H. H. Berger, "Contact resistance and contact resistivity," *]. Electrochem. Soc.*, Vol. 119, pp. 507-514, 1972

[26] H. H. Berger, "Contact resistance on diffused resistors," *Digest of Technical Papers*, Vol. 12, pp. 160-161, 1969

[27] A. S. Zoolfakar, N. A. Shahrol, "Modelling of NPN Bipolar Junction Transistor Characteristics Using Gummel Plot Technique," *2010 International Conference on Intelligent Systems, Modelling and Simulation*, pp. 396-400, 2010

[28] Z. Yu; R. W Dutton, "Gummel plot nonlinearities in polysilicon emitter transistors—Including negative differential resistance behavior," *IEEE Electron Device Letters*, Vol. 6, No. 10, pp. 507-509

[29] R. Ivental, L. Green, *Semiconductor Modelling*, 1st ed., 2006

[30] G. L. Miller, D. V. Lang, L. C. Kimerling, "Capacitance Transient Spectroscopy," *Annual Review of Materials Science*, pp. 377-448, 1977

[31] A. L. Tóth, L. Dózsa, J. Gyulai, F. Giannazzo, V. Raineri, "SCTS: scanning capacitance transient spectroscopy," *Materials Science in Semiconductor Processing*, Vol. 4, No. 1-3, pp. 89-91, 2001

[32] D. V. Lang, "Deep- level transient spectroscopy: A new method to characterize traps in semiconductors," *Journal of Applied Physics*, Vol. 45, No. 7, p. 3023, 1974

[33] G. Papaioannou, G. Kiriakidis, A. Georgakilas, A. Christou, "Comprehensive Investigation of Traps in GaAs/AlGaAs Heterostructures and Superlattices by DLTS," *MRS Proceedings*, Vol. 144, 1988

[34] J. M. Woodall, J. L. Freeouf, "GaAs metallization: Some problems and trends," *Journal of Vacuum Science and Technology*, Vol. 19, No. 3, pp. 794-798, 1981

[35] A. Piotrowska, "Ohmic Contacts to GaAs: Fundamentals and Practice," *Acta Physica Polonica A*, Vol. 84, No. 3, pp. 491-504, 1993

[36] N. Braslau, "Contact and metallization problems in GaAs integrated circuits," *Journal of Vacuum Science & Technology A: Vacuum, Surfaces, and Films*, Vol. 4, p. 3085, 1986

[37] W. O. Barnard, "Au-Ge/In ohmic contacts to n-type GaAs," *Thin Solid Films*, Vol. 165, No. 1, pp. 77-82, 1988

[38] L. F. Eastman, "Semi- insulating GaAs substrates for integrated circuit devices: promises and problems," *Journal of Vacuum Science and Technology*, Vol. 16, No. 6, pp. 2050-2053, 1979

[39] C. -H. Hsu, H. -J. Chang, H.-W. Yu, H. Q. Nguyen, E. Y. Chang, "Gold-Free Fully Cu-Metallized InGaP/InGaAs/Ge multi-junction solar cell," in *International Conference on Solid State Devices and Materials*, Fukuoka, Japan, 2013, pp. 1153-1153

[40] K. -S. Chen, E. Y. Changa, C. -C. Lin, C. -S. Lee, W. -C. Huang, C. -T. Lee, "A Cu-based alloyed Ohmic contact system on n-type GaAs," *Appl. Phys. Lett.*, Vol. 91, p. 233511, 2007

[41] K. Tanahashi, H. J. Takata, A. Otuki, M. Murakami, "Thermally stable nongold Ohmic contacts to ntype GaAs. I. NiGe contact metal," *Journal of Applied Physics*, Vol. 72, p. 4183, 1992

[42] H. J. Takata, K. Tanahashi, A. Otsuki, H. Inui, M. Murakami, "Thermally stable nongold Ohmic contacts to ntype GaAs. II. NiSiW contact metal," *Journal of Applied Physics*, Vol. 72, p. 4191, 1992

[43] M. S. Islam, P. J. McNally, D. C. Cameron, P. A. F. Herbert, "Properties of Pd/Sn Ohmic contacts on n-GaAs," *Journal of Materials Processing Technology*, Vol. 77, pp. 42-49, 1998

[44] M. L. Lovejoy, A. J. Howard, K. R. Zavadil, D. J. Rieger, R. J. Shul, "Low resistivity ohmic contacts to moderately doped n- GaAs with low-temperature processing," *Journal of Vacuum Science & Technology A: Vacuum, Surfaces, and Films*, Vol. 13, p. 758, 1995

[45] S. S. Lau, W. X. Chen, E. D. Marshall, C. S. Pai, "Thermal and chemical stability of Schottky metallization on GaAs," *Appl. Phys. Lett*, Vol. 47, No. 12, p. 1298

[46] E. O. Hall, *Interfacial Phenomena in Metals and Alloys*, 1st ed. New York, USA: Plenum Press, 1970

[47] A. M. Cazabat, "Wetting from macroscopic to microscopic scale," *Advances in Colloid and Interface Science*, Vol. 42, pp. 65-87, 1992

[48] K. Kendall, "Energy Analysis of Adhesion," in *The Mechanics of Adhesion*, D.A. Dillard, Ed. New York: Elsevier, 2002, pp. 77-110

[49] O. Dezellus, N. Eustathopoulos, "Fundamental issues of reactive wetting by liquid metals," *Journal of Materials Science*, Vol. 45, No. 16, pp. 4256-4264, 2010

[50] A. Piotrowska, A. Guivarch, G. Pelous, "Ohmic contacts to III–V compound semiconductors: A review of fabrication techniques," *Solid-State Electronics*, Vol. 26, No. 3, pp. 179-197, 1983

[51] I. Mojzes, R. Veresegyházy, B. Pécz, B. Kovács , "Thermal decomposition of compound semiconductors covered with thin metallic layers ," *PERIODICA POLYTECHNICA SER. EL. ENG.*, Vol. 35, No. 4, pp. 135-249, 1991

[52] L. Dobos, B. Kovács, I. Mojzes, V. Malina, B. Pécz (a1), J. Karányi, "The Volatile Component Loss and the Surface Morphology of the Gold-Palladium Metallizations to the Compound Semiconductor Structures," *MRS Proceedings*, Vol. 260, 1992

[53] I. Mojzes, R. Veresegyházy. B. Kovács, B. Pécz, "Metal film barriers against the evaporation of volatile components during the heat treatment of metal-compound semiconductor contacts," *Thin Solid Films*, Vol. 164, pp. 1-4, 1988

[54] I. Mojzes, V. Malina, L. Dobos, J. Karányi, B. Pécz, B. Kovács, "PALLADIUM BASED CONTACTS TO GaAs AND InP," *Period. Polytech. Elec. Eng.*, Vol. 37, No. 1, pp. 21-30, 1993

[55] B. Pécz, R. Veresegyházy, I. Mojzes, G. Radnóczi, A. Sulyok, V. Malina, "Thermal Behaviour of Au/Pd/GaAs Contacts," *MRS Proceedings*, Vol. 181, 1990

[56] B. Pécz, E. Jároli, G. Radnóczi, R. Veresegyházy, I. Mojzes, "Pyramidal pit formation at the Au/GaAs interface during heat treatment," *Phys. Stat. Sol. A, 94: 507-513*, Vol. 94, pp. 507-513

[57] A. K. Rai, R. S. Bhattacharya, "Alloying behavior of gold, Au-Ge and Au-Ge-Ni on GaAs," *Thin Solid Films*, Vol. 114, No. 4, pp. 379-398, 1984

[58] D. G. Ivey; D. Wang; D. Yang; R. Bruce; G. Knight, "Au/Ge/Ni ohmic contacts to n-Type InP," *Journal of Electronic Materials*, Vol. 23, No. 5, pp. 441-446, 1994

[59] R. A. Bruce, G. R. Percy, "An improved Au/Ge/Ni ohmic contact to n-type GaAs," *Solid-State Electronics*, Vol. 30, No. 7, pp. 729-737, 1987

[60] M. Wittmer, R. Pretorius, J.W. Mayer, M-A. Nicolet, "Investigation of the Au-Ge-Ni system used for alloyed contacts to GaAs," *Solid-State Electronics*, Vol. 20, No. 5, pp. 433-436, 1977

[61] I. Mojzes, B. Kovács, M. Schuszter, I. Kun, L. Máté, L. Dobos, L. Dávid, "Fractal behaviour of the surface of in situ heat treated metal–InP contacts," *Thin Solid Films*, Vol. 317, No. 1-2, pp. 69-71, 1998

[62] L. Dávid; L. Dobos; B. Kovács; I. Mojzes; B. Pécz, "Fractal character of in situ heat treated metal-compound semiconductor contacts," *Journal of Materials Science: Materials in Electronics*, Vol. 17, No. 4, pp. 321-324, 2006

[63] M. Schuszter, Z. Bodnár, L. Dobos, I. Mojzes, "Surface fractal phenomena observed in the investigation of compound semiconductors," *Fizikai Szemle (In Hungarian)*, Vol. LI, p. 80, Marcius 2001

[64] I. Mojzes, B. Kovacs, I. Kun, L. Mate, M. Schuszter, L. Dobos, "Surface pattern formation and the volatile component loss of heat treated metallisations of InP," in *IEEE*, Sinaia, Romania, 1996, pp. 629-632

[65] I. Mojzes, R. Veresegyházy, "Thermal dissociation of InP covered with metallic contact layers," *Thin Solid Films*, Vol. 144, No. 1, pp. 29-40, 1986

[66] F. Riesz, L. Dobos, C. Vignali, C. Pelosi, "Thermal decomposition of InP surfaces: volatile component loss, morphological changes, and pattern formation," *Materials Science and Engineering: B*, Vol. 80, No. 1-3, pp. 54-59, 2001

[67] M. Kardar, G. Parisi, Y.-C. Zhang, "Dynamic Scaling of Growing Interfaces," *Phys. Rev. Lett.* , Vol. 56, p. 889, 1986

[68] A. Ballestad, T. Tiedje, J.H. Schmid, B.J. Ruck, M. Adamcyk, "Predicting GaAs surface shapes during MBE regrowth on patterned substrates," *Journal of Crystal Growth*, Vol. 271, No. 1-2, pp. 13-21, 2004

[69] Albert-Laszlo Barabasi and Harry Eugene Stanley, "Kardar-Parisi-Zhang equation," in *Fractal concepts in surface growth*. ISBN 978-0-521-48318-6, Uk: Cambridge University Press, 1995, ch. 6

[70] L. Nurminen, A. Kuronen, K. Kaski, "Kinetic Monte Carlo simulation of nucleation on patterned substrates," *Phys. Rev. B*, Vol. 63, No. 3, p. 035407, December 2000

[71] W. Miller, "Simulation of Epitaxial Growth by Means of Density Functional Theory, Kinetic Monte Carlo, and Phase Field Methods," in *Handbook of Crystal Growth: Fundamentals (Volume I, Part A: Thermodynamics and Kinetics)* 2nd ed. New York: Elsevier B.V, 2015, pp. 521-559

[72] M. Biehl, "Lattice gas models and Kinetic Monte Carlo simulations of epitaxial growth," in *Birkhäuser Basel*, Vol. 149, ISNM International Series of Numerical Mathematics, 2004, pp. 3-18

[73] Z. Erdélyi, M. Pasichnyy, V. Bezpalchuk, J. J. Tomán, B. Gajdics, A. M. Gusak, "Stochastic kinetic mean field model," *Computer Physics Communications*, Vol. 204, pp. 31-37, July 2016

[74] Antal Ürmös, Szilvia Nagy, Imre Mojzes Bernadett Varga, "Fractal properties of gold, paladium and gold-palladium thin films on InP," *Vacuum*, 2009

[75] Á. Nemcsics, M. Schuszter, L. Dobos, P. Turmezei, "Image processing in the material science or fractal behaviour on the GaAs/electrolyte interface," in *6th International Symposium on Intelligent Systems and Informatics,* Subotica, Serbia, 2008, pp. 1-3

[76] Á. Nemcsics, M. Schuszter, L. Dobos, P. Turmezei, "Investigation of Electrochemically Etched GaAs (001) Surface with the Help of Image Processing," *Acta Polytechnica Hungarica*, Vol. 6, No. 1, pp. 95-102, 2009

[77] T. Vicsek, *Fractal Growth Phenomena*, 2nd ed. Singapore, New Jersey: World Scientific, 1992

[78] T. Vicsek, *Fractals in Natural Sciences*, 1st ed., M. Shlesinger, M. Matsushita T. Vicsek, Ed. Singapore, New Yersey: World Scientific, 1994

[79] F. Family, T. Vicsek, *Dynamics of Fractal Surfaces*, F. Family and T. Vicsek, Ed. Singapore, New Jersey: World Scientific, 1991

[80] J. Pipek, I. Varga, "Mathematical characterization and shape analysis of localized, fractal, and complex distributions in extended systems," *International Journal of Quantum Chemistry*, Vol. 51, No. 6, pp. 539-553, 1994

[81] J. Pipek, I. Varga, "Universal classification scheme for the spatial-localization properties of one-particle states in finite d-dimensional systems," *Phys. Rev. A*, Vol. 46, p. 3148, 1992

[82] B. Mandelbrot, *The Fractal Geometry of Nature*. New York: W. H. Freeman, 1982

[83] F. Hausdorff, "Dimension und äusseres Mass," *Mathematische Annalen*, Vol. 79, No. 1, pp. 157-179, 1918

[84] I. Varga, J. Pipek, "Rényi entropies characterizing the shape and the extension of the phase space representation of quantum wave functions in disordered systems," *Phys. Rev. E.*, Vol. 68, p. 026202, 2003

[85] I. Varga, J. Pipek, "The generalized localization lengths in one-dimensional systems with correlated disorder," *Journal of Physics: Condensed Matter*, Vol. 10, No. 2, pp. 305-331, 1998

[86] J. Pipek, I. Varga, "Scaling behavior of energy functionals of highly complex electron distributions," *International Journal of Quantum Chemistry*, Vol. 70, No. 1, pp. 125-131, 1998

[87] A. Bonyár, L. M. Molnár, G. Harsányi, "Localization factor: A new parameter for the quantitative characterization of surface structure with atomic force microscopy (AFM)," *Micron*, Vol. 43, No. 2-3, pp. 305-310, 2012

[88] L. Dobos ; I. Mojzes ; M. Schuszter, "Fractal behaviour of in situ heat treated metal-compound semiconductor structures," in *IEEE*, 1997, pp. 229-232

[89] Sz. Nagy, I. Mojzes L. M. Molnár, "Structural entropy in detecting background patterns of AFM images," *Vacuum*, Vol. 84, pp. 179-183, 2009

[90] J. Eun, J. A. Cooper Jr, "High Temperature Ohmic Contact Technology to N-Type GaAs," Purdue University, ECE Technical Reports, 1993

[91] Jialin Zheng,Wei Zhuang, Nian Yan, Gang Kou, Hui Peng, Clancy McNally, David Erichsen, Abby Cheloha, Shelley Herek, Chris Shi, Yong Shi, "Classification of HIV-I-Mediated neuronal dendritic and synaptic damage using multiple criteria linear programming," *Neuroinformatics*, Vol. 2, No. 3, pp. 303-326, 2004

[92] Claudiu Pozna, Nicuşor Minculete, Radu-Emil Precup, László T. Kóczy, Áron Ballagi, "Signatures: Definitions, operators and applications to fuzzy modeling," *Fuzzy Sets and Systems*, Vol. 201, pp. 86-104, 2012

[93] Jian Sheng Guan, Lo Yi Lin, Guo Li Ji, Chih Min Lin, Tien Loc Le, Imre J. Rudas, "Breast tumor computer-aided diagnosis using self-validating cerebellar model neural networks," *Acta Polytechnica Hungarica*, Vol. 13, No. 4, pp. 39-52, 2016

[94] Sasa Vrkalovic, Teodor-Adrian Teban, Ioan-Daniel Borlea, "Stable Takagi-Sugeno fuzzy control designed by optimization," *International Journal of Artificial Intelligence*, Vol. 15, No. 2, pp. 17-29, 2017

[95] A. G. Baca, F. Ren, J. C. Zolper, R. D. Briggsa, S. J. Peartonc, "A survey of ohmic contacts to III-V compound semiconductors," *Thin Solid Films*, Vol. 308-309, pp. 599-606, 1997

External Motivation, the Key to Success in the MOOCs Framework

Žolt Namestovski[1], Lenke Major[1], György Molnár[2], Zoltán Szűts[2], Péter Esztelecki[3], Gábor Kőrösi[3]

[1]University of Novi Sad, Teacher Training Faculty, Štrosmajerova 11, 24000 Subotica, Serbia, zsolt.namesztovszki@magister.uns.ac.rs, major.lenke@magister.uns.ac.rs

[2]Budapest University of Technology and Economics, Department of Technical Education, Műegyetem rkp. 3, 1111 Budapest, Hungary, molnar.gy@eik.bme.hu, szuts.z@eik.bme.hu

[3]University of Szeged, Institute of Informatics, Árpád tér 2, 6720 Szeged, Hungary, epeter@inf.u-szeged.hu, korosig@inf.u-szeged.hu

Abstract: This paper aims at presenting the findings and sharing the experiences of a case study whose data were gathered from an experimental MOOC (massive open online course) platform. The content was designed with an end view of favoring media-based education, students' activities, and their interactive communication. The main advantage of the devised system is that students were able to learn using their mother tongue, Hungarian. This research involved 208 students, enabling the authors to test the following variables by applying statistical methods: residence (country), sex, occupation, age, external (offline) motivation, amount of time spent in front of the computer, length of time in the LMS (learning management system) and achievements during a specific course. Statistical analysis revealed correlations between numerous factors, which may later serve as a solid ground for further studies in this field.

Keywords: student achievements; e-learning; external motivation; LMS; MOOC; K-MOOC

1 Introduction and Literature Review

Massive open online courses (MOOCs) are the latest revolution in online teaching and learning [1]. These academic courses are available to the general public, worldwide; there are no preconditions; and they are usually free of charge. [2], [3], [1], [4], [5]

"The field of open and distributed learning has experienced a surge of media coverage and public interest in the last several years, largely focusing on the

phenomenon of massive open online courses (MOOCs). The term MOOC has been used to describe a diverse set of approaches and rationales for offering large-scale online learning experiences. MOOCs have been delivered using both centralized platforms and services including learning management systems (LMSs) and decentralized networks based on aggregations of blog sites and social media feeds. MOOCs have been designed to support university curricula, academic scholarship, community outreach, professional development, and corporate training applications". [6]

"MOOCs are offered by a variety of development initiatives, such as Coursera, Udemy, MITx, edX, Udacity, which include the world's leading universities: Stanford, Harvard, and MIT. The courses are taught by leading-edge professors around the world, in various fields of science. They allow for flexible learning at any time and any place, integrating a variety of tasks into the course structure. The structure and scope of each course varies, depending on the characteristics and needs of the course curriculum, and the instructor's decision". [7]

Similar to some popular MOOC systems, the authors created their own MOOC, and placed emphasis on students' activities and multimedia contents. Although the impact of video and multimedia technologies in educational outcomes is a field of ongoing research, the pedagogical impact of using videos can be summarized by three key concepts. [8]

The following summary chart shows the history of MOOCs. The initiating higher education institutions were: MIT (2009), Stanford (2010) Harvard (2012).

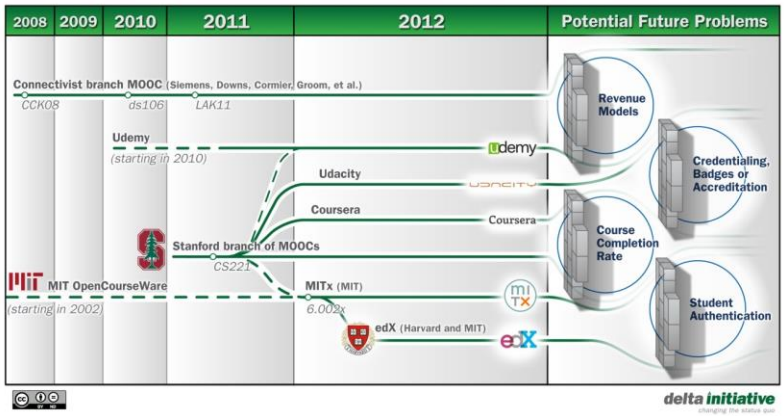

Figure 1

MOOC development between 2008-2012, source: http://mfeldstein.com/four-barriers-that-moocs-must-overcome-to-become-sustainable-model/ (downloaded: 2013. 03. 10.)

- "Interactivity with the content (the student relates to visual content, whether verbally, by note taking or thinking, or by applying concepts)

- Engagement (the student connects to the visual content, becoming drawn in by video, whether on-demand or real-time)
- Knowledge transfer and memory (the student may remember and retain concepts better than via other instructional media)" [9]

Since video combines many types of data (images, motion, sounds, and text) in a complementary fashion, learning can be adjusted more easily than with other tools to diverse learning styles and the individual learning pace of students. With video, the learner has more control over the information they receive and an additional opportunity for deeper learning by being able to stop, rewind, fast-forward, and replay the content as many times as needed. [9]

The authors kept the following principles in mind when constructing their videos: the main findings are that shorter videos are much more engaging, that informal talking-head videos are more engaging, that Khan-style tablet drawings are more engaging, that even high-quality pre-recorded classroom lectures might not make for engaging online videos, and that students engage differently with lecture and tutorial videos. [10]

"Understanding motivation to learn in online environments is gaining much interest among researchers. For example, Shroff, Vogel, and Coombes [11] found that online learners were more intrinsically motivated than their on-campus counterparts. Online learners' intrinsic motivation is positively related to their learning performance". [12] Studies on online learning suggest that unmotivated students may fail to use cognitive and meta-cognitive strategies, such as mastery learning or self-monitoring. In the context of MOOCs, because it is an open and free learning environment, participants tend to choose only segments of the learning environment, following their goals and interests. [13], [14] For example, Wang and Baker [14] found that course completers tend to be more interested in the course content, whereas non-completers tend to be more interested in MOOCs as a type of learning experience. In a wider perspective, [13] found that different motivational goals (e.g. relevant to job, career change, meet new friends), may predict different behavioral patterns for MOOC learners. In specific, they found that learners who enrolled with friends were more likely to be engaged with course materials than their counterparts [13]. These results correspond with other studies, showing that MOOC participants who were engaged in significant interactions with peers were less likely to dropout. [15], [16] Research on MOOCs, as described above, examined social engagement via large online groups. [17], [15], [13] Research also examined social engagement via small face-to-face groups, indicating a positive effect on MOOC completion [18]. To date, MOOC research lacks knowledge about the relationships between motivation and learning in small online groups. In addition, given that social engagement is mediated by language, this construct may also play a significant role in MOOC participants' motivation to learn. [12]

All the advantages of e-learning were combined in the educational framework that was used during the study; additionally, it has to be mentioned that it is suitable to launch further courses in the future. [19] However, it is important to emphasize the theoretical and practical aspects of such studies, besides the technical background, which can guarantee a successful and dynamic course, and would make it possible to involve and activate students in a greater number (several hundred) in learning. Such background support includes videos that summarize topics, students' activities, and expert groups surrounding a course [20]. It is possible to create a form of co-operative learning between students to blur the borderline between students and tutors; furthermore, it enables one to create an environment which allows carrying out modern pedagogical methods to eliminate inactivity, to enhance interactivity, student centeredness, collaborative and lifelong learning. On top of that, such an approach to learning opens the door to eliminating geographical obstacles and towards unifying regions for at least the time of a course. One of the main achievements of the course was the fact that students could use their mother tongue during learning. It should also be mentioned that all tutors were located in Serbia belonging to the Hungarian minority.

2 K-MOOC

A Hungarian innovative project was started in 2014 called K-MOOC (Carpathian Basin Online Education Center), where several MOOC courses were offered in Hungarian [27], [28]. One of the sources can be seen on the screenshot.

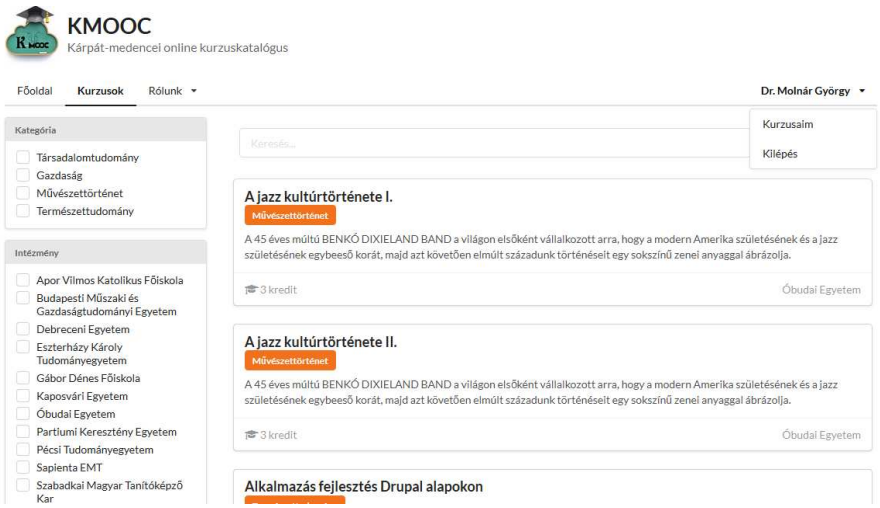

Figure 2
K-MOOC courses, source: own screenshot

As part of the K-MOOC system, our own course entitled Digital Pedagogy was launched a second time. The set-up of the course was in accordance with the e-learning rules as well as the requirements drawn up by the ministerial application, which was designed in the course – module – thematic content – lesson model. The direct aim of this application was to encourage universities who were part of the K-MOOC Network to design and launch online courses, enriching the palette of courses and scientific fields submitted by Óbuda University. Owing to the project, 45 K-MOOC courses were run in the first semester of 2016 and 49 courses in the second semester [27].

The interested students could sign up for the courses on their own on this website: https://www.kmooc.uni-obuda.hu/. When choosing a course, the accepted and offered credits and the topic were dominating. The biggest challenge semed to be the lack of knowing the evaluation time. Most users spent 2 hours with the course on a weekly basis [28]. Completing was satisfactory given the fact that 80-90% of the subscribers passed the course.

Regarding our course, based on the experiences we gathered we can claim that many students chose Digital Pedagogy because of the topic, the innovative methods and out of curiosity or for the sake of trying it out. Therefore, those students had not been motivated for completing the course. After every thematic unit or lesson the students were given questions for self-evaluation, tasks to be uploaded and tests as part of evaluation. The final assessment consisted of an online written examination paper and an essay. The participants lost interest in the latter one but were confident in completing the online tasks and other test-based solutions. This result is in accordance with the set-up for MOOCs [29].

Our course materials were centred around 15-20 screenshots that combined texts, media objects, examples, simulations and practical questions. Those who were continuously attending the class were seemingly active during the term, showing steady loading and activity. The following figure depicts our Digital Pedagogy course page (in Hungarian):

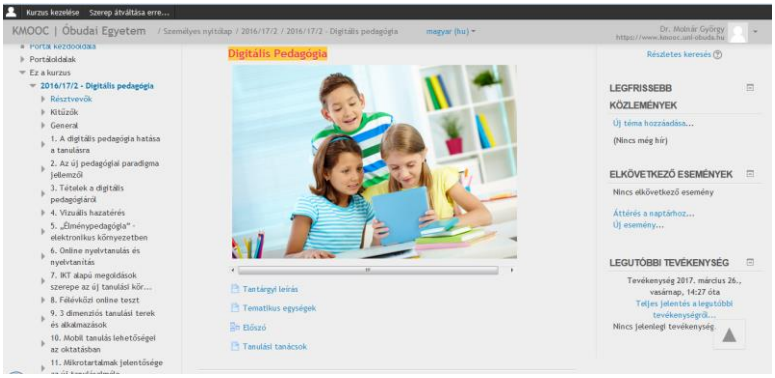

Figure 3
Our Digital pedagogy K-MOOC course, source: own screenshot

Taking everything into consideration, the first-term K-MOOC course was successful. Therefore, we wish to continue our work and launch the course again in the next semester in the hope of acquiring more students' attention.

3 Aims and Methods

In the first phase of the research, authors conducted an examination of the current educational environments and methodological tools. The duration of this MOOC course initiative was five weeks, altogether it consisted of a three week long training, a daily studying session of three-four hours, and activities required for its completion, without any necessary prerequisites. The primary target group of this MOOC was composed of Hungarian secondary school students in Serbia. The online course was conducted between February 8, 2015 and March 1, 2015. MOODLE (LMS - learning management system) was designated to serve as an online educational environment. Each set of topics was constructed using videos, which mediated the most important learning contents. The course was named "Conscious and safe internet usage", and was divided into sub-modules/weeks:

• Introduction to the course (5:58 minutes)

• Week 1 - Digital footprint (25:46 minutes)

• Week 2 - Conscious and safe internet usage (22:57)

• Week 3 - Online bullying(19:50)

The activities were divided into compulsory and optional units that ended with the completion of assignments on a weekly basis. The topics of the assignments were created in accordance with the subscribers' personal preferences, experience and recommendations. Deadlines and the start of a new week were always set to Sunday. The forms of an assignment varied including texts, pictures, and multimedia documents, while each assessment was conducted by the tutor. The point averages, then, were administered and recorded into the system. In line with the compulsory assignments, participants could gain additional points by taking an active part in forum discussions.

The point distribution during the "Conscious and safe internet usage" course was as follows:

• 20 points by the end of the first week

• 20 points by the end of the second week

• 20 points by the end of the third week

• 10 points for involvement in forum discussions

• 20 points for the final assignment

• 10 points for the final test

• Total: 100 points

The amount of points necessary to successfully complete the course was set to 75 points. Those who scored above the threshold limit were given a certificate issued with the tutors' signature (in electronic format).

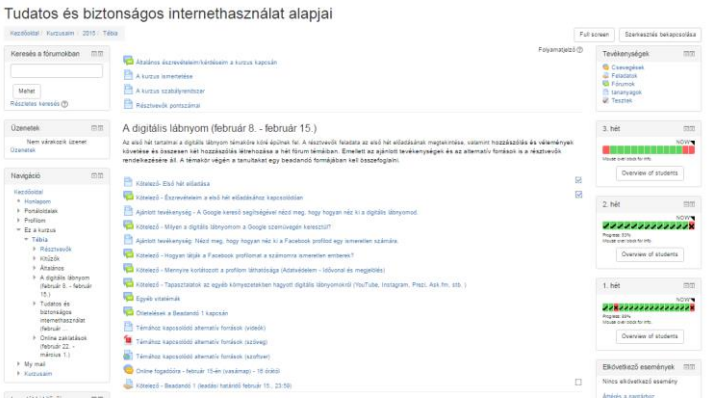

Figure 4
First sub-module/week in MOODLE

4 Research Questions

Background variables were either collected during the application phase with the help of a questionnaire or was generated by the system (MOODLE administrative platform).

The online application contained the following questions:

Open ended questions:

- Student's email address
- Student's sex
- Student's age
- Student's residence (country)
- External (offline) motivation

Multiple choice questions:

- Student's occupation (student, teacher, other)

- Student's host institution (elementary school, secondary school – vocational school, secondary school – grammar school, college, university, none)
- Length of time in front of the computer (less than 1 hour, between 1-3 hours, 3-5 hours, more than 5 hours)

Information provided by the MOODLE:

- Time spent in LMS
- Achievement during the course

5 Results

208 students enrolled on this given course, in the following composition: 79% (165) female and 21% (43) male students, as opposed to statistics in the available international literature [21], [22], [23] where male participants composed the significant majority. The age demographics of the participating students was similar to edX [23], given that a major part (59%) of them were under the age of 30.

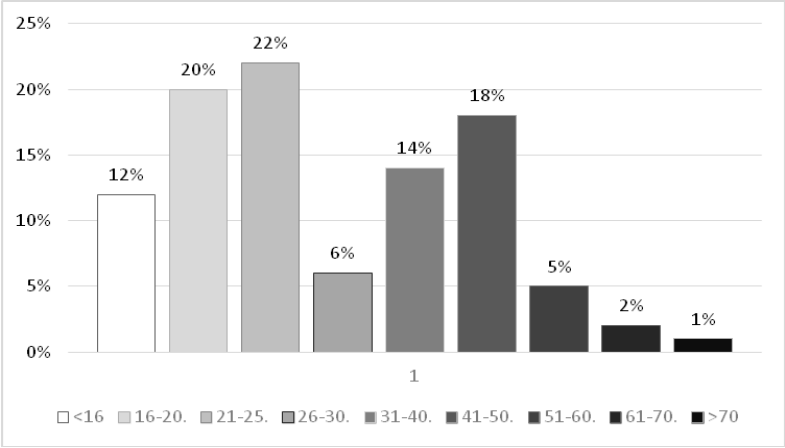

Figure 5
Sample by age group

The online course involved not only Hungarian secondary school students in Serbia, but also a number of educators were involved, who had a chance to indirectly develop study materials. Apart from students in Serbia, students from Hungary could also sign up for to the course, which, in turn, further differentiated the expert community. They answered questions by engaging in an intensive and constructive series of discussions with the aim of untangling possible solutions.

Based on their origins of country of all participants, 135 students (65%) were from Serbia, 71 students (34%) from Hungary, while 2 students (1%) were from Romania. The occupational distribution of the participants showed was as follows: 99 (48%) were students, 86 (41%) of them were teachers, whereas 23 – a total of 11% listed themselves as having another profession.

Given that MOOCs are becoming more and more popular worldwide, learners' motivation should be further studied from various aspects. [12], [13], [24] This paper examines the impact of "external motivation". By “external motivation” the authors mean points, obtained on a MOOC platform, which can be added to those acquired in formal education. This method, during our studies, served as a motivational tool for university students at the University of Novi Sad, Faculty of Hungarian Teacher Training –for first and second year students. Compared to the overall number of students (N=208), this group is made up of 44 students, i.e.: 21% of the entire sample. They accounted for 10% of the total number of points gained from the courses Introduction to Informatics and Educational Informatics.

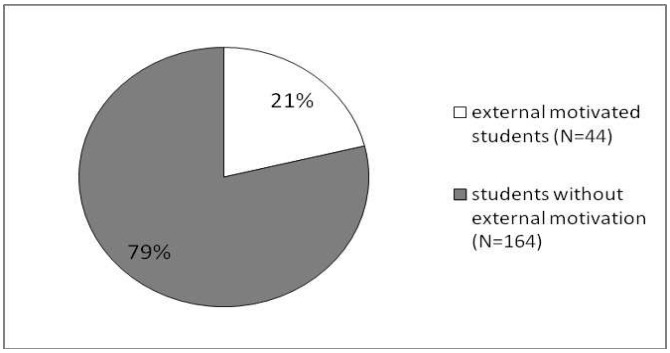

Figure 6
Sample by external motivation

The students, based on their own estimation, provided the amount of time spent in front of the computer during their online application. According to the obtained data from the registered students, 12% (26 students) spent less than one hour in front of the computer, 46% (95 students) one to three hours, 27% (56 students) three to five hours, and 15% (31 students) more than five hours a day.

Based on the authors’ experience and compared to other MOOC systems, an average of 540 minutes of active learning was set as necessary to successfully complete the course. The amount of time spent in a MOODLE system was recorded and later it was retrieved for further study. The conclusion was reached that it showed a heterogeneous picture. Students were logged in to the system 235 minutes on average, though the standard deviation of 225 was quite significant.

Table 1
Distribution of the time spent in the system (N=208)

Time spent in the system	n	%
Between 0 and 100 minutes	83	40
Between 100 and 200 minutes	36	17
Between 200 and 300 minutes	14	7
Between 300 and 400 minutes	10	5
Between 400 and 500 minutes	21	10
Between 500 and 600 minutes	30	14
Between 600 and 700 minutes	14	7

104 students (50%) completed the course successfully (by acquiring 75% or more points). This score is usually regarded as low in formal offline courses; however, in the category of non-formal online courses it is thought to be an outstanding result. These results were higher than the results available in the works of other authors, such as 10% [25] and 15% [26].

Those students who performed successfully spent an average of 387 minutes online with a standard deviation of 192. Students who finished the course successfully achieved high scores, on average 93.64, with a standard deviation of 4.60.

Table 2
Distribution of students' achievement (N=208)

	N	%
Successfully completed the course (75% or more points achieved)	104	50%
Completed pre-requisites without passing the course (did not achieve 75%)	2	1%
Tasks and the course were not completed.	31	15%
Registered in the system without earning any points	44	21%
Did not signing into the system	27	13%

During the statistical analysis, the authors did not find any correlation between the variables of sex, external motivation, length of time in front of computer and students achievement.

There are significant differences between the groups formed on the basis of residence and external motivation. While only two students enrolled in the course from Romania, we removed this group from this investigation. Analysing only the students from Serbia and Hungary, using two-sample t-tests we can conclude that there are detectable differences in variables of external motivation and achievement.

Based on the average value of external motivation, for the 100% participants from Hungary showed an impact of this factor, whereas the corresponding figure was only 67% for participants from Serbia. The significant differences were proven using t-test (t=8,04 p=0,001). Future research will further examine the nature of these differences.

External motivation and the variable of time spent in this framework demonstrated an apparent relationship (Pearson correlation factor=0.38, p=0.001).According to these, motivated participants took part more actively in the acquisition of knowledge.

Authors were also able to point out an observable correlation, based on the entire sample, between the amount of time spent in the LMS and student achievements - amount of acquired points (Pearson correlation factor r= 0.75, p= 0.001).

Table 3
Correlations between time spent in the LMS and student achievement

		Time spent in an educational framework	Student achievements
Time spent in the LMS	Pearson Correlation	1	,750
	Sig. (2-tailed)		,000
	N	208	208
Student achievements	Pearson Correlation	,750	1
	Sig. (2-tailed)	,000	
	N	208	208

In this case of narrowing down the sample (leaving those participants out who, while having enrolled in the course, but never logged in into the learning environment), a statistically outstanding correlation emerges between the external motivation and time spent in LMS (Pearson correlation factor = 0.25, p= 0.003).

Table 4
Correlations between external motivation and time spent in LMS

		External motivation	Time spent in the LMS
External motivation	Pearson Correlation	1	,247
	Sig. (2-tailed)		,003
	N	141	141
Time spent in the LMS	Pearson Correlation	,247	1
	Sig. (2-tailed)	,003	
	N	141	141

Through the analysis of the sample that was narrowed down (active students in learning environment), we could demonstrate that the amount of time spent in the LMS and the variable of student achievements show a significant correlation (Pearson correlation factor = 0.46, p=0.001).

Table 5

Correlations between student achievements and time spent in the LMS (sample of active students in LMS)

		Time spent in the LMS	Student achievements
Student achievements	Pearson Correlation	1	,465
	Sig. (2-tailed)		,000
	N	141	141
Time spent in the LMS	Pearson Correlation	,465	1
	Sig. (2-tailed)	,000	
	N	141	141

Variables, based on a two-sample t-test, provided the difference for the correlation of sexes and the results achieved by the end of the course. The variables of the place of residence (country), age, and occupation affected the participants' efficiency. There are statistical differences in the achievements between the groups of students, those from Hungary and Serbia, based on the two-sample t-test. The rate of having successfully completed the course shows that 73% for the participants from Serbia as opposed to 58% for participants from Hungary (t=-2,15 p=0,03).

The group of teachers and students were analysed through a two-sample t-test and the results showed a statistically significant difference concerning their achievements (F=5,9 p=0,01 t=3,4 p=0,001).

Table 6

Independent Samples Test

Independent Samples Test					
		F	Sig.	t	Sig. (2-tailed)
Student achievements	Equal variances not assumed	5.903	,016	-3.400	,001

The authors established three groups on the basis of the participants' age. The one-way ANOVA analysis pointed to the fact that there was a significant difference between the students' achievements of the following age groups:10-19, 20-40, and above 40 amounting to (F=10.7, p=0.001).The post hoc (Tukey's-b test) analysis established two groups, according to which achievements of younger and elderly groups are different from the middle-age group [elderly, young]<[middle-age].

Table 7

One-way ANOVA

ANOVA					
Student achievements					
	Sum of Squares	df	Mean Square	F	Sig.
Between Groups	39488,776	2	19744.388	10.674	,000

Table 8
Tukey's range test

Tukey B[a,b]			
Student achievements			
1	N	Subset for alpha = 0.05	
		1	2
elderly (above 40)	53	35.66	
young (aged 10 -19)	47	43.02	
middleage (aged 20 -40)	108		66.22

In line with the amount of time spent in front of the computer, we form four groups of the applicants. The one-way ANOVA test also showed that a significant difference indeed existed (F=6,7 p=0,001) in the groups whose members spent less than one or more than five hours in front of the computer. The authors also analyzed participants who spent one-thre or three-five hours of their time at the PC compared for student achievements during the course. Tukey's b-test demonstrated the following correlation between the groups: [less than one hour, less than five hours]<[one-three hours, three-five hours].These tests do not prove that students who spent more time at the PC will perform more successfully in MOOCs. For a more detailed explanation of these results, these variables will have to be subjected to a deeper analysis.

Table 9
One-way ANOVA

ANOVA					
Student achievements					
	Sum of Squares	df	Mean Square	F	Sig.
In-between groups	37879.414	3	12626.471	6.764	,000

Table 10
Tukey's range test

Tukey B[a,b]			
Student achievements			
Time in front of the computer	N	Subset for alpha = 0.05	
		1	2
less than 1 hour	26	30.77	
more than 5 hours	31	32.42	
3-5 hours	56		57.27
1-3 hours	95		63.71

Using the two-sample t-test method, the authors investigated the question if there was a difference in external motivation between those participants who succeeded and those who failed. The results obtained from this research indicate that the external motivation of successful participants is significantly higher than those who achieved zero points (F=185.9 p<0.01; t=6.09 p<0.01). It may thus be said that those students who were extrinsically motivated (by the fact that points from

the completed courses can be transferred to some school subjects) would persist with a higher probability until the end of the online course.

Table 11
Independent Samples Test

Independent Samples Test					
		F	Sig.	t	Sig. (2-tailed)
External motivation	Equal variances assumed	185.936	,000	4.624	,000
	Equal variances not assumed			**6.097**	**,000**

5 Discussion

This experimental study involving 208 students from 3 countries revealed significant statistical correlations with the help of an experimental MOOC system (Conscious and safe internet usage). Authors gained a great amount of experience regarding online learning. Such observations could pave the path to further studies or may serve as a basis for future online learning courses.

Significant results in research related to time spent in LMS:

- It has been concluded that students who spent more time in LMS would be more successful within the framework MOOC.
- The most significant observation is the fact that external motivation showed a correlation not only with the quantity of time spent in the educational framework but also with the performance during the course.
- The amount of time spent in the educational framework is intertwined with the efficiency variable on a MOOC platform.
- Students who spent more time in LMS would be more successful within the framework MOOC.
- Students who had external motivation, spent more time in the LMS than students, who did not have external motivation.
- Those students who spent more time on a MOOC platform, and presumably completed not only the obligatory tasks but also the recommended ones and other activities.
- To sum up, the students who were motivated to not only gain access to online contents and earn online certificates but also by the offline contents, in this case, points earned during "real" (physical) courses, were also the ones who achieved better at learning online and at completing the MOOC courses.

Significant results in research related to achievement during the course:

- External motivation showed a correlation not only with the quantity of time spent in the educational framework but also with the performance during the course.
- Regular computer users have a better chance at completing an online course.
- In addition, they participated in online forums communicating intensively with their peers were significantly more efficient.

The results of the pilot study contributed to the better understanding of an alternative learning environment, where one of the greatest disadvantages is the low achievements of participating students.

6 Limitations

The statistical analysis presented in this study are limited to a special segment of students. The sample size of the study was relatively small. In their future work authors intend to implement longitudinal research in which multiple MOOC cohorts are analyzed under the same statistical model and also among the same qualitative framework.

References

[1] H. Najafi, C. Rolheiser, S. Håklev, L. Harrison: Variations in Pedagogical Design of Massive Open Online Courses (MOOCs) Across Disciplines. Teachning Learning Inquiry, 2017 5(2) pp. 47-64

[2] F. C. Bonafini, C. Chae, E. Park, K. W. Jablokow: How Much Does Student Engagement with Videos and Forums in a MOOC Affect Their Achievement? Online Learning Journal, Online Learning, 2017, 21(4) pp. 223-240

[3] E. Allen, J. Seaman: *Grade Change: Tracking Online Education in the United States.* Babson Survey Research Group and Quahog Research Group, LLC, 2014

[4] A. Fini: The Technological Dimension of a Massive Open Online Course: The Case of The CCK08 Course Tools. *International Review of Research in Open and Distance Learning*, 2009, 10(5) pp. 74-96

[5] B. Stewart: Massiveness + openness = New literacies of participation? *MERLOT Journal of Online Learning and Teaching*, 2013, 9(2), pp. 228-238. Retrieved from: http://jolt.merlot.org/vol9no2/stewart_bonnie_0613.htm

[6] A. Anders: Theories and Applications of Massive Online Open Courses (MOOCs): The Case for Hybrid Design. *International Review of Research in Open and Distance Learning*, 2015, 16(6) pp. 39-61

[7] S. Halawa, D. Greene, J. Mitchell: Dropout Prediction in MOOCs Using Learner Activity Features. In *U. Cress, & C. D. Kloos (Eds.), Proceeding of the European MOOC stakeholder summit*, Lausanne, Switzerland, February 10-12, 2014, pp. 58-65

[8] M. Castells: *The Rise of the Network Society. Classics of the Information Society. The Information Age. Economy, Society, Culture. Volume I*. Thinking – Infonia, 2005

[9] A. D. Greenberg, J. Zanetis: *The Impact of Broadcast and Streaming Video in Education*. Report commissioned by Cisco Systems Inc. to Wainhouse Research, LLC. Ainhouse Research, 2012

[10] J. P. Guo, J. Kim, R. Rubin: How Video Production Affects Student Engagement: An Empirical Study of MOOC Videos. *Proceedings of the first ACM conference on Learning @ scale conference,* 2014

[11] R. H. Shroff, D. R. Vogel, J. Coombes: Assessing Individual-Level Factors Supporting Student Intrinsic Motivation in Online Discussions: a Qualitative Study. *Journal of Information Systems Education*, 2008, 19(1), pp. 111-125

[12] M. Barak, A. Watted: *Nanotechnology for All: Examining Students' Motivation and Learning Outcomes in a Massive Online Open Course*. Chicago, USA: National Association for Research in Science Teaching (NARST) 2016

[13] R. F. Kizilcec, E. Schneider: Motivation as a Lens to Understand Online Learners: Toward Data-driven Design with the OLEI Scale. *ACM Transactions on Computer-Human Interactions*, 2015, 22(2)

[14] Y. Wang, R. Baker: Content or Platform: Why do Students Complete MOOCs? *MERLOT Journal of Online Learning and Teaching*, 2015, 11(1) pp. 17-30

[15] A. Brooker, L. Corrin, P. de Barba, J. Lodge, G. Kennedy: A Tale of Two MOOCs: How Student Motivation and Participation Predict Learning Outcomes in Different MOOCs. Australasian Journal of Educational Technology, 2018, 34(1) pp. 73-87

[16] D. F. O. Onah, J. Sinclair, R. Boyatt: Dropout Rates of Massive Open Online Courses: Behavioral Patterns. In *Proceedings of EDULEARN14,* Barcelona: Spain, 2014, pp. 5825-5834

[17] C. Alario-Hoyos, M. Perez-Sanagustín, C. Delgado Kloos, G. Parada, , M. Munoz-Organero, A. Rodríguez-de-las-Heras: Analysing the Impact of Built-in and External Social Tools in a MOOC on Educational

Technologies. In D. Hernandez-Leo, T. Ley, R. Klamma, A. Harrer (Eds.), *Lecture notes in computer science*: Vol. 8095, Proceedings 8th European Conference on technology enhanced learning, 2013, pp. 5-18

[18] N. Li, V. Himanshu, A. Skevi, G. Zufferey, J. Blom, P.: Dillenbourg: Watching MOOCs Together: Investigating Co-located MOOC Study Groups. *Distance Education*, 2014, 35, pp. 217-233

[19] G. Siemens: Connectivism: *A Learning Theory for the Digital Age*, 2004 http://www.elearnspace.org/Articles/connectivism.htm (Last accessed: 28.03.2016.)

[20] A. Plessis: Student-Teachers' Pedagogical Beliefs: Learner-centred or Teacher-centred When Using Ict in the Science Classroom?, *Journal of Baltic Science Education*, 2016, 15(2) pp.140-158

[21] L. B. Breslow, D. E. Pritchard, J. DeBoer, G. S. Stump, A. D. Ho, D. T. Seaton: Studying Learning in the Worldwide Classroom: Research into edX's First MOOC. *Research & Practice in Assessment*, 2013, 8, pp. 13-25

[22] Coursera Blog: Coursera Hits 1 Million Students across 196 Countries. Coursera. Retrieved from: http://blog.coursera.org/post/29062736760/coursera-hits-1-million-students-across-196, 2012

[23] edX (2015). Age Demographics. edX. http://edx.readthedocs.org/projects/edx insights/en/latest/enrollment/Demographics_Age.html (Last accessed: December 7, 2015), edX (2015). Gender Demographics. edX, Retrieved from: http://edx.readthedocs.org/projects/edx-insights/en/latest/enrollment/Demographics_Gender.html

[24] T. Sinha: Together We Stand, Together We Fall, Together We Win: Dynamic Team Formation in Massive Open Online Courses. In *Proceedings of the 5th IEEE International Conference on application of digital information & web technologies (ICADIWT)* India, 2014

[25] J. Wilkowski, A. Deutsch, M. D. Russell: Student Skill and Goal Achievement in the Mapping with Google MOOC. L@S '14 *Proceedings of the first ACM conference on Learning @ scale conference*. ACM New York, NY, USA, 2014, pp. 3-10

[26] K. Jordan: MOOC Completion Rates: The Data. 2013. www.ktyjordan.com. Retrieved from: http://www.katyjordan.com/MOOCproject.html

[27] F. Hegyesi, K. Némethy, A. Szakál, J. Gáti, G. Kártyás: Human Interactions in the Context of K-MOOC, Óbuda University Courses - Source of the Document SISY 2016 - IEEE 14th International Symposium on Intelligent Systems and Informatics, Proceedings 7601511, 2016, pp. 271-274

[28] F. Hegyesi, Gy. Kártyás: MOOC in Higher Education - Source of The Document ICETA 2013 - *11th IEEE International Conference on Emerging eLearning Technologies and Applications*, Proceedings 06674415, 2013, pp. 119-122

[29] M. György: Pillanatképek az IKT szakképzésben alkalmazható megoldásairól - avagy kételyek és jó gyakorlatok az innovatív pedagógiai módszerek útján - visszatekintés az EDU elmúlt időszakára, EDU SZAKKÉPZÉS ÉS KÖRNYEZETPEDAGÓGIA ELEKTRONIKUS SZAKFOLYÓIRAT (ISSN: 2062-3763) 6: (2) pp. 7-18 (2016)

Preliminary Results of Size and Slide-Roll Effect on the Kinematics of Total Knee Replacements

Gusztáv Fekete[1,2], Dong Sun[1,2,3], Gongju Liu[1], Yao Dong Gu[2] Gábor P. Balassa[4], István Bíró[5], Patric D. Neis[6], Endre Jánosi[1]

[1] Eötvös Loránd University, Faculty of Informatics,
Savaria Institute of Technology
Károlyi Gáspár tér 4, H-9700 Szombathely, Hungary
fg@inf.elte.hu, je@inf.elte.hu, 1611042084@nbu.edu.cn

[2] Ningbo University, Research Academy of Grand Health
Fenghua Road 818, 315211 Ningbo, China
feketegusztav@nbu.edu.cn, 1511042066@nbu.edu.cn, guyaodong@nbu.edu.cn

[3] Pannon University, Faculty of Engineering
Egyetem u. 10, H-8200 Veszprém, Hungary

[4] Szent István University, Faculty of Mechanical Engineering,
Institute of Mechanics and Machinery
Páter Károly utca 1, H-2100 Gödöllő, Hungary
balassa.gabor.peter@hallgato.szie.hu

[5] Szeged University, Faculty of Engineering, Institute of Technology
Mars tér 4, H-6724 Szeged, Hungary, biro-i@mk.u-szeged.hu

[6] Federal University of Rio Grande do Sul, Laboratory of Tribology,
90050-170 Porto Alegre, Brazil, patric.neis@ufrgs.br

Abstract: This paper deals with two fundamental questions with regard to total knee replacement kinematics. First, it provides quantitative information about the effect of knee prosthesis size on restored knee rotation by the so-called performance function. Second, the paper introduces a hypothesis which considers the effect of slide-roll on the performance function. By means of statistical methods, a strong linear correlation between slide-roll and performance-function of the examined total knee replacements was deduced. This result can be interpreted as follows: alteration of slide-roll ratio may enhance the overall performance of total knee replacements with regard to the restored kinematics, or in this specific case, the rotation.

Keywords: qualification method; total knee replacement; rotation; slide-roll; size-effect

1 Introduction

A wide range of choice regarding the brands (Stryker©, Zimmer©, BioTech©, CeramTec© or Sanatmetal©) and sizes (S, M, L, XL, etc.) of commercial knee replacements and supporting telesurgical technologies [1] are available for surgeons to carry out knee operations to restore closely the same kinematics of the physiological knee joint.

Multiple, substantial studies have been published about how total knee replacement (TKR) design affects the kinetics [2, 3] and kinematics [4] of the knee joint. It is also worth mentioning the indirect changes caused by TKR positioning during operation [5] or the effect of foot impairs in the general health of the knee joint [6]. However, no generally accepted methods have been introduced to qualify TKRs about their performance of restoring original knee joint kinematics.

The term of "TKR quality" should describe how closely the commercial TKRs can reproduce the rotation-ad/abduction of the physiological joint with respect to the original kinematics of the knee joint. This new area has been recently researched and a novel qualification method was introduced by the use of a so-called *performance-function* [7]. This function provides a percentile value of the measured rotation of a commercial prosthesis relative to a *reference-rotation* [8], which is the averaged and statistically determined rotation function based on a set of cadaver knee joints.

The basic idea of this qualification method can be further expanded to other knee related kinematical-kinetical values, such as ad/abduction, slide-roll or the acting tibiofemoral force between the contact surfaces. The above-mentioned parameters play key role in TKR lifetime. It has been proven that abnormally high adduction implies osteoarthritis progression in the medial compartment of the knee joint [9, 10], while the latter two phenomena are key-parameters in wear propagation between TKR surfaces. Based on the latest results, it was quantitatively determined that the effect of the tibiofemoral force and the slide-roll cause 65% and 15% more removed volume on TKR surfaces respectively [11, 12].

It is worth noting that the examined TKRs showed fairly low performance ratio compared to the reference-function, since they only achieved 18-35% of the original physiological rotation described by the reference rotation [7]. Whether TKR size has significant role in this performance, has not been further discussed.

The effect of implant size has only been focused on a few knee kinematics-related issues, e.g., the individual effect of the tibial implant thickness on the tibiofemoral angle (TFA) [13] or TKR wear [14]. With regard to wear, TKR size has been proven to be a contradictory parameter since the experimental results of Affatato et al. [15], demonstrated that under the same condition larger tibial UHMWPE inserts resulted in higher wear ratios than those of the small implants.

This is a significant contradiction since a large implant has also larger contact surface, which provides lower contact pressure. According to the literature, with regard to wear in implants, the precondition of low wear is low pressure [16].

These results support the fact that the effect of TKR size on wear propagation can be rather unexpected and controversial. Due to the lack of studies regarding the influence of knee implant size (small, medium, large, etc.) on restored kinematics, this paper aims to provide firsthand information on this topic.

Besides the analysis of the size-influence, a so-far undiscussed question between performance-function (considering only rotation) and slide-roll of commercial TKRs is also presented. It is assumed that correlation may exist between these parameters. If it does, then an overall enhancement could be achieved by altering the slide-roll as a parameter. Therefore, this existence will be statistically examined as well.

2 Methods

2.1 Concept of Qualification

The concept of the qualification method is based on the theoretical introduction of a so-called *performance-function* (κ), which provides a percentile value of the measured rotation ($\rho_{pr}(\varphi)$) of a commercial prosthesis relative to the *reference-rotation* ($\rho_{ref}(\varphi)$). This has been introduced by Katona et al. [8]:

$$\kappa(\varphi) = \frac{\rho_{pr}(\varphi)}{\rho_{ref}(\varphi)} \cdot 100 \tag{1}$$

where:

$\rho_{pr}(\varphi)$: measured rotation function of a commercial prosthesis, as a function of flexion angle,

$\rho_{ref}(\varphi)$: measured and averaged rotation function, obtained from multiple cadaver knee joints, as a function of flexion angle.

In order to estimate a performance-function of an arbitrary TKR, e.g. with regard to rotation, both the rotation function ($\rho_{pr}(\varphi)$) of the examined prosthesis and the reference-rotation function ($\rho_{ref}(\varphi)$) needed to be determined. To carry out the necessary experiments our research group designed and manufactured a multi-purpose test rig [17] which allowed us to carry out measurements both on cadavers and TKRs as well (Fig. 1).

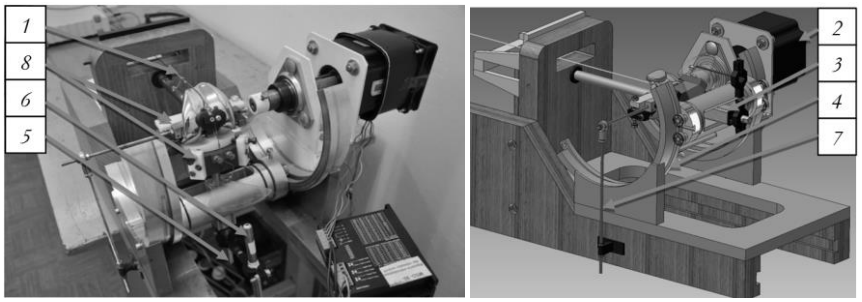

Figure 1
The test rig

To fulfill other purposes, the design was carried out in a way that the test rig, together with the measuring and processing method, would be identically adequate to measure cadaver knees or TKR systems. The fixture in the test rig ensures that during the flexion of cadaver knee or TKR system, which is exerted by the quadriceps under the effect of self-weight or the stepper motor, the same type of movement would be carried out.

The test rig includes the following main parts:

1. The loading system (1), together with the bending mechanism of the knee joint. The load is transmitted through a rubber-muscle model, while the bending movement is exerted by a DPM 110SH99 stepper motor.
2. The stepper motor (2) with a maximum 11.5 Nm holding torque. With this motor, the knee joint can be bent up to 80^{o} of flexion angle. Due to the design of the test rig, the tibia can carry out unconstrained movement. This feature is essential since the movement has to be controlled only by the quadriceps, the self-weight and the surfaces of the condyles.
3. The bushing and the rail. The unconstrained movement is secured by the use of bushing- and planar bearings (3). The flexion is performed along a controlled curved rail (4).
4. The measuring system. The rotation can be directly measured by a laser (6), which shows the rotation on the attached plexiglass plate. In case of TKR measurement, the tibia plateau is attached to the tibial shaft (5). The tibial shaft represents the direction of the medullar cavity or canal (containing the bone marrow). During the experiments, both TKRs and cadavers are measured in the same anatomical system.
5. Additional fixture system. The test rig also includes a special fixture system (8), which ensures that the inserted TKRs (or cadavers) can be secured identically, and the experiment can be carried out according to a pre-defined protocol [8].

During the experiments, first the reference-rotation function was determined based on multiple cadavers, which was followed by the rotation functions of several commercial TKRs, and eventually the statistical determination of the performance-function [7, 8].

To carry out the test qualification, the following TKRs were tested: three cruciate-retaining TKR from the manufacturer of Bio-Tech (prostheses 1, 3 and 5), one cruciate-retaining and posterior-stabilized TKR from Sanatmetal (prosthesis 7) and two cruciate-retaining TKRs (prosthesis 0 and 4), from unknown manufacturer (Table 1).

Table 1
Tested prostheses [7]

Number	Manufacturer	Femoral size	Tibia plateu size	Leg	Type
0	Unknown	L-LARGE	XLGE 12	L	CR
1	BioTech	Med. Right B140	B105 M10	R	CR
3	BioTech	B102 XL-L	B106 L10	L	CR
4	Unknown	M-LARGE	MED 10	L	CR
5	BioTech	Med. Right B146	B104 S10	R	CR
7	Sanatmetal	D	EF 5-6 10 PE	L	PS

After the cadaver measurements and the determination of the reference-function, the rotation of six commercial TKRs were measured as a function of flexion angle (Fig. 2).

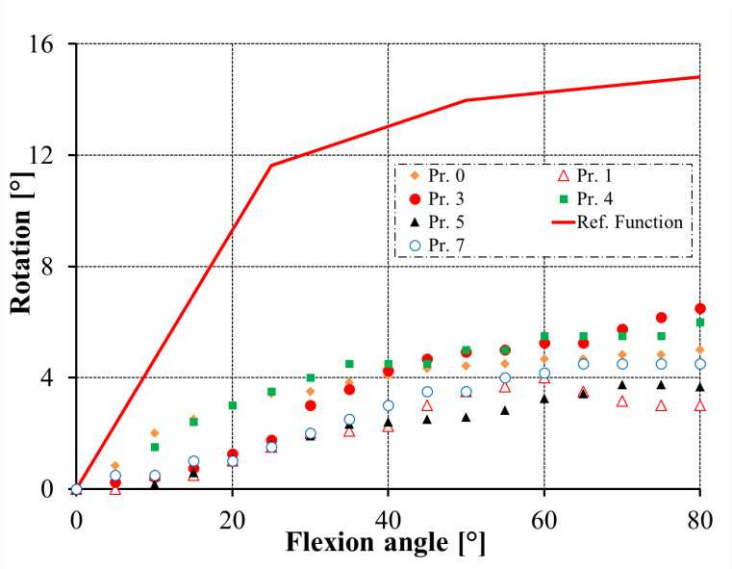

Figure 2
Reference-function and the rotations of the commerical TKRs [6]

The reference-function is approximated as a tri-linear function, which includes three major breakpoints at 25˚, 50˚ and 80˚ of flexion angle. These breakpoints have been statistically determined [8].

2.2 Effect of TKR Size

To classify the results and draw a more appropriate conclusion regarding the kinematical performance of the tested TKRs, an averaged performance ratio has been introduced (Eq. (2)). This ratio was determined based on the values of the major breakpoints (25˚, 50˚ and 80˚of flexion angle). Therefore, it can provide a general overview about the performance of each TKR.

$$\kappa_{Av.pro.i}(\varphi) = \frac{\kappa_i(25^\circ) + \kappa_i(50^\circ) + \kappa_i(80^\circ)}{3} \tag{2}$$

Where *i* denotes the tested prosthesis.

Data for the evaluation of the TKR size effect have been taken from contemporary literature [7], where examined six TKRs were chosen to demonstrate the phenomenon (Table 2). The TKRs were separated as follows: prosthesis 1, 5, and 7 were medium sized TKRs, while prosthesis 0, 3, and 4 were large sized. By the separation of the TKRs according to their sizes, the possible effect can be detected.

Table 2
Values of performance-function [7] and the calculated average performances

i	κ (25°) [%]	κ (50°) [%]	κ (80°) [%]	$\kappa_{averaged}$ [%]	Size [-]
Pr. 0	32.4	31.1	34.1	32.5	L
Pr. 1	10.9	24.3	21.6	18.9	M
Pr. 3	13.3	39	41.3	31.2	L
Pr. 4	31.5	35.7	39.9	35.7	L
Pr. 5	10.9	20.6	26.2	19.2	M
Pr. 7	12.5	27.1	31.9	23.8	M

After determining the averaged performance value of each TKR, the results have been summarized in Figure 3 as a function of TKR size. By separating the results based on their size, a clear difference can be distinguished between the sizes, which confirm the hypothesis that TKR size has a significant effect on the functionality of the prosthesis and the restored kinematics.

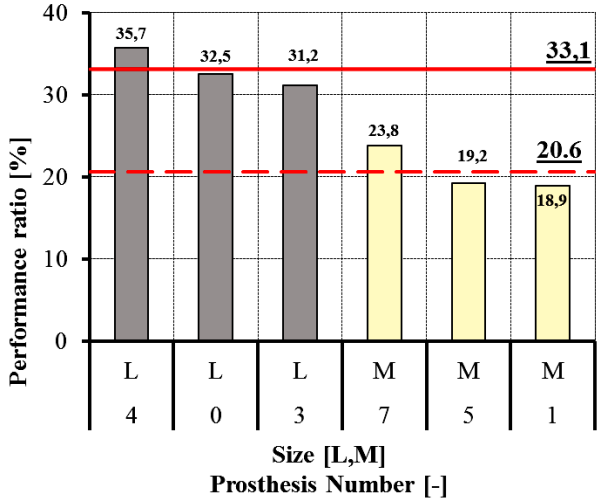

Figure 3
Averaged performance ratio of the commercial TKRs

2.3 Correlation between Performance-Function and Slide-Roll

When the averaged performances in the major breakpoints were plotted in Figure 4, an interesting trend was observed. If the function of the averaged slide-roll ratio [4], which has been deduced from actual TKR geometries, was compared to these discrete points (0°, 25°, 50°, and 80°), then it became apparent that the observed functions had similar tendency (Fig. 4).

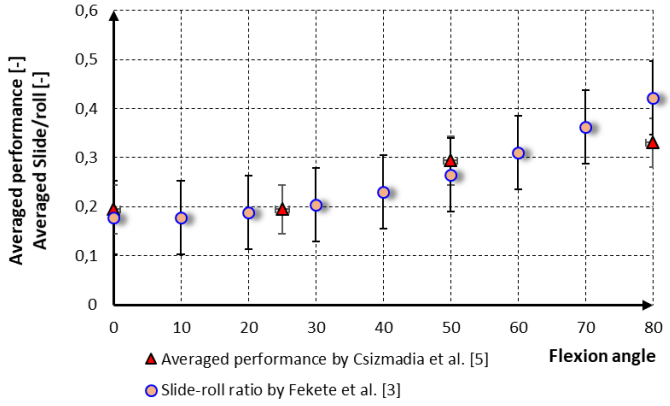

Figure 4
Averaged performance and slide-roll ratio of the prostheses

According to Figure 4, a possible correlation can exist between the averaged slide-roll and the averaged performance-function. If this correlation exists, it can be assumed that the alteration of TKR slide-roll may also lead to better performance in TKR rotation.

To statistically prove and qualify the level of correlation, the Pearson correlation coefficient (r) was determined, which equaled to 0.9774. The analysis considered all the examined TKRs regardless their sizes. The obtained result showed strong positive correlation, which was further analyzed in order to decide whether the result significant was. Since the data were available in four points (0°, 25°, 50°, and 80°), the degree of freedom of the set was 4 ($n = 4$), with an r score of 0.9774 while the significance level was set to 0.05.

P-value, which denotes the probability of an observed result assuming a true null hypothesis, was found to be 0.0226. Thereby it was confirmed that the result was significant at the level of $p < 0.05$. To investigate a size-based dependence as well, prostheses with size L and M were investigated separately (Fig. 5).

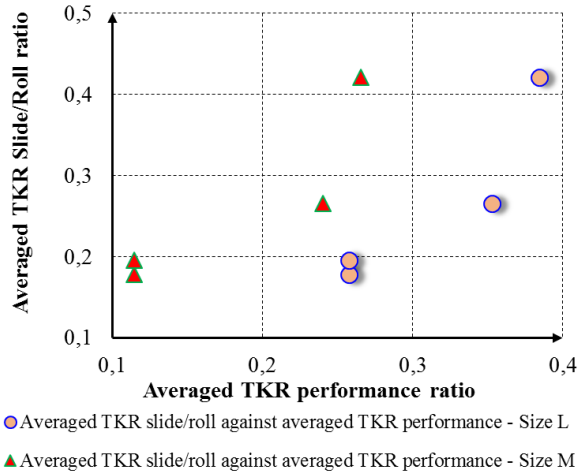

Figure 5
Correlation analysis between TKR performance and slide-roll

By carrying out the same statistical analysis on the data set, the following results were obtained and summarized in Table 3.

Table 3
Pearson correlation coefficients and significance on the examined TKRs

	n [-]	r [-]	p-value [-]	Significant at 0.05?
All TKRs	4	0.9774	0.0226	Yes
TKRs (size M)	4	0.8273	0.1727	No
TKRs (size L)	4	0.9657	0.0343	Yes

Conclusions

The averaged performance-function of all six prostheses were calculated, and their results were summarized in a cluster column chart (Fig. 3) as a function of prosthesis size (L, M). The continuous line, with a percentile value of 33.1%, represented the averaged performance-function of the large-sized prostheses, while the dashed line, with a percentile value of 20.6%, represented the averaged performance-function of the medium-sized prostheses. The effect of TKR size became immediately apparent since by this study it has been quantitatively determined that TKRs with large size (L) can restore the functional kinematics 12.5% superior than TKRs of medium size (M).

In fact, this result means that large-sized prostheses have a 60.7% ({33.1 – 20.6}/20.6) superior performance than medium-sized prostheses. Therefore, it has been confirmed that among other factors, e.g., tibial implant thickness [13, 14], TKR size also has a significant effect on knee kinematics, or more precisely on the restored rotation.

Nevertheless, the question why larger TKRs behave kinematically differently is still not answered. According to Affatato et al. [15], large prostheses are characterized by a wider area that undergoes more sliding, therefore, more friction and wear, which could produce discrepancies in their kinematics. This size-related phenomenon was also confirmed by Kang et al., [18] in case of hip prostheses. The authors found higher volumetric wear rate in large size hip replacements, possibly due to the result of higher sliding distance and lower contact pressure. Even though a confirmed explanation is still missing, the problem may be partially answered if a separated analysis on the rotation segments [8] and on slide-roll function would be carried out as a future step.

Another important hypothesis has also been proven, namely the strong linear correlation between the averaged slide-roll ratio and the averaged performance-function. Separately, the TKRs were also investigated according to their size; the results showed significance in the case of large sized TKRs, however they did not indicate the same condition in the case of middle sized TKRs.

This last result can be interpreted as follows: alteration of slide-roll ratio may enhance positively the overall performance of total knee replacements with regard to the restored kinematics. This question will be further analyzed on multibody modell.

Acknowledgements

This paper was supported by: National Natural Science Foundation of China (81772423), Anta Sports Products Limited (HK2015000090), Zhejiang Social Science Program - Zhi Jiang Youth Project (Project number: 6ZJQN021YB), Savaria Institute of Technology, Eötvös Loránd University, Szent István University, University of Szeged and the Research Academy of Grand Health, Ningbo University.

References

[1] Takács, Á., Kovács, L., Rudas, I. J., Precup, R-E., Haidegger, T. Models for Force Control in Telesurgical Robot Systems. Acta Polytechnica Hungarica, 12 (8), pp. 95-114, 2015

[2] Ramírez, J. F., Muñoz, E. J. and Vélez, J. A. Algorhytm for the Prediction of the Reactive Forces Developed in the Socket of Transfemoral Amputees. Dyna, 79 (173), pp. 89-95, 2012

[3] Innocenti, B., Pianigiani, S., Labey, L., Victor, J. and Bellemans, J. Contact Forces in Several TKA Designs during Squatting: A Numerical Sensitivity Analysis. Journal of Biomechanics, 44 (8), pp. 1573-1581, 2011

[4] Fekete, G., De Baets, P., Wahab, M. A., Csizmadia, M. B., Katona, G., Vanegas-Useche, L. V., Solanilla, J. A. Sliding-Rolling Ratio during Deep Squat with Regard to Different Knee Prostheses. Acta Polytechnica Hungarica, 9 (5), pp. 5-24, 2012

[5] Kessler, O., Bull, A. M. J. and Amis, A. A. A Method to Quantify Alteration of Knee Kinematics Caused by Changes of TKR Positioning. Journal of Biomechanics, 42 (6), pp. 665-670, 2009

[6] Feng, Y., Song, Y. The categories of AFO and its Effect on Patients with Foot Impairs: A Systematic Review. Physical Activity and Health, 1 (1), pp. 8-16, 2017

[7] Csizmadia, B. M., Balassa G. P. and Katona, G. The First Steps to the Development of the Knee Prosthesis Rating Method. Biomechanica Hungarica, 6 (1), pp. 39-45, 2014

[8] Katona, G., Csizmadia, B. M. and Andrónyi, K. Determination of Reference-Function to Knee Prosthesis Rating. Biomechanica Hungarica, 6 (1), pp. 293-301, 2013

[9] Chang, A. H., Moisio, K. C., Chmiel, J. S., Eckstein, F., Guermazi, A., Prasad, P. V., Zhang, Y., Almagor, O., Belisle, L., Hayes, K., Sharma, L. External Knee Adduction and Flexion Moments during Gait and Medial Tibiofemoral Disease Progression in Knee Osteoarthritis. Osteoarthritis and Cartilage, 23 (7), pp. 1099-1106, 2015

[10] Morgenroth, D. C., Medverd, J. R., Seyedali, M., Czerniecki, J. M. The Relationship between Knee Joint Loading Rate during Walking and Degenerative Changes on Magnetic Resonance Imaging. Clinical Biomechanics 29 (6), pp. 664-670, 2014

[11] Fekete, G., Sun, D., Gu, Y., Neis, P. D., Ferreira, N. F., Innocenti, B., Csizmadia, B. M. Comparative Study on Wear between Tibiofemoral Connection under Standard and Non-Standard Squat. Muscle, Ligaments and Tendons Journal, 7 (4), pp. 518-526, 2017

[12] Fekete, G., Bíró I., Csizmadia B. M. Mechanikai Modell a tibio-femorális kapcsolat során fellépő kopás meghatározására térdimplantátumokban. Biomechanica Hungarica, 10 (1), pp. 55-63, 2017

[13] Hopgood, P., Martin, C. P. and Rae, P. J. The Effect of Tibial Implant Size on Post-Operative Alignment Follwing Medial Unicompartmental Knee Replacement. The Knee, 11 (5), pp. 385-388, 2004

[14] Battaglia, S., Taddei, P., Castiello, E., Tozzi, S., Sudanese, A. and Affatato, S. Combined Effect of the Body Mass Index and Implant Size on the Wear of Retrieved Total Knee Prostheses. Journal of Mechanical Behavior of Biomedical Materials, 38, pp. 69-77, 2014

[15] Affatato, S., Grillini, L., Battaglia, S., Taddei, P., Modena, E. and Sudanese, A. Does Knee Implant Size Affect Wear Variability? Tribology International, 66, pp. 174-181, 2013

[16] Pellenghar, C., Müller, P. E., Dürr, H. R., Maier, M., Birkenmaier, C., Mazoochian, F., Pfhaler, M., Troillier, H., Lienemann, A. and Jansson, V. The Influence of the Implant Size on the Outcome of Unconstrained Total Knee Arthroplasty. Acta Chirurgica Belgica, 105 (5), pp. 508-510, 2005

[17] Szakál, Z. Mérőberendezés térdízület mozgásvizsgálatához. GÉP, 57 (1), pp. 37-40, 2006

[18] Kang, L., Galvin, A. L., Fisher, J., Jin, J. Enhanced Computational Prediction of Polyethylene Wear in Hip Joints by Incorporating Cross-Hear and Pressure in Addition to Load and Sliding Distance: Effect of Head Diameter. Journal of Biomechanics, 42 (7), pp. 912-918, 2009

Potential of Low Cost Motion Sensors Compared to Programming Environments

Juraj Mihaľov, Emília Pietriková, Anton Baláž, Branislav Madoš, Norbert Ádám

Department of Computers and Informatics, Faculty of Electrical Engineering and Informatics, Technical University of Košice, Letná 9, 04200 Košice, Slovakia

Email: {juraj.mihalov, emilia.pietrikova, anton.balaz, branislav.mados, norbert.adam}@tuke.sk

Abstract: The article investigates systems, which represent a modern and popular approach to Virtual Reality and controlling systems. We would like to focus on low-cost motion sensors used in applications which are oriented on object tracking and gesture recognition. There are various types of sensors. Some of them measure the infrared light reflected from the opposing surface, previously emitted by the device in to gather information about any movement in the observed environment. Another way how to recognize not only a moving object present in the environment, but also its gestures and further characteristics of the movement is to use the Kinect. Therefore, we included Kinect also in our research. There is also a sensoric device called Leap Motion, which is specially developed to analyze gestures of human hands and track their motion with very high accuracy. We will provide pros and cons of every mentioned type of sensors or sensoric devices. Our aim is to summarize specific characteristics of mentioned devices to evaluate their ability to be beneficial in the recently very intensively expanding IoT sector. Considering new trends, we decided to focus on low cost sensors in to make our research more relevant also for small businesses and start-ups whose initiative leads to further development of sensoric soloutions and involving them in IoT. We decided to include also Myo Armband. It uses eight electromyography sensors, combined with a gyroscope and an accelerometer to sense electrical activity produced by the muscles of the forearm. Of the multiple programming environments available, we decided to compare and evaluate three programming engines most frequently used for programming applications processing sensoric data. For gaming purposes, the Unreal and Unity 3D engines are the most frequent. For robotics, medicine or for industrial purposes usually LabVIEW is the best choice. In this, we compare the aforementioned three programming environments using different algorithms, utilizing the three motion controllers, and we discuss their (dis)advantages and programming perspectives.

Keywords: Leap Motion; LabVIEW; Myo Armband; Unity 3D; Unreal Engine

1 Introduction

As a motion controller, Kinect provides an intuitive way of controlling a computer, eliminating the need of a keyboard, a mouse or other input devices. It can track up to six people simultaneously and adjust its microphone field, so it can recognize the talking person. This low-cost device has changed the meaning of computer control. However, from our point of view, the main disadvantage of Kinect is its field of view. This can be partly solved by using a Leap Motion device, which – similarly to Kinect – employs reflected infrared light. Though it is not able to track the entire body, only the hands, it can recognize gestures and moves at a high-level, including real-time reactions. A combination of Kinect with Leap Motion could upgrade the sensed area and allow high-precision hand tracking, close to the sensor [1]. Since a direct view of the sensors (using the infrared spectrum) is required, they mainly recognize gestures. That is why current research focuses on the ability to track the user, to allow him/her to turn back or sideways to the sensors and have gesture recognition still sufficiently accurate. In addition to infrared light measurement, another possibility is to use electromyographic sensors, gyroscopes or accelerometers affixed directly to the human body [2]. An example of such a peripheral device, utilizing the aforementioned technologies, is the Myo Armband. From our point of view, combining low-cost sensors, such as Myo Armband, Kinect and Leap Motion, can result in tracking users to a distance of up to 4 meters and reliably recognize gestures even in case of poor visibility. Moreover, such a combination may lead to integration with CAVE systems (Cave Automatic Virtual Environment), representing a fully immersive virtual reality system [3]. To exploit their full potential, one has to evaluate the accuracy of the sensors in the available programming environments (including sensor control features). CAVE consists of several subsystems, in fact separate agents, working in parallel with a huge amount of data [4]. Currently, the market offers several possibilities. To select the optimal movement recognition technology and user's gestures is as important as to choose corresponding development environment. It is important to consider also its reliability, availability of plugins and updates. Our first two choices were the Unreal and Unity engines, both mostly used in computer games and entertainment applications. These softwares are ideal for households and for private purposes; however, they are not sufficient for industrial purposes. Therefore, our third choice was LabVIEW, a programming environment preferred in the industry and robotics [5]. In this paper, we evaluate these three programming engines using small applications created to control three motion sensors, focusing on their effectiveness as well as their user-friendliness [6].

2 Motion Sensors

As already stated, current research is aimed at creating a sensor network, consisting of several various sensors employing infrared light. Notable examples of infrared depth sensors include Kinect, DUO3D, Intel Realsense, Leap Motion and, in case of outdoor environment analysis, Fotonic [7]. Of these, we selected Kinect and Leap Motion, being low-cost devices and, as stated in [8] and [9], their data may be combined in a complementary way. From Kinect data, we generate 3D images of the target, while Leap Motion data allow accurate tracking of hands and fingers. Authors of [10] discuss a combination of Kinect and Leap Motion, testing their accuracy and reliability in ASL (American Sign Language) gesture recognition. From user view, we focus on research on sensors that are radiating infrared light spectrum. It is important to examine the reliability and accuracy of current motion sensors in order to increase their quality. There are projects like DMF (Deformable Model Fitting), an algorithm for 3D face recognition using Kinect to classify mimics with maximum probability, or the Microsoft Avatar Kinect tool, imitating the user, including his/her facial expressions. Motion sensors like Kinect has a high potential of utilization in virtual reality, environment analysis, and – using a combination of sensors and state-of-the-art technology – even in health-care. It is used by therapists to help people with various physical disabilities who tend to lack enthusiasm for physical exercise. Games and other physical activities based on Kinect motivate patients to move more and have fun while doing exercises. Another well-known use is Adora[1], an operation assistant controlled by voice and hand gestures, enabling surgeons to access patient data. The Virtualrehab project uses Kinect or Leap Motion to track and capture movements of patients and allows them to play games. Patients can do physical exercises by playing games using Leap Motion – to train hands – or Kinect – to train their entire body. Such games focus on balance, coordination and posture of the patient and they use customized rehabilitation programs to treat physical health problems. Kinteract software, utilizing motion-based games in the rehabilitation process, is described in [11]. The added value resides in providing a motion sensor server that supports a growing array of motion sensors and merges their data into a single protocol. Authors interconnect Kinect, Leap Motion and Orbotix Sphero devices[2]. In this combination of sensors, Orbotix Sphero is a hand-held durable" robotic ball", with a diameter less than 12cm and weight of 200g, communicating with devices compatible with iOS, Android and Windows. Sphero is a low-cost device to be controlled by other devices; however, it can also be used as a controller due to the powerful integrated IMU (Inertial Measurement Unit). Sphero can be used as a motion sensor thanks to its gyroscope and

[1] Adora homepage, http://adora-med.com/.

[2] Sphero homepage, http://www.sphero.com/.

accelerometer sensors. It is programmable within Lightning Lab, which allows programming Sphero with a compatible device.

2.1 Infrared Motion Sensors

Infrared technology is utilized within the Leap Motion sensor to track one or both hands in a fast and accurate fashion. It usually monitors space from the top of a desk, in a range of 25 mm and 600 mm. As a great advantage, it may be attached to virtual reality headsets, most often Oculus Rift or HTC Vive. The device recognizes simple gestures, hand movements and their location at 200 Hz. In order to get the relative location of the tracking point, Leap Motion utilizes frames, subsequently placing this point into the Cartesian coordinate system. It contains three infrared LEDs and two infrared cameras. When sensing the environment, it immediately sends coordinate data via USB and calculates the framed scene [12]. Since Leap Motion was released with an SDK (Software Development Kit), it is possible to merge it with the fields of view of other motion controllers, such as the Kinect – in case of the latter, it is up to 150×120°.

2.2 Sensor Combinations in Gaming Controllers

Kinect is a well-known motion controller created as a combination of several sensors in a single device. Microsoft unexpectedly stopped producing Kinect 2018 25th October and sold Apple's patent[3]. Apple has already integrated it into the iPhone X. The modified Kinect in this smartphone is placed in the upper ramp and uses it on FaceID. FaceID emits 30,000 infrared beams and monitors their return time to measure depth and recognize the user[4]. Kinect was produced in two versions: Kinect 360 and Kinect v2. Authors of [13] directed their attention to these sensors, confirming that Kinect v2 is more accurate and has better parameters in comparison with the first-generation sensor (see Table 1). Authors of [14] described an experiment leading to the conclusion that the main technical advantage of v2 over v1 was that it provided better resolution. This was achieved through distance measurement performed for each pixel of the captured depth maps, allowing more accurate detection of small objects and better color images [15]. In general, Kinect is a combination of an infrared depth camera, a color camera and a microphone array of four microphones. Thanks to the microphone array, Kinect can recognize the talking person even if there are more users in front of it and it can be controlled by voice as well. Kinect can sense up to six users together and it is able to recognize 26 joints per person.

[3] Microsoft kills Kinect, Stop manufacturing it, http://www.theverge.com/.

[4] Kinect is officially dead. Really. Offcially. It's dead, http://www.polygon.com/.

Table 1
Comparison of Kinect sensors

	Kinect 360	**Kinect v2**
RGB camera (pixels)/(Hz)	1280×1024/15	1920×1080/15 or 30
Depth camera (pixels)	640×480	512×424
Min. depth (m)	0.8	0.5
Max. depth (m)	4	4
Tilt motor	Yes	No
Horizontal Field of View (°)	57	70
Vertical Field of View	43	60
Defined skeleton joints	20	26
Full tracked skeletons	2	6
USB version	2.0	3.0

Originally, Kinect was produced as part of the Xbox game console; however, following a massive demand from users, Microsoft developed Kinect for Windows [16]. Similarly, other controllers like Playstation Move or Nintendo Wii were produced, mostly to control games and other devices. Readers interested in virtual reality are advised to check the very innovative sensor combinations available in the Oculus Rift and Oculus Touch devices. Authors of [17] published an interactive virtual museum, combining Oculus Rift and Kinect, allowing hand gestures. In case of Oculus Touch, the user must hold a pair of controllers and push their buttons. In [18], Kinect and Nintendo Wii were compared, focusing on their possibilities for home use, as a rehabilitation tool. Participants tested the devices for ten weeks during their rehabilitation process and finally inclined to use Kinect for their future rehabilitation.

2.3 Wearable Motion Sensors

Sensors using infrared light to monitor the users 'moves and gestures need direct visibility [19]. On the other hand, Myo Armband monitors forearm muscles with the help of eight electromyographs: the user puts this device on his/her dominant arm, similarly to a bracelet, right below the elbow. The muscle sensor cooperates with a nine-axis inertial measure unit, a three-axis accelerometer and a gyroscopic sensor. Then, on the skin surface, the device measures the EMG signal known as MUAP (Motor Unit Action Potential), created by multiple small muscle strings. Myo Armband monitors the skin surface at a frequency of 200 Hz [20], while the IMU works at 50 Hz. Myo Armband does not provide RAW EMG data since it only offers the user classified output. Data are processed by algorithms within Myo Armband. The classified output of Myo Armband shows which gesture corresponds to the sensed signal. Currently, the set of available gestures includes wave in/out, spread fingers, fist and hand in relaxed position. RAW data are available through the Myo Data Capture application. To its advantage, Myo

Armband is compatible with almost every platform, including MS Windows, iOS or Android from version 4.3. However, it can connect only to low energy Bluetooth 4.1, using a unique USB dongle. Currently, the official release does not provide support for Linux, though Myo community developers released PyoConnect to access Myo Armband devices. In [21], it was experimentally combined with Kinect. The authors claim that the connection was established without any issues. Myoware, similarly to Myo Armband, is a wearable sensor measuring EMG muscle signals [22]. This sensor has neither an accelerometer nor a gyroscope. However, it provides both standard and RAW EMG output. The lack of a case or cover makes it an attractive sensor; it provides various connection options, such as the Cable Shield for more cables, the Proto Shield for a prototype board, the Power Shield for batteries and the Mighty Master Shield. The Master Shield contains LEDs indicating the intensity of muscle workout. A great advantage of Myoware is that it can be easily combined with other sensors. Thus, it is possible to create special "costumes" reacting to muscle activity or it is possible to create a unique prosthesis. Moreover, Myoware is an Arduino-compatible sensor, providing many opportunities, e.g. to sense any muscle of the human body. On the other hand, Myoware needs a permanent connection via cable. The aim of the current research is to accomplish an accurate combination of low-cost sensors, requiring wireless as well as case-covered sensors. Therefore, we used Myo Armband to experimentally evaluate the programming engines described in this study.

2.4 Comparison of Selected Motion Sensors

In [23], the authors tested these three sensors in 250 applications and they analysed 15 common gestures. The main disadvantage of Myo Armband, compared to Leap Motion is that while Myo Armband enables a limited set of gestures, resulting in a more consistent use of gestures across applications. Leap Motion enables a wider range of gestures and hence it provides greater variability of gestures. Gestures involving fingers and hand movements are less commonly used in Microsoft Kinect application due to its current hand-tracking limitations. The experiment was not focused on testing security matters (e.g. intrusion detection) of the respective sensors [24]. We tested these sensors in our experiment [25] to evaluate the recognition effectiveness of gestures: pointing, waving, hand rotation, fist gesture and fist rotation. The results of the experiment are available in Figure 1, displayed by gestures and sensors. Figure 1 also shows the percentage of recognition accuracy for all sensors. The following sections discuss achieved results, recorded also in Figure 1. The graph includes percentage results on efficiency with five gestures performed by three sensors. In pointing measurements we tried to aim with the cursor in the application at the desired place and monitored whether by our hand movement the cursor reached the intended destination. We start with Leap Motion. We went through different applications whether it was a desktop cursor controller or a game in which we

tried to select the desired button in the game menu. We aimed with our index finger directly above the Leap Motion sensor. The results were very pleasurable, the cursor almost each time stopped at the place we expected. With Myo Armband we had to move all our hand to point somewhere and often it was just too slow. Although the cursor hit the mark on 90% precision with Leap Motion, 79% with Myo Armband and 80% with Micorosoft Kinect. Similar results were achieved with Kinect and Myo Armband. One must use the whole arm to move the cursor, but it is meant to be so as Kinect scans the whole body recognizing the body joints. Nevertheless, aiming was uncouth and needed much effort same as with Armband. Accurately sensor in this category was without the doubt the Leap Motion with its 90% accuracy. Waving was different for each of the three devices. For Leap Motion we performed a motion with a hand very similar to petting an object. Leap Motion took the challenge very well, our hand gesture actions were followed by the expected reactions. Since Myo Armband scans the muscles, it does not recognize the movement of the gestures, rather their starting and ending position. These two gestures may seem dull, but they work very well for their purpose. For Kinect, we took the whole arm waving into account once watching the bone recognition viewing the body joints, then different crates punching activities with our arms. The results were ample, with no big deviations. We liked the performance of Kinect in waving category the most. Kinect and Leap Motion achived 95% success and Myo Armband only 90%. We took hand rotation movement as turning one's arm around the arm's own axis. For Leap Motion, It showed just a negligible error. With Myo Armband, the hand rotation movement was pretty nice. It noticed even the smallest changes of rotation and reacted accordingly. So Leap Motion and Myo Armband achieve 98% and 97% success. For Kinect there were only a few applications using hand rotation, so we focused at bone recognition with this gesture and watched whether the body joints of the arm are moving accordingly. With a maximal deviation 10%, they copied our movements. For this gesture, we decided to recommend Myo Armband. Fist gesture for fist recognition we decided not only to scan the process of making and ceasing the fist gesture but also holding the gesture and performing arm motion. It is one of the most used gestures within each of the three devices. Leap Motion offers very accurate finger detection. It sensed the closed fist or in other words the absence of the fingers very well, although sometimes it showed one or more fingers spread apart. For Myo Armband, motion recognition was not such a big problem, since the band tracks the muscles. The problem was if one was already too comfortable with a fist holding they sometimes accidentally released the grip for a moment. Armband calibration plays a big role here as we all have different sized arms. Kinect applied fist gesture mainly on holding things, similarly as Leap Motion, uses the grab gesture. Despite some finger leaks we selected the Leap Motion as the best device for fist gesture recognition. After a long software procedure and after 50 measurements for three devices, we finally step into the result evaluation. Changing the results into percentage values we made the final graphs as we state them in Figure 1. The results are pretty straightforward, Leap

Motion showed the best results. When waving is concerned the results were similar, we selected Kinect for a subjective reasons. Although Leap Motion had slightly better measured results in hand rotation, we selected Armband as the best due to its comfortability. In fist recognition both passive and active, Leap Motion provided the best results. As we can see each device is satisfactory in different matters. When taking the cursor controlling in front of the computer, the Leap Motion is the clear answer. But when controlling the cursor from distance, like it may be at some presentations, one should rather choose, Armband or Kinect. As waving has different purposes and different ways of performance through each device, we cannot tell which one is the best. When hand rotating the best choice is Myo Armband as it is very reliable and at the same time, one can just have their arm hanged next to their body. If we want to make fist recognition, again we watch the distance from the computer. Leap Motion seems as the best but only in close distances.

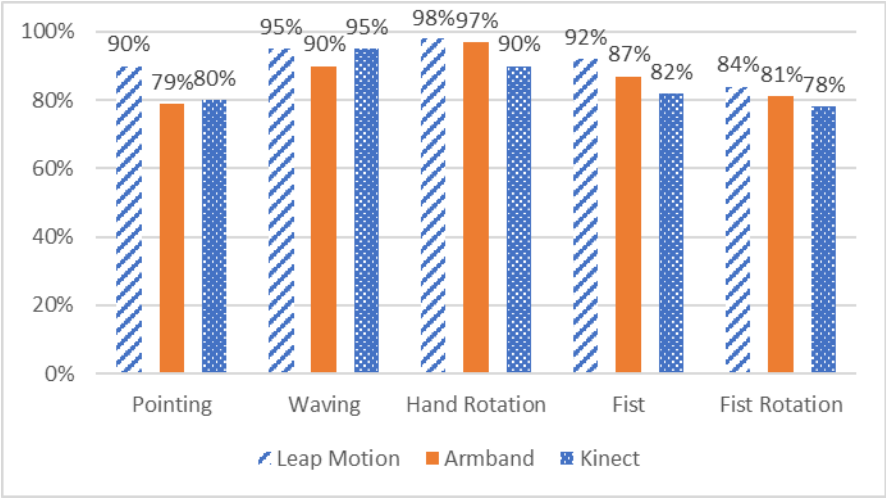

Figure 1
Summary of sensor efficiency

3 Unity3D Engine

In this study, we created simple programs interacting with three sensors: Kinect, Leap Motion, and Myo Armband. In general, we either created software using the official SDKs released with the respective sensors by their manufacturers (usually published with newer firmware versions) or we used game engines. Manufacturers and third-party developers produce drivers and plug-ins enabling creation of programs within popular game engines. Their benefits as well as their limitations

are described in the following chapter. As far as game engines are concerned, there are three key factors to be considered by programmers[5]. The first one is usability – i.e. mainly its user friendliness. The second is functionality, defining the exact capabilities of the particular engine. The last key factor is price. In this case, we should take into account what platform the final solution utilizes. Unity3D Engine[6] and Unreal Engine[7] are game-based programming environments currently dominating the market, which includes other engines like Frostbite, CryEngine or Source. In the following chapters, we evaluate these two engines using simple algorithms, all operating with three motion controllers: Kinect, Leap Motion, and Myo Armband. Authors [26] developed via Unity in cooperation with Kinect and Arduino The Robot Engine. Computer tracks and simulate user's gestures via Kinect sensor, recognizes users voice commands and accordingly to the command performs a required action. A survey performed by TNW Deals[8] showed that almost half of game developers focus primarily on Unity3D. Contrary to C++, which is preferred by most of other engines, this engine works in C#, providing better scripting features, e.g. to create a game world, as well as advanced programming aspects [27]. Moreover, it provides UnityScript – its own scripting language similar to JavaScript – intended mainly for inexperienced programmers.

Unity3D is multiplatform; it supports 2D and 3D scenes, including virtual and augmented reality. The most popular games developed in this engine are Assassin's Creed, Deus Ex, Lara Croft etc. It offers thousands of free game assets. On the other hand, the free version of Unity3D does not provide Unity Profiler, which is in general intended for game optimizing. The price of the Unity Pro is $ 1500 for lifetime support or $ 75 for a month. Authors of [28] explained how they developed a game called Callory Battle AR. They developed two types of the game: one created without a 3D game engine and the second one with a free game engine from the Unity3D suite. They described their challenges with augmented reality issues as well. Authors of [29] used Unity3D to collect large amounts of customer data concerning their participation in games and they used clustering and visualization techniques. They described a prediction model based on the technology acceptance model to improve the sales performance of innovative products. Another use of Unity3D is described in [30], where the authors described how they developed a robotic platform to evaluate cooperative bilateral telerehabilitation approaches. The main goal was to evaluate the stability and performance of the force reflection strategy in the cooperative bilateral

5 Gamesparks: Game Engine Analysis and Comparison, http://www.gamesparks.com/blog/game-engine-analysis-and-comparison/.

6 Unity 3D homepage, https://Unity3D.com/.

7 Unreal Engine homepage, https://www.unrealengine.com/.

8 TNW Deals: This engine is dominating the gaming industry right now, http://thenextweb.com/gaming/2016/03/24/engine-dominating-gaming-industry-right-now.

configuration and three robotic teleoperation techniques. In the following sections we describe the experience gained during the integration of three motion sensors with Unity3D. Step by step, we downloaded all drivers released by the sensor manufacturers and performed the correct installation of the employed sensors.

3.1 Cube Movement and Color Change using Myo Armband

Before creating a project for Myo Armband in Unity3D, it is important to import the package containing the SDK, available for download at the official website. Since every project using the engine requires the addition of a separate plug-in, this step is necessary as well. Then, an abstract camera – sensing moves from Myo Armband – and the Sun – representing natural light in the environment – appear on the screen. Our scenario involves a simple push of the right mouse button, resulting in the addition of a cube. Although writing a C# script is necessary (e.g. in Visual Studio), Unity3D compiles it by default and discovers the utilized objects.

In our case, we use an input script to move the cube by means of a motion controller, the Myo Armband – support for this is built into the system. The script has a simple behavior: following a fist gesture, the Myo Armband vibrates. The cube (visible on the screen) represents the end of a simple "hand" following the movements. Following a wave in/out gesture, the color of the cube changes from green to blue. The default color can be set by a double tap, as shown in Figure 2. The library of Myo Armband includes gestures like fist, wave in/out, spread fingers, or relax.

Figure 2
Myo Armband program in Unity3D

3.2 Cube Movement and Color Change through Kinect

Since the Kinect plug-in is not compatible with the newest version of Unity3D, our first issue was to find and install a compatible version of the engine. After connecting Kinect to a USB port, creating a new project in C# is simple. Again, the addition of the SDK is required, as well as importing the package and input plug-ins. An existing script can be edited in Visual Studio, containing two public

void functions: start and update. The start function works only with a starting script – it can be used for setting parameters and values of variables. The update function is called every 10 milliseconds, as fast as Kinect senses the scene. After dealing with hand scanning and movement, we apply the data to the cube object again. In Figure 3 is shown application which copy users right hand movement. Box change color when user moves his hand to the left to red color, to the right to green color and when user hold his hand still, box is white.

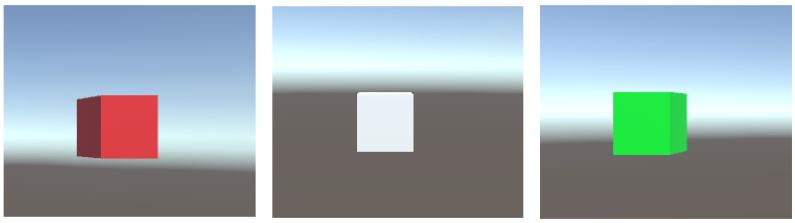

Figure 3
Kinect program in Unity 3D

3.3 Cube Movement and Color Change through Leap Motion

Similarly, to Myo Armband and Kinect, the official Leap Motion SDK contains a Unity3D plug-in, which we downloaded and imported into the compatible version of the engine and the project directory. However, here the engine encountered a problem since gestures have been removed from the library. Again, the script included two public void functions: start and update. The first one worked only with a starting script, which means it can be used for a controller which, however, Leap Motion does not contain. Therefore, we added a Controller class to call particular functions and switching the controller on/off. The update function operates every 10 milliseconds, as fast as Leap Motion senses a scene and turns it into a frame. Then, the script for hand scanning and movement is put into the cube object and set within graphic environment. The resulting script sets the cube color to green, if user moves his/her hand to the left. Movement to the right changes the cube color to red. It is important to create materials having different parameters, e.g. color or a material (see Figure 4).

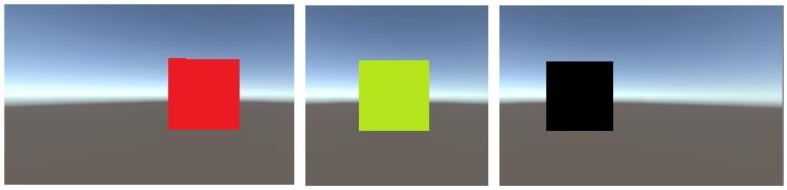

Figure 4
Leap Motion test in Unity 3D

3.4 Unity3D Engine Conclusion

We made three simple applications for motion sensors in Unity3D Engine and after that we can conclude Unity3D Engine is usable C# based programming environment for this purpose. We found huge support and libraries on the internet for Leap Motion and Myo Armband. Kinect has limited support of this environment and it was hardwork to find supported plugins. Work with C# and UnityScript is for programmer very intuitive and we can recommend this environment to work mainly with Myo Armband thanks to greater support and actual plugins.

4 Unreal Game Engine

As already stated, Unity3D covers almost half of the gaming industry software. On the other hand, there is a number of popular, high quality games created within another game engine: Unreal. Such games include Alone in The Dark or Tekken. A major difference of the two competing engines is programming language: Unity3D utilizes both C# and UnityScript (similar to JavaScript), while Unreal utilizes C++ or a graphic programming environment. This visual scripting environment utilizes components called Blueprints, claimed to be very user-friendly[9]. Authors of [31] described their experiment with six different popular game engines and compared them from many points of view, e.g. supported platforms, language support, physics engine or forward/backward compatibility of particular engines. They compared GPU and CPU usage of the games created using the respective engines. The results revealed that the Unreal engine was one of the most popular engines among visual programmers. Unreal Engine 4 has different pricing structure than Unity3D 4. It costs $ 19 per month plus 5% anytime you have earned some revenue.

4.1 Orb Jump through Myo Armband

When creating a new project for Myo Armband within the Unreal engine, first it is necessary to import the binaries and the Kinect 4 Unreal plug-in[10]. Myo Armband can be used as a controller only if the input mapping is set. After performing these settings, we attached a character to a PhysicsBallBp blueprint. To receive Myo events, an interface is necessary. Then, MyoComponent was added to the Component. Figure 5 depicts our settings saved to DefaultInput. Next, MyoInterface was added, allowing the performance of poses like fingersSpread,

9 Pluralsight homepage, https://www.pluralsight.com/.

10 Myo Developer blog, http://developerblog.myo.com/.

doubleTap, unknown, rest and waves. Our choice was to use "fist" to make a jump, as shown in Figure 6. After we played the scene, it was possible to control the orb's movements in the virtual world. By performing a fist gesture, it was possible to make the orb jump, as shown in Figure 7.

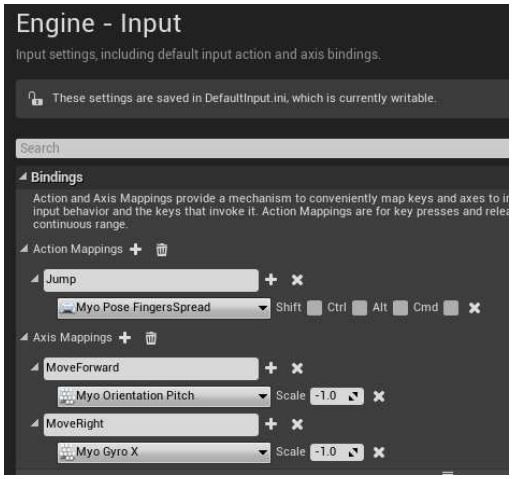

Figure 5
Input setting for Myo Armband in Unreal

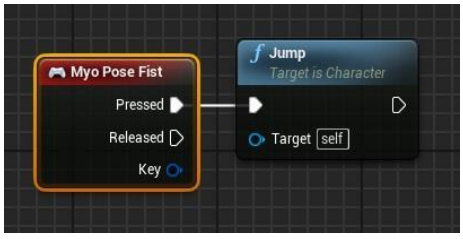

Figure 6
Blueprint for orb jump through Myo Armband

Figure 7
Orb jump controlled by Myo Armband

4.2 Orb Movement through Kinect

Again, the Kinect 4 Unreal plug-in must be imported. We selected a plug-in with API documentation, which is a primary interface to a component-based system[11]. This should be activated through the plug-in menu. Part of the plug-in is developed within the Introduction environment, where we were able to test functionality of Kinect in Unreal. Figure 8 depicts an image from IR and RGB Kinect cameras.

Figure 8
Kinect 4 Unreal Introduction test

Kinect tracking data is exposed via the Blueprint interface. Integration of Kinect with the Unreal engine requires the same steps as with Myo Armband or Leap Motion. First, the plug-in has to be downloaded into the root directory. The last necessary step is the configuration of the controller. In our experiment, we were able to sense our moving hands, as shown in Figure 9.

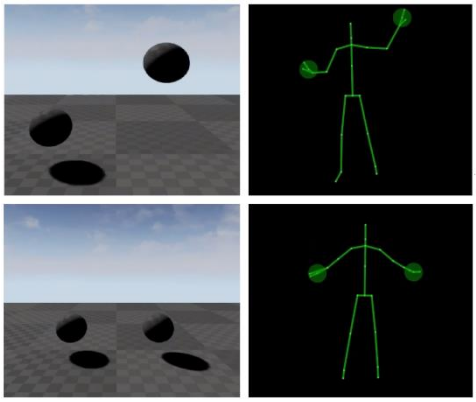

Figure 9
Kinect in Unreal Engine

[11] Opaque homepage, http://www.opaque.media/.

4.3 Object Movement through Leap Motion

Similarly to the other two controllers, binaries and plug-ins – downloadable from an official web page as part of the official plug-in Leap Motion for Unreal Engine[12]-were added. After the first steps, we could see an environment depicted in Figure 10. Convenience Rigged Characters are automatically included since version 0.9 has plug-in content. So, in order to use these characters, we changed our game mode to `LeapRiggedCharacter` or `LeapFloatingHandsCharacter` as a default mode. We modified our pass through character by changing collision preset to `PhysicsActor`. The `BasicBody_Physics Viewport` allows modification of collision shapes colliding with the world. Here, the `LeapBasicRiggedCharacter` was used, being the only one skeletal mesh available for a non-virtual reality environment. Using this character allowed us to modify any aspect of rigging. After a few steps, it was possible to test Leap Motion's features from many views, e.g. we tried to grab objects, move them from one place to another, or shake them in space. We made 50 tries and 45 of them were successful that means a 90% success rate.

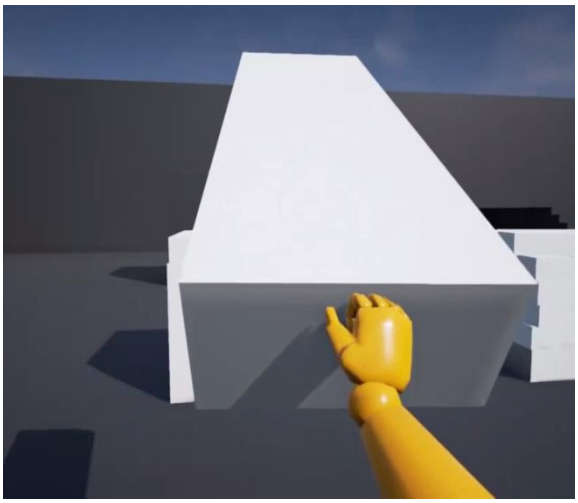

Figure 10
Leap Motion in Unreal Engine

4.4 Unreal Game Engine Conclusion

In Unreal Game Engine we prepared three environments for three different motion sensors. It is not programming as in Unity3D Engine. In Unreal Engine, work with

12 Leap Motion Developer page, https://developer.LeapMotion.com/.

motion sensors is about setting sensors as controllers and just setting up the environment. Compared to Unity3D Engine environments that we tested we completed in 50% of the time thanks to using blueprints. Thanks to blueprints, actual plugins and better license terms we encourage using Unreal Game Engine against Unity 3D.

5 Low-Cost Sensors in LabVIEW

To create software for low-cost sensors like Kinect, Myo Armband or Leap Motion, there is a wide variety of possibilities. In addition to official SDKs or the already demonstrated game engines like Unity3D and Unreal, many other visual programming environments are available [32]. One of these is LabVIEW, produced by National Instruments, aimed at the development of engineering applications. It works with many hardware targets and programming languages, utilizing plug-ins or toolkits. In this environment, programmers can count on support for third-party devices as well as on many open-source toolkits and useful add-ons. The LabVIEW environment workspace contains two main parts – Front Panel and Block Diagram. The Block Diagram contains the graphical source code of the program, while the Front Panel shows graphical output of the running program. Objects are added using the Functions Pallete that automatically appears by right-clicking the block diagram workspace. Unlike Unity3D or Unreal, LabVIEW is not free. This is a great disadvantage in case of low-cost programming, even though it offers many possibilities. Nevertheless, we will demonstrate low-cost sensor utilization in LabVIEW as an alternative way of program development for industrial, or robotics applications, aimed mainly at small and medium enterprises [33] and for Smart Cities. The trial version and student license are free; however, the LabVIEW 2016 for Analysing and Signal Processing version costs more than 3500 €[13].

5.1 Myo Armband in LabVIEW

Authors of [34] described recognition of six elementary hand movements in LabVIEW by sensing RAW EMG data of Myo Armband, while authors of [35] used them to control wheelchair motion. At the National Instruments forum[14] and student competition, a student created an intuitively controlled prosthetic hand prototype, identifying and mimicking hand gestures. The cost of this prosthetic hand, utilizing Myo Armband with LabVIEW, was less than £ 300. National

[13] National Instruments homepage, http://www.ni.com/.

[14] National Instruments forum, http://forums.ni.com/t5/LabVIEW-Student-Design/Robotic-Hand-Control-Through-EMG-Classification/ta-p/3538008.

Instruments created a forum called the LabVIEW MakerHub[15] for developers working with the LabVIEW environment, with a lot of helpful third-party content. In order to interconnect Myo Armband with LabVIEW, we downloaded Myo UDP to LabVIEW – this enables LabVIEW to work with an UDP stream of data sensed by Myo Armband's EMG sensors, as shown in Figure 11.

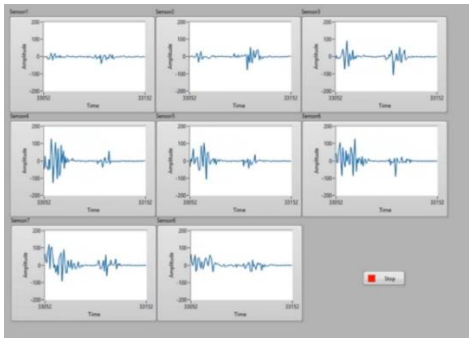

Figure 11
Front Panel for Myo Armband with the Functions Palette open in LabVIEW

5.2 Leap Motion in LabVIEW

The LabVIEW MakerHub interface for Leap Motion is a free open-source LabVIEW add-on, which makes it easy to use Leap Motion to track hand and fingertip positions with sub-millimeter accuracy, to get velocity and acceleration vectors and to recognize gestures like swipes, taps and circles. This interface made it possible to read all RAW data from Leap Motion and to use them in block diagrams. See Figure 12 and Figure 13 for an example of this – measurement of hand velocity.

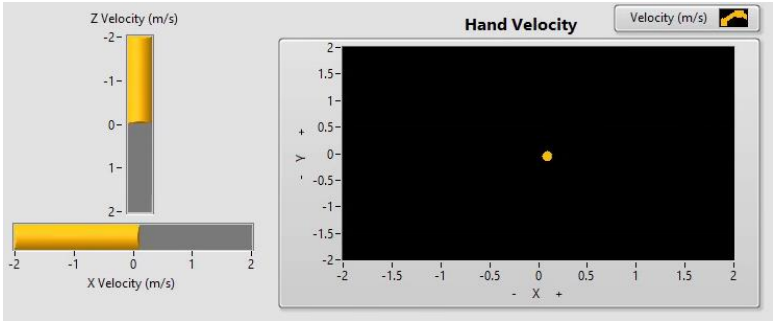

Figure 12
Front Panel for Myo Armband with the Functions Palette open in LabVIEW

15 LabVIEW MakerHub homepage, https://www.LabVIEWmakerhub.com/.

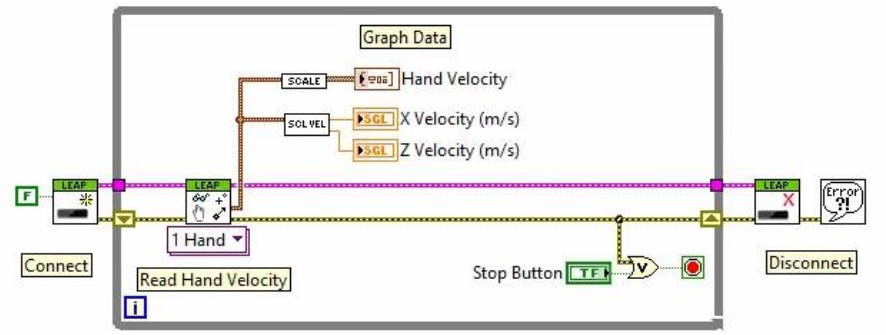

Figure 13
Block Diagram for Myo Armband with the Functions Palette open in LabVIEW

5.2 Kinect in LabVIEW

In order to utilize Kinect within LabVIEW, again, it is required to install the Kinect plug-in from MakerHub or just to use the built-in Kinect API. All Kinect possibilities can be utilized by developers to create block diagrams such as color, depth, skeletal or infrared video streams, as shown in Figure 14.

Figure 14
View on RGB-D map from LabView included Hand Gesture recognition

5.3 LabVIEW Conclusion

Work in Labview programming environment was different when compared with Unity3D and Unreal Game Engine mainly thanks to block diagram and front panel. Similar to Unreal Game Engine we spend only 50% of the time to prepare a fully functional application able to sense users movements and gestures. In Labview there are no options to prepare game environments and game applications but after our experience with Labview we decided to use it for our next experiments with motion sensors aimed toward industry and Smart Cities.

Conclusion

We presented three low-cost sensors, which we used in three different programming environments. Kinect and Leap Motion are infrared light sensing depth sensors, while Myo Armband is a sensor sensing EMG skin surface signals. These three sensors are fully compatible with both Unity3D and Unreal engines, mostly used for entertainment and gaming. The sensors are also compatible with the LabVIEW programming environment, mostly utilized for robotics and industry.

However, the free version of LabVIEW may not be used for our purposes of low-cost sensor combination, disqualifying it from such a challenge. However, in the paid (expensive) version, both its usage and software development are rather easy. We made an experiment showing how the three motion sensors work within the three programming environments. In Unity3D, we used C#, in Unreal we used the Blueprints workspace, while in LabVIEW we used the standard front panel and block diagram workspace. In these environments, working with the sensors was comfortable and highly accurate. However, to create a low-cost sensor combination, Unreal seems to be the best choice. Both Unity3D and Unreal Engine support virtual reality and they are compatible with 2D as well as 3D and 2D/3D worlds. Blueprints may be easily used with the Unreal engine, making this environment the most appropriate. The Unreal engine is the most user-friendly, with a wide range of capabilities and useful extensions. Even though it is said to be a game engine, it is a powerful programming environment. At the time we wrote this article, we thought Kinect would be ideal for our research needs.

We were considering whether Leap Motion and Myo Armband would be suitable for our research. We are focusing on sensors that are used by both, households and industry. They could be part of intelligent homes, serve as a controller for controlling non-contact computer games, and so on. They could be helpful in operations and save lives like Adora and Virtualrehab. Therefore, their reliability is important. From an industrial point of view, their consumption is also important. Various development environments are used to integrate these sensors in different areas. For playing games, is the best way to use Unity 3D and Unreal Engine, and is advisable to use LabView for sensor networks development or to implement is Smart City. After our experiments we can say that Kinect is suitable for controlling games and creating simple Smart Home soloutions. We do not consider Kinect suitable for Smart City and industrial purposes.

Acknowledgement

This work was supported by KEGA Agency of the Ministry of Education, Science, Research and Sport of the Slovak Republic under Grant No. 077TUKE-4/2015 „Promoting the interconnection of Computer and Software Engineering using the KPIkit“.

This work was supported by KEGA Agency of the Ministry of Education, Science, Research and Sport of the Slovak Republic under Grant No. 003TUKE-4/2017 Implementation of Modern Methods and Education Forms in the Area of Security of Information and Communication Technologies towards Requirements of Labour Market. This support is very gratefully acknowledged.

References

[1] Craig A. and Krishnan S., "Fusion of Leap Motion and Kinect Sensor for Impreved Field of View and Accuracy for VR Applications" In: 2016, Stanford EE26, [online] [quoted: 29.6.2018], Available at: http://stanford.edu/class/ee267/Spring2016/report_craig_krishnan.pdf

[2] Kainz, O. et al., "Low-cost Assistive Device for Hand Gesture Recognition using sEMG", Proceedings of SPIE, Bellingham 2016, pp. 1-7

[3] Nan X., Zhang Z., Zhang N., Guo F., He Y., Guan L., "VDesing: Toward Image Segmentation and Composition in Cave Using Finger Interactions", IN: 2013 IEEE China Summit & International Conference, DOI: 10.1109/ChinaSIP.2013.6625382, ISBN: 978-1-4799-1043-4

[4] Szabó C., Korečko Š., Sobota B., "Data Processing for Virtual Reality," In: Advances in Robotics and Virtual Reality: Intelligent Systems Reference Library: Volume 26. - Berlin Heidelberg: Springer-Verlag, 2012, pp. 333-361, ISBN 978-3-642-23362-3 - ISSN 1868-4394

[5] Vokorokos L., Hartinger M., Ádám N., Chovancová E., Radušovský J., "Increasing Efficiency of the Sequential Algorithms Programs Execution Using CUDA," In: SAMI 2014: IEEE 12th International Symposium on Applied Machine Intelligence and Informatics : Proceedings : January 23-25, 2014, Herl'any, Slovakia. - Danvers: IEEE Computer Society, 2014, pp. 281-284, ISBN 978-1-4799-3441-6

[6] Lor Johan P., "International and Comparative Librarianship: A Thematic Approach", 2014, ISBN 13: 9783110268003

[7] Vokorokos L., Mihaľov J. and Leščišin Ľ., "Possibilities of Depth Cameras and Ultra Wide Band Sensor", In: SAMI 2016, IEEE, 2016, pp. 57-61, DOI: 10.1109/SAMI.2016.7422982, ISBN 978-1-4673-8739-2

[8] Penelle B., Debeir O., "Multi-Sensor Data Fusion for Hand Tracking using Kinect and Leap Motion", In: VRIC '14 Proceedings of the 2014 Virtual Reality International Conference, Article No. 22, DOI: 10.1145/2617841.2620710

[9] Kopják J, Kovács, "Event driven software modeling for combinational logic networks based control programs" In: Szakál Anikó (szerk.), Proceedings of the 16th IEEE Conference International Conference on Intelligent Engineering System 2012. Lisszabon, Portugália, 2012.06.11-2012.06.13. Lisszabon: Institute of Electrical and Electronics Engineers (IEEE), 2012, pp. 253-257, ISBN: 978-1-4673-2695-7

[10] Marin. G., Dominio F., Zanuttigh P., "Hand gesture recognition with Leap Motion and Kinect devices", IN: Image Processing (ICIP), 2014 IEEE International Conference, DOI: 10.1109/ICIP.2014.7025313

[11] Matos N., Santos A., Vasconcelos A.," Kinteract: a multi-sensor physical rehabilitation solution based on interactive games", IN: PervasiveHealth'14 Proceedings of th 8th International Conference on pervasive Computing Technologies for Healthcare, pp. 350-353, DOI: 10.4108/icst.pervasivehealth.2014.255325

[12] Weichert F., Bachmann D., Rudak B., Fisseler D., 2013, "Analysis of the accuracy and robustness of the Leap Motion Controller.", IN: Sensors 2013, DOI: 10.3390/s130506380, ISSN 1424-8220

[13] Pagliari D., and Pinto L.,"Calibration of Kinect for Xbox One and Comparison between the Two Generations of Microsoft Sensors ", Sensors 2015, 27569-27589, ISSN 1424-8220, 2015. DOI:10.3390/s151127569

[14] Lachat E., Macher H., Mittet M. A., Landes T., Grussenmeyer P., "First Experiences with KinectV2 Sensor for Close Range 3d Modelling. " In Proceedings of the Conference on 3D VirtualReconstruction and Visualization of Complex Architectures, Avila, Spain, 25-27 February 2015; pp. 93-100, DOI: 10.5194/isprsarchives-XL-5-W4-93-2015

[15] Chovanec M., Bíly J., Chovancová E., Radušovský J., "Algorithms for User Detection and Authentication based on Face Analysis", In: ICETA 2013: 11th IEEE International Conference on Emerging eLearning Technologies and Applications, October 24-25, 2013, Stary Smokovec. - Danvers: IEEE, 2013, pp. 63-66, ISBN 978-1-4799-2161-4

[16] Kainz, O. et al., "Detection of Persons and Height Esatimation in Video Sequence", International Journal of Engineering Sciences & Research Technology. Vol. 5, No. 3, 2016, pp. 603-609

[17] Pinto J., Dais P., Eliseu S., Santos B. S.," Interactive configurable virtual environment with Kinect navigation and interaction", IN: Sciences and Technologies of Interaction 2015, Online: 30.3.2017

[18] Beaulieu-Boire L., Belzile-Lachapelle S., Blanchette A., Desmarais P.O., Lamontagne-Montminy L., Tremblay C., Corriveau H., Tousignant M., "Balance Rehabilitation using Xbox Kinect among an Elderly Population: A Pilot Study" IN: Novel Physiotherapies 2015, DOI: http://doi.org/10.4172/2165-7025.1000261

[19] Zug S. et al. "Are laser scanners replaceable bz Kinect sensors in robotic applications?" IN: IEEE International Symposium on Robotic and Sensors Environments, 2012, DOI: http://doi.org/10.1109/ROSE.2012.6402619

[20] Mulling T., and Sathiyanarayanan M., 2015, "Characteristics of Hand Gesture Navigation: a case study using a wearable device (MYO)", IN: Proc. of the 29th British Human Computer Interaction (HCI), pp. 283-284,

ACM, July 2015, DOI: http://doi.org/10.1145/2783446.2783612, ISBN: 978-1-4503-3643-7

[21] Kainz O., Jakab F., "Approach to Hand Tracking and Gesture Recognition Based on Depth-Sensing Cameras and EMG Monitoring", IN: Acta Informatica Pragensia 3, 2014, 104-112, DOI: 10.18267/j.aip.38

[22] Jobes S. K., Bernier J. M., Dryer S. L., Douglas E. D., "Arm Mounted Exoskeleton to Mechanically Assist Activities of Daily Living", IN: American society for engineering education 2016 Conference, Online 30.3.2017

[23] Cabreira A. T. and Hwang F., "An Analysis of Mid-air Gestures Used Across Three Platforms," in Proceedings of the 2015 British HCI Conference, ser. British HCI '15. ACM, 2015, pp. 257-258, doi: 10.1145/2783446.2783599

[24] Ennert M., Chovancová E., Dudláková Z., "Testing of IDS model using several intrusion detection tools," In: Journal of Applied Mathematics and Computational Mechanics. Vol. 14, No. 1 (2015), pp. 55-62, ISSN 2353-0588

[25] Vokorokos L., Mihaľov J., Chovancová E., "Motion Sensors: Gesticulation Efficiency Across Multiple Platform", 20th Jubilee IEEE International conference on Intelligent engineering systems, pp 293-298, 2016, doi: 10.1109/INES.2016.7555139

[26] Bartneck, C., Soucy, M., Fleuret, K., & Sandoval, E. B. (2015). "The Robot Engine - Making The Unity 3D Game Engine Work For HRI ". Proceedings of the IEEE International Symposium on Robot and Human Interactive Communication, Kobe pp. 431-437, DOI: 10.1109/ROMAN.2015.7333561

[27] Jakab, F. et al.: Rich Media Delivery, Computer Science and Technology Research Survey (CSTRS), Vol. 3, 2008, pp. 31-36

[28] Kim L. S., Suk H. J., Kang J. H., Jung J. M., Laine T. H., Westlin J., "Using Unity3D to Facilitate Mobile Augmented Reality Game Development", IN: 2014 IEEE World Forum on Internet of Things, DOI: 10.1109/WF-IoT.2014.6803110

[29] György Györök, "Embedded hybrid Controller with programmable Analog Circuit", In: IEEE 14th International Conference on Intelligent Systems. Gran Canaria, Spain, 05/05/2010-07/05/2010. Gran Canaria: pp. 1-4, Paper 59, ISBN: 978-4244-7651-0

[30] Felipe A. Pires, Wilian M. Santos, Kleber de O. Andrade, Glauco A. P. Caurin, Adriano A. G. Siqueira, "Robotic Platform for Telerehabilitation Studies based on Unity Game Engine", In: Serious Games and Applications for Health (SeGAH), 2014 IEEE 3rd International Conference, 14-16 May 2014, DOI: 10.1109/SeGAH.2014.7067094, ISBN: 978-1-4799-4823-9

[31] Mishra P., Shrawankar U., "Comparison between Famous Game Engines and Eminent Games", IN: International Journal of Interactive Multimedia and Artificial Intelligence, 2016, ISSN: 1989-1660, DOI: 10.9781/ijimai.2016.4113

[32] Madoš B., Hurtuk J., Čajkovský M., Kudra E., "Visual programming tool for computer with data flow computation control" In: Acta Electrotechnica et Informatica, year. 14, č. 4 (2014), pp. 27-30, ISSN 1335-8243

[33] Chovancová E., Vokorokos L., Chovanec M., "Cloud computing system for small and medium corporations," In: SAMI 2015. - Danvers: IEEE, 2015 S. 171-174. - ISBN 978-147998221-9

[34] Navarro J.C., León-Vargas F., Pérez J.B., "EMG-Based System for basic hand movement recognition", IN: Dyna, year 79, pp. 41-49, Medellin, 2012, ISSN 0012-7553

[35] Sathish S., Nithyakalyani K., Vinurajkumar S., Vijayalakshmi C., Sivaraman J., "Control of Robotic Wheel Chair using EMG Signals for Paralysed Persons", IN: Indian Journalof Sience and Technology, Vol. 9, January 2016, DOI: 10.17485/ijst/2016/v9i1/85726, ISSN: 0974-6846

Survey of Ethical Managerial Behavior – a Three Country Comparative Study

Andrea Bencsik, Renáta Machová, Lilla Csókás

Faculty of Economics, J. Selye University
Bratislaská cesta 3322, 945 01 Komárno, Slovak Republik,
e-mail: bencsika@ujs.sk; machovar@ujs.sk; 107564@student.ujs.sk

Tímea Juhász

SAP-consultant, Hostlogic Co., Hungary, e-mail: tjuhasz@hostlogic.hu

Kornélia Lazányi

Keleti Károly Faculty of Business and Management, Óbuda University
Tavaszmező u. 17, 1084 Budapest, Hungary
e-mail: lazanyi.kornelia@kgk.uni-obuda.hu

Abstract: The research presented in this study is focusing on upright managerial skills, considering the expectations towards the manager and ethical leadership behavior. The research, including quantitative and qualitative elements have addressed 3 countries (Hungary, Slovakia, Czech Republic). The questions of the survey focused on differences between upright managerial and leadership qualities, as well as the questions of ethical managerial behavior. In addition to employee opinion and considering the managerial aspects, the authors conducted a questionnaire survey to complement the research results. The results of the descritive and complex statistical analysis have shown that there is significant difference in the opinion of respondents of the mentioned countries regarding the leadership qualities and expectations, as well as the ethical behavior.

Keywords: leader; leadership; ethics; code of ethics

1 Introduction

The changes on the labour market require a new type of leadership (Mura et al., 2017, Poór et al., 2017). Earlier, high-level of intelligence and professional competence were the key features of managerial success. Nowadays, the importance

of emotions is in focus, as human factors are becoming more and more appreciated. Commitment of the employee and the need for ethical leadership behavior are also widely discussed issues, when we consider leadership efficiency and success of the workplace as a community.

Rational behavior was expected from leaders in the past, while emotions were considered an irrational factor (Lazányi, 2009 a,b). Nowadays, communication and decisions of managers should be influenced by emotions, so the role of emotions cannot be excluded. Since the 1980s it has been widely accepted that managers have to deal with emotions of their subordinates because ignoring emotions can result in decreased management efficiency (Lazányi, 2011). A good manager has the appropriate mental skills and expertice, but emotional intelligence is a key to succeed (Poór, 2009). However, besides cognitive and emotive components, ethical factors also seem inevitaable when describing an upright manager or leader. As ethical leaders are moral agents of their organisation (Xu et al., 2016) they are key determinants of organization-focused justice. Just and ethical leaders engender employees' trust in their employing organization, which in turn promotes their justice perceptions toward their organisation.

Hence, to achieve success and recognition of the organization it is necessary to introduce a leadership style, where emotional involvment and ethical behavior are emphasized. To achieve efficiency and employee satisfaction we need managers with a focus on emotions, rather than managers exercising their power. These managers are called,leaders" and have distinctive characteristics of their behavior and leadership style. The main objective of the research is to detect a relationship between these factors and explore their application in practice.

2 Theoretical Overview – Leadership

The basics of leadership as a science are connected with the origin of the civilization. The rulers of Egypt, the Greek heroes and the biblical patriarchs have one thing in common – leadership style.

Numerous definitions and theories emerged about the concept, content and meaning of management and leadership. Based on the scientific background, it is a process influencing the behavior between the superior and the subordinate. Our main objective was to find out how the behavior and qualities of superiors influence the business processes, how the superiors tend to motivate their employees to meet objectives that serve the goals, needs and expectations of both sides (Bakacsi, 2004); (Day, Antonakis, online, 2015); (Stoner,Patterson, online, 2005). The leadership expectations and the qualities of a good leader had been defined by the Greek philosopher, Plato (The Republic). There are four qualities that make a good leader. These qualities are: wisdom, courage, moderation and justice. Numerous

researchers and professionals addressed the theoretical and practical aspects of leadership. The question "Who is a good leader?" reoccurs in most of the publications. The 20th century has become the decade of development of the management science. The science is a subject to constant change, which is constantly influenced by social and economic systems (Sedlák, 2009); (Szűcs, Rády, Matkó, 2013); (Tureckiová, 2007). The research of Kurt Lewin (2015), a representative of behavioral science became a pioneer in several aspects. He outlined the conclusions about leadership styles in 1938, and summarized the results of a series of experiments based on simulated problem solving in a team. He interpreted three different management styles (Bakacsi, 2004); (Heidrich, 2011).

His theory is based on three types of behavior:

1. **Autocratic leadership style:** all the important issues are managed by the leader; he is sets the tasks and organizesthe teams. He is solely responsible for decision making, controlling, evaluation and providing reward for the employees. The leader's behavior can be characterized rather friendly and impersonal than hostile.
   The experiments of Lewin have shown the highest performance in this group (74%), but the performance was combined with stress. Resignation of the leader was followed by declining performance (29%). The autocratic leader is significantly limiting the independence of team members.
2. **Democratic leadership style:** the most important issues are decided by team members following a debate. The leader acts as a facilitator and encourages members of the team. The members of the team can decide who they want to work with, and the team is responsible for sharing tasks among the team members. The leader is objective or realistic. This style of leadership leads to 50% of performance. The activity can be characterized by creativity.
3. **Laissez-faire/ delegative leadership style:** the leaders are hands-off and allow team members and individuals to make decisions; they do not cooperate. The leader provides different tasks to team members and encourages the staff to ask for further information, if necessary. He is not involved in debate or consultation. The Laissez-faire style of leadership is characterized by low quality of work. The team performance is only 33%.

The research results show that the team members found democratic and laissez-faire style of leadership the most appropriate, but autcratic style of leadership proved to be better in case of solving tasks (Dobák, Antal, 2013); (Dobák, Antal, 2010). However, it is true about all the styles introduced above that the leader–follower relationship is a dyadic one-on-one relationship, hence there is no leader without a follower (Lussier, Achua, 2004).

The concept of management and leadership, as well as the correlation between them has been addressed by many researchers. It is not the aim of this study to discuss this issue in detail. However, we find it important to highlight the issue relevant to

our research, to emphasize the difference between leadership and management. It is a question of debate, whether difference between leadership and management exists or not. New theories emerged in the field of leadership science in the 1980s. Conger and Kanungo (1998) have made an influence with the concept of charismatic leadership in the organization (Karácsonyi, 2006). Charismatic leadership is the attribution of leadership behavior, perceived by the employees. Based on the theory, leadership can be defined as a kind of behavior. The charismatic leader is differentiated from non-charismatic leaders by the following behavioral elements:

- Vision for the future
- Personal risk taking
- Sensitivity towards the environment
- Sensitivity to followers needs
- Behavior different than the usual

By articulating a vision, having sensitivity to followers needs and developing a sense of collective identity, charismatic leaders may strengthen identity-based trust (Lewicki, Bunker, 1996). Caldwell and Karri (2005) have defined 15 characteristics of great leaders. In his model integrity, as the main initiator of organizational and interpersonal trust creates congruence and alignment of organizational rules and values, while an upright moral position and ethical principles accertain that the leader honoures his duties and that the interests of all parties will be taken into account and protected (Caldwell et al. 2008).

The introduction of one of the oldest and the most basic theories of human sensibility is only a brief excerp of the models and theories, which focus on leadership behavior aimed at achieving success. We will not provide a detailed presentation, but their importance is undisputable regarding the research of successful leadership. We wanted to know in what measure the respondents agree with the existence of leadership qualities.

The good leader has excellent interpersonal skills and can motivate the team of his employees. He is systematic and can handle the unexpected situations; can exercise his authority and build mutual respect; emphasizes cooperation and enthusiastically involved in it. He is able to adapt to specific situations and accept different opinions and perspectives, thus enabling the staff to accept the vision of the organization and common objectives. A leader is able to generate trust in his subordinates, where they do not only enter into a social contract with another party, but willingly accept the risks involved within that relationship as well (Mayer, Gavin, 2005), (Lazányi et al. 2017). Subordinates, by their choice of following a leader relinquish their personal choice to another person hoping that the leader will honor his duties (Caldwell, Clapham, 2003). Hence, trust is a basic function of the leader-follower relation. What is more, according to Brown's findings (Brown et al. 2005) trust and the perceived level of the leader's fairness play vital roles in the formation of employee perceptions about their leaders' ethics and the organization's ethical climate, influencing the subordinates' motivation and their behavior.

2.1 Business Ethics

Ethics means moralization, so we can conclude that it is related to morality and morals (Bláha, Dytrt, 2003); (Jankovský, 2003); (Lewis, 1985).

According to an ancient hypothesis, ethical or moral behavior expresses self inspiration of an individual to control their behavior in order to benefit ourselves and others, without being harmful for anyone.

Ethics is a science dealing with moral principles. Its main objective is to explore specific rules and principles, which define what is acceptable or not in certain situations. These rules and principles are called ethical theroy (Crane, Matten, 2007).Business ethics became a discussed issue about 50 years ago in the USA. In 1990s, Zsolnai and Kindler (1993) published a comprehensive study about the impact of ethics on the economy. Boda and Radácsi (2002) emphasized the function of strengthening social expectations in the development of business ethics, highlighting that not only the environment but the corporate executives themselves required the fixing of ethical norms to deal with internal moral conflicts. According to the authors, the primary objective of corporate ethics is to provide an analysis framework for decision making and suggest solutions to enhance ethical behavior of management (Varsányi, 2006).

The emergence of business ethics in the 1980s was a revolutionary paradigm shift that brought a new way of thinking. Beside profit maximization, ethical corporate behavior became important. This period is linked to the social audit of The Body Shop, and the People, Planet and Profit strategy of Shell and the spread of CSR programmes. This period was the age of business ethics (Crane, Matten, 2010); (Zsolnai, 2015).

Several factors are listed below about the key role of business ethics:

- The public is often disturbed by new developments in the companies, but corporate ethics help to understand and accept the changes difficult to tolerate and the new situations.
- The businesses provide opportunities that make a significant contribution to the society, e.g. products, services, workplaces and pay tax. These are the pillars of the economic development.
- The violation of busines law can cause enermous damage to individuals, the community and the environment as well.
- Some businessmen have already participated in training about business ethics in Europe and elsewhere. Business ethics can help in ethical decision-making by providing leaders with appropriate knowledge and tools and enable them to identify and analyze the situations precisely and find solutions to ethical issues and dilemmas they face.
- Ethics violations are still present in the business world. According to a recent research in England, which focuses on workplace ethics, one out of four

employees felt heavy pressure when they had to compromise between their own and the company standards.
- Business ethics is providing knowledge beyond the traditional framework of economic studies and confronts us with important issues of the society (Crane, Matten, 2007).

Ethical principles and behavioral rules are summarized in the Code of Ethics that should be respected by the members of the organizations.

2.1.1 Ethical Expectations

Ethical behavior is important for all of us. In the corporate environment, managers are the people who should serve as role models for their employees. Trust in managers is proved to be related to the perceived level of ethical leadership and a have positive effect on work engagement as well (Chughtai, 2015). In line with this Trong Tuan (2012) emphasised the importance of congruence between espoused and enacted values since this is one of the cornerstones for the development of employees' trust in managers.
This is equally relevant to ethical behavior and decision making. The concept of ethical leadership was formulated by Brown, Treviño and Harrison (2005). According to them, ethical leadership is based on two pillars: a moral person and a moral leader. They suggest that the ethical leader must be more than just a moral person. He must act as an ethical leader. However, ethical decision-making is not enough for the leaders to be ethical people. The followers have to see their leaders as an example for ethical behavior. This can be manifested in visible actions, rewards, discipline and mediating values (Donlevy, Walker, 2011); (Lasthuizen, 2008); (Spangenberg, Theron, 2005). Howell and Avolio (1992) defined the factors that determine the ethical and non-ethical behavior of the leader. The following table summarizes the factors.

Table 1
The characteristics of ethical and non-ethical leaders

Ethical leader	Non-ethical leader
The power is exercised for the interests of others	The power is exercised for individual interest
The vision is based on the needs and desires of followers	Realises his own personal vision, the vision is communicated to followers
Considers the criticism and learns from the mistakes	The critical opinion is censored
Inspires independent thinking of the followers	Requires to agree with his decisions without doubt
Practices two-way communication	Practices one-way communication
Supports and develops the followers	Does not consider the needs of his followers

Respecting the internal moral rules, represents the interests of the organization	Takes into account the external moral rules to fulfill his own interests

Source: Howell and Avolio, 1992 Page 45

The authors studied the relation and validity of the concept leadership-leader-ethics, based on the answers of respondents of three nations.

3 Research Methodology – The Research Sample

The survey was conducted in 2017 in Hungary, Slovakia and the Czech Republic. The listed countries belong to the group of Central and Eastern European countries and were recognized as socialist countries until the political transition. Nearly three decades have passed on since the political transition, both the societies and the economy struggle with some characteristic features of the past regime. All of the mentioned states have a very similar political past, which has had impact on the economic achievements of these countries. The closed borders did not provide possibility for proper development. The influx of foreign capital started after removing the borders, and different level of development has started in the mentioned countries. The common past and similar economic conditions were the factors to examine these countries.

3.1 Methodology

The research was conducted using a questionnaire survey and personal interviews. The questionnaires were distributed in the selected countries. The issue was researched from the perspective of the employees. The submitted questionnaires satisfied the requirements of representation on the basis of statistical registers. The questionnaires were sent to 5000 employees, 486 questionnaires were returned completed. The willingness to respond was more than 9%, but the research sample is not representative. The specification of our respondents will be presented in the next chapter. In order to confirm the results of the questionnaire survey, we conducted interviews with the managers of individual countries. This paper will present the results of the quantitative research. The questionnaire consisted of closed questions, based on nominal and metric scales. The questionnaire was divided into three main parts. The first part of the questionnaire focused on the issue of leadership; the second big question group concentrated on the issue of ethics; and finally the authors examined the correlation between the leadership and ethics.

The researchers have differentiated the concept of leader and manager in the survey, so the questions focused on the required characteristics of the manager, characteristics of a good leader and elements of behavior. Rest of the survey

questions focused on ethical behavior, examined the ethical values of the leaders and included questions about the Code of Ethics in the companies. We were interested in how the companies respect regulations, whether the employees are familiar and respect them. In the third phase the ethical behavior of the leader and its impact on employee satisfaction has been examined.

3.2 Methodology of Analysis

The analysis was performed by using a single and multivariate statistical methods (frequency, standard deviation, mean analysis, cross-table interpretations, nonparametric tests, cluster and factor analyzes) applying the SPSS programme. The research results are presented on the basis of the following hypothesis.

Hypothesis:

The respondents of the surveyed countries had different opinions about the relationship between leadership and ethics.

4 Research Results

The introduction of research results we will start by specifying the research sample. The tables below contain the most important characteristics. Table 2a presents the characteristics in figures, while in Table 2b the results are expressed in percentages.

Table 2a
Sample characteristics in figures

	Hungary	Slovakia	Czech Republic
Gender			
Male	62	80	54
Female	94	118	78
together	156	198	132
Age			
18-25	22	32	24
26-35	85	70	49
36-45	41	60	35
> 45	8	36	24
Type of the company			
Micro enterprise	2	34	18
Small enterprise	20	58	28
Medium-sized enterprise	20	66	26
Big enterprise	114	40	60

Source: Authors' own research

Table 2b
Sample characteristics in %

	Hungary	Slovakia	Czech Republic
Gender			
Male	12.8%	16.5%	11.1%
Female	19.3%	24.3%	16.0%
total	32.1%	40.8%	27.1%
Age			
18-25	4.5%	6.6%	4.9%
26-35	17.5%	14.4%	10.1%
36-45	8.4%	12.3%	7.2%
> 45	1.6%	7.4%	4.9%
Type of the company			
Micro enterprise	0.4%	7.0%	3.7%
Small enterprise	4.1%	11.9%	5.8%
Medium-sized enterprise	4.1%	13.6%	5.3%
Big enterprise	23.5%	8.2%	12.3%

Source: Authors' own research

The first part of the questionnaire deals with the leadership qualities. The respondents had to express their opinion about the qualities emphasized by Plato (wisdom, courage, moderation and justice). The respondents had to decide on 5-point Likert Scale how much they agree with the ideas mentioned above. The scale is used to express the opinion of respondents, where 1 = not characteristic at all, 5=absolutely characteristic. 82.1% of the respondents agreed with the definition; the average was 4.2, while deviation was low (838), which means that the respondents had a relatively unanimous opinion on the issue. The authors examined whether the respondents in different countries have different opinion on the issue discussed. As the metric variable did not show normal distribution, the researchers conducted a Kruskall-Wallis Test. The results showed no significant disagreement among the respondents of different countries (Chi-Square: 4.418 df: 2 sign.: .110 $p>0.05$). Mainly the Slovak respondents accepted the definition (average: 4.24), while the lowest level of acceptance was shown by the Hungaian respondents (average: 4.13). To consider what is expected from the leader, the authors used the qualities defined by Conger and Kanungo. These qualities had to be valued on 5-point Likert Scale, where 1 = not characteristic at all, 5=absolutely characteristic. Table 3 presents the average and standard deviation of the answers.

Table 3

Qualities of a good leader (mean value, standard deviation)

Qualities	N		Average	Standard deviation
	Valid	Missing		
Future vision	486	0	4.15	.880
Personal risk taking	486	0	3.80	.941
Sensitivity towards the environment	486	0	3.84	1.010
Sensitivity to followers needs	486	0	3.94	1.005
Behavior different than the usual	486	0	3.08	1.082

Source: Authors' own research

Based on the collected data from the respondents, the leader should represent the future vision in the company, while being open to his employees. Presentation and symbolization of the future vision does not imply that he should also represent a behavior different than the usual. Based on the results of Kruskall-Wallis Test, the opinion of respondents about the qualities listed differed only in one case. Mainly the Hungarian respondents agreed with the future vision (Chi-Square: 4.078 df: 2 sig:,130 $p>0.05$); average: 4.29), while Slovak respondents agreed the least (average: 4.09).

The next focus of the research was to evaluate, whether the respondents accept their subordinate as a leader or rather a manager. To make a decision, the respondents were provided a definition by the authors. The following definition was formulated: "We think about the manager as a leader, who is providing an added value by enhancing the self-confidence of his employees, their belief in their skills and experience. He is able to motivate his team and can be characterized with excellent interpersonal skills; can handle uncertain situations; manages with prestige and puts great emphasis on teamwork; respects colleagues and capable of adapting to different situations and act accordingly. The good leader can accept the diversity of colleagues, who accepts the vision and goal of the organization, as well as work hard to achieve it."

Based on the definition, 70% (340 respondents) of the respondents considered their superiors to be a leader. Those respondents, who thought about their superior as a leader expressed their opinion about the importance of further qualities of a good leader. A 5-point scale was used for evaluation, where 1= not characteristic at all and 5= absolutely characteristic.

Table 4

Leadership characteristics (average, standard deviation)

Characteristics	N		Average	Standard deviation
	Valid	Missing		
strengthens the self-confidence of the staff	340	0	3.83	.955

inspires the team in different situations	340	0	3.85	.914
has strong interpersonal skills	340	0	3.90	.893
is able to handle uncertain situations	340	0	4.11	.794
instead of exercising power leads with prestige	340	0	4.00	.910
respects his colleagues	340	0	4.16	.911
emphasizes teamwork	340	0	3.99	1.006
accepts the diversity of colleagues	340	0	4.10	.914
can inspire colleagues to accept the future vision and goals of the ogatnization, as well as work hard to achieve it	340	0	3.92	.851

Source: Authors' own research

According to the answers of respondents about their superiors, the leader respects his colleagues, does not discriminate and can handle different situations. The respondents had a relatively similar opinion. The qualities mentioned in the table had been converted into factors for further analysis. All variables corresponded to factor formation (KMO value .916, Barlett-test: approximate Chi-square: 1652.878 df: 36 sign.: .000). The proportion explained was 66.552%, while Varimax rotation was used for factor formation. Two factors have been introduced:

1. The first factor covers the characteristics regarding the emotional intelligence of the leader. (accepts diversity of his colleagues; respects his colleagues; emphasizes teamwork; can inspire colleagues to accept the future vision and goal of the organization and works hard to achieve it; instead of exercising his power manages with prestige)
2. The second factor covers the characteristics connected to the management of the organization (the leader has excellent interpersonal skills; can handle uncertain situations; can inspire the staff; is able to strengthen the self-confidence of employees)

Based on the opinion of the respondents, the authors conducted further analysis. The factors were used to create homogeneous groups by clustering. 3 clusters were created, and the cluster centers are demonstrated in Table 5.

Table 5

The Cluster centres

	Cluster		
	1	2	3
REGR factor score 1 for analysis 1	.47997	-1.41107	.38284
REGR factor score 2 for analysis 1	-1.22804	-.06517	.58408

Source: Authors' own research

Based on the cluster centers, the following clusters have been formed:

1. The leader's qualities are weak to manage the organization.
2. Both factors in the cluster are weak, especially the first factor (emotional intelligence) is strongly negative.
3. Both the emotional intelligence and managerial skills of the leader are strong.

According to the respondents, 82 managers belonged to the first, 77 to the second and 181 to the third cluster.

It was also a subject of the analysis, if there is difference between the classification of managers of the surveyed countries into different clusters. The Chi-square test showed a significant difference: Chi-square: 11.206 df: 1 sign.:, 024 $p<0.05$. The results showed that more than half of the Hungarian respondents ranked their superiors in the third cluster, while each sixth of the respondents ranked them into the second cluster. 46.5% of the Slovak respondents ranked their superiors into the third cluster, while each second respondent placed them into the second. The respondents of the Czech Republic ranked their superiors into the third cluster, while each fifth of the respondents placed them in the second cluster. According to answers of respondents, their managers are rather leaders, while their emotional intelligence should be improved.

The following questions focused on the respondents' satisfaction with their managers. About 65% of the respondents were satisfied with their superior, who were evaluated on 5-point scale (1=absolutely dissatisfied and 5= absolutely satisfied). The authors also examined, if there is a difference in level of satisfaction between those, who considered their superior a leader or not. The non-papermetic Mann-Whitney U test 8068.00 sign.: .000 signalled a significant difference. Those who categorized their superiors as leaders have reached a satisfaction rate of 4.11 combined with a low-level of standard deviation .844. Those, who did not think about their superiors as leader had a very low rate of satisfaction 2.77 with a higher level of standard deviation (standard deviation: 1.033).

The respondents had to position their superior according to Lewin's leadership styles. According to 32.7% of the respondents their superiors are autocratic, 52.9% apply democratic style of management and 14.4% fall into Laissez-faire style. The classification of leadership style had no significant effect on the nationality of the respondents (Pearson Chi-square: 5.365 df : 4 sign.: .252 $p>0,05$).

The authors have analyzed whether there is a correlation in the pattern between the satisfaction with the leader and the leadership style. The Kruskal-Walis test proved a significant correlation (Chi-square: 123.592 df: 2 sign.: .000 $p<0.05$). The respondents were mainly satisfied with democratic style of leadership (average: 4.18), followed by Laissez-faire style of leadership (average 3.73) and the least popular was the autocratic style of management (average: 2.93).

The next part of the questionnaire focused on opinion about ethical issues. According to an ancient belief, the moral or ethical behavior expresses that individuals control their behavior to benefit others or cause no harm to anyone.

The first questions the authors examined were,whether ethical misconduct or problems occur on the workplace and if the companies have already introduced the Code of Ethics, including the required ethical principles to respect in the company. The analysis was also interested in how much the employees know about the Code of Ethics and how familiar they are with the principles involved in the document.
About a third of the respondents have already experienced ethical misconduct in their workplaces. 33.3% of the Hunagrian 22.2% of the Slovak and 33.3% of the Czech respondents had experience with ethical violation on their workplaces. The authors have collected several options regarding ethical violation. The respondents had to decide in what measure the listed options are characteristic for their organizations. They had to evaluate the listed options on the 5-point Likert Scale (1= not characteristic at all, 5- absolutely characteristic). The standard deviation and the average are presented in the table below:

Table 6
Non-ethical forms of behavior

Non-ethical forms of behavior	N		Average	Standard deviation
	Valid	Missing		
Lie	486	0	2.37	1.106
Deception	486	0	2.33	1.035
Bluffing	486	0	2.44	1.084
Abuse of power	486	0	2.54	1.236
Fail to comply with the law	486	0	1.97	1.019
Remain quiet about the key information	486	0	2.28	1.077
Agression	486	0	1.72	.958
Bribery	486	0	1.69	.903
Sexual orientation discrimination	486	0	1.66	.936
Companies ignore their negative impact on the external environment	486	0	1.83	.987

Source: Authors' own research

The low average values show that the listed non-ethical forms of behavior and procedures are relatively uncommon on the workplaces of the respondents. The highest average among the listed ones was shown in case of abuse of power. The standard deviation is the highest, which means that the respondents did not share the same opinion. Sexual discrimination was considered to be the least typical and respondents had a relatively similar opinion.

The authors have also analyzed whether there is difference in terms of ethical forms of behavior listed between the individual countries. The test has shown a significant difference in the following cases:

Table 7

Kruskal-Wallis-test (p<0,05)

	Chi- Square	df	Asymp. Sig.
Deception	8.036	2	.018
Bluffing	7.094	2	.029
Abuse of power	6.232	2	.044
Bribery	9.873	2	.007

Source: Authors' own research

In terms of deception, the highest average was for the Hungarian respondents (average: 2.5), the lowest for Czechs (average 2.24). Bluff was the most typical for Hungarians (average 2.56) and the least typical for Czechs (average: 2.29). Abuse of power has shown the highest value with Hungarians (average: 2.71), the lowest value was achieved by Slovak respondents (average: 2.40). In case of bribery, the highest average was given by the Checz respondents (average: 1.79), while the lowest value by Hungarians (average 1.51).

According to the respondents, 36.6% of the organizations have Code of Ethics that employees have to be familiar with. 9.1% of the respondents know about the Code of Ethics, but do not control whether the principles are kept or not. 13.2% of the organizations have Code of Ethics, but the employees are not familiar with it. 41% of the respondents answered that the organizations they work for do not have a written set of principles in the form of Code of Ethics. There was significant difference regarding the nationality (Pearson's Chi-Square test: 62.280 df: 6 sign.: .000 p<0.05). The Hungarian organizations follow the principles of the Code of Ethics (48.7%). The most frequent answer of Czech and Slovak respondents was the absence of Code of Ethics (Slovak respondents 57.0%, Czech respondents 43.9%).

The respondents were asked about their reaction if they recognize that colleagues or superiors do not respect the principles of the Code of Ethics. Most of the respondents (40.6%) signal that the principles of the document were not respected; 24.4% of the respondents showed no reaction at all; 20.6% would announce any unfair action; 14.4% warn the attention of the person for unfair action. During the examination of the question in different countries, the authors identified a significant difference (Pearson's Chi-Square: 20.743 df: 6 sign.: .002 p<0.05). The majority of Hungarian respondents (30.8%) take no action, while 58% of the Slovak and 50% of the Czech respondents warn the attention for unfair action.

Further question was whether the manager always respects the principles of Code of Ethics. The respondents had to provide their answers on 5-point Likert scale, where 1= not characteristic at all and 5= absolutely characteristic. The average value was 4.35 and the standard deviation .709, which suggests that the phenomenon is

really characteristic. The low average value shows that respondents have similar opinion. The Kruskall-Wallis Test also presented different opinion of the countries involved in our research (Chi-Square: 11.226 df: 2 sign.:, 004 $p<0.05$). The most characteristic was the statement in case of the Czech respondents (average 4.49) and the least characteristic was in case of the Slovak respondents (average: 4.17). According to 68.7% of the respondents, the managers show ethical behavior, while 13.6% of the respondents experienced unethical behavior.
Finally, several forms of unethical behavior were listed and respondents had to choose, which form of unethical behavior and to what extent was characteristic for their managers (where 1= not characteristic at all and 5= absolutely characteristic). The average of answers and the standard deviation is presented in Table 8.

Table 8
Unethical forms of behavior

Forms of behavior	N		Average	Standard deviation
	Valid	Missing		
Different treatment of employees	486	0	2.32	1.189
Using inappropriate tone	486	0	2.27	1.173
Abuse of power	486	0	2.23	1.222
Unfair evaluation	486	0	2.23	1.187
Retaining information	486	0	2.25	1.118
Distrust	486	0	2.24	1.154

Source: Authors' own research

Low averages have emerged in case of different forms of behavior, which show that unethical forms of behavior are not really characteristic. The high value of deviations proves that respondents had very different opinion regarding different forms of behavior. Significant difference in opinion is shown in case of two forms of unethical behavior: "using inappropriate tone" and "retaining information". The Slovak average (2.39%) was the highest in case of the first (using inappropriate tone), while highest average (2.41%) in case of the lattest (retaining information) was shown by the Hungarian respondents. *Summarizing the results above, the hypothesis was accepted.*

Conslusions

The present paper presents the results of survey conducted in 2017. The research focused on management vs leadership and ethical issues in three different countries. Based on the result sample of the survey, the Hungarian, Czech and Slovak respondents had different opinion about the relationship between ethics and leadership.

Our respondents have agreed on the most important qualities of a good leader, emphasized by Plato. These are the following: wisdom, courage, moderation and justice. In addition, the most important feature of the good leader is to represent the

vision of the organization, to remain open to employees and consider the needs of them. However, the mentioned characteristics do not determine a different behavior as a manager. Marcus Buckingham (2009) also emphasized that a good leader can recognize the value and unique qualities of the employee, as well as he can utilize them.

We have also examined the ratio of those, who are called leaders by their employees in the mentioned Central and Eastern European countries. A relatively high ratio (70%) of respondents think that their superior is a leader. This can be seen as a very positive achievment and it also reflects that our region is dominated by leaders respecting their employees, who do not practice discrimination and are able to handle different situations. Our research has shown that all the employees, who think about their superiors as leaders were more satisfied with the superior. We came to conclusion that it has impact on the employee's satisfaction if their superior is considered to be a leader.

Based on the Lewin's experiment, we have examined which style of management is the most widespread among the managers. More than half of the managers practice democratic style of management. This is followed by the autocratic style of management, represented by one-third of the managers. The smallest ratio was achieved by managers practicing Laissez-faire style of management. We have also analyzed which management style the employees were the most satisfied with. Respondents were the most satisfied with the democratic style of management, followed by Laissez-faire. The least satisfied were with the autocratic style of management. This result matches the research results of Lewin, however Lewin studied employee efficiency influenced by different styles of leadership. We have recognized a correlation between employee efficiency and their satisfaction. As a result, those superiors will make their employees satisfied, who consider the interests of their subordinates. This is a key to cooperation and efficiency. This result is supported by the research results conducted earlier (Vlacseková , Mura, 2017).

The second part of the research focused on ethics. We have primarily studied the ethics violation on workplaces in the Central and Eastern European countries mentioned above. The Hungarian and Czech employees have experienced workplace ethics violation at a similar rate of 33.3%. The employees of Slovak businesses have experienced ethical misconduct in a lowest measure of 22.2%. The Hungarian respondents experience several examples of ethical misconduct, but the majority of them do not react after recognizing it. It is also true that the unethical form of superior behavior shows a low average, similarly to other countries. The Slovak respondents encounter a relatively low rate of ethical misconduct, but there is low number of companies with a Code of Ethics, while the majority of Czech respondents warn the attention in case of any ethical misconduct.

The low average value shows that ethical violation is not common on the workplaces of the surveyed Central and Eastern European countries. It is true that

the ratio of these cases is relatively low, but we were interested in the possibility to decrease their occurrence on the workplaces. We believe that development and implementation of the Code of Ethics can serve as a good basis. Our survey shows that nearly 60% of the respondents emphasized the existence of Code of Ethics on their workplaces. The ratio is relatively high, but our survey results show that only 36.6% of the companies require their employees to respect the requirements included in the document. To respect the Code of Ethics was the most characteristic for the Hungarian organizations. The data presented shows that there is a need to introduce the Code of Ethics and comply with the requirements involved in the document. We think, it will help employees of the company to make good decisions, and will contribute to efficient operation of the company. It also provides guidance both for employees and their superiors about the behavior expected on the workplace. In addition to guidelines, the Code of Ethics clearly outlines the implications of non-ethical behavior. Being familiar with the consequences may reduce the frequency of ethical violation.

We found it important to examine whether a good leader respects the Code of Ethics in every situation. We believe that the leader should act as a positive example in front of the employees. If they do not respect the Code of Ethics, it cannot be required from the employees as well. Our research results show that compliance with the rules of the Code of Ethics is important, and the leaders should respect them. Only a small percentage of managers can be characterized by unethical behavior. We can conclude that they are genuinely aware of their role to be an example for employees.

The behavior of the manager has a strong impact on the employee satisfaction. Those employees are satisfied with their managers, who are A type of leader and exercise democratic style of management. Our research also emphasizes that ethical behavior is an essential attribute of a good manager. Hassan and colleagues (2013) reached similar results in their research. Attention is drawn to the fact, that managers have recently encountered difficulties in motivating their employees, but practising ethical behavior has positive impact on their employees and will increase their satisfaction.

Acknowledgements

The scientific article is a partial result of the research carried out with the support of the Hungarian Academy of Sciences (1051 Budapest, Nádor utca 7) by the DOMUS HUNGARICA scholarship and the New National Excellence Program supported by Hungarian Ministry of Human Resources.

References

[1] Bakacsi, Gy. 2004.: Szervezeti magatartás és vezetés, Budapest: Aula Kiadó, 2004, 344 pp.

[2] Bláha, J. and Dytrt, Z. 2003.: Manažerská etika, Praha: Management Press, 2003, 155 pp.

[3] Buckingham, M. 2005.: What Great Managers Do, Harvard Business Review, 2005, Accessed: 03.11.2017., https://hbr.org/2005/03/what-great-managers-do
[4] Boda, Zs. and Radácsi, L. 2002. : Vállalati etika. BKE Vezetőképző, Budapest, 2002.
[5] Brown, M. E., Treviño, L. K. and Harrison, D. A. 2005. : Ethical leadership: A social learning perspective for construct development and testing, Organizational Behavior and Human Decision Process, 2005, 97 (2), 117 pp.
[6] Caldwell, C. and Clapham, S. E. 2003. : Organizational Trustworthiness: An International Perspective, Journal of Business Ethics, 2003, 47(4), 349–364 pp.
[7] Caldwell, C., Hayes, L. A., Bernal, P., and Karri, R. 2008. : Ethical stewardship–implications for leadership and trust, Journal of business ethics, 2008, 78(1-2), 153-164 pp.
[8] Caldwell, C. and Karri, R. 2005. : Organizational Governance and Ethical Choices: A Covenantal Approach to Building Trust, Journal of Business Ethics, 2005, 58 (1), 249–259 pp.
[9] Chughtai, A., Byrne, M., and Flood, B. 2015. : Linking ethical leadership to employee well-being: The role of trust in supervisor, Journal of Business Ethics, 2015, 128(3), 653-663 pp.
[10] Conger, J. A. and Kanungo, R. N. 1998.: Charismatic Leadership in Organizations, SAGE Publications, 1998.
[11] Crane, A. and Matten, D. 2007. : Business Ethics: Managing Corporate Citizenship and Sustainability in the Age of Globalization, 2nd Edition, Oxford: Oxford University Press, 2007, 566 pp.
[12] Crane, A. and Matten, D. 2010. : Business Ethics: Managing Corporate Citizenship and Sustainability in the Age of Globalization, 3rd Edition, Oxford: Oxford University Press, 2010, 591 pp.
[13] Day, J. V. and Antonakis J. Leadership: Past, Present, and Future,Accessed: 31.10.2017., http://www.sagepub.com/sites/default/files/upm-binaries/41161_1.pdf
[14] Dobák, M. and Antal, Zs. 2010. : Vezetés és szervezés, Szervezetek kialakítása és működtetése, Budapest: Aula Kiadó Kft, 2010 483 pp.
[15] Dobák, M. and Antal, Zs. 2013.: Vezetés és szervezés, Szervezetek kialakítása és működtetése, Budapest: Akadémia Kiadó, 2013, 483 pp.
[16] Donlevy, J. K. and Walker, K. D. 2011.: Working Through Ethics in Education and Leadership, Rotterdam: Sense Publishers, 2011, 156 pp.
[17] Hassan, S., Mahsud, R., Yukl, G. and Prussia, G.E. 20113. : Ethical and empowering leadership and leader effectiveness, Journal of Managerial Psychology, 2013, 28 (2), 133-146 pp.
[18] Heidrich, B.: Alkalmazottak vezetése BGF, 2011,Accessed: 23.11.2017., http://www.tankonyvtar.hu/hu/tartalom/tamop412A/0007_e6_alkalmazotti_vezetes_scorm/lewin_kiserlete_aD6dEhuZiAH3zK03.html

[19] Howell, J. M. and Avolio, B. J. 1992.: The ethics of charismatic leadership: Submission or Liberation?, Academy of Management Perspectives, 1992, 6 (2), 43-54 pp.
[20] Jankovský, J. 2003. : Etika pro pomáhající profese, Praha: Triton, 2003, 219 pp.
[21] Karácsonyi, A. 2006.: A leadership, a szervezeti kultúra és kapcsolatuk jellegzetességei a magyar szervezetek esetében: Ph.D értekezés, Budapest: Budapesti Corvinus Egyetem, 2006, 184 pp.
[22] Lasthuizen, K. 2008. : Leading to Integrity, Empirical Research into the Effects of Leadership on Ethics and Integrity, 2008,Accessed: 31.10.2017., http://dare.ubvu.vu.nl/bitstream/handle/1871/12872/8385.pdf
[23] Lazányi, K. 2009.: Érzelem és vezetés - a vezetők érzelmei, MUNKAÜGYI SZEMLE, 2009a, 53 (4), 16-24 pp.
[24] Lazányi, K. 2009. : The Role of Leaders' Emotions. ABSTRACT - APPLIED STUDIES IN AGROBUSINESS AND COMMERCE, 2009b, 3 (3-4), 103-109 pp.
[25] Lazányi, K. 2011.: Organizational consequences of emotional labour in management. ABSTRACT - APPLIED STUDIES IN AGROBUSINESS AND COMMERCE, 2011, (3-4) 125-130 pp.
[26] Lazányi, K., Virglerová, Z., Dvorský, J., and Dapkus, R. 2017. : An Analysis of Factors Related to "Taking Risks", according to Selected Socio-Demographic Factors, Acta Polytechnica Hungarica, 2017, 14 (7), 35-50 pp.
[27] Lewicki, R.J. Bunker, B.B. 1996 : Developing and maintaining trust in work relationships, in Kramer, R.M. and Tyler, T.R. (Eds), Trust in Organisations: Frontiers of Theory and Research, Sage, Thousand Oaks, CA, 1996, 114-39 pp.
[28] Lewin, K. 2015: Principles of Topological Psychology. Format Paperback, Publisher Martino Fine Books, 2015, ISBN-139781614277903.
[29] Lewis, P. V. 1985: Defining 'business ethics': Like nailing jello to a wall. Journal of Business Ethics, 1985, 4 (5), 377-383 pp.
[30] Lussier, R. N. C. F. Achua 2004: Leadership: Theory, Application, Skill Development, South-Western Publishing, Eagan, MN, 2004.
[31] Mayer, R. C. and Gavin, M. B. 2005: Trust in Management and Performance: Who Minds the Shop while the Employees Watch the Boss?, Academy of Management Journal, 2005, 48 (5), 874–888 pp.
[32] Mura, L., Ključnikov, A., Tvaronavičienė, M., and Androniceanu, A. 2017: Development Trends in Human Resource Management in Small and Medium Enterprises in the Visegrad Group, Acta Polytechnica Hungarica, 2017, 14 (7).
[33] Plato: Állam,in: Platón összes művei, Európa, 1984.
[34] Poór, J. 2009:International Human Resource Management under changes - Eastern European Perspectives. In: Striving for Competitive Advantige and Sustainability - New Challenges of Globalization : Proceedings of the 11th International Conference of SGBED. - Bratislava, 2009, ISBN 9780979765957.

[35] Schwartz, M. S. 2005 : Universal Moral Values for Corporate Codes of Ethics, Journal of Business Ethics, 2005, 59 (1-2), 27-44 pp.
[36] Sedlák, M. 2009 : Manažment. 4th Edition, Bratislava: Iura Edition, 2009, 434 pp.
[37] Šimo, D. - Mura, L. 2015. Manažment organizácií. Bratislava: Wolters Kluwer, 2015, 264 s. ISBN 978-80-8168-242-1
[38] Spangenbert, H. and Theron, C. C. 2005 :Promoting ethical follower behavior through leadership of ethics: the development of the ethical leadership inventory (ELI), South African Journal of Business Management, 2005, 36 (2), 1-18 pp.
[39] Szegedi, K. 2001 : A magyar vállalatok etikai érzékenysége: Ph.D. értekezés, Miskolc: Miskolci Egyetem, 2001, 211 pp.
[40] Takala, T. 2017 : Dark Leadership, Charisma and Trust, 2010, Accessed: 29.10.2017., http://file.scirp.org/pdf/Psych.20100100009_40146739.pdf
[41] Trong Tuan, L. 2012 : The linkages among leadership, trust, and business ethics, Social Responsibility Journal, 2012, 8(1), 133-148 pp.
[42] Tureckiová, M. 2007 : Klíč k účinnému vedení lidí, Praha: Grada Publishing, 2007, 122 pp.
[43] Varsányi, J. 2006 : Vállalati menedzsment, Széchényi István Egyetem, 2006, Available: 01.11.2017., http://sozediva.atw.hu/alt_man2006_jegyzet.pdf
[44] Vlacseková, D. and Mura, L. 2017 : Effect of motivational tools on employee satisfaction in small and medium enterprises, Oeconomia Copernicana, 2017, 8 (1), 111-130 pp.
[45] Xu, A. J., Loi, R., and Ngo, H. Y. 2016 : Ethical leadership behavior and employee justice perceptions: The mediating role of trust in organization, Journal of Business Ethics, 2016, 134(3), 493-504 pp.
[46] Zsolnai, L. 2015: The Spiritual Dimension of Business Ethics and Sustainability Management, Cham: Springer International Publishing,2015, 218 pp.
[47] Zsolnai, L. and Kindler, J. 1993: Etika a gazdaságban, Budapest: Keraban Kiadó, 1993

Short Supply Chain: Goals, Objectives and Attitudes of Producers

Anna Dunay, József Lehota, Éva Mácsai, Csaba Bálint Illés

Szent István University, Páter K. u. 1, H-2100 Gödöllő, Hungary,
dunay.anna@gtk.szie.hu, lehota.jozsef@gtk.szie.hu, macsai.eva@gtk.szie.hu,
illes.b.csaba@gtk.szie.hu

Abstract: The research discusses the objectives, goals and attitudes of Hungarian fruit and vegetable producers using the method of Theory of Planned Behaviour. The objective of the paper is to explore the factors which may influence the decision-making process of agricultural producers in choosing the appropriate marketing channel. Research results showed that main goals of producers using direct sales are focused on economic issues, but non-economic goals (tradition, consumer relations, local values, environmental aspects) were highly preferred in their business processes. Producers, who prefer direct sales activities, generally have a wider product supply and undertake to build closer relations with their consumers. They consider stability and traditional products produced by conventional technologies as the key business success factor.

Keywords: short food supply chain; Theory of Planned Behaviour; marketing channel; fruit and vegetable producer; agricultural enterprises

1 Introduction

The aim of our research was to assess the role and acceptance of direct sales as a marketing channel among Hungarian vegetable and fruit producers. The theoretical approach of the research was developed based on the theoretical model of Bergevoet et al. (2004) which was elaborated using Ajzen's Theory of Planned Behaviour (Ajzen 1991; Ajzen 2006). Bergevoet et al. (2004) conducted a survey on the entrepreneurial behaviour of Dutch dairy farmers focusing on their main goals, objectives and attitudes, where they used the psychological model of Theory of Planned Behaviour (TPB) to explore how these psychological factors might influence economic performance and farm sizes.

Present research adapts this approach for describing the main goals, objectives and attitudes of Hungarian vegetable and fruit producers about applying direct sales as a marketing channel. The main aims of our research were to answer the following: (1) what are the main goals, attitudes and intentions of Hungarian vegetable and

fruit producers; (2) how these goals, attitudes and intentions could affect producers' entrepreneurial behaviour and strategic decisions; and finally, (3) how these elements may influence producer's selection among different marketing channels and direct sales in particular.

Although TPB was used by different researchers for understanding farmers' beliefs and motivations (Fairweather et al. 1994; Fielding et al. 2008; Hansson et al. 2012) and for the examination of farmers' managerial decisions (Bergevoet et al. 2004; Rehman et al. 2003), but – according to our experiences – it was not used for analysing farmers' perceptions towards direct sales activities either in Hungarian or international literature. The research was started for the assessment of the role and acceptance of direct sale as marketing channel among Hungarian fruit and vegetable producers by conducting a questionnaire survey. The results of the research give insight into the background of producers' decision-making process and risk taking attitude (Lazányi et al. 2017) and underline the importance of non-economic goals, such as traditional farming, improving local communities, maintaining direct relations with consumers, using environment-friendly technologies and keeping the lifestyle feature of family farms.

2 Literature Review

In the past decade, the role of short food supply chains in the agricultural sector and their impacts on the development of small agricultural enterprises and on rural communities was discussed by many academic studies. Alternative or short food supply chains are good examples for creating new links between agricultural production and society or between producers and consumers, as consumers get closer to the origins of their food and in some cases they are involved more directly in the production (Renting et al. 2003). The definition of short food supply chain by Marsden et al. (2000) emphasized that 'it is not the number of times a product is handled or the distance over which it is ultimately transported which is necessarily critical, but the fact that the product reaches the consumer embedded with information.' (Marsden et al. 2000, p. 424).

Renting et al. (2003), identified three main types of short food supply chains, all of which show a special connection between the food consumer and producer (Marija et al. 2015). Face-to-face type (1) is characterized by physical connection between producers and consumers, i.e. consumers buy directly from the producer or the processor (e.g. farm shops, farmers' markets, roadside sales, pick-your-own, home delivery, e-commerce). Spatial proximity (2) means that products are produced and retailed in the region of production and consumers consider the local nature of the product. This category includes specialist retailers – bakeries, butchers, grocers – who sell local products and the representatives of the hospitality industry selling local foods (e.g. farm shop groups, community

supported agriculture (CSA), special events, thematic routes, catering for institutions, etc.). Spatially extended category (3) means that consumers are outside of the region of the product, but the information about the place and processes of production is communicated to the consumer (e.g. fair trade products or protected denominations of origin).

Renting et al. (2003) also underlined the importance of information; according to their opinion the critical difference between 'alternative' or short food supply chains (SFSC) and conventional networks is that the food reaches the consumer together with specific information about the product. Venn et al. (2006) draw attention to the ability of these networks "to 'resocialize' and 'respatialize' food through supposedly 'closer' and more 'authentic' relationships between producers, consumers and their food" (Venn et al. 2006, p. 248), which will have significant impacts both on the development of rural communities and the viability of agricultural enterprises. In many cases, short food supply chains might be identified as examples of 'resistance' of farmers to modernization of the food system. Ubrežiová et al. (2015) underlined the importance of alternative networks in activating local human potential and local sources, and they may support strengthening of local social ties. Szegedi et al. (2014) pointed out that cooperation between the members of the chain might improve competitiveness and shorten the cycle-time of the supply chain.

In alternative or short chains, farmers can reach higher revenues because of skipping retailers, and transport and packaging costs. On the other hand, consumers may gain fresh, healthy food at a reasonable price. The wider community may also benefit from these networks because alternative food networks (AFNs) have ecological impacts represented by reduced food miles and carbon emissions that favour sustainable farming (Tudisca et al. 2014). Fehér (2007) highlighted the importance of local products, which represent a common local value. These products reach the consumer in relatively small quantities, the main marketing channel is direct sale, and products represent high quality. They often attached to services of agri-tourism, which show that direct sales activities tend to benefit both farms and rural communities (Aguglia et al. 2009).

In Hungary, alternative food supply systems (farmers' markets, farm sales, pick-your-own, local food festivals, thematic routes) play a more important role in Hungary, whereas other specific forms of SFSCs (food box delivery, buying groups, CSA and community gardens) are usually initiated by urban, well-educated people in urban areas or their agglomeration (Kneafsey et al. 2013). The most important feature of face-to-face or direct channels is the direct connection between producer or processor and the consumer, and a main advantage of direct sales is the opportunity to reduce marketing costs and to add value to the product. Lehota and Csíkné Mácsai (2012) classified direct sales channels according to the profit creating impacts (Fig. 1).

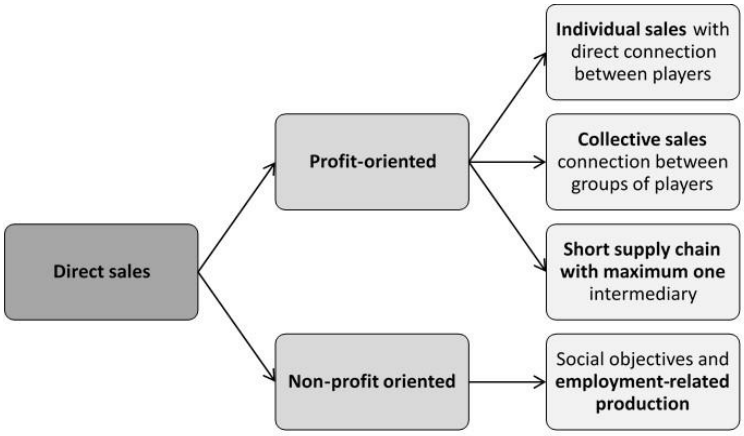

Figure 1
Types of direct sales

Types of direct selling could also be differentiated based on the venue of sale activities. In case of on-farm activities, the producer does not move from the farm and stays at the place of production, for example farm shops, pick-your-own sales (when consumers pick the products on the spot and buy it), or different agri-tourism or village tourism activities (which are emerging sectors of the tourism industry). Off farm activities covers such activities, where the producer does not stay at the place of production, for example farmers markets, farm-to-restaurant sales, e-commerce or mail-order, or taking part at special events, local food festivals (Lehota and Csíkné Mácsai, 2012).

3 Material and Methods

3.1 Theoretical Background

Theory of Planned Behaviour of Ajzen (1991) is a psychological theory that links beliefs and behaviour of individuals (Fig. 2); it states that a person's behaviour depends on the person's goals and intentions, which is influenced by attitudes (behavioural beliefs), subjective norms (normative beliefs) and perceived behavioural control (control beliefs).

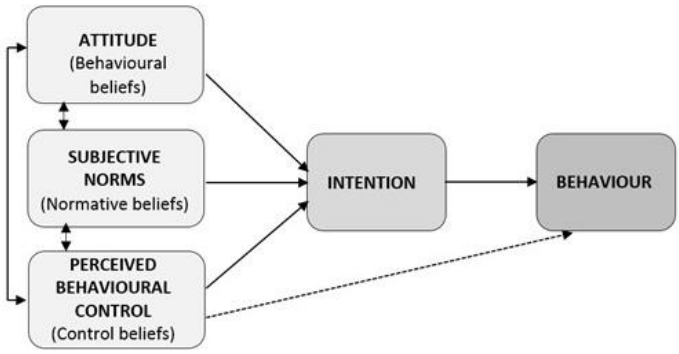

Figure 2
Elements of the Theory of Planned Behaviour

Bergevoet et al. (2004) supposed that farmers' goals, intentions and decisions are influenced not only by economic but also by non-economic factors during their business decision-making process. Their research results proved that farmers' behaviour shows a correlation with their personal and farm-related goals and objectives, which are also influenced by their attitudes, subjective standards and observed behaviour control. They concluded that goals, objectives and attitudes of the farmers determine their strategic and entrepreneurial behaviour and are in close correlation with their farm sizes. In the course of the present research we applied this theory, thus, the steps of our research were formulated in accordance with this approach.

3.2 Sampling Process and Questionnaire Survey

Based on the literature sources and a formerly conducted qualitative research, the main hypothesis of present research was that intentions, preferences and driving forces are different in the case of producers who use different marketing channels, and the acceptance of direct selling as a marketing channel is also different.

The research was conducted among Hungarian vegetable and fruit producers in order to explore the role and acceptance of direct sales as a marketing channel. Before starting the questionnaire survey, the research team conducted a set of semi-structured interviews, which results and experiences were used for finalizing the questionnaire (Csíkné Mácsai 2014). Based on the findings of the qualitative research, we supposed that direct sales is differently assessed by those agricultural producers who are engaged in this marketing channel, and by those who do not apply direct sales.

As the main aspect of our research was to unfold the differences in producers' viewpoint about direct sales, the crucial task was to represent the different opinions. Therefore, in the sampling process we wanted to cover both parties, i.e.

producers who apply and producers who do not apply direct sale as a marketing channel. As there is not any database available about producers who apply direct sales exclusively as a marketing channel, we conducted the research among producers who sell their products directly to the consumers at market halls or local markets. For surveying producers who use direct sales as a supplementary source of income, we interviewed the members of Producers' Organizations because – according to the main rule – members must sell their products through the PO.

The questionnaires were filled in through personal interviews, as in this way we got detailed and valuable background information from the respondents. In each case, the managers of the farms were interviewed, as they are responsible for decision-making and future plans of the enterprise.

The questionnaire survey was realized at four locations. Three markets are situated in the capital, Budapest. Two of them are operated by the Municipality of Budapest (Fehérvári Street Market Hall and Bosnyák Square Market Hall), the third is an Organic Market operated by the Hungarian Bioculture Association (the number of sample at Budapest locations was n=90). The fourth location is in Kecel (a city in the Southern Great Plain region of Hungary, approximately 130 km southward from Budapest) where the members of the Fresh Producers' Organization were interviewed (n=46).

3.3 Statistical Analysis

The gathered data were processed and filtered by SPSS 16.0 working package. As the main focus of the research was to explore the role and importance of direct sales, the analyses were taken in three main steps: (1) identifying the main goals, objectives and preferences of the farmers based on the analysis of the questionnaire statements; (2) analysing the relationship between the different attitudes, subjective norms and components affecting perceived behavioural control and the goal factors resulted by the first step of the calculations; and (3) analysing the relationship between goal factors and sales channels.

After descriptive statistical analyses, we conducted bi- and multivariate correlation analyses using the methods of linear regression and factor analysis. It should be noted, that due to the sampling method, the results shall not be considered as representative and the conclusions cannot be applied for the whole population.

4 Research Results

4.1 Producers' Goals and Objectives

As a first step, main goals and objectives of producers were analysed based on their farming goals, when respondents were asked to score each goal on a 5-grade Likert scale (Table 1). (In this aspect broad, general and long-term intentions are considered as 'goals', while 'objectives' represent the more specific targets of business performance.)

Table 1
Goals and objectives of producers in the examined sample (Average of a 5-grade Likert scale: 1- not important 5-very important; N=136)

Responds on goals and objectives	**Average score**
Produce high quality products	4.82
Maintain the present production level	4.68
Realise the highest income level	4.52
Enjoy own work	4.47
Contribute to the positive image of farming as a profession	4.43
Preserve regional/local values (nature, landscape, cultural heritage)	4.38
Increase the share of direct sales	4.12
Earn respect from other farmers	4.05
Have more leisure time after work	3.95
Create an existence for my successor	3.40
Implement new farming technologies	3.18
Increase farm size	2.67
Increase non-agricultural revenue	2.48

According to the results, the most important goals of producers were economic goals: producing high quality products, maintaining present production level and realising the highest income level. However, statements representing non-economic values (e.g. 'enjoy own work', 'contribute to the positive image of farming as a profession' and 'preserve regional/local values') were also considered as important by the respondents. Increasing the share of direct sales was also mentioned as an important goal, while objectives like 'implement new production technologies', 'increase farm size' and 'increase non-agricultural revenue' were assessed as least important. These results show that farmers focus on maintaining their present production level and they do not prefer improving technologies or developing their farm. A correlation analysis was conducted to analyse the relationship between the preference of goals and the share of direct sales, which results showed that there is a medium strong positive correlation between the share of direct sales and the following goals: 'earn respect of other

farmers' (0.426), 'preserve regional/local values' (0.374), 'contribute to the positive image of farming as profession' (0.455), 'produce high quality products' (0.312). Besides exploring the goals and objectives of the producers, we examined which farm types are preferred by the farmers in order to meet their goals and objectives (Table 2).

Table 2

Farm-related goals of the farmers (preferred farm types) (Average of a 5-grade Likert scale: 1- not important 5-very important; N=136)

Responds on farm-related goals and objectives	**Average score**
Farm with environment friendly production	4.38
Farm based on direct sales activities	4.26
Family farm	4.26
High-tech farm	3.38
Organic/Ecological farm	3.24
Innovative farm	2.99
Large-scale farm	2.27
Farm with agri-tourism/village tourism activities	1.86

It is concluded that respondents prefer farms with environment friendly production, farms based on directs sales activities and family farms. Other types, like high-tech farms, ecological farms, innovative farms, large-scale farms and farms with agri-tourism activities were less attractive for the respondents.

After analysing the goals and the preferred farm types, we conducted a factor analysis to explore the connections between the variables. Thus, we could describe the structure between the preferred objectives and preferred farm types, which results are summarized in Table 3.

Table 3

Factors influencing the selection of marketing channels (Rotated factor matrix)

Objectives and preferred farm types	**CV**	**Factors**				
		LS	**MO**	**DS**	**FS**	**FD**
Preserve regional/local values	0.8946	0.9237	-0.0939	0.0970	0.0142	-0.152
Enjoy own work	0.4868	0.6854	-0.0440	0.0002	-0.0054	0.123
Have more leisure time after work	0.3926	0.5817	0.0387	0.0505	-0.0250	0.222
Earn respect from other farmers	0.5211	0.5759	-0.0829	0.4189	-0.0730	0.042
Increase the share of direct sales	0.2707	0.3884	-0.0319	0.2204	0.0013	0.265
Farm with environment friendly production	0.2695	0.3812	0.1278	0.3135	0.0975	-0.004

Innovative farm	0.9603	-0.0728	0.9332	0.0538	0.2840	0.025
High-tech farm	0.6752	-0.0103	0.7660	-0.0561	0.2809	0.078
Contribute to the positive image of farming as profession	0.6587	0.5664	0.0117	0.5694	-0.0784	0.086
Farm based on direct sales activities	0.4143	0.1248	-0.2267	0.5435	0.2191	-0.063
Produce high quality products	0.3219	0.0684	0.0738	0.5337	-0.1495	0.067
Large-scale farm	0.6105	-0.0188	0.2813	0.2087	0.6148	0.331
Increase farm size	0.6814	-0.0770	0.3297	-0.0855	0.5998	0.447
Farm with agri-tourism activities	0.3192	0.0175	0.1884	-0.0882	0.5217	-0.058
Implement new farming technologies	0.5914	0.0594	0.4538	-0.1087	0.1285	0.595
Create an existence for my successor	0.4013	0.3148	-0.0873	0.1243	0.0854	0.521

Legend: CV: Communality values, LS: Lifestyle, MO: Modernization, DS: Direct sales, FS: Increasing farm size, FD: Farm development. Extraction Method: Maximum Likelihood. Rotation Method: Varimax with Kaiser Normalization. Rotation converged in 6 iterations. KMO=0.780, Bartlett: (Approx. Chi Sq.) 775.749 (Sig.) 0.000; Communalities: 0.270-0.960, Total Variance Explained: 52.931; Goodness-of-fit Test (Chi Square) 35.042 (Sig) 0.946 N=136.

For conducting the factor analysis, 5 variables from the original 21 (specified in Table 2 and 3) should be excluded from the analysis because their communality values did not reach the 0.25 limiting value. (In the factor analysis we applied the method of Sajtos and Mitev (2007) and included only those variables which reached a communality value higher than 0,25.) The remained variables were classified into five factor groups – Lifestyle (LS), Modernization (MO), Direct sales (DS), Increasing farm size (FS) and Farm development (FD) – which main characteristics are as follows:

Factor 1: Lifestyle (explained variance: 17.155%): Those factors were included into this group which were related to non-economic values, i.e. to farmers' personal life quality objectives or goals with social, cultural or environmental values. Analysing the skewness (S) of the factor, it can be stated that the distribution is significantly right-skewed for the total sample (S=-2.106) that means, these objectives have an increased importance for the respondents in connection with the future of the farm.

Factor 2: Modernization (explained variance: 12.425%): Farm types with innovative targets and values were included into this group, so the focus of this group is on farm modernization aspects. The skewness of the factor is minimally left-skewed (S=0.048), i.e. these goals are less dominant for the producers for the future of their farms. This is in line with the former results of the research, i.e. the

use high-tech technologies and innovative farming was among less important objectives of the respondents.

Factor 3: Direct sales (explained variance: 8.318%): This group includes farms based primarily on direct sales activities and objectives 'Produce high-quality products' and 'Contribute to the positive image of farming as profession'. The skewness of the factor (S=-0.934), is moderately right-skewed, i.e. these goals are considered as important for the future of the farm.

Factor 4: Increasing farm size (explained variance: 8.034%): This factor includes variables 'Increase farm size', 'Large-scale farm' and 'Farm with agri-tourism activities'. The skewness of the factor (S=0.358) is minimally left-skewed, i.e. these aspects are not dominant for the producers. This result is also in line with the former conclusions of the research, namely farmers do not plan increasing farm size and do not consider leading large-scale farms in the future.

Factor 5: Farm development (explained variance: 6.999 %): This group includes the objectives 'Implement new farming technologies' and 'Create an existence for my successor'. Based on the skewness (S=-0.393) it can be concluded that factor is a dominant perspective for the producers.

4.2 Relationship between Producers' Goals and Objectives and their Statements on Attitudes, Subjective Norms and Perceived Behavioural Control related to Direct Sales

As a next step of the research, the relationship between the attitudes, subjective norms and components affecting the perceived behavioural control (i.e. the elements of Ajzen's Theory of Planned Behaviour model) and the previously determined groups of objectives was examined, for which we used stepwise method of linear regression analysis. Stepwise method is a method for selecting the best explanatory variables (Sajtos and Mitev 2007), where the strongest correlated variable is added at first to the model and then the weaker variables are added gradually. The algorithm does multiple regression a number of times, each time removing the weakest correlated variable in such way that it would not decrease the R2 value significantly. At the end, those variables are left, which explains the distribution in the best way. The results of stepwise regression analysis are summarized by Table 5.

Table 5

Relationship between producers' goals and their statements on attitudes, subjective norms, perceived behavioural control (regression results)

	Statements	**Goal factors**				
		LS	**MO**	**DS**	**FS**	**FD**
S	The opinion of other producers is important for me	0.388		0.197		

P	I try to reduce chemical use	0.210				
A	I can sell fresh products	0.740				
P	I am open for technical and professional novelties		0.395			
P	I produce wide range of products		-0.235			
P	I produce less common fruits and vegetables		0.173			
A	Vulnerability to retailers will decrease		0.243			
A	I can sell products with higher price		-0.186			
P	I can harmonize production and sales			0.223		
P	I try to produce quality products			0.288	-0.182	
P	I use direct sale as marketing channel			0.256	0.322	
A	The vulnerability to retailers will decrease				0.344	
A	The period between production and sales will be reduced				-0.245	
A	Labour-intensive form of sales				-0.204	
P	I try to employ less employees					-0.267
A	Direct sale is applicable only for selling small amount of products					0.227
P	We can manage production & sales by the help of family					0.232
P	I am able to build appropriate relationship with consumers					-0.226
	Adjusted R^2	**0.318**	**0.251**	**0.487**	**0.217**	**0.122**

Legend: elements of TPB in statements: A: attitude, S: subjective norm, P: perceived behavioural control. Goal factors: LS: Lifestyle, MO: Modernization, DS: Direct sales, FS: Increasing farm size, FD: Farm development. One-Way ANOVA sig<0.05, N=136, only significant (P<0,001) β values are displayed in the table.

This step of the analysis was related to the statements on attitudes, social norms and perceived behavioural control and the identified five goal factors. The results of the regression analysis show that the variance of Direct sales factor is explained most significantly by the selected variables (48.7%). Based on this, it is concluded that producers, who marked direct sales as a targeted marketing channel will focus on the production of high quality products, use direct sales as a main marketing channel, they can harmonize the level of production and sales and they consider the opinion of their colleagues, i.e. other producers.

Variables that have significant positive relation with Lifestyle factor explain 31.8% of the factor's variance. For those producers who focus on non-economic

goals, the opinion of other producers is a highlighted factor, they try to minimise chemical use and consider the delivery of fresh products as a main advantage of direct sales.

The variance of Modernization factor is explained by 25.1% of variables added by the model. Producers, who focused on modernization, were more open for professional and technological novelties, and they produce special, less common fruits and vegetables. The variable 'wide range of products' showed a negative significant relation with the Modernization factor, which suggests that modernization is not associated with broadening of the scale of products, it is rather related to technical modernization. The main advantage of direct sales for those producers, who preferred modernization, was that their vulnerability to retailers would decrease.

Increasing farm size was preferred by farmers who typically deal with direct sales and consider this marketing channel as an appropriate tool for reducing the vulnerability of producers to retailers. They did not consider the production of high-quality products and fresh product delivery as quite important.

The variance of Farm development factor was explained least by the added variables (12.2%). Producers who preferred farm development use the help of their family members in production and sales and do not try to employ others. They do not consider themselves to be able to build appropriate relations with the consumers and in their opinion direct sale is applicable only for selling limited amount of products.

4.3 Relationship between Goal Factors and Sales Channels

In the next step of the research, the relationship between the five factors formulated by the objectives of the farmers and the proportion of direct sales and sales through POs were compared to the total sales. The selection of this method was motivated by the importance of these two channels because according to the answers, 61.6% of the respondents sell their products directly to the consumers, while 22.56% use selling through POs as a marketing channel, while the use of other channels were minimal.

A stepwise linear regression was used for identifying the relationship between the components, which resulted that four factors contribute significantly to the variations in selecting direct sales as marketing channels, which results are shown by Equation (1). It should be noted that the in this aspect the share of direct sales is referred as *Individual sales,* in order to distinguish it from the Direct sales (DS) factor.

$$\text{Individual sales} = 61{,}60 + 30{,}43 * \text{DS} + 12{,}27 * \text{LS} - 11{,}75 * \text{MO} - 7{,}30 * \text{FD} \quad (1)$$

$$p<0.001;\ \text{Adjusted } R^2=0.491$$

Legend: DS: Direct sale; LS: Lifestyle; MO: Modernization; FD: Farm development. (In this equation the constant and the partial regression coefficients B_i are given.)

All elements of the model were significant in relation with the share of direct sales in the producers' selection of marketing channels, and the four factors explained 49.1% of the differences in the share of direct sales.

The results of linear regression analysis reflect that the share of direct sales is related positively to *Direct sales* (DS) and *Lifestyle* (LS) factors, while *Modernization* (MO) and *Farm development* (FD) are negatively related to it. Thus, it is concluded that modernization and farm development are not among the key preferences of the responding farmers, which confirm the results of the previous interviews, when producers expressed their preferences for using conventional farming methods. The same analysis was carried out for identifying the share of *sales through POs*, which results are expressed by Equation (2).

$$\text{Sales with POs} = 22{,}56 - 7{,}74 * \text{LS} + 6{,}44 * \text{MO} - 22{,}63 * \text{DS} \qquad (2)$$

$p<0.001$; Adjusted $R2=0.624$

Legend: LS: Lifestyle; MO: Modernization; DS: Direct sales

The results of linear regression analysis reflect that the share of sales through POs is related negatively to *Lifestyle* (LS) and *Direct sales* (DS) factors, which means these factors are not important for those producers who sell their products through POs. However, *Modernization* (MO) factor showed a positive relation, which suggests that modernization of the farm has an increased importance for these producers. Three factors were added to the model and they explained 62.4% of the share of sales through POs in all sales channels. The results are in consistent with the results of the formerly conducted variance analysis, which concluded that PO members do not prefer the statements related to *Lifestyle* and *Direct sales* factors.

Further analyses were carried out to explore how the explained variance would change if selected variables from the farmers' statements on attitudes, social norms and perceived behavioural control were also included in the equations in addition to the farmers' goals. For this reason, a linear regression of was performed, where the previously included objectives entered to the model as fixed variables, while the variables of the statements were entered in a stepwise procedure in addition to these fixed variables. Equation (3) describes the role of *Individual sales* among other sales channels:

$$\text{Individual sales} = -86.16 + 6.32*LS - 4.61*MO + 11.35*DS - 2.68*FD +$$

$$+12.31*S1 + 12.20*S2 - 7.00*S3 + 5.00*S4 + 6.62*S5 \qquad (3)$$

$p<0.01$; Adjusted $R2=0.718$

Legend: LS: Lifestyle; MO: Modernization; DS: Direct sale; FD: Farm development; S1: I am able to build appropriate relationship with

consumers/buyers; S2: Direct sale is a time-consuming form of sales; S3: I produce products on larger farm size than it is appropriate for using direct sales; S4: I produce a wide range of products; S5: I can sell fresh products

By adding more variables into the model, the variance explained increased from 49.1% to 71.8%. Based on the regression equation it is can be observed that farmers who apply direct sales at a greater share, have a wide range of products, use less chemicals, are able to build good relationship with consumers. They consider direct sales as a time-consuming form of sales, but its main advantage that they can sell fresh products.

Analysing the *sales through POs* resulted Equation (4):

$$\text{Sales through POs} = 175.68 - 2.94*LS + 0.86*MO - 4.26*DS - 11.70*S1 - 7.31*S2 - 9.46*S3 - 7.49*S4 + 2.46*S5 \quad (4)$$

$$p < 0.01;\ \text{Adjusted } R^2 = 0.600$$

Legend: LS: Lifestyle; MO: Modernization; DS: Direct sale; S1: I am able to build appropriate relation with consumers/buyers; S2: I use direct sale as marketing channel; S3: Direct sale is a time-consuming form of sales; S4: I try to reduce chemical use; S5: Administrative tasks lay a heavy load on me

The results of *Sales through POs* show that the variance explained decreased by including more variables into the model which so it is not reasonable to add the statements (S) into the model. Nevertheless, we performed this step in order to make a comparison between PO members and farmers using direct sales as a marketing channel. Compared to farmers with direct sales activities – Equation (3) – in case of farmers who sell products through POs, the share of *Sales through POs* showed negative relationship with *Lifestyle* and *Direct sales* factors, but it was positively correlated with *Modernization* factor. Statement regarding the relationship with consumers (S1) showed negative correlation with the share of *Sales through POs*, which also underline the differences in their goals and attitudes.

Discussion and Conclusions

The main aim of this research was to identify the main features of vegetable and fruit producers' decision-making process in the selection between marketing channels, and to explore their entrepreneurial attitudes and behaviour, with a particular focus of direct sales as marketing activity. It should be underlined that present research results should not be considered as representative thus general conclusions cannot be drawn for the total population, but might be used for detecting the main directions of farmers' attitudes and assessment on direct sales as marketing channel.

The main hypotheses of present research – i.e. intentions, preferences and driving forces of farmers using different marketing channels and their assessment on direct sale as a marketing channel are different – was verified by research results.

The research results justified that the goals and objectives of farmers might be differentiated as economic and non-economic goals. These findings are consistent with former literature sources (Fairweather and Keating 1994; Bergevoet et al. 2004; Menozzi et al. 2015). Besides economic goals, non-economic objectives (such as sustainability, preservation of natural and cultural landscape, private goals connected to work-life balance, etc.) are also important for the farmers. The assessment of preferences and intentions are varying in farms using different sales channels. Farms applying direct sales as main marketing channel are focusing on the production of high quality products and non-economic goals like contribution to the more positive image of farming as a profession or the preservation of natural and cultural landscape.

By analysing the economic goals, it can be stated that farm development and modernization aspects have less preferences for farmers who apply direct sales. This observation is consistent with the results of Kuhnert (1998), which highlighted that agricultural enterprises can be characterized by traditional organizational culture, they are less innovative and profit-oriented approach. Besides this, managing and organizing the activities connected to direct sales is a time-consuming task (Juhász et al. 2012) which will take many resources and time from farm planning, innovative ideas, product and production level development (Wirthgen and Maurer 2000; Martinez et al. 2010). This result is also justified by the results of Bietsch and Hintze (2004), concluding that agricultural enterprises which do not apply directs sales use only 10 percent of their working hours for sales, while this proportion for farms based on direct selling is 55% (Bietsch and Hintze 2004). The low preferences of farms applying direct sales in modernization aspects are justified by using conventional technologies and fewer chemicals for the production. These features refer to the use of sustainable technologies, which might increase the recognition and uniqueness of the products. These findings are consistent with some observations of King et al. (2010), Menozzi et al. (2012), Benedek and Fertő (2015), Canfora (2016).

Although respondents indicated that they use less chemicals, most of them were not open for integrated or organic production (except for those respondents who sold their products at the organic markets), but they indicated production of high quality products as one of the most preferred goals. An important result of the present research was that environment friendly production was ranked as first among farm-related goals of the respondents, while large-scale production and increasing farm size were less important aspects for the farmers. Research results confirmed that farms based on direct sale have a wide range of products, which is considered as a success factor of this marketing activity. It affects profitability of farms as well (Uematsu and Mishra 2011). The conclusions of a former Hungarian research (Juhász et al. 2012) highlighted that the main advantage of direct sales is the close connection between seller and buyer, (see also Marsden et al. 2000; Renting et al. 2003). These findings were justified by the present research results,

namely, the opinion of consumers was ranked differently by farmers who sell products directly and those who sell products through POs.

As a summary, it can be stated that those producers who apply direct sales as the main marketing channel give a higher priority for non-economic objectives and direct sales-related objectives, while farm modernization and farm development are less important for them. These findings might be justified by the results of the previously conducted qualitative research, which showed that producers, who use direct sales as the main marketing channel, preferred to build a stable group of consumers and they did not intend apply other marketing channels, which should be essential in case of increasing production level. They considered stability as the key success factor and traditional products produced by conventional technologies were considered as their main competitive advantage. On the contrary, producers who sell their products through POs, had higher preferences on farm modernization and farm development, as they are able to sell their surplus yields through the POs.

Research results indicated that attitudes and subjective norms are determinants of producers' behavior; therefore, they will strongly influence the formulation of their economic and non economic goals and their managerial decisions. In addition, these goals and objectives will determine the preferences of producers in the selection between marketing channels.

References

[1] Aguglia L., De Santis F. and Salvioni C.: Direct Selling: a Marketing Strategy to Shorten Distances between Production and Consumption. Paper presented at 113th EAAE Seminar, Chania, Crete, 13 p., 2006 http://ageconsearch.umn.edu/bitstream/57657/2/Aguglia.pdf. Accessed 06-04-2016

[2] Ajzen I.: The Theory of Planned Behavior. Organizational Behavior and Human Decision Processes, 50: pp. 179–211, 1991 doi: 10.1016/0749-5978(91)90020-T

[3] Ajzen I.: Constructing a TPB questionnaire: Conceptual and methodological considerations. 2006. Available at: http://people.umass.edu/aizen/tpb.html. Accessed 06-07-2016.

[4] Benedek Zs., Fertő I.:. Miért választják a termelők a rövid ellátási láncokat? Why do producers prefer short supply chains? Statisztikai Szemle, 93: pp. 580–597, 2015

[5] Bergevoet R.H.M., Ondersteijn C.J.M., Saatkamp H.W.,van Woerkum C.M.J., Huirne R.B.M.: Entrepreneurial behaviour of Dutch dairy farmers under a milk quota system: goals, objectives and attitudes. Agricultural Systems 80: pp. 1–21, 2004 doi:10.1016/j.agsy.2003.05.001

[6] Bietsch M., Hintze C.: Economic sustainability of organic vegetable growing in Baden-Württemberg), LVG Heidelberg, 72 p., 2003

[7] Canfora I.: Is the Short Food Supply Chain an Efficient Solution for Sustainability in Food Market? Agriculture and Agriculture Science Procedia 8: pp. 402-407, 2016 doi: 10.1016/j.aaspro.2016.02.036

[8] Csíkné Mácsai É.:. Közvetlen értékesítés a mezőgazdasági termékek piacán (Direct selling on the market of agricultural products) PhD thesis, Szent István University, Gödöllő. 191 p, 2014

[9] Fairweather J.R., Keating N.C.: Goals and management styles of New-Zealand farmers. Agricultural Systems 44: pp. 181-200, 1994 doi: 10.1016/0308-521X(94)90160-H

[10] Fehér I.: Direct Marketing Practice in Hungarian Agriculture. Agricultural Economics 53: pp, 230–234, 2007

[11] Fielding, K.S., Terry, D.J., Masser, B.M., Hogg, M.A.: Integrating social identity theory and the theory of planned behaviour to explain decisions to engage in sustainable agricultural practices. British Journal of Social Psychology 47:pp. 23–48, 2008 doi:10.1348/014466607X206792

[12] Hansson, H., Ferguson, R., Olofsson, C.: Psychological constructs underlying farmers' decisions to diversify or specialize their businesses. An application of Theory of Planned Behaviour. Journal of Agricultural Economics 63: pp. 465–482, 2012 doi:10.1111/j.1477-9552.2012.00344.x

[13] Juhász, A., Mácsai, É., Kujáni, K., Hamza, E., Györe, D.: Role and opportunities of direct sales in the market position of food products. Agrárgazdasági Kutató Intézet, Budapest, 121 p, 2012

[14] King, R.P., Hand, M.S., DiGiacomo, G., Clancy, K., Gómez, M.I., Hardesty, S.D., Lev, L., McLaughin, E.W.: Comparing the structure, size and performance of local and mainstream food supply chain, USDA, ERS, Report No. 99, 73 p. 2010

[15] Kneafsey, M., Venn, L., Schmutz, U., Balázs, B., Trenchard, L., Eyden-Wood, T., Bos, E., Sutton, G., Blackett, M.: Short Food Supply Chains and Local Food Systems in the EU. A State of Play of their Socio-Economic Characteristics. JRC Report 25911, 6/2013. 123 p, 2013 doi:10.2791/88784

[16] Kuhnert, H.: Direct marketing in conventional and organic farming: A direct market survey as a form of individual farm diversification. Wissenschaftsverlag Vauk Kiel KG, Kiel 210 p, 1998

[17] Lazányi, K., Virglerová, Z., Dvorský, J., & Dapkus, R. (2017). An Analysis of Factors Related to" Taking Risks", according to Selected Socio-Demographic Factors. Acta Polytechnica Hungarica, 14(7).DOI: 10.12700/APH.14.7.2017.7.3

[18] Lehota, J., Csíkné Mácsai, Features of sales activities – channels of direct sales, In: Szakály, Z., Szente, V. :Direct sales and marketing of agricultural products, Szaktudás, Budapest, pp. 117-155, 2012

[19] Marija, Matotek Marija, Barać Ivan, Regodić Dušan, Grubor Gojko, Supply chain risk management using software tools. Acta Polytechnica Hungarica, 2015, 12.4: 167-182.DOI: 10.12700/APH.12.4.2015.4.10

[20] Marsden T., Banks J., Bristow G.: Food Supply Chain Approaches: Exploring their Role in Rural Development. Sociologia Ruralis 40: pp. 424–438, 2000 doi: 10.1111/1467-9523.00158

[21] Martinez, S., Hand, M., Da Pra, M., Pollack, S., Ralston, K., Smith, T., Vogel, S., Clark, S., Lohr, L., Low, S., Newman, C.: Local Food System: Concepts, Impacts and Issues. Economic Research Service Report Summary, U.S. Department of Agriculture. 80 p, 2010

[22] Menozzi, D., Fioravanzi, M., Donati, M.: Farmer's motivation to adopt sustainable agricultural practices. Bio-based and Applied Economics 4: pp. 125–147.2015 doi:10.13128/BAE-14776

[23] Rehman, T., McKemey, K., Garforth, C., Huggins, R., Yates, C.M., Cook, R.J., Tranter, R.B., Park, J.R., Dorward, P.T.: Theory of Reasoned Action and Its Integration with Economic Modelling in Linking Farmers' Attitudes and Adoption Behavior – An Illustration from the Analysis of the Uptake of Livestock Technologies in the South West of England, IFMA 14th Congress, Perth, Australia. 19 p. 2003

[24] Renting, H., Marsden, T., Banks, J.: Understanding Alternative Food Networks: Exploring the Role of Short Food Supply Chains in Rural Development. Environment and Planning A 35: pp. 393–411. 2003. doi: 10.1068/a3510

[25] Sajtos, L., Mitev, A.: SPSS kutatási és adatelemzési kézikönyv (SPSS research and data analysis manual), Alinea Kiadó, Budapest, 402 p, 2007

[26] Szegedi, Z., Vinogradov, S., Domjan, E., Störkel, M., Valentinyi, Z.: Problems of the co-operative attitude of supply chain members in the Hungarian FMCG sector. Journal of International Scientific Publications: Agriculture and Food 2: pp. 472-479, 2014

[27] Tudisca, S., Di Trapani, A.M., Sgroi, F., Testa, R., Giamporcaro, G.: Role of alternative food networks in Sicilian farms, International Journal on Entrepreneurship and Small Business 22: pp. 50–63. 2014. doi: 10.1504/IJESB.2014.062130

[28] Uematsu, H., Mishra, A.K.: Use of Direct Marketing Strategies by Farmers and their Impact on Farm Business Income. Agricultural and Resource Economics Review 40: pp. 1–19. 2011. doi: 10.1017/S1068280500004482

[29] Ubrežiová, I., Horská, E., Moravčíková, K., Ubrežiová, A.: Glocalization and Local Alternative Economic Systems: the Case of the Slovak Republic. In: Raupelienė A. (ed.): Proceedings of the 7th International Scientific Conference, Rural Development 2015: Towards the Transfer of

Knowledge, Innovations and Social Progress, Akademija, Lithuania. 2015. doi: 10.15544/RD.2015.081

[30] Venn, L., Kneafsey, M., Holloway, L., Cox, R., Dowler, E., Tuomainen, H.: Researching European 'alternative' food networks: some methodological considerations. Area 38: pp. 248–258. 2006. doi: 10.1111/j.1475-4762.2006.00694.x

[31] Wirthgen, B., Maurer, O.: Direktvermarktung: Verarbeitung, Absatz, Rentabilität, Recht (Direct marketing: processing, sales, profitability and legal rules), Verlag Ulmer, Stuttgart, 236 p, 2000

Influence of Design Methods a Discrete Model of Separately Excited DC Motor on Parameters Estimation

István Vajda*, Alexander Glazyrin, Irina Ustinova***, Evgeniy Bolovin****

* Kandó Kálmán Faculty of Electrical Engineering, Óbuda University, Bécsi út 96/b, H-1034 Budapest, Hungary, vajda.istvan@kvk.uni-obuda.hu

** Department of Electrical Drive and Equipment, National Research Tomsk Polytechnic University, Lenin Ave. 30, Tomsk, Russia, 634034, asglazyrin@tpu.ru, orange@tpu.ru

*** Department of Higher Mathematics, National Research Tomsk Polytechnic University, Lenin Ave. 30, Tomsk, Russia, 634034, igu@tpu.ru

Abstract: The authors have developed the methods of preparing the difference schemes required for dynamic identification of the parameters of a DC motor as an object of the electric drives with control system during idling start-up. A system of differential equations describing the separately excited DC motor is reduced to the system of difference equations for constructing the discrete model. The authors have used three methods: direct difference, bilinear transformation method and multipoint approximation for writing the difference equations system. The estimations of the parameters of the discrete model based on the linear algebraic equations system applied this way were obtained by the matrix method. Comparing the estimates obtained the authors detected the influence of the methods of constructing the object discrete model on the error in the parameters' estimations obtained.

Keywords: discrete model; difference equations; bilinear transformation method; multipoint approximation; direct difference; linear algebraic equations system; dynamic identification; parameters estimations

1 Introduction

Dynamic identification of control objects [1] consists in determination of its model parameters based on supplied system input and output information during time limited by transition process continuance. It is necessary to understand that the identification procedure is an ill-posed problem. For transition into

consideration of an ill-posed problem, it is necessary to understand what is the well-posed problem by Jacques Hadamard. Consider the operator equation:

$$\mathbf{A}\cdot x=\mathbf{B} \tag{1}$$

where **A** is an operator acting from a space with infinite dimension x in a space with infinite dimension B. The essence of the problem is to reduce to finding solutions of the equations **x**, the corresponding of the given right side **B**. This problem will be positively posed if its mathematical solution has the following properties:

1.The solution exists.

2. The solution is unique. This condition provided if **A** has one-to-one correspondence [2].

It should be noted that the first and second conditions indicate the existence of the inverse operator $\mathbf{A}^{-1}$, and its domain of definition coincides with the domain of definition of the space **B**.

3. The solution's behavior changes continuously with the initial conditions, i.e. if $\mathbf{B}_n \to \mathbf{B}$, $\mathbf{A}\cdot\mathbf{x}_n = \mathbf{B}_n$, $\mathbf{A}\cdot\mathbf{x} = \mathbf{B}$, then $\mathbf{x}_n \to \mathbf{x}$. This means that the inverse operator $\mathbf{A}^{-1}$ is continuous.

Accordingly, ill-posed problem is considered when at least one of these properties is violated.

Equation (1) is a typical mathematical model for many physical phenomena [3], provided that the operator **A** relates the characteristics of the object **x** with the data **B**. It's necessary to understand that x can't be measured and **B** can't be obtained during the experiment. This problem is called inverse [4] and solution concludes in finding the characteristics of the object **x**. Such an inverse problem often has to be discretized in order to obtain a numerical solution. A functional analysis of inverse problems shows the continuity of the solutions [5], which implies the fulfillment of the third condition. But in connection with the transition to the discrete domain, this condition is violated, which leads to instability of the numerical solutions in calculations with finite accuracy.

Error in the statement of the operator **A** is affected on the fulfillment of the correctness conditions and methods of solving inverse problems. At the same time, it is impossible to completely get rid of the noise component [5-7]. Taking into account the noise of equation (1), it looks as follows:

$$\mathbf{A}\cdot\mathbf{x} + \boldsymbol{\varepsilon} = \mathbf{B}$$

where **ε** are the errors arising from the transition from a continuous coordinate system to a discrete one [8]. 1. Presence of natural noise components of signals received by sensors. 2. Vulnerability of digital differentiation to the presence of noise. 3. The value of the sampling period must not contradict the requirements of

the Nyquist–Shannon theorem [9, 10]. Thus, the correct designing of a discrete model of the object and the influence of the quality of digital differentiation is an integral task for solving problems' parameters identification of a separately excited DC motor

2 Possible Schemes of Numerical Differentiation

There are many methods of numerical differentiation [11, 12]:

1. Forward differences (direct difference) where $x'(t_0) \approx \frac{x(t_0 + \Delta t)\text{-}x(t_0)}{\Delta t}$.

The estimation of the numerical differentiation formula error using Taylor's formula with remainder term in integral form is: $\left|\frac{x(t_0 + \Delta t) - x(t_0)}{\Delta t} - x'(t_0)\right| \le c_1 \int_{t_0}^{t_0+\Delta t} |x''(\xi)| d\xi$, where c_1 is the constant independent of $x(t)$, Δt and $x(t) \in C^{(2)}$, so $x(t)$ has continuous derivatives up to the second order and including on the interval $[t_0, t_0 + \Delta t]$.

2. Backward differences (inverted difference). Estimation of errors of such approximation is: $\left|\frac{x(t_0) - x(t_0 - \Delta t)}{\Delta t} - x'(t_0)\right| \le c_2 \cdot \int_{t_0-\Delta t}^{t_0} |x''(\xi)| d\xi$, where we make the same assumptions as in the previous paragraph relatively to c_2, $x(t)$ and Δt.

3. Central difference $x'(t_0) \approx \frac{x(t_0 + \Delta t) - x(t_0 - \Delta t)}{2\Delta t}$ which approximation error is given by the expression $\left|\frac{x(t_0 + \Delta t) - x(t_0 - \Delta t)}{2\Delta t} - x'(t_0)\right| \le c_3 \cdot \Delta t \cdot \int_{t_0-\Delta t}^{t_0+\Delta t} |x'''(\xi)| d\xi$.

4. The method of multipoint approximation to approximate the derivative. The approximation order can be improved significantly if we use more points, and namely: $t = t_0 - 2\Delta t, t = t_0 - \Delta t$, $t = t_0 + \Delta t$, $t = t_0 + 2\Delta t$ at decomposition of continuous function by the Taylor's formula:

$$x(t) = x(t_0) + (t - t_0)x'(t_0) + \frac{(t - t_0)^2}{2!}x''(t_0) + \frac{(t - t_0)^3}{3!}x'''(t_0) + o((t - t_0)^3) \qquad (2)$$

So we obtain

$$x'(t) \approx \frac{x(t_0 - 2\Delta t) - 8x(t_0 - \Delta t) + 8x(t_0 + \Delta t) - x(t_0 + 2\Delta t)}{12\Delta t} \qquad (3)$$

from the system of linear equations:

$$\begin{cases} x(t_0-2\Delta t)=x(t_0)-2\Delta t x'(t_0)+2\Delta t^2 x''(t_0)-\dfrac{4\Delta t^3}{3}x'''(t_0)+o(\Delta t^3), \\ x(t_0-\Delta t)=x(t_0)-\Delta t x'(t_0)+\dfrac{\Delta t^2}{2}x''(t_0)-\dfrac{\Delta t^3}{6}x'''(t_0)+o(\Delta t^3), \\ x(t_0+\Delta t)=x(t_0)+\Delta t x'(t_0)+\dfrac{\Delta t^2}{2}x''(t_0)+\dfrac{\Delta t^3}{6}x'''(t_0)+o(\Delta t^3) \\ x(t_0+2\Delta t)=x(t_0)+2\Delta t x'(t_0)+2\Delta t^2 x''(t_0)+\dfrac{4\Delta t^3}{3}x'''(t_0)+o(\Delta t^3). \end{cases} \quad (4)$$

The estimation of this approximation error has the form:

$$\left|\frac{x(t_0-2\Delta t)-8x(t_0-\Delta t)+8x(t_0+\Delta t)-x(t_0+2\Delta t)}{12\Delta t}-x'(t_0)\right| \le$$
$$\le c_4\Delta t^3\left\{\int_{t_0-\Delta t}^{t_0+\Delta t}\left|x'''(\xi)\right|d\xi-2\int_{t_0-2\Delta t}^{t_0+2\Delta t}\left|x''''(\xi)\right|d\xi\right\},\ x(t)\in C^{(4)} \quad (5)$$

3 Methods for Imaging Derivatives

The examined schemes of numerical differentiation allow moving from differential equations to difference ones, which are widely used to describe the stationary discrete systems. z-transform is the convenient tool for solving differential equations, so let us consider separately some methods for imaging derivatives from the Laplace-domain to the z-domain.

Let us consider the method of direct difference as the derivative transformation. The method consists in derivative approximation by the finite difference $\frac{dx}{dt}\to\frac{x(n\cdot\Delta t+1\cdot\Delta t)-x(n\cdot\Delta t)}{\Delta t}$.

Applying the Laplace transform of the left side and z-transform of the right one, we obtain $xX(s)\to\frac{z-1}{\Delta t}X(z)$. The explicit form of this transformation is $s\to\frac{z-1}{\Delta t}$. The inverse transformation $z\leftarrow s\cdot\Delta t+1$ was obtained from the latter relation. According to [13, 14] in order to construct the filters with desired properties the conversion of the derivative into the finite difference must satisfy the following conditions:

1. The imaginary axis of s-plane must be displayed into the unit circle of z-plane.

2. The left half-plane of Laplace-domain $\mathrm{Re}(s)\leq 0$ must be displayed into the interior part of a unit circle of z-domain $|z|<1$.

3. The conversion should be rational.

The left half-plane of s-plane moves into the left half-domain $Re(s)<1$ of z-domain based on the inverse transform $z\leftarrow s\cdot\Delta t+$, so the second condition is not satisfied. The imaginary axis of s-plane moves into a straight $Re(s)=1$ of z-domain, so the first condition is not satisfied. These conditions can be fulfilled near the point $z=1$ of the complex z-domain, so when $\Delta t\rightarrow 0$ the direct difference method should give a satisfacto-ry result.

The inverse difference method, in which the derivative is approximated by the backward difference: $\frac{d\mathrm{x}}{d\mathrm{t}}\rightarrow\frac{x(n\cdot\Delta t)-x(n\cdot\Delta t-1\cdot\Delta t)}{\Delta t}$. Applying the Laplace transform of the left part and z-transform of right part, we obtain $s\cdot X(s)\rightarrow\frac{1-z^{-1}}{\Delta t}\cdot X(z)$ whence the explicit form of this transformation $s\rightarrow\frac{1-z^{-1}}{\Delta t}$ was obtained. The inverse transformation is as follows $z\leftarrow\frac{1}{1-s\cdot\Delta t}$. Since $\mathrm{Re}\left(\frac{1}{1-j\cdot\omega\cdot\Delta t}\right)=\frac{1}{1+\omega^2\cdot\Delta t^2}$ and $\mathrm{Im}\left(\frac{1}{1-j\cdot\omega\cdot\Delta t}\right)=\frac{\omega\cdot\Delta t}{1+\omega^2\cdot\Delta t^2}$, then

$$\left(\mathrm{Re}\left(\frac{1}{1-j\cdot\omega\cdot\Delta t}\right)-\frac{1}{2}\right)^2+\left(\mathrm{Im}\left(\frac{1}{1-j\cdot\omega\cdot\Delta t}\right)\right)^2=\left(\frac{1}{1+\omega^2\cdot\Delta t^2}-\frac{1}{2}\right)^2+$$

$$+\frac{\omega^2\cdot\Delta t^2}{\left(1+\omega^2\cdot\Delta t^2\right)^2}=\frac{1}{4},$$

so the points of the imaginary axis $s=j\cdot\omega$ the backward difference method transforms into the points of circle on z-plane with center in $z=\frac{1}{2}$ and radius equal to $\frac{1}{2}$. The point $s=0$ is imaged into the point $z=1$, so if $s\rightarrow+\infty$ then $z\rightarrow -j\cdot 0$, and if $s\rightarrow-\infty$ then $z\rightarrow+j\cdot 0$. Under this imaging the left half-plane of Laplace-domain is displayed inside the circle.

Let us consider the bilinear transformation $s \to \frac{2}{\Delta t} \cdot \frac{1-z^{-1}}{1+z^{-1}}$ that allows the inverse transformation $z \leftarrow \frac{\frac{2}{\Delta t}+s}{\frac{2}{\Delta t}-s}$. The last expression shows that the points of the imaginary axis $s=j\cdot\omega$ are transformed into the point of circle $|z|=1$ by bilinear transformation. As $\frac{\frac{2}{\Delta t}+\mathrm{j}\omega}{\frac{2}{\Delta t}-j\omega}=\frac{\frac{4}{\Delta t^2}+\frac{4}{\Delta t}\omega j-\omega^2}{\frac{4}{\Delta t^2}+\omega^2}$, so $\mathrm{Re}\left(\frac{\frac{2}{\Delta t}+\mathrm{j}\omega}{\frac{2}{\Delta t}-j\omega}\right)=\frac{\frac{4}{\Delta t^2}-\omega^2}{\frac{4}{\Delta t^2}+\omega^2}$ and $\mathrm{Im}\left(\frac{\frac{2}{\Delta t}+\mathrm{j}\omega}{\frac{2}{\Delta t}-j\omega}\right)=\frac{\frac{4}{\Delta t}\omega}{\frac{4}{\Delta t^2}+\omega^2}$, therefore $\mathrm{Re}^2\left(\frac{\frac{2}{\Delta t}+\mathrm{j}\omega}{\frac{2}{\Delta t}-j\omega}\right)+\mathrm{Im}^2\left(\frac{\frac{2}{\Delta t}+\mathrm{j}\omega}{\frac{2}{\Delta t}-j\omega}\right)=1$.

Points of the left half-plane $\mathrm{Re}(s)<0$ are transformed into the region bounded by a circle $|z|<1$. The transformation must be linear fractional and is fulfilled as well. It is the third condition.

Finally, applying the Laplace transform of the left part and z-transform of the right part of the expression (1), we obtain $s \cdot X(s) \to \frac{z^{-2}-8z^{-1}+8z-8z^2}{12\Delta t} X(z)$ and its ex-plicit form $s \to \frac{z^{-2}-8z^{-1}+8z-8z^2}{12\Delta t}$. The authors did not manage to find the inverse transformation in the last expression, so the analysis of conversion when displaying the derivative found by the formula (3) is not given in the paper.

4 The Difference Scheme to Identify the Separate Excitation DC Motor Parameters Applying the Direct Difference Method

The separately excited DC motor model at idle is described by a differential equations system [15]:

$$\begin{cases} U(t) = R \cdot i(t) + L \cdot \frac{di(t)}{dt} + c \cdot \omega(t) \\ J \cdot \frac{d\omega(t)}{dt} = c \cdot i(t) \end{cases} \quad (6)$$

where $U(t)$ is the voltage (V), applied to the anchor at time t; R is the resistance of the armature circuit (Ohm); $i(t)$ is the armature current (A); L is the anchor circuit inductance (H); c is the special coefficient (V•sec/rad); J is the equivalent inertia moment, cast to the motor shaft; $\omega(t)$ is the shaft rotation frequency of DC motor.

Taking into account the sampling time interval Δt of the measurement system let us move from the differential equation $U(t) = R \cdot i(t) + L \cdot \frac{di(t)}{dt} + c \cdot \omega(t)$ to the differential equations system for the current $n \cdot \Delta t$ and previous time $n \cdot \Delta t$-$1 \cdot \Delta t$ at a constant assessment of resistance and inductance:

$$\begin{cases} i(n \cdot \Delta t) \cdot \hat{R} + D^{(1)}\left[i(n \cdot \Delta t)\right] \cdot \hat{L} = U(n \cdot \Delta t) - c \cdot \omega(n \cdot \Delta t), \\ i(n \cdot \Delta t - 1 \cdot \Delta t) \cdot \hat{R} + D^{(1)}\left[i(n \cdot \Delta t - 1 \cdot \Delta t)\right] \cdot \hat{L} = U(n \cdot \Delta t - 1 \cdot \Delta t) - c \cdot \omega(n \cdot \Delta t - 1 \cdot \Delta t), \end{cases} \tag{7}$$

where $i(n \cdot \Delta t)$, $i(n \cdot \Delta t\text{-}1 \cdot \Delta t)$ are the currents; $D^{(1)}[i(n \cdot \Delta t)]$, $D^{(1)}[i(n \cdot \Delta t\text{-}1 \cdot \Delta t)]$ are the derived currents; $U(n \cdot \Delta t)$, $U(n \cdot \Delta t\text{-}1 \cdot \Delta t)$ are the voltages; $\omega(n \cdot \Delta t)$, $\omega(n \cdot \Delta t\text{-}1 \cdot \Delta t)$ are the shaft rotation frequencies of DC motor on the current and previous steps, respectively. The last system can be written in matrix form:

$$\begin{bmatrix} i(n \cdot \Delta t) & D^{(1)}\left[i(n \cdot \Delta t)\right] \\ i(n \cdot \Delta t - 1 \cdot \Delta t) & D^{(1)}\left[i(n \cdot \Delta t - 1 \cdot \Delta t)\right] \end{bmatrix} \cdot \begin{bmatrix} \hat{R} \\ \hat{L} \end{bmatrix} = \begin{bmatrix} U(n \cdot \Delta t) - c \cdot \omega(n \cdot \Delta t) \\ U(n \cdot \Delta t - 1 \cdot \Delta t) - c \cdot \omega(n \cdot \Delta t - 1 \cdot \Delta t) \end{bmatrix} \tag{8}$$

The solution of this system explicitly by the matrix method at the current step of time sampling has the form:

$$\begin{bmatrix} \hat{R}(n \cdot \Delta t) \\ \hat{L}(n \cdot \Delta t) \end{bmatrix} = \frac{1}{i(n \cdot \Delta t) \cdot D^{(1)}\left[i(n \cdot \Delta t - 1 \cdot \Delta t)\right] - i_{j-1} \cdot D^{(1)}\left[i(n \cdot \Delta t)\right]} \cdot$$
$$\cdot \begin{bmatrix} \left(U(n \cdot \Delta t) - c \cdot \omega(n \cdot \Delta t)\right) \cdot D^{(1)}\left[i(n \cdot \Delta t - 1 \cdot \Delta t)\right] - \\ \left(U(n \cdot \Delta t - 1 \cdot \Delta t) - c \cdot \omega(n \cdot \Delta t - 1 \cdot \Delta t)\right) \cdot i(n \cdot \Delta t) - \\ - \left(U(n \cdot \Delta t - 1 \cdot \Delta t) - c \cdot \omega(n \cdot \Delta t - 1 \cdot \Delta t)\right) \cdot D^{(1)}\left[i(n \cdot \Delta t)\right] \\ - \left(U(n \cdot \Delta t) - c \cdot \omega(n \cdot \Delta t)\right) \cdot i(n \cdot \Delta t - 1 \cdot \Delta t) \end{bmatrix} \tag{9}$$

Substituting $D^{(1)}\left[i(n \cdot \Delta t)\right]$ as the estimation of the derivatives in the form of a direct difference $\frac{i(n \cdot \Delta t) - i(n \cdot \Delta t - 1 \cdot \Delta t)}{\Delta t}$, we finally obtain:

$$\begin{bmatrix}\hat{R}(n\cdot\Delta t)\\ \hat{L}(n\cdot\Delta t)\end{bmatrix}=\frac{1}{\left[i(n\cdot\Delta t-1\cdot\Delta t)\right]^2-i(n\cdot\Delta t)i(n\cdot\Delta t-1\cdot\Delta t)}\cdot$$
$$\cdot\begin{bmatrix}\left(U(n\cdot\Delta t)-c\cdot\omega(n\cdot\Delta t)\right)\cdot\dfrac{i(n\cdot\Delta t-1\cdot\Delta t)-i(n\cdot\Delta t-2\cdot\Delta t)}{\Delta\mathrm{t}}-\\ \left(U(n\cdot\Delta t-1\cdot\Delta t)-c\cdot\omega(n\cdot\Delta t-1\cdot\Delta t)\right)\cdot i(n\cdot\Delta t)-\\ -\left(U(n\cdot\Delta t-1\cdot\Delta t)-c\cdot\omega(n\cdot\Delta t-1\cdot\Delta t)\right)\cdot\dfrac{i(n\cdot\Delta t)-i_{j-1}}{\Delta t}\\ -\left(U(n\cdot\Delta t)-c\cdot\omega(n\cdot\Delta t)\right)\cdot i(n\cdot\Delta t-1\cdot\Delta t)\end{bmatrix} \tag{10}$$

Based on the second equation of the system (2) let us find the estimation of the inertia moment transforming the equation to the form

$$\frac{d\omega(t)}{dt}\cdot\hat{J}=c\cdot i(t) \tag{11}$$

Taking into account the comments given in the derivation of the previous system of difference equations, let us form according to the equation (11) the proper difference equation $\dfrac{\omega(n\cdot\Delta t)-\omega(n\cdot\Delta t-1\cdot\Delta t)}{\Delta\mathrm{t}}\cdot\hat{J}(n\cdot\Delta t)=c\cdot i(n\cdot\Delta t)$ from which we directly obtain $\hat{J}(n\cdot\Delta t)$.

5 The Difference Scheme to Identify the Separate Excitation DC Motor Parameters Applying the Bilinear Transformation Method

Applying the Laplace transform to the system (6) we obtain:

$$\begin{cases}L\cdot s\cdot i(s)+R\cdot i(s)=U(s)\text{-}c\cdot\omega(s),\\ J\cdot s\cdot\omega(s)=c\cdot i(s).\end{cases} \tag{12}$$

Then using the bilinear transformation [16] $\mathrm{s}\rightarrow\dfrac{2}{\Delta\mathrm{t}}\cdot\dfrac{1-z^{-1}}{1+z^{-1}}$ we obtain:

$$\begin{cases}\dfrac{2}{\Delta t}\cdot\left(1-z^{-1}\right)\cdot i(z)\cdot L+\left(1+z^{-1}\right)\cdot i(z)\cdot R=\left(U(z)-c\cdot\omega(z)\right)\cdot\left(1+z^{-1}\right),\\ \dfrac{2}{\Delta t}\cdot\left(1-z^{-1}\right)\cdot J\cdot\omega(z)=c\cdot i(z).\end{cases} \tag{13}$$

Let us write down the first equation of the system (13) relative to the current $n\cdot\Delta t$ and the previous time $n\cdot\Delta t\Delta t$ considering the fact that according to z-transform the image multiplication by z^{-1} corresponds to a delay per one sample:

$$\begin{cases} \dfrac{2}{\Delta t}\cdot\big(i(n\cdot\Delta t)-i(n\cdot\Delta t-1\cdot\Delta t)\big)\cdot L+\big(i(n\cdot\Delta t)+i(n\cdot\Delta t-1\cdot\Delta t)\big)\cdot R= \\ =U(n\cdot\Delta t)+U(n\cdot\Delta t-1\cdot\Delta t)-c\cdot\big(\omega(n\cdot\Delta t)+\omega(n\cdot\Delta t-1\cdot\Delta t)\big) \\ \dfrac{2}{\Delta t}\cdot\big(i(n\cdot\Delta t-1\cdot\Delta t)-i(n\cdot\Delta t-2\cdot\Delta t)\big)\cdot L+\big(i(n\cdot\Delta t-1\cdot\Delta t)+i(n\cdot\Delta t-2\cdot\Delta t)\big)\cdot R= \\ =U(n\cdot\Delta t-1\cdot\Delta t)+U(n\cdot\Delta t-2\cdot\Delta t)-c\cdot\big(\omega(n\cdot\Delta t-1\cdot\Delta t)+\omega(n\cdot\Delta t-2\cdot\Delta t)\big) \end{cases} \tag{14}$$

In matrix form this system has the form:

$$\begin{bmatrix} \dfrac{2}{\Delta t}\cdot\big(i(n\cdot\Delta t)-i(n\cdot\Delta t-1\cdot\Delta t)\big) & i(n\cdot\Delta t)+i(n\cdot\Delta t-1\cdot\Delta t) \\ \dfrac{2}{\Delta t}\cdot\big(i(n\cdot\Delta t-1\cdot\Delta t)-i(n\cdot\Delta t-2\cdot\Delta t)\big) & i(n\cdot\Delta t-1\cdot\Delta t)+i(n\cdot\Delta t-2\cdot\Delta t) \end{bmatrix}\cdot\begin{bmatrix}\hat{L}(n\cdot\Delta t)\\ \hat{R}(n\cdot\Delta t)\end{bmatrix}= \tag{15}$$
$$=\begin{bmatrix} U(n\cdot\Delta t)+U(n\cdot\Delta t-1\cdot\Delta t)-c\cdot\big(\omega(n\cdot\Delta t)+\omega(n\cdot\Delta t-1\cdot\Delta t)\big) \\ U(n\cdot\Delta t-1\cdot\Delta t)+U(n\cdot\Delta t-2\cdot\Delta t)-c\cdot\big(\omega(n\cdot\Delta t-1\cdot\Delta t)+\omega(n\cdot\Delta t-2\cdot\Delta t)\big)\end{bmatrix}$$

We obtain the solution of the latter system explicitly:

$$\begin{aligned} &\hat{L}(n\cdot\Delta t)=\frac{\Delta t}{4\cdot\Big(i(n\cdot\Delta t)\cdot i(n\cdot\Delta t-1\cdot\Delta t)-\big[i(n\cdot\Delta t-1\cdot\Delta t)\big]^2\Big)}\cdot \\ &\cdot\Big\{\big(i(n\cdot\Delta t-1\cdot\Delta t)+i(n\cdot\Delta t-2\cdot\Delta t)\big)\cdot \\ &\cdot\big[U(n\cdot\Delta t)+U(n\cdot\Delta t-1\cdot\Delta t)-c\cdot\big(\omega(n\cdot\Delta t)+\omega(n\cdot\Delta t-1\cdot\Delta t)\big)\big]- \\ &-\big(i(n\cdot\Delta t)+i(n\cdot\Delta t-1\cdot\Delta t)\big)\cdot \\ &\cdot\big[U(n\cdot\Delta t-1\cdot\Delta t)+U(n\cdot\Delta t-2\cdot\Delta t)-c\cdot\big(\omega(n\cdot\Delta t-1\cdot\Delta t)+\omega_{j-2}\big)\big]\Big\}, \end{aligned} \tag{16}$$

$$\begin{aligned} &\hat{R}(n\cdot\Delta t)=\frac{1}{2\cdot\Big(i(n\cdot\Delta t)\cdot i(n\cdot\Delta t-1\cdot\Delta t)-\big[i(n\cdot\Delta t-1\cdot\Delta t)\big]^2\Big)}\cdot \\ &\Big\{\big(i(n\cdot\Delta t)-i(n\cdot\Delta t-1\cdot\Delta t)\big)\cdot \\ &\cdot\big[U(n\cdot\Delta t-1\cdot\Delta t)+U(n\cdot\Delta t-2\cdot\Delta t)-c\cdot\big(\omega(n\cdot\Delta t-1\cdot\Delta t)+\omega(n\cdot\Delta t-2\cdot\Delta t)\big)\big]- \\ &-\big(i(n\cdot\Delta t-1\cdot\Delta t)-i(n\cdot\Delta t-2\cdot\Delta t)\big)\cdot \\ &\cdot\big[U(n\cdot\Delta t)+U(n\cdot\Delta t-1\cdot\Delta t)-c\cdot\big(\omega(n\cdot\Delta t)+\omega(n\cdot\Delta t-1\cdot\Delta t)\big)\big]\Big\}. \end{aligned} \tag{17}$$

From the second equation of the system (13) obtain the estimation of the equivalent inertia moment J in a similar way

$$\hat{J}(n\cdot\Delta t)=\frac{\Delta t}{2}\cdot c\cdot\frac{i(n\cdot\Delta t)+i(n\cdot\Delta t-1\cdot\Delta t)}{\omega(n\cdot\Delta t)-\omega(n\cdot\Delta t-1\cdot\Delta t)} \tag{18}$$

Estimations of the parameters $\hat{L},\quad \hat{R},\quad \hat{J}$ are delivered by the expressions (9) and (11), in which the derivatives are approximated by the formula (3).

6 The Results of Numerical Modeling of Dynamic Identification of Separate Excitation DC Motor Parameters

For solution of the identification problem [17] the authors found the analytical solution of the system (3), which is shown in Figure 1. The identification processes for the parameters $\hat{L}$, $\hat{R}$, $\hat{J}$ were plotted for the direct difference method, bilinear transformation, multipoint approximation (Figure 2–4) and compared with the actual values. The lack of transients in Figure 2–4 can be explained by the fact that the noise component was not taken into account at simulation.

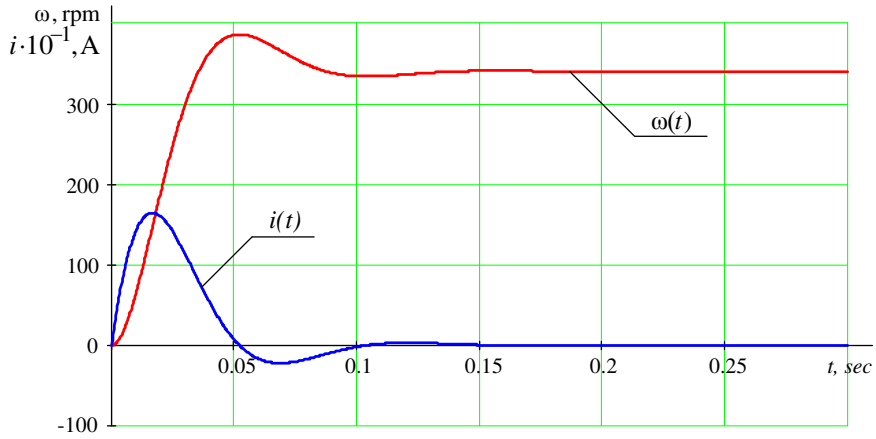

Figure 1
Transition processes of current i(t) and rotor speed ω(t)

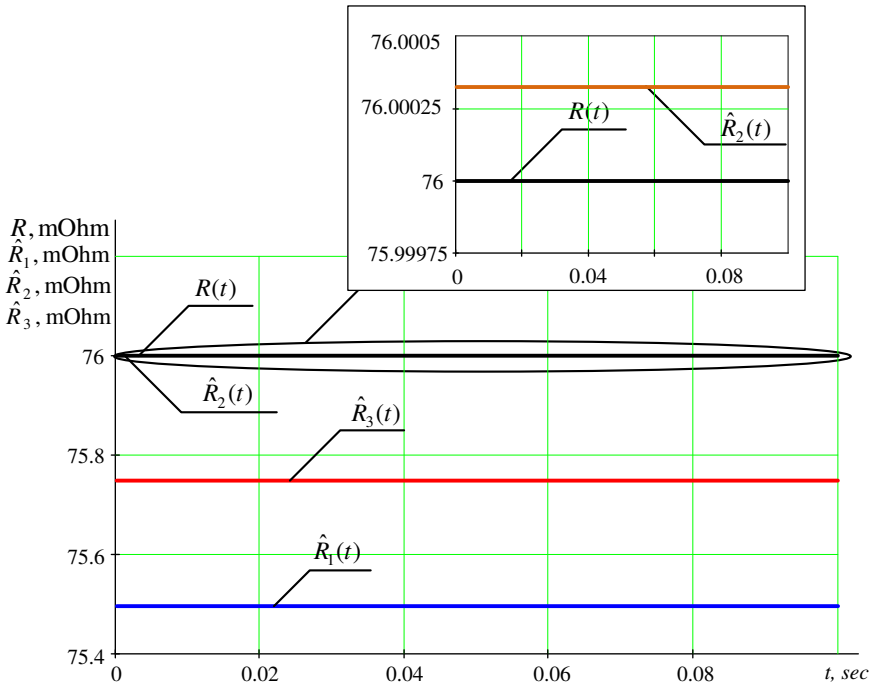

Figure 2

The dynamic of DC motor resistance estimation. *R* is the real resistance value; $\hat{R}_1$ − the resistance estimation by direct difference method; $\hat{R}_2$ is the resistance estimation by bilinear transformation method; $\hat{R}_3$ is the resistance estimation by multipoint approximation

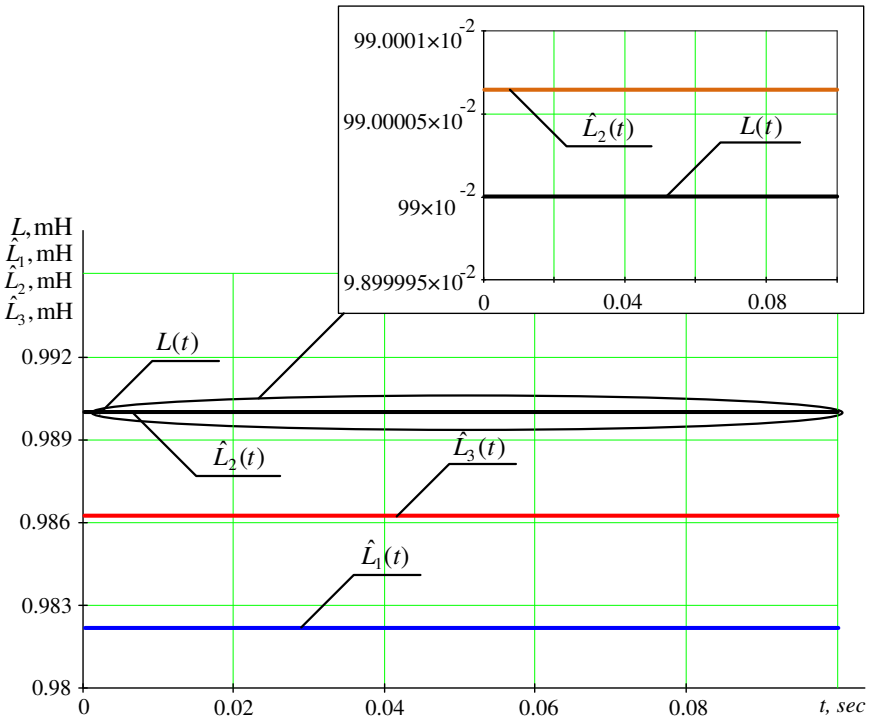

Figure 3

The dynamic of DC motor inductance estimation. L is the real inductance value; $\hat{L}_1$ is the inductance estimation by the direct difference method; $\hat{L}_2$ is the inductance estimation by the bilinear transformation method; $\hat{L}_3$ is the inductance estimation by the multipoint approximation

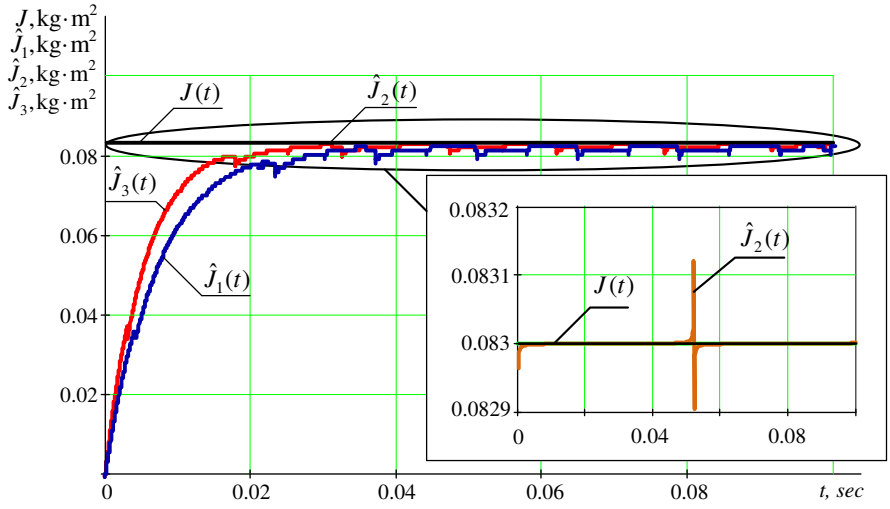

Figure 4

The dynamics of estimation of DC motor equivalent inertia moment. J is the real value of the equivalent inertia moment; $\hat{J}_1$ is the equivalent inertia moment estimation by the direct difference method; $\hat{J}_2$ is the equivalent inertia moment estimation by the bilinear transformation method; $\hat{J}_3$ is the equivalent inertia moment estimation by multipoint approximation

To analyze the quality of the evaluation process of the parameter x (respectively) in Figure 2–4 the authors considered the integral mean-square error of the parameter estimation during the load-on $\delta_x = \sqrt{\frac{1}{j_{fin} - j_{st}} \cdot \sum_{k=j_{fin}}^{j_{st}} \left(\frac{x - \hat{x}_k}{x} \right)^2} \cdot 100\%$ corresponding to the numbers $j_{st} = 2$ and $j_{fin} = 1002$. All errors are presented in Table 1.

Estimations of the equivalent inertia moment by the direct difference method $\hat{J}_1$ and by the multipoint approximation $\hat{J}_3$ were subjected to nonlinear predictive filter. The filtration is required due to the presence of a large dispersed component of the estimates which value is many times higher than the actual value of the inertia moment. This leads to inability to obtain adequate estimates.

Table 1
Indicators of quality estimates

	Estimate	Real value	Estimated value	δ_x, %
Resistance, mOhm	$\hat{R}_1$	76	75.49	0.66
	$\hat{R}_2$		76.032	$43 \cdot 10^{-5}$
	$\hat{R}_3$		75.66	0.437
Equivalent moment of inertia estimates, kg·m²	$\hat{J}_1$	0.083	0.08	2.61
	$\hat{J}_2$		0.083	$78 \cdot 10^{-4}$
	$\hat{J}_3$		0.081	1.48
Inductance, mH	$\hat{L}_1$	99	98.24	0.76
	$\hat{L}_2$		99	$65 \cdot 10^{-6}$
	$\hat{L}_3$		98.6238	0.38

Thus the estimation calculation errors are considerably lower (Table 1) in the equations obtained by the bilinear transformation than in the dif-ference equations, obtained by the methods of direct difference and multipoint difference approximation, so using the bilinear transformation for identifying the estimates of the separate excitation DC motor parameters is preferred as the filtration is not required in this case.

References

[1] Bolovin E. V., Glazyrin A. S. "Method for identifying parameters of submersible induction motors of electrical submersible pump units for oil production", Bulletin of the Tomsk Polytechnic University, Geo Assets Engineering, Tomsk, 2017, pp. 123-131

[2] J. Hefferon. Linear algebra. – Saint Michael's College Colchester, Vermont USA, 2014 – 496 p.

[3] G. J. Sussman, J. Wisdom. Structure and interpretation of classical mechanics. – MIT Press, MA, USA, 2015 – 584 p.

[4] A. Tarantola. Inverse problem theory and methods for model parameter estimation. – Institut de Physique du Globe de Paris, Université de Paris 6, Paris, France, 2005 – 358 p.

[5] A. N. Tihonov, A. S. Leonov, A. G. Yagola. Nonlinear Ill-Posed Problems – Dordrecht, Netherlands: Springer Netherlands, 2014 – 386 p.

[6] Tkachuk R. Yu., Glazyrin A. S., Polichshuk V. I. “Induction motor drive's parameters identification using genetic algorithms”,7th International Forum on Strategic Technology, IFOST 2012. Tomsk, 2012, Vol. 2, pp. 586-589

[7] Fadali M., Visioli A. Digital control engineering: analysis and design. 2nd ed. New York, NY, USA: Academic Press, 2012

[8] Kozlova, L., Bolovin, E., Payuk, L. “Angular Velocity's Neural Network Observer of the Electric Drive of TVR - Im Type Implemented in Software Environment LabVIEW”, IOP Conference Series: Materials Science and Engineering, 2016, pp. 1-7

[9] Kotelnikov V. A. On the carrying capacity of the ether and wire in telecommunica-tions. Moscow, USSR: Izd. red. upr. Svyazi RKKA, 1933

[10] Blanchard P., Devaney R. L., Hall G.R. Differential Equations. London, England: Thompson, 2006

[11] Chang Shu. Differential Quadrature and its Application in Engineering: Engineer-ing Application. London, England: Springer-Verlag London, 2000

[12] Burden R. L., Faires J. D. Numerical Analysis, 7th ed. Brooks/Cole, 2000

[13] Roberts G., Taenzler F. An Introduction to Mixed-Signal IC Test and Measure-ment. Oxford Series in Electrical and Computer Engineering (Hardco), 2011

[14] Smith St. M. The Scientist and Engineer's Guide to Digital Signal Processing. 2nd ed. San Diego, CA, USA: California Technical Publishing, 1999

[15] Glazyrin A. S. Mathematical modeling of electromechanical systems. Analytical methods. Tomsk, Russia: Publishing House of Tomsk Polytechnic University, 2009

[16] Openheim A. V., Schafer R. W., Buck J. R. Discrete-Time Signal Processing. 2nd ed. Bergen, New Jersey, USA: Upper Saddle River Inc., 1998

[17] Bolovin E. V., Glazyrin A. S., Brendakov V. N., “The Influence of the Design Method for Induction Motor With Stationary Rotor on Identification of Its Parameters”, 2015 International Siberian Conference on Control and Communications (SIBCON): proceedings, 2015, pp. 1-7

Statistics based landmark selection model for cone-beam CT derived three-dimensional cephalometry

Adrienn Dobai[1], **Zsolt Markella**[2], **Miklós Mezei**[2], **Tamás Vizkelety**[1]

[1] Department of Oral and Maxillofacial Surgery and Dentistry, Semmelweis University
[2] Kandó Kálmán Faculty of Electrical Engineering, Óbuda University, Budapest, Hungary
{dobai.adrienn_gyongyi,vizkelety.tamas}@med.semmelweis-univ.hu,
{markella.zsolt,mezei.miklos}@kvk.uni-obuda.hu

Abstract: Although some articles have already assessed the reliability of three dimensional (3D) cephalometric landmarks, but the results were questionable because most of them analized the landmarks using linear or angular measurements instead of the coordinates. Therefore, the aim of this study was to eliminate the mistakes of the 3D landmark selection by the means of statistics based landmark selection model and a practically useable decision tree. In our study three medical doctors – the "examiners" – identified 55 particular landmarks on 30 non–orthodontic Cone Beam Computed Tomography (CBCT) scans using the Cranioviewer software. The identification process has been done three times in order to increase the accuracy. Intraclass correlation coefficient and analysis of variance were applied to decrease the intra- and inter- examiner variability, while standard deviation (SD) and mean absolute difference (MAD) were used for characterization of landmark locations. Inaccurate coordinates were grouped according to both the intra- and the inter-examiner deviation of $\geq$ 1mm and the difference between the two statistical methods (SD vs. MAD). The intra-examiner identification errors were $\leq$ 1mm. The inter-examiner SD and MAD were $\geq$ 1mm except in cases of four landmarks with MAD and in cases of two with SD. Inter-examiner deviations were always higher than intra-examiner deviations. Standard deviation distorted more than mean absolute difference. Based on these result we have created a decision tree for landmark selection. Most of the coordinates belong to the landmarks can be reliably adapted to 3D cephalometric, but the statistics based decision model could be useful to eliminate mistakes in landmark selection as well. Since, the statistical rules are summarized like a decision tree it can be easily used in practice.

Keywords: Cephalometry, Planning Techniques, Computer-Generated 3D Imaging, Cone-Beam Computerized Tomography, Dimensional Measurement Accuracy

1 Introduction

Cephalometric analysis is widely used for orthodontic diagnosis and presurgical planning in orthognathic surgery. By applying CBCT three-dimensional volumes of the particular target appear. In this way almost all errors coming from two-dimensional (2D) radiography can be eliminated. These errors include the magnification, distortion and superimposition of anatomical structures [1] as well. CBCT allows more exact representation of craniofacial asymmetries. Although one disadvantage of CBCT is the relatively high radiation dose, however, thanks to low-dose modules the effective doses of modern CBCT devices have been decreased. Furthermore, for presurgical planning of orthognathic cases, many additional exposures such as periapical, occlusal and posteroanterior radiographies are needed in addition to panoramic and lateral cephalometric X-rays [2]. The sum of the effective doses of these multiple exposures can be higher than with CBCT. Therefore, in more complex cases the CBCT is a more recommended tool for the presurgical planning [3,4] than other methods with similar purposes.
Many cephalometric analytical protocols and norms have been created for 2D imaging. These norms are not proper for the three-dimensional cephalometric measurement because of methodological differences between the common lateral cephalogram and the CBCT. Thus, new cephalometric norms are required for the CBCT based 3D cephalometry. The selection of acceptable landmarks for 3D craniometry is the basis for cephalometric reliability and repeatability. While landmark identification errors have already been published in numerous articles [5] many of them use angles or lines and not factual reference points [6, 7], which could be the base for creating a three-dimensional cephalometric analysis. There are three important considerations in landmark selection, which were not assessed in the previous articles [5–7]:

1. In three-dimensional measurements not all coordinates of a landmark are as important as others from the analysis point of view. Hence, we should not only analyze the accuracy of a landmark, but rather its reliable coordinates.
2. Other decisions can be made about the reliability considering different statistical tests, such as the SD or MAD. Since, the previously published studies in this regard [5–7] have applied only SD or MAD, they did not represent the differences in the results of two calculations.
3. Many factors contribute to the reproducibility of reference points such as image quality, anatomic complexity, experience of the examiners, correct definitions and so on [8, 9]. As these effects – with the exception of the anatomical structure – can be reduced by modern technology and precise measurement methods. Namely, if we know the reasons of inaccurate landmark detection then we will be able to eliminate the errors.

Due to the purpose of this study were fourfold:

1. To assess the intra- and inter-examiner reliability of the landmarks;

2. To demonstrate the most and least determinable coordinates by the means of two statistical markers (SD and MAD);
3. To analyze the identification problem of the unreliable coordinates;
4. To use these findings in order to develop a decision tree of landmark selection for 3D cephalometric analysis.

The paper is structured as follows: first, we introduce the applied methodology including the selection process, landmark detection and applied tool for statistical analysis. After, the outcomes are presented. Then, the results are assessed in the discussion section. Finally, the conclusions of the research are presented.

2 Applied Methodology

2.1 CBCT Scan Selection

This research (number: TUKEB 2/2008) was approved by the ethical committee of Semmelweis University. Thirty (n=30) existing CBCT scans were finally selected, 19 females and 11 males (aged 18 to 30 years), who underwent CBCT scanning for non orthodontic reasons.
During the selection of CBCT images we have taken into account the ethnicity and the age of patients, the field of view, the quality of the images and the facial form. Thus, the scans have been selected by using the following inclusion and exclusion criteria:

Inclusion criteria

a) sufficient image quality
b) large field of view (FOV)
c) bilateral Class I molar relationship
d) European ethnicity

Exclusion criteria

a) filling on the contact points of molar teeth
b) diasthema or crowding
c) anatomic anomalies or skeletal asymmetries
d) evidence of previous or current orthodontic treatment

The CBCT scans were obtained by using an i-CAT Classic scanner (Xoran Technologies, Ann Arbour Michigan, USA) at 120KV and 36 mA. The FOV was 16cm (H) x 22cm (D), and the isotropic voxel size was 0.4 x 0.4 x 0.4 mm. The 30 heads were fixed with the standardized head-holder and scanned parallel to the Frankfurt horizontal.

2.2 Landmark detection

The data of CBCT were transferred as DICOM (Digital Imaging and Communications in Medicine) files into the Cranioviewer software (Cranioviewer, Budapest, Hungary) in which the landmark locations have been calculated. In the multiplanar view (MPR) three axes have been defined as follows: X moved from left to right, Y moved from front to back and Z moved from top to bottom. After the detection of the landmarks the Cranioviewer automatically determined the coordinates of each point in millimeters and it shows the distance from the center of the coordinate system. Four imaging procedures are available in the program: slice X-ray, CT, MIP (Maximum Intensity Projection), AMIP (Advanced Maximum Intensity Projection). We used the AMIP and MIP only for the rough approximation of landmarks but all points were marked accurately on the CT projection. After detection, the program is able to create a 3D frame view from the determined points. A total of 55 landmarks (11 unpaired and 22 paired) on the hard tissue have been selected on CBCT images based on the 3D definitions of each landmark – as it can be seen in Table 1. The landmark locations are also shown on a typical 3D CBCT scan in Figure 1 - 2.

The landmark identifications have been repeated three times inside one week long interval. The identification was done by three experienced medical doctors (two dentists and one radiologist). Because of the experiences and training background of the examiners were quite similar these had minimal effect on the identification error.

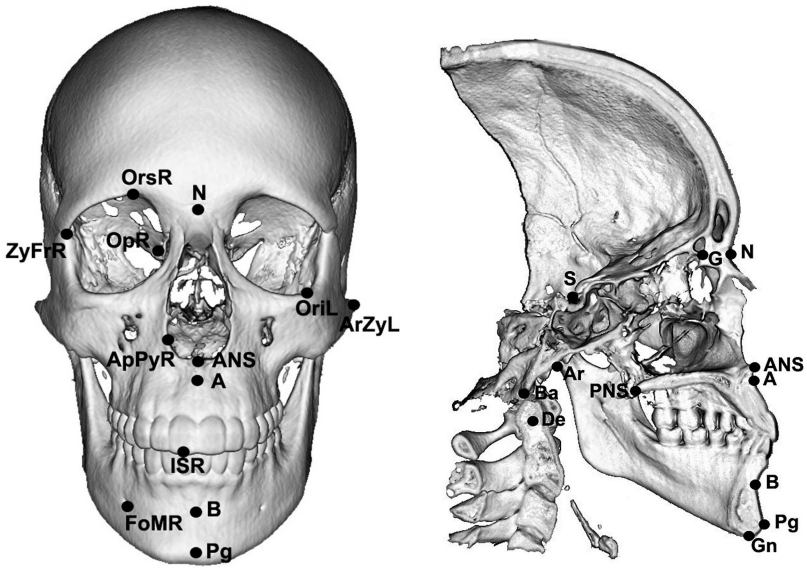

Figure 1
Position of cephalometric landmarks on the frontal and midsagittal view, respectively.

LANDMARK	DEFINITION
N (Nasion)	The crossing point of the sutura nasofrontalis and the sutura internasalis.
G (Galli)	Crossing point of the crista galli and the lamina cribrosa under the highest point of the crista galli.
S (Sella)	Crossing points of the sagittal and transversal diameter maximums of the cavum of the sella turcica where the transversal diameter is a constructed one determined by the proc. clinoideus ant. et post projected caudally to the level of the sagittal diameter.
Ba (Basion)	The most caudal and dorsal point of the clivus in the midplane of the skull.
De (Dens)	The crossing point of the greatest anteroposterior and transversal diameter of the dens axis.
ANS (Anterior nasal spine)	The most ventral end of the nasal floor, the tip of the spina nasalis anterior.
A (Point-A)	The deepest (most dorsal) point on the ventral surface curve of the maxilla in the sagittal midplane.
PNS (Posterior nasal spine)	The most dorsal extent of the hard palate in the midsagittal plane.
B (Point-B)	The deepest (most dorsal) point on the anterior curvature of the mandible symphisis in the midsagittal plane.
Pg (Pogonion)	The most ventral point along the curvature of the chin in the midsagittal plane.
Gn (Gnathion)	The most caudal point along the curvature of the chin in the midsagittal plane.
PtmR (Pterygomaxillare Right)	The contact point of the tuber maxillae with the pterygoid blade at the vertical level of the spina nasalis posterior on the right side.
ArR (Articulare Right)	A lateral view of the intersection of the external contour of the cranial base and the dorsal contour of the right ramus mandibulae.
ArZyR (Arcus Zygomaticus Right)	The most lateral/widest point of the zygomatic arch on the right side.
ZyFrR (Sutura Zygomaticofrontale Right)	The most ventral point of the right sutura zygomaticofrontalis.
ApPyR (Apertura Pyriformis Right)	The most lateral/widest point on the right side of the apertura pyriformis in the frontal view.
SemR (Semicircularis Right)	The most cranial point of the canalis semicircularis ant. seu sup. at the right side.
OriR (Orbitale inferius Right)	The most caudal point of the left orbita aperture.
OrsR (Orbitale superius Right)	The most cranial point of the right orbita aperture.
FmsR (Sutura Frontomaxillaris Right)	The distal end of the right sutura frontomaxillaris.
OpR (Opticus Right)	The intraorbital end of the canalis opticus at 9 o'clock at the right side of the orbit.
JR (Point-J Right)	The deepest point of the curvature formed at a junction of the anterior portion of the right ramus and corpus of the mandible.
PrCoR (Processus Coronoideus Right)	The most cranial point of the right processus coronoideus.
CmR (Condylus medialis Right)	Medial pole of the right condyle.
ClR (Condylus lateralis Right)	Lateral pole of the right condyle.
GoR (Gonion Right)	Bisection tangent of the lowest edge of the corpus and the most posterior edge of the ramus mandibulae.
IGoR (Inferior Gonion Right)	The most inferior point on the camber of the corpus mandibulae on the right side.
PGoR (Posterior Gonion Right)	The most dorsal point on the dorsal camber of the ramus mandibulae on the right side.
FoMR (Foramen mentale Right)	The most proximal/distal point of the right foramen mentale.
IIR (Incision inferior Right)	The mesiodistal midpoint of the incisor edge of the lower right incisor.
ISR (Incision superior Right)	The mesiodistal midpoint of the incisor edge of the upper right incisor.
IIAR (Incision inferior apicale Right)	The apex of the right lower incisor.
ISAR (Incision superior apicale Right)	The apex of the right upper incisor.

Table 1
Three-dimensional definitions of cephalometric landmarks.

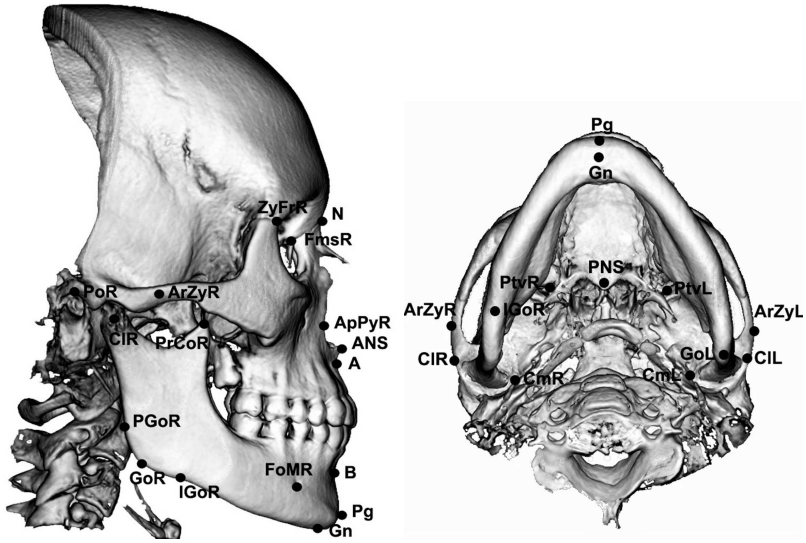

Figure 2
Position of cephalometric landmarks on the lateral and from the inferior view, respectively.

2.3 Statistical analysis

In order to establish intra- and inter-examiner reliability, values were assessed by an intraclass correlation coefficient (ICC) using SPSS statistical package 20.0 (IBM Corporation, Chicago, USA) [10]. The determination of the real position of the landmarks is impossible in case of in vivo research; therefore in order to evaluate the precision of landmark location we used descriptive statistics.

Similar to the previously published articles [2, 11, 12] in which SD or MAD have been applied, in this study we compared these two statistical estimations. Intra-examiner SD and MAD showed the repeatability of landmark identification and the inter-examiner SD and MAD characterized the reproducibility. We selected the most (SD or MAD was ≤ 0.2 mm) and less (SD or MAD was ≥ 1.0 mm) reliable coordinates in case of intra- and inter-examiner analysis, respectively. The inaccurate coordinates were divided into three groups based on the magnitude of SD of intra-examiner, inter-examiner or both deviations. By observing the differences we could determine the cause of difficulty regard to the unreliable landmark detection.The results are summarized and a decision model – including the main guidelines of landmark selection – is presented in the next section.

3 Results

In the followings we summarize the completed tests and provide a picture about the performance of the suggested technique.

Intra- and inter-examiner investigation: the reliability of the examiners was determined by calculating the ICC values for all landmarks of the X, Y and Z coordinates. To get a more detailed picture about the reliability of landmark positions, separate X, Y, Z coordinate values were used instead of three dimensional distances. The intraclass correlation coefficient was greater than 0.9 for all axes and for each landmark in intra-examiner measurements and it was greater than 0.9 in inter-examiner measurements.

Intra-examiner test for repeatability: in case of the intra-examiner test the standard deviation and the mean absolute difference of each landmark were assessed for each examiner trial. In most cases the values of SD were low ($\leq$1 mm), only by the following cases were between 1.03 and 2.00 mm: Orbitale Inferior (ob3:X-axis), bilateral Inferior Gonion (ob1,2,3:Y-axis), Orbitale Inferior (ob3:Y-axis), bilateral Posterior Gonion (ob1,2,3:Z-axis), J-point (ob2,3:Z-axis), Apertura Piriformis (ob3:Z-axis). The mean absolute differences were lower than 1 mm except the Orbitale Inferior (ob3:X-axis), bilateral Inferior Gonion (ob2,3:Y-axis), Apertura Piriformis (ob3:Z-axes) and bilateral Posterior Gonion (ob 1,2, 3:Z-axis).

Inter-examiner test for reproducibility: by using the inter-examiner test the SD and MAD were determined from the averaged intra-examiner trials of the 3 medical staff members (see Table 2.).

The inter-examiner standard deviation corresponded each landmark for X, Y and Z coordinates were evaluated from the average coordinates of the three investigators. For the most part the deviation was lower than 1mm. Only in case of the following structures was higher than 1 mm:

- On the X axis: Orbitale inferior right (3.44 mm) and left (3.56 mm), J-point right (1.55 mm) and left (1.77 mm).
- On the Y axis: Orbitale inferior right (2.44 mm) and left (2.23 mm), J-point right (1.8 mm) and left (1.78 mm), Inferior Gonion right (2.9 mm) and left (3.38 mm), Sutura Zygomaticofrontale right (1.32 mm) and left (1.28 mm).
- On the Z axis: Orbitale inferior right (2.27 mm) and left (2.25 mm), J-point right (3.37 mm) and left (3.34 mm), Sutura Frontomaxillare right (1,07 mm) bilateral Apertura Piriformis (2.59 mm; 2.56 mm) and Posterior Gonion (2.34 mm; 1.99 mm).

The measurement errors were also determined as the average of mean absolute differences for all coordinates for each landmark. The average mean differences on the X, Y and Z axis were bigger than 1 mm in these cases:

- On the X axis: Orbitale inferior right and left (2.6 and 2.64 mm), J-point right and left (1.15mm and 1.3mm)
- On the Y-axis: inferior Gonion right and left (1,68 and 2.8mm) and J-point right and left (1.34mm and 1.32mm), Orbitale inferior right and left (1.88mm and 1.8 mm)
- On the Z-axis: J-point right and left (2.14mm and 2.1mm), inferior Gonion right and left (1.71mm and 1.91mm)

Landmark	SD_X (mm)	SD_Y (mm)	SD_Z (mm)	MAD_X (mm)	MAD_Y (mm)	MAD_Z (mm)
N	0,21	0,24	0,33	0,16	0,18	0,20
G	0,29	0,86	0,58	0,22	0,64	0,54
S	0,38	0,24	0,29	0,28	0,17	0,20
Ba	0,23	0,39	0,27	0,16	0,26	0,28
De	0,18	0,23	0,36	0,13	0,16	0,21
ANS	0,21	0,31	0,26	0,16	0,22	0,21
A	0,19	0,15	0,55	0,14	0,11	0,27
PNS	0,23	0,28	0,31	0,17	0,18	0,24
B	0,23	0,18	0,52	0,17	0,12	0,22
Pg	0,26	0,16	0,58	0,19	0,13	0,24
Gn	0,30	0,39	0,24	0,23	0,31	0,22
PtmR	0,47	0,40	0,76	0,34	0,26	0,49
PtmL	0,44	0,43	0,78	0,33	0,28	0,52
ArR	0,31	0,22	0,49	0,24	0,18	0,32
ArL	0,36	0,35	0,48	0,27	0,27	0,36
ArZyR	0,14	0,66	0,54	0,10	0,47	0,44
ArZyL	0,15	0,84	0,68	0,11	0,62	0,48
ZyFrR	0,62	1,32	1,00	0,46	0,76	1,00
ZyFrL	0,44	1,28	0,84	0,33	0,74	1,00
ApPyR	0,42	0,33	2,59	0,31	0,21	0,77
ApPyL	0,34	0,43	2,56	0,25	0,28	0,83
SemR	0,29	0,30	0,24	0,21	0,22	0,19
SemL	0,32	0,28	0,31	0,24	0,22	0,19
OriR	3,44	2,42	2,27	2,60	1,88	1,61
OriL	3,56	2,23	2,25	2,64	1,80	1,57
OrsR	0,96	1,00	0,46	0,70	0,83	0,59
OrsL	0,83	1,00	0,47	0,60	1,00	0,69
FmsR	0,58	0,92	1,07	0,53	0,74	0,57
FmsL	0,65	0,79	0,89	0,48	0,62	0,51
OpR	0,68	0,89	0,88	0,64	0,69	0,72
OpL	0,51	0,97	0,97	0,38	0,70	0,84
JR	1,55	1,85	3,37	1,15	1,34	2,14
JL	1,77	1,78	3,34	1,30	1,32	2,10
PrCoR	0,26	0,33	0,28	0,19	0,20	0,23
PrCoL	0,28	0,28	0,31	0,21	0,20	0,19
CmR	0,21	0,32	0,55	0,15	0,25	0,33
CmL	0,20	0,33	0,55	0,14	0,23	0,33
ClR	0,16	0,32	0,58	0,12	0,23	0,35
ClL	0,15	0,27	0,54	0,11	0,20	0,29
GoR	0,27	0,65	0,68	0,19	0,49	0,47
GoL	0,33	0,70	0,71	0,24	0,53	0,53
IGoR	0,89	2,90	0,91	0,66	1,68	1,71
IGoL	1,00	3,38	1,00	0,74	2,08	1,91
PGoR	0,39	0,81	2,34	0,29	0,47	1,00
PGoL	0,39	0,66	1,99	0,29	0,47	0,93
FoMR	0,56	0,55	0,86	0,41	0,31	0,52
FoML	0,59	0,63	0,93	0,43	0,37	0,57
IIR	0,61	0,28	0,35	0,46	0,20	0,27
IIL	0,63	0,24	0,33	0,47	0,17	0,25
ISR	1,00	0,21	0,16	0,80	0,16	0,14
ISL	0,89	0,25	0,17	0,67	0,19	0,15
IIAR	0,33	0,46	0,72	0,24	0,36	0,46
IIAL	0,24	0,51	0,74	0,18	0,36	0,54
ISAR	0,25	0,30	0,41	0,18	0,24	0,25
ISAL	0,29	0,43	0,43	0,21	0,30	0,30

Table 2
Standard deviation and mean absolute difference characteristics for each landmark (dark grey - the most unreliable reference points, light grey - the most reliable reference points).

The most reliable points (SD $<$ 0.2 mm) are quoted below:

- On the X axis: Dens (0.18 mm) and Point-A (0.19 mm), Arcus Zygomaticus left and right (0.14 mm; 0.15 mm), Lateral Condyle left (0.15 mm) and right (0.16 mm).
- On the Y axis: Point-A (0.15 mm), Pogonion (0.16 mm) and Point-B (0.18 mm)
- On the Z axis: Incision Superior right and left (0.16 mm; 0.17 mm)

By the calculation of average MAD more reference points had lower dispersion (< 0.2 mm) than in case of SD, such as Nasion, Sella, Basion, Posterior Nasal Spine, Coronoid Process, Medial Condyle, Semicirculare, Incision Inferior, Incision Inferior and Superior Apicale.

Unreliable landmark characterization: the MAD values were lower than the SD values in case of the same coordinates which proves the fact that the standard deviation distorts more - because of the outliers - than the absolute difference. Therefore, we divided the unreliable landmarks into different groups in accordance with the high intra-or inter-examiner standard deviation (see Table 2.). The inter-examiner differences dependent mainly on the training and experience of the examiners [13] and definitions of landmarks contrary to the intra-examiner analysis, in which the image quality and the position of the anatomical structures played important roles (see Table 2.). The investigators were close or equally qualified. Those coordinates - where only the intra-examiner deviation was high – are not usable in the future for 3D cephalometry, because the anatomical structure was fixed and the image – provided by the iCAT machine – had high quality. Those points which had problem with the deviation only in the inter-examiner test can be improved by using better definition or training courses. The most problematic coordinates were those which had unreliable detection by both tests, these coordinates are not suggested for use in 3D measurement.

Decision tree: when starting to plan surgical treatment, it is important to know which reference points can be used. Therefore in the evaluation of the two statistics (SD and MAD) of the repeatability and reproducibility of landmark detection we focused to the most unreliable coordinates. These conclusions are relevant for the selection of the proper points for the 3D cephalometry:

1. The coordinates of the same landmarks may exhibit a high degree of variance. Since not every landmark plays important role in presurgical planning we should focus not on the landmarks themselves, but on their coordinates.

2. Standard deviation can be more distorted than mean absolute difference.

3. Inter-examiner SD or MAD is mainly higher than intra-examiner value.

Figure 3. shows the suggested method for landmark selection. By considering the results and these conclusions, the following method is suggested when planning:

1. One must respect those coordinates, which are necessary for the planning of the treatment.

2. Looking at the inter-examiner standard deviation of the questionable coordinate:

    a) If the inter-examiner SD is low in those coordinates which are necessary then the landmark can be used safely.

    b) If the inter-examiner SD is high (> 1mm), it is recommended to check the MAD.

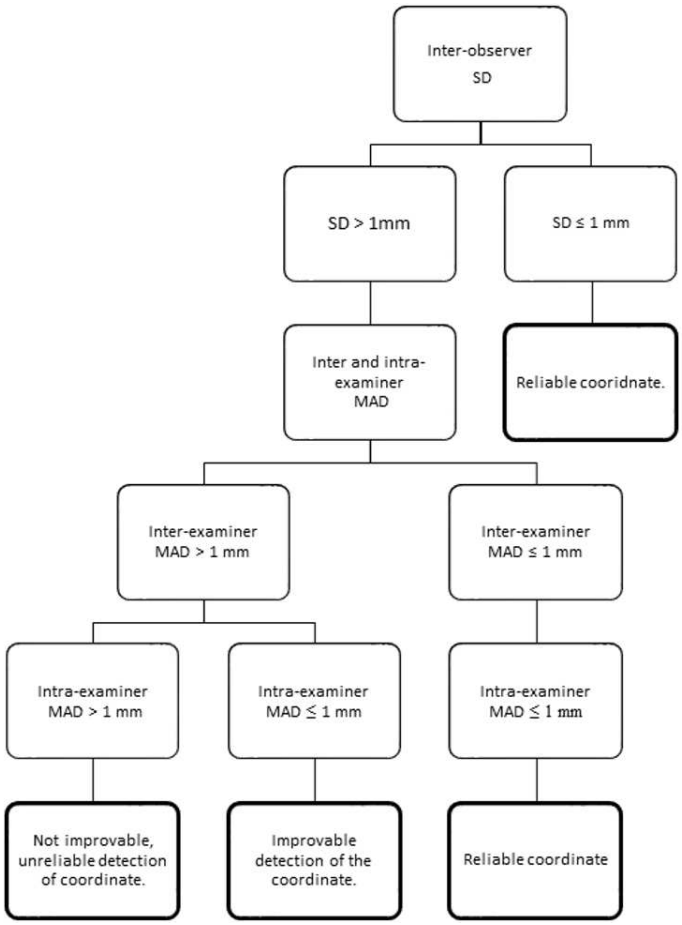

Figure 3
Decision tree for landmark selection.

3. Looking at the inter- and intra-examiner mean absolute difference of the coordinate:

   a) When inter- and intra-examiner MAD are high ($>$ 1mm), many factors, such as image quality, facial anatomy, incorrect definition of the landmark, and the examiner could influence the identification error. Due to the various sources of the problem the accuracy of the detection is not improvable.

   b) When inter-examiner MAD is high ($>$ 1mm), but the intra-examiner MAD is low ($\leq$1 1mm) this can be useful but during the detection paying attention to the source of the problem is needed. The lack of precise definition of landmarks and different training level of examiners can cause the non unambiguous marking. In these cases the problem can only be solved with a new, more accurate definition or with training of

the examiners at a higher quality level.

c) If the inter-examiner MAD is low, the intra-examiner MAD will also be low, so these coordinates are adaptable in 3D accurately.

4 Discussion

Three-dimensional cephalometry plays an important role in the planning of the clinical treatment especially in the field of orthognathic surgery. Therefore in the present study the repeatability and reproducibility of the cephalometric landmarks were analyzed for creating a selection method. Other studies used dry skulls, lateral cephalograms or CBCTs to evaluate landmark identification, but most of them used only lines and angles [14–18], and not the reference points. Previously published studies concluded which reference points were not accurate. However, in 3D cephalometry often happens that we need only one direction of the landmark during the analysis, thus we need to focus the coordinates and not lines or angles.
30 patients with normal occlusion were included in this study and 55 landmarks were located by three examiners three times using Cranioviewer cephalometric software. The members of the examined group had normal occlusion, thus these data can be useful for creating cephalometric analyses in the future, which characterize the ideal state of the face in the presurgical planning.
Some studies have already contrasted the precision of landmark location based on multiplanar reconstructed images and volume rendered 3D cephalometry with the in vitro examination based on dried skulls. Fernandes et al. in 2014 and Neiva et al. in 2015 have reported that measurements performed on multiplanar reconstructed images were more accurate than measurements in volume rendering compared by using digital calipers [19, 20]. Another study stated, that the inter-raters ICCs were higher for multiplanar (ICC $\geq$ 0.90 in 82.16 %) than 3D reconstruction (ICC $>$ 0.90 in 67.76 %) [20]. Besides, Katkar et al. stated that the surface-rendered method increased the evaluation time without improving the precision of identification [21]. Therefore in this study the landmarks were investigated using surface-rendered methods.
According to Bookstein the basic problem with the landmark detection is the lack of suitable, practical definitions of 3D landmarks [22], therefore in this research a reference guide was defined accurately allowed for each plane.
In this study the intra-and inter-examiner intraclass correlation coefficients of each landmark were high (ICC $\geq$ 0.9) in every axis, similar results were reported by Zamora et al. [2]. The results of Oliveria et al. showed less correlations than we calculated. The ICC $\geq$ 0.9 was found for 85 % of the intra-examiner and for 65.5 % of the inter–examiner measurements [23] . To sum up we showed that the ICCs in the 3D cephalometry are mainly high ($\geq$ 0.9) and the inter-examiner reliability is generally higher than intra–examiner [24].
The repeatability and reliability of reference points were characterized with SDs and MADs because of two considerations: *(i)* with the help of the two statistics we could compare the results also to those published articles in which only SD or only MAD was applied and *(ii)* this calculation serves for providing the difference between the

two statistical parameters.
If we compare the results from viewpoint of SD and MAD values, then we can see that the standard deviation was always higher than mean absolute difference, which can be, because the standard deviation is more sensitive to the outliers. Many articles report only the SD values [2]. Due to this fact we could not do exact comparison with the existing literature. However, we compared the results of Zamora et al. with the calculation of this study in the case of midplane landmarks including: Na, S, Ba, Me, Gn, A and B-point, and we found lower MAD than SD in each case. In this study the unreliable coordinates (SD $\geq$ 1 mm or MAD $\geq$ 1 mm) were the same by the two statistics except for Apertura Piriformis and J-Point, whereby the SDs were higher than 1mm, but the MAD was lower. So a landmark selection based on only MAD or only SD can result maybe two different decisions. Therefore during the selection of the landmarks for the presurgical planning we cannot ignore this fact.
If we look at the difference between the intra and inter-examiner results, then we note the same situation as with the ICC, so the intra-rater SD or MAD was lower than inter-rater values. Lagrave et al. analyzed the inter and intra reliability and results showed that inter-examiner mean measurement differences were higher than intra-examiner [11,12,25]. In this study the intra–examiner MADs (0.04 - 1.58 mm) were less than inter-examiner errors, which have been between 0.09 - 2.64 mm.
However, many studies determined the imprecise landmarks, but this problem was not explored, therefore we have created groups based on the type of deviation (Table 3). With the help of Table 3. we can conclude that by some coordinates of the following landmarks – J-point, Zygomaticofrontal suture, Frontomaxillary suture and Infrerior orbitale – the landmark identification error can be reduced with correct definition or more training. With the Y coordinate of the Zygomatic Arch the anatomy and the image quality play important role in the identification. Regarding image quality, Katkar et al. reported a study, in which they compared the landmark identification error with two difference CBCT machines. They stated, that machine differences were significant for almost all landmarks, but some landmarks were more accurate on Galileos and some of them were more accurate on i-CAT machines [21]. Therefore, by those coordinates which had high intra- and low inter-examiner SD, the identification error can be hardly reduced.

Axis	Intraexaminer test	Interexaminer test	Intra–and interexaminer test
X	–	J-point	Orbitale Inferior
Y	Zygomatic Arch	J-point Sutura Zygomaticofrontale	Inferior Gonion Orbitale Inferior
Z	–	Orbitale inferior Sutura Frontomaxillare	J-point Apertura Piriformis Posterior Gonion

Table 3
Anatomical structures, which have had high standard deviation in the intra-examiner, in the inter-examiner or by both test.

Conclusions

In this study most coordinates of the landmarks were reliably adapted to the three-dimensional measurement based CBCT scans. We suggest caution in selection of the coordinates of the following landmarks: Zygomatic Arch, J-point, Zygomaticofrontal suture, Frontomaxillary suture, Inferior Orbitale, Inferior Gonion, Posterior Gonion and the Piriform Aperture.
The characterization of coordinates by SD and MAD showed that the enrollment decision of landmark for 3D cephalometry depends strongly on the statistics.
The analysis of the unreliable coordinates revealed the source of the identification problem, we could improve the detection.
The decision tree can be useful to eliminate the mistakes for the presurgical planning in the practice.

Acknowledgement

M. Mezei thankfully acknowledges the support of the Robotics Special College and the Applied Informatics and Applied Mathematics Doctoral School of Óbuda University.

References

[1] M. A. Papadopoulos, C. Jannowitz, P. Boettcher, J. Henke, R. Stolla, H. F. Zeilhofer, L. Kovacs, W. Erhardt, E. Biemer, and N. A. Papadopulos. Three-dimensional fetal cephalometry: an evaluation of the reliability of cephalometric measurements based on three-dimensional CT reconstructions and on dry skulls of sheep fetuses. *J Craniomaxillofac Surg*, 33(4):229–237, 2005.

[2] N. Zamora, J. M. Llamas, R. Cibrian, J. L. Gandia, and V. Paredes. A study on the reproducibility of cephalometric landmarks when undertaking a three-dimensional (3D) cephalometric analysis. *Med Oral Patol Oral Cir Bucal*, 17(4):e678–e688, 2012.

[3] W. De Vos, J. Casselman, and G. R. Swennen. Cone-beam computerized tomography (CBCT) imaging of the oral and maxillofacial region: a systematic review of the literature. *Int J Oral Maxillofac Surg*, 38(6):609–625, 2009.

[4] P. M. Cattaneo and B. Melsen. The use of cone-beam computed tomography in an orthodontic department in between research and daily clinic. *World J Orthod*, 9(3):269–282, 2008.

[5] O. Lisboa Cde, D. Masterson, A. F. da Motta, and A. T. Motta. Reliability and reproducibility of three-dimensional cephalometric landmarks using CBCT: a systematic review. *J Appl Oral Sci*, 23(2):112–119, 2015.

[6] O. J. van Vlijmen, T. Maal, S. J. Berge, E. M. Bronkhorst, C. Katsaros, and A. M. Kuijpers-Jagtman. A comparison between 2D and 3D cephalometry on CBCT scans of human skulls. *Int J Oral Maxillofac Surg*, 39(2):156–160, 2010.

[7] C. Michele, A. Federica, D. G. Roberto, and S. Alessandro. Two-Dimensional and Three-Dimensional Cephalometry Using Cone Beam Computed Tomography Scans. *J Craniofac Surg*, 26(4):e311–e315, 2015.

[8] M. Fuyamada, M. Shibata, H. Nawa, K. Yoshida, Y. Kise, A. Katsumata, E. Ariji, and S. Goto. Reproducibility of maxillofacial landmark identification on three-dimensional cone-beam computed tomography images of patients with mandibular prognathism: Comparative study of a tentative method and traditional cephalometric analysis. *Angle Orthod*, 84(6):966–973, 2014.

[9] W. J. Houston, R. E. Maher, D. McElroy, and M. Sherriff. Sources of error in measurements from cephalometric radiographs. *Eur J Orthod*, 8(3):149–151, 1986.

[10] R. N. Landers. Computing Intraclass Correlations (ICC) as Estimates of Interrater Reliability in SPSS. https://thewinnower.com/papers/1113-computing-intraclass-correlations-icc-as-estimates-of-interrater-reliability-in-spss. Accessed: 2017-06-20.

[11] M. O. Lagravere, J. M. Gordon, I. H. Guedes, C. Flores-Mir, J. P. Carey, G. Heo, and P. W. Major. Reliability of traditional cephalometric landmarks as seen in three-dimensional analysis in maxillary expansion treatments. *Angle Orthod*, 79(6):1047–1056, 2009.

[12] M. O. Lagravere, C. Low, C. Flores-Mir, R. Chung, J. P. Carey, G. Heo, and P. W. Major. Intraexaminer and interexaminer reliabilities of landmark identification on digitized lateral cephalograms and formatted 3-dimensional cone-beam computerized tomography images. *Am J Orthod Dentofacial Orthop*, 137(5):598–604, 2010.

[13] W. Schlicher, I. Nielsen, J. C. Huang, K. Maki, D. C. Hatcher, and A. J. Miller. Consistency and precision of landmark identification in three-dimensional cone beam computed tomography scans. *Eur J Orthod*, 34(3):263–275, 2012.

[14] P. W. Major, D. E. Johnson, K. L. Hesse, and K. E. Glover. Landmark identification error in posterior anterior cephalometrics. *Angle Orthod*, 64(6):447–454, 1994.

[15] E. L. Delamare, G. S. Liedke, M. B. Vizzotto, H. L. da Silveira, J. L. Ribeiro, and H. E. Silveira. Influence of a programme of professional calibration in the variability of landmark identification using cone beam computed tomography-synthesized and conventional radiographic cephalograms. *Dentomaxillofac Radiol*, 39(7):414–423, 2010.

[16] S. A. Stratemann, J. C. Huang, K. Maki, A. J. Miller, and D. C. Hatcher. Comparison of cone beam computed tomography imaging with physical measures. *Dentomaxillofac Radiol*, 37(2):80–93, 2008.

[17] D. R. Periago, W. C. Scarfe, M. Moshiri, J. P. Scheetz, A. M. Silveira, and A. G. Farman. Linear accuracy and reliability of cone beam CT derived 3-dimensional images constructed using an orthodontic volumetric rendering program. *Angle Orthod*, 78(3):387–395, 2008.

[18] A. A. Brown, W. C. Scarfe, J. P. Scheetz, A. M. Silveira, and A. G. Farman. Linear accuracy of cone beam CT derived 3D images. *Angle Orthod*, 79(1):150–157, 2009.

[19] T. M. Fernandes, J. Adamczyk, M. L. Poleti, J. F. Henriques, B. Friedland, and D. G. Garib. Comparison between 3D volumetric rendering and multiplanar slices on the reliability of linear measurements on CBCT images: an in vitro study. *J Appl Oral Sci*, 23:1, 2014.

[20] M. B. Neiva, A. C. Soares, O. Lisboa Cde, V. Vilella Ode, and A. T. Motta. Evaluation of cephalometric landmark identification on CBCT multiplanar and 3D reconstructions. *Angle Orthod*, 85(1):11–17, 2015.

[21] R. A. Katkar, C. Kummet, D. Dawson, L. Moreno Uribe, V. Allareddy, M. Finkelstein, and A. Ruprecht. Comparison of observer reliability of three-dimensional cephalometric landmark identification on subject images from Galileos and i-CAT cone beam CT. *Dentomaxillofac Radiol*, 42(9):20130059:1–11, 2013.

[22] F. L. Bookstein. Morphometric Tools for Landmark Data. *Cambrige University Press*, page p453, 1991.

[23] A. E. de Oliveira, L. H. Cevidanes, C. Phillips, A. Motta, B. Burke, and D. Tyndall. Observer reliability of three-dimensional cephalometric landmark identification on cone-beam computerized tomography. *Oral Surg Oral Med Oral Pathol Oral Radiol Endod*, 107(2):256–265, 2009.

[24] J. F. Gravely and P. M. Benzies. The clinical significance of tracing error in cephalometry. *Br J Orthod*, 1(3):95–101, 1974.

[25] Gy. Eigner, J.K. Tar, I. Rudas, and L. Kivács. LPV-based quality interpretations on modeling and control of diabetes. *ACTA Pol Hung*, 13(1):171–190, 2016.